

PhD THESIS

**EXPERIMENTAL AND NUMERICAL ANALYSIS OF
WEAR FLAT GENERATION AND GROWTH IN
ALUMINA GRINDING WHEELS**

Presented to obtain the degree of

Doctor in Industrial Engineering

Presented by:

Leire Godino Fernández

Thesis supervisors:

Dr. Iñigo Pombo Rodilla

Prof. Dr. Jose Antonio Sánchez Galíndez

February 2019, Bilbao

4 years and "only" 183 pages...

ACKNOWLEDGMENTS

Este trabajo no hubiera sido posible sin todas aquellas personas que de una manera u otra habéis contribuido en mi formación no sólo como investigadora sino también como persona. A vosotros...

... mis directores, Iñigo y Jose Antonio. La calidad y consistencia de este trabajo es vuestra. Qué decir de vuestro apoyo constante y esfuerzo para que día a día sea más autónoma en mi carrera como investigadora. ¿Y vuestro papel como psicólogos en los momentos más críticos? Encomiable.

... Professor Ivan Iordanoff. I am grateful for giving me a chance to be part of your team in the ENSAM in Talance. Thank you for your wisdom and your dedication. I also would like to acknowledge Jeremie for your support and commitment. I have learned a lot working with you.

... Iván, siempre a pie de máquina para afrontar esos ensayos tan caóticos. ¡Buen equipo! Suerte en tu nueva etapa.

... mis compañeros, los recién llegados, los que ya no estáis y los que habéis compartido conmigo estos cuatro años. Los días han sido más entretenidos junto a vosotros. Me llevo grandes amigos.

... “my personal English reviewers”, because your corrections have put the icing on the cake of this work. Is it correct? ¡Paciencia es poca!

...mis amigas, siempre dispuestas. Juntas desde niñas y por muchos años, por muy diferentes que sean nuestros caminos.

...mi familia que desde pequeña me habéis inculcado la importancia de la constancia y el esfuerzo para conseguir lo que me proponga. Con esto se acaba mi etapa de estudiante, creo...

... Jorge, sobran las palabras. 4 años escuchando mis penurias con las máquinas, te han convertido en un experto en la materia ¡Quién te lo iba a decir! Has sabido cómo levantarme el ánimo cuando más lo necesitaba, y también, ponerme las pilas cuando me relajaba. Has puesto el equilibrio a esta carrera de fondo. ¡Gracias por estar ahí!

¡MUCHAS GRACIAS!

SUMMARY

Grinding is an abrasive machining operation commonly known as a finishing process, which gives great added value to the final product in a wide range of fields such as automotive, aerospace or energy industry. Thus, a continuous research is required in order to meet the industrial demand. Current industrial requirements are related to the minimization of grinding cost and, consequently, the increase of process efficiency. In this sense, new abrasives are being developed to increase tool life and removal rates. Microcrystalline sintered alumina creates this new generation, which seems to be more durable comparing with conventional alumina, being its behavior not deeply analyzed. Likewise, tool life is directly related to grinding wheel wear, being wear flat one of the most harmful, leading to a real industrial problem of thermal damage and decrease of process efficiency.

In this respect, this research work is developed in order to tackle the problem of wear flat in abrasive grains of alumina, taking into account the influence of crystalline structure. The study is focused on the characterization of wear flat analyzing its generation and evolution under grinding contact conditions. The wear flat is addressed from both experimental and numerical points of view, dividing the work in real grinding tests, tribological tests and a numerical analysis of the wear.

Real grinding tests are carried out isolating wear flat, studying this phenomenon depending on the crystalline structure and grinding parameters. This work shows the importance of tribochemical reactions and the third body in the contact and the influence of crystalline structure in both wear flat generation and worn surface appearance. After that, to control contact conditions, an original design of pin-on-disk tribometer is implemented. The tribometer reproduces the thermal cycle of abrasive grains at 30 m/s achieving 190 MPa. These results show a higher depth of groove for WFA comparing to SG. Finally, a numerical analysis of an abrasive grain is done. The thermal model shows higher contact temperature for SG. Moreover, DEM wear model of a single abrasive grain presents the evolution of the third body wear, achieving higher wear for WFA.

In consequences, higher %A is achieved for SG abrasive wheel. In contrast, the tribometer tests and the numerical analysis reveal a higher influence of tribochemical reactions in the case of WFA. This is explained due to the higher temperature achieved in the contact for SG, which modifies the bond around SG abrasive grains, enhancing the adhesion of third body to the all worn surface.

CONTENT

I. INTRODUCTION.....	3
I.1. Industrial context.....	3
I.2. Objectives and contributions	4
I.3. Content layout.....	6
II. STATE OF THE ART.....	11
II.1. Abstract	11
II.2. Grinding process	11
II.2.1. Introduction	11
II.2.2. Latest developments in grinding	13
II.2.3. Basis of grinding process	16
II.3. Grinding wheels	17
II.3.1. General classification	17
II.3.2. Alumina: crystallographic structure	19
II.3.3. Grinding wheel wear	23
II.4. Tribology of abrasive machining processes	26
II.4.1. Alumina-steel contact.....	29
II.4.2. Material removal mechanisms in grinding process	33
II.4.3. Approaches for the characterization of grinding process	35
II.4.4. Alumina-steel contact under grinding conditions: approaches.....	37
II.4.5. Third body generation under grinding contact conditions	39
II.5. Wear Flat of alumina grinding wheels	41
II.5.1. Wear Mechanisms involves in wear flat generation.....	41

II.5.2.	Wear Flat characterization during grinding.....	42
II.5.3.	Wear Flat and wheel topography measurement techniques	46
II.6.	Simulation of grinding process	49
II.6.1.	Modeling of grinding wheel topography.....	52
II.6.2.	Modeling of grinding wheel wear	54
II.6.3.	Application of DEM to tribological studies	56
II.7.	Conclusions	57

III. ON THE DEVELOPMENT OF WEAR FLAT OCCURRENCE ON ALUMINA GRINDING WHEEL DURING GRINDING..... 63

III.1.	Introduction.....	63
III.2.	Experimental set up for grinding tests.....	63
III.3.	Grinding tests methodology	68
III.3.1.	Methodology for wear flat generation and quantification during grinding	68
III.3.2.	Methodology for wheel surface analysis.....	72
III.4.	Experimental results.....	73
III.4.1.	Grinding analysis.....	74
III.4.1.1.	<i>The importance of measuring real depth of cut.....</i>	74
III.4.1.2.	<i>Error in wear flat quantification</i>	75
III.4.1.3.	<i>Influence of crystalline structure of abrasive grains on wear flat evolution .</i>	75
III.4.1.4.	<i>Influence of grinding parameters of abrasive grains on wear flat evolution.</i>	77
III.4.1.5.	<i>Wear flat influence on grinding forces and friction coefficient.....</i>	79
III.4.2.	Microscopic analysis of wheel surface.....	83
III.4.2.1.	<i>3D functional roughness parameters analysis</i>	83
III.4.2.2.	<i>SEM and EDXA analysis</i>	86
III.5.	Preliminary conclusions	95

IV. NEW DESIGN OF A PIN-ON-DISK TRIBOMETER FOR ALUMINA ABRASIVE GRAIN WEAR ANALYSIS 101

IV.1.	Introduction	101
IV.2.	New design of a pin-on-disk tribometer.....	102
IV.3.	Experimental set up for pin-on-disk tests.....	105
IV.4.	Methodology for tribological tests to characterize abrasive grain wear.....	107
IV.4.1.	Real contact area quantification	107
IV.4.2.	Methodology for Pin-on-disk tests.....	109
IV.4.3.	Methodology for abrasive grain wear measurement	111
IV.5.	Pin-on-disk experimental results	114
IV.5.1.	Real contact area quantification	115
IV.5.2.	Influence of the contact conditions in the wear of the abrasive grains.....	117
IV.5.3.	Influence of crystalline structure of abrasive grains in the wear.....	120
IV.6.	Preliminary conclusions	124

V. FIRST APPROACH TO MODELING THE WEAR OF ALUMINA ABRASIVE GRAINS..... 129

V.1.	Introduction	129
V.2.	Alumina abrasive grain wear model.....	130
V.2.1.	Objectives of the wear model.....	130
V.2.2.	Basis of the wear model	131
V.3.	Determination of 2 domains in the abrasive grain.....	134
V.3.1.	Variation of Al ₂ O ₃ properties with temperature.....	134
V.3.2.	2D finite element thermal model of alumina abrasive grain	135
V.3.2.1.	<i>Simplifications for the finite element thermal model.....</i>	<i>136</i>

V.3.2.2.	<i>Thermal model definition</i>	138
V.3.2.3.	<i>Results of 2D thermal simulations</i>	139
V.4.	Abrasive grain wear simulation model.....	142
V.4.1.	DEM for alumina abrasive grain wear simulation: GranOO.....	142
V.4.2.	Main algorithm of the abrasive grain wear model.....	142
V.4.3.	Discrete element model definition	143
V.4.4.	3D cohesive beam model to alumina modeling	146
V.4.4.1.	<i>Calibration of mechanical properties of the abrasive grain</i>	147
V.4.4.2.	<i>Failure criteria calibration and wear criteria definition.</i>	149
V.4.5.	Model inputs.....	151
V.4.5.1.	<i>Sliding speed</i>	151
V.4.5.2.	<i>Pressure</i>	152
V.4.6.	Boundary conditions	153
V.4.7.	Contact problem: definition of contact laws	154
V.5.	Validation of the abrasive grain wear DEM model.....	155
V.5.1.	Verification of only <i>down domain</i> simulation.....	155
V.5.2.	Wear model for WFA abrasive grains.....	157
V.5.3.	Model variations to reproduce SG abrasive grain wear	159
V.6.	Preliminary conclusions	161
VI. CONCLUSIONS AND FUTURE WORKS.....		167
VI.1.	Conclusions	167
VI.2.	Future works.....	171
REFERENCES		175

FIGURES

Figure 1: Ground workpieces of different material for different field of application	12
Figure 2: Horizontal grinding machine [4].....	13
Figure 3: (a) Wire Dress system developed by Studer company, integrated on grinding machines, (b) tool exchange of Studer S33 grinding machine [6]	14
Figure 4: (a) Scheme of designs of textured grinding wheel with different TD [18], (b) Real circumferential textured grinding wheel [19].....	15
Figure 5: Design of 2 zone tool for gear grinding [20].	15
Figure 6: Grinding basis.(a) Main elements of grinding process [26],(b) Surface grinding cutting parameters [1]	16
Figure 7: Crystalline structures of alumina abrasive grains	20
Figure 8: Detail of sharp edges on grain surface of microcrystalline structure of SG abrasive [29].....	21
Figure 9: TG TM with aspect ratio 5:1 manufactured by Norton [30]	22
Figure 10: Macrogeometric grinding wheel wear [1]	23
Figure 11: Microgeometric abrasive grain wear	24
Figure 12: Wear pattern of grinding wheel [9].....	25
Figure 13: Friction coefficient evolution with sliding speed and contact pressure for steel-steel dry sliding [41].....	28
Figure 14: Friction coefficient evolution with sliding distance for alumina steel contact on dry and water lubricated conditions [62].....	31
Figure 15: Material removal mechanisms in grinding [65]: (a) rubbing, (b) ploughing and (c) cutting [65]	33
Figure 16: Evolution of grinding specific energy (a) with equivalent chip thickness and (b) wear flat area. The influence of wear mechanisms in specific energy is highlighted [27].	35

Figure content

Figure 17: Pin-on-disk test set up [75]	36
Figure 18: Main findings of TEM analysis of worn alumina [16]	38
Figure 19: Fe ₂ O ₃ -Al ₂ O ₃ phase diagram [82]	40
Figure 20: Evolution of grinding forces with wear flat [27]	43
Figure 21: Plastic flow of SG abrasive grains and third body adhesion (a) a complete worn abrasive grain and (b) detailed flat grain and third body adhesion [34].....	44
Figure 22: Thermal cycle experiment on conventional and SG alumina carried out by Klocke [16].....	45
Figure 23: Automatic image processing device implemented on surface grinding machine [88]	47
Figure 24: Schematic diagram of wheel surface analysis [88].....	49
Figure 25: Application and classification of different types of grinding models [92].	50
Figure 26: Groove scratching tests with 2 grains 360 000 time steps, 144ps. (a) side view, (b) top view [92].	51
Figure 27: Scheme of 3D topography physical approach [110].....	53
Figure 28: Evolution of normal specific grinding force with wear flat increase. 4 simulated cases are represented varying cutting parameters [121].	55
Figure 29: DEM simulation of the contact between two bodies and third body generation [124]	56
Figure 30: (a) The 3 grinding wheels used during tests, (b) dressed 3SG grinding wheel surface combining conventional an microcrystalline abrasive grains.	64
Figure 31: Workpiece (a) dimensions and two tests carried out, test A and test B and (b) side view of the workpiece highlighting grinding width and depth of cut of the grinding tests.....	65
Figure 32: Set up of wheel, workpiece on a clamp, dynamometric device and dial gauge on grinding machine.....	66
Figure 33: (a) Wheel-workpiece positioning during tests and (b) tests scheme in order to analyze just dressed and worn surfaces	69
Figure 34: Methodology of accumulative grinding tests.....	70

Figure 35: Optical microscope set on grinding machine. Light direction is perpendicular to wheel surface in order to apply coaxial light technique.....	71
Figure 36: Coaxial light of microscope (a) light hitting a rough surface (b) light hitting flat surface	71
Figure 37: Steps for wear flat quantification (a) raw 2D image, (b) automatically flat areas detection and (c) filtered image.....	72
Figure 38: Evolution of wear flat with specific material removal representing the error of wear flat measurement corresponding to <i>Test 1</i> and the differences of studied <i>new</i> wheel surfaces... 75	75
Figure 39: Influence of crystalline structure of abrasive grains on wear flat evolution with specific material removal for $v_w=15000\text{mm/min}$ and $a_e=5\mu\text{m}$ (<i>Test 2</i>).....	76
Figure 40: Influence of real depth of cut on wear flat evolution with specific removed material. (a) Results of 3SG grinding wheel and (b) results of MA grinding wheel.....	77
Figure 41: Influence of workpiece speed on wear flat evolution with specific removed material. (a) Results of 3SG grinding wheel and (b) results of WFA grinding wheel.	78
Figure 42: Grinding kinematic, force directions representation.....	79
Figure 43: Specific grinding forces evolution with specific removed material (<i>Test 2</i>)	80
Figure 44: Contact evolution between abrasive grains and workpiece. (a) Initial contact of <i>new</i> surface, (b) abrasive grain wear just in the beginning of the contact and (c) the contact of <i>worn</i> surface.	80
Figure 45: Friction coefficient evolution with specific removed material for <i>Test 2</i>	81
Figure 46: Representation of S_k , S_{kp} and S_{vk} parameters obtained from Abbott-Firestone curve for <i>new</i> WFA.	85
Figure 47: Wheel surface after grinding tests highlighting transition zone between <i>new</i> and worn surface.	87
Figure 48: Detailed grain surface (a) SG <i>new</i> abrasive grain and (b) WFA <i>new</i> abrasive grain.	91
Figure 49: EDXA analysis for third body analysis	92
Figure 50: EDXA analysis for the distinction between abrasive grain and bond.....	93

Figure 51: Set up of pneumatic control of pin-on-disk	102
Figure 52: Pin holder and guide system of pneumatic cylinder to avoid pin rotation during tests ..	103
Figure 53: Reproduction of thermal cycle of one abrasive grain (in pink) with designed pin-on-disk set up.....	104
Figure 54: Set up of tribometer mounted on a surface grinding machine.	104
Figure 55: (a) Pin dimensions, (b) dressing set up of vertical surface of the wheel.....	106
Figure 56: Abbot Firestone curve and the attainment of functional parameters.	108
Figure 57: Steps to achieve reference plane of dressed disk surface using 3D functional parameters.	108
Figure 58: Parallel slice to reference plane sets in order to quantify real contact area depending on wear depth.	109
Figure 59: Set up of the first contact between pin and disk (a) schematic representation of the set up and (b) real tribological tests set up. In both cases force directions are represented.....	110
Figure 60: (a) 3 tests conducted on flat vertical surface of the disk. (b) Comparison between new and worn pins, generated burr and the marks of sliding direction in pin surface.....	111
Figure 61: (a) WFA disk highlighted measured area, (b) 2D representation of digitalized area and (c) 3D surface digitalization	112
Figure 62: Representation of (a) closing and (B) opening morphological filters [127]	113
Figure 63: Depth of worn alumina quantification: 1 st step, profiles superimposition, 2 nd step, upper line profile, 3 rd step, profile after morphological filter application and 4 th step, leveled profile and depth quantification	114
Figure 64: Quantification of groove depth generated on WFA and 3SG alumina disks. Variation with sliding speed, pneumatic pressure and the mean value is represented.	115
Figure 65: Real contact area quantification from wear depth. Reference plane and contact depth slices for WFA and 3SG disk.	116
Figure 66: Normal and tangential forces evolution with sliding speed for 0.6MPa (test1a, test1b and test1c)	117

Figure 67: Normal and tangential force evolution with pneumatic pressure for 30m/s (<i>Test1c</i> , <i>Test2c</i> and <i>Test3c</i>)	118
Figure 68: Normal and tangential force signals and contact time for <i>Test 1a</i> on WFA.....	119
Figure 69: Variation of real contact pressure with sliding speed and crystalline structure.....	120
Figure 70: Comparison between <i>new</i> and <i>worn</i> states of WFA and 3SG alumina disk (a) reduced peak height and (b) peak material proportion	121
Figure 71: Valley material proportion to compare of <i>new</i> and <i>worn</i> states of WFA and 3SG disk.....	122
Figure 72: 3D wheel surface digitalization and envelope of filtered superimposed profiles for (a) WFA and (b) 3SG alumina.....	123
Figure 73: Number of contacts of each type of abrasive grain with the steel pin on a complete test.	124
Figure 74: Scheme of contact modeling, two bodies in contact and the model solicitations....	132
Figure 75: Domains division regarding the temperature in the contact.	133
Figure 76: Variation of alumina properties with temperature [134]	135
Figure 77: Heat distribution in grinding.....	136
Figure 78: Values of heat partitioning ratio to workpiece depending on equivalent chip thickness and crystalline structure of alumina abrasive grains [63].....	137
Figure 79: Abrasive grain boundary conditions and mesh density	138
Figure 80: (a) Temperature maxima reached in the abrasive grain and (b) the height of 200°C isotherm.....	140
Figure 81: 2D thermal simulations results for the six cases of study.....	141
Figure 82: Flowchart to predict alumina abrasive grain wear	143
Figure 83: (a) Front view of model disposition and (b) upper view	144
Figure 84: Domains and pressure surface definition on (a) WFA and (b) SG abrasive grains.	145
Figure 85: Cohesive beam bond [133]	146

Figure content

Figure 86: Force applied in tensile tests on a cylinder generated with 10000 DEs [133] 147

Figure 87: Results of the first tensile test. r_μ calibration obtaining stable and constant macro Poisson ratio. 148

Figure 88: Results of the last tensile test. E_μ calibration obtaining stable and constant macro Poisson ratio and macro Young's modulus. 148

Figure 89: (a) First body set of DE pointing the break of beams (b) detached element in green due to the break of beams supporting it 150

Figure 90: Regularized Coulomb Law 152

Figure 91: Model solicitations: (a) Micro tangential force applied in the contact to impose the sliding speed and (b) force imposed in the *Pressure Surface* to impose the real contact pressure..... 153

Figure 92: Abrasive grain oscillation due to micro tangential force effect 153

Figure 93: Discretization of semi-sphere and only the *down domain* of WFA abrasive grain . 156

Figure 94: Third body generation on semi-sphere and only *down domain*..... 156

Figure 95: Incorrect micro failure stress (0.8GPa) of WFA abrasive grain, down view..... 157

Figure 96: Third body generation in WFA abrasive grain 158

Figure 97: Third body evolution with contact time for WFA 159

Figure 98: Beams stress of WFA and SG abrasive grains 160

Figure 99: Comparison of the third body generation on WFA and SG abrasive grains..... 160

TABLES

Table 1: Properties of abrasive grain materials [27]	18
Table 2: Third body composition depending on contact conditions	39
Table 3: Chemical composition of AISI D2.....	64
Table 4: Surface grinding machine main characteristics.....	65
Table 5: Devices used for real parameter measurement during the tests	66
Table 6: Main equipment used for wear flat characterization and surface analysis.....	67
Table 7: Grinding tests real parameters.....	69
Table 8: Dressing parameters.....	69
Table 9: Parameters used to wear flat characterization and wheel surface analysis on the three microscopes.....	73
Table 10: Differences between real and measured depth of cut and specific material removal rate.....	74
Table 11: 3D topography and Abbott-Firestone curve of <i>new</i> and <i>worn</i> topography for WFA, 3SG and MA.	84
Table 12: Wheel surface representative functional roughness parameters.	85
Table 13: Atomic weight of the main chemical elements found in the wheel surfaces.	87
Table 14: SEM analysis of the transition between <i>new</i> and <i>worn</i> surface. for the three types of crystalline structure. The images in the right are taken with contrast.	88
Table 15: Worn surface at 50x magnification and flat areas remarked.....	89
Table 16: SEM images taken at magnification of 500x. Detailed <i>new</i> and flat abrasive grins...	90
Table 17: Specification of pneumatic elements	102
Table 18: Set up of Pin-on-disk tests	105
Table 19: Dressing parameters of vertical surface	107

Tables content

Table 20: Pin-on-disk parameters	110
Table 21: Input parameters for 2D thermal model.	139
Table 22: Alumina properties at 200°C [134]	139
Table 23: Mean values of 200°C isotherm height to define DEM	141
Table 24: Alumina macro properties for the different domains.	145
Table 25: Micro properties of alumina for down and <i>up domains</i>	149
Table 26: Discrete volume of abrasive grains wear obtained on pin-on-disk tests	151
Table 27: Set of DE and bond used on the model	154
Table 28: Micro properties and model solicitations for semi-sphere and <i>down domain</i>	156
Table 29: Parameters in which the effect of the crystalline structure of abrasive grains is considered	159

NOMENCLATURE

$\% A$	[-]	Percentage of area corresponding to wear flat
A_a	[mm ²]	Apparent contact area
a_e	[μm]	Depth of cut
a_d	[μm]	Dressing depth
A_r	[mm ²]	Real contact area
Al_2O_3	[-]	Alumina or aluminum oxide
b_w	[mm]	Grinding width
C	[-]	Failure constant
CBN	[-]	Cubic boron nitride
COR	[-]	Coefficient of restitution in DEM
c_p	[J/kgK]	Specific heat capacity
DEM	[-]	Discrete element method
DE	[-]	Discrete element
$E=E_M$	[GPa]	Young's modulus or Macro Young's modulus, corresponding to real properties
E_μ	[GPa]	Micro Young's modulus, calibrated Young's modulus of beams in DEM
e_c	[J/mm ²]	Grinding specific energy

Nomenclature

e_{cu}	[J/mm ²]	Cutting specific energy
e_{pl}	[J/mm ²]	Ploughing specific energy
e_{sl}	[J/mm ²]	Rubbing specific energy
FEM	[-]	Finite element method
<i>G-ratio</i>	[-]	Volumetric wear of grinding wheel
h_{eq}	[-]	Equivalent chip thickness
K	[W/mK]	Thermal conductivity
L_{μ}	[-]	Cohesive beam length
MA	[-]	Monocrystalline alumina
P	[W]	Grinding process Power consumption
p_a	[MPa-GPa]	Apparent contact pressure
p_r	[MPa-GPa]	Real contact pressure
Q'_w	[mm ³ /mm·s]	Specific material removal rate
Q_w	[mm ³ /s]	Material removal rate
q_{ch}	[W/m ²]	Heat flux to the chip
q_f	[W/m ²]	Heat flux to the fluid
q_g	[W/m ²]	Heat flux to the grain
q_s	[-]	Speed ratio v_w/v_s
q_t	[W/m ²]	Total heat flux

q_w	[W/m ²]	Heat flux to the workpiece
R_w	[-]	Partition of heat that is directed to the workpiece
r_μ	[-]	Ratio between cohesive beam radius and average DE radius
s	[m/s]	Sliding speed
SiC	[-]	Silicon carbide
SG	[-]	Sintered sol gel alumina
3SG	[-]	Wheel composed by 30% of SG abrasive grains
S_k	[μm]	Core roughness depth
S_{mr1}	[%]	Areal material ratio that divides the reduced peaks from core roughness
S_{mr2}	[%]	Areal material ratio that divides the reduced valleys from core roughness
S_{pk}	[μm]	Reduced peak height
S_{vk}	[μm]	Reduced valley depth
t_c	[s]	Contact time
v_d	[mm/min]	Dresser speed
v_s	[m/s]	Wheel speed
v_w	[mm/min]	Workpiece speed
V_M	[m ³]	Macro volume: volume of the real body

Nomenclature

V_s	[mm ³]	Grinding wheel volume lost
V_w	[mm ³]	Workpiece material removal
V'_w	[mm ³ /mm]	Specific material removal
$V_{\mu i}, V_{\mu}$	[m ³]	Volume of one DE or Discrete volume of the modeled body
WFA	[-]	White fused alumina
ZTA	[-]	Zirconia toughened alumina
γ	[-]	Adhesion parameter in DEM
κ	[-]	Stiffness parameter in DEM
μ	[-]	Friction coefficient
μ_{μ}	[-]	Micro friction coefficient, corresponding to friction between DEs in DEM.
ν_M	[-]	Poisson's ratio or macro Poisson's ratio, corresponding to real properties
ν_{μ}	[-]	Micro Poisson's ratio: calibrated Poisson's ratio of beams in DEM
$\rho=\rho_M$	[kg/m ³]	Density or Macro density, corresponding to real properties
ρ_{μ}	[kg/m ³]	Micro density: calibrated density of beams in DEM
$\sigma_{f\mu}$	[MPa]	Micro failure stress of DEM beams
σ_{vm}	[MPa]	Von Mises stress

Chapter I: Introduction

I. INTRODUCTION

Grinding is an abrasive machining process in which the material is removed by thousands of abrasive particles with a higher hardness than the workpiece material. These abrasive grains, together with the bond and the porosity, constitute abrasive grinding wheel. Abrasive tools present non-defined cutting edges. Combining this with grinding machining conditions, high quality workpieces of hard materials can be obtained.

Grinding is commonly known as a finishing process. Constant research of the process and industrial necessities lead to improvements in grinding machines, in abrasive materials and hence in grinding wheels configuration. These technological advances allow higher depth of cut and cutting speeds (Creep Feed Grinding, High Efficiency Depth Grinding), leading to a more efficient process with higher material removal rates ($Q'=1000 \text{ mm}^3/\text{mm s}$), lower machining times and improved surface quality. All of these enhancements allows the grinding process to be more competitive than other machining processes and hence to extend the application field.

I.1. Industrial context

The continuous industrial requirements in a wide range of fields such as automotive, aerospace or energy make the need to continuously research in grinding to meet industrial demand and to be competitors with respect to other manufacturing processes. This way, the aim of researchers should be to reduce the gap between industrial necessities and academic research in a shorter period of time as much as possible. However, not only researches close to industry are acknowledged, but also fundamental studies enable a better understanding of the process, helping to reach industrial solutions.

New industrial requirements related to the increase of grinding process efficiency and ground surfaces quality imply a constant adaptation of the process. Advanced materials, which have in general high hardness and low machinability, have to be ground, meeting all industrial requirements. Thus, a new generation of abrasives and grinding wheels are being developed over the past years with the aim of increasing tool life and removal rates, improving process time and costs. The development of microcrystalline sintered alumina created a new abrasive generation, which, nowadays, is submitted to continuous improvements to be competitive with superabrasives in more critical operations, in aeronautical sector between others. Regarding wheel life, SG is more durable and more efficient than conventional alumina, with the particularity of self-sharpening. However, to ensure the optimum design and application of microcrystalline grinding wheels, a deeper analysis of the contact and wear mechanisms during

grinding is required. The present work is developed in order to fill the lack of knowledge of microcrystalline grains behavior under grinding conditions.

Concerning tool life, this is directly related to grinding wheel wear, which produces dimensional, geometrical or surface quality errors, leading to rejected parts and, consequently, economic losses. From the different wear mechanisms, wear flat occurrence leads to the most damaging impact for the workpiece, thermal damage. Likewise, this type of wear is not taken into account for microcrystalline abrasives due to its ability to self-sharpen. However, depending on grinding parameters and wheel conditioning, the flatness of microcrystalline grinding wheels also occurs.

In this sense, this research work addressed the problematic of wear flat from a scientific point of view, applying fundamental studies to the real industrial problem of thermal damage and small grinding wheel life. The study is focused on the characterization of wear flat occurrence under grinding contact conditions. Firstly, carefully designed experimental grinding tests are carried out with the aim to analyze the influence of crystalline structure of abrasive grains in wear flat generation. Moreover, this tests show the importance of tribochemical reactions which leads to wear flat occurrence and contact condition changes. To avoid the randomness of grinding process, tribological tests are carried out. The original design of a tribometer allows to control contact conditions and to reproduce the real contact of abrasive grains, reproducing also their thermal cycle. A thermal model of abrasive grain is accomplished to determinate the part of the abrasive grain affected by the temperature and, hence, the part more susceptible to worn. Finally, to better understand wear during the complete contact, and not only to compare the initial and final states of abrasive grains, a first approach of abrasive grain wear model is developed using DEM. Both the tribometer and the numerical model are good tools for grinding wheel manufacturers to characterize the behavior of abrasive grains for specific grinding conditions.

I.2. Objectives and contributions

The main objectives of the present research work and the contributions arisen from them are summarized in this section.

To determinate the influence of crystalline structure of abrasive grains on wear flat occurrence during real grinding operation.

The isolation of wear flat from other types of wear allows to carry out an exhaustive characterization of the evolution of grinding wheel flatness depending on the crystalline structure and grinding parameters.

To study the tribochemical nature of wear flat and analyze the influence of the third body generation in the contact between abrasive grains and workpiece.

Tribochemical reactions in the contact lead to the flatness of abrasive grains and to the third body generation. Depending on the crystalline structure of abrasive grains, not only the smooth appearance of flat wheel surface varies, but also the quantity and composition of the third body. Thus, the contact and grinding conditions are different.

To perform an original design of pin-on-disk tribometer implemented on a surface grinding machine.

The main characteristic of designed pin-on-disk tribometer is the ability of reproduce a discontinuous contact between abrasive grains and workpiece, simulating the real thermal cycle of abrasive grains. Moreover, real contact conditions of grinding process are reproduced, exhaustively controlled and quantified during the contact.

To quantify real contact pressure and real wear of abrasive grains depending on the crystalline structure.

Real contact area is quantified establishing a methodology to analyze surface topography. Moreover, the wear generated in abrasive disk is quantified and, depending on its characteristics, the predominant type of wear is established.

To provide a useful industrial tool for the design of grinding wheels for specific applications.

Real contact conditions can be reproduced and the wear of abrasive grains can be characterized before manufacture required grinding wheel.

To determinate the alumina abrasive grain affected zone by the temperature under real contact conditions.

The aim is to analyze the influence of high temperatures achieved in the contact between alumina abrasive grain and the workpiece. A thermal model is developed in order to establish two domains in the abrasive grain, the part affected by the temperature and the part at room temperature.

To propose an abrasive grain wear model to analyze the influence of the third body generation in the contact between alumina and steel under grinding contact conditions.

A discrete element wear model is developed with the aim of reproducing the influence of tribochemical reactions in the contact. The model considers the third body generation, its adhesion to flat part of abrasive grain and the wear of the abrasive grain.

I.3. Content layout

The work is divided in six chapters, being the first one the present chapter, *Chapter I*, in which the introduction of the work is done.

Chapter II gathers a bibliographic review of the State of the Art in grinding. The main grinding wheels wear aspects which have been essential as starting point of the present research work, are addressed. The different crystalline structure of alumina and the different types of wear of grinding wheels and abrasive grain are analyzed. The attention is focused in wear flat, the tribochemical nature wear. Thus, tribological studies of the wear of alumina against steel are analyzed, emphasizing on grinding contact applications. Finally, to better understand the grinding process, grinding models are analyzed, focusing on wear models.

Chapter III presents experimental grinding tests in which the main objective is to characterize the wear flat occurrence in different crystalline structures abrasive grains. Wear flat evolution and its effect on grinding parameters during real grinding process are analyzed. Also grinding wheel surface is exhaustively characterized for a better understanding of the tribochemical mechanism that take place in the contact between abrasive grains and workpiece.

In *Chapter IV* an original design of pin-on-disk tribometer is developed. A real grinding wheel is used as a disk and a workpiece material as a pin. This fact allows reproducing real thermal cycle of abrasive grains. The tribometer is implemented on a grinding machine in order to achieve grinding contact conditions. Tribological tests are carried out for different crystalline structures. New methodology to characterize the wear of abrasive grains under real heavy contact conditions is implemented, being useful for the grinding wheel manufacturer to know the behavior of new abrasive grains before implement the wheel on a real process.

Chapter V gathers the abrasive wear simulation. Firstly, a thermal model of alumina abrasive grain is accomplished in order to establish the part of the abrasive grain affected by the temperature. After that, using contact conditions of tribometer tests, the DEM is used to model the wear of a single alumina abrasive grain. This first approach of wear model allows a better understanding of the influence of adhered third body to flat grains and the influence of crystalline structure to wear generation.

Finally, *Chapter VI* summarizes the main contributions and conclusions taken from the present work. Moreover, the future research work on the analysis and characterization of grinding wheel wear are proposed.

Chapter II: State of the art

II. STATE OF THE ART

II.1. Abstract

This chapter gathers the review of the main grinding aspects which have been essential as starting point of the present research work. Non defined cutting edges of grinding wheel together with heavy contact conditions of abrasive grains (cutting speed higher than 30 m/s and pressures about 1-2 GPa) hinder the characterization of the contact during grinding. From the different types of wear that take place during grinding, wear flat presents the most harmful effects for the process. The specific energy consumption is mainly turned into heat, increasing the temperature in the contact, resulting in thermal damage and loss of accuracy in workpieces and in the acceleration of tribochemical reactions in the contact.

Moreover, new generation of abrasives are emerged due to the continuous research works and industrial requirements. In this sense, wear flat occurrence depending on the abrasive material or abrasive grain structure is of interest in order to prevent harmful effects in the process. One of the handicap to characterize wear flat is the %A measurement and quantification, being the studies based on non-contact methods the most relevant. Likewise, tribological approaches are developed in order to reproducing the wear flat occurrence during grinding, being the extrapolation of results to real grinding the main inconvenience of this approach.

Finally, process modeling and simulation is a critical predictive tool to avoid problems once the process is implemented on the industry or for a better understanding of the influence of each parameters from a research point of view. Different type of models to simulate diverse variables have been developed: temperature, forces and specific energy simulations are the most popular. However, few works referred to wear flat prediction are found, and the presence of third body in the contact is not taken into account for wear modeling.

II.2. Grinding process

II.2.1. Introduction

Grinding process is an abrasive process in which the material is removed by a serial of very hard abrasive grains, harder than workpiece material. Randomly positioned abrasive grains are embedded on a bond, creating an abrasive grinding wheel. Non-defined cutting edges hinder the

characterization of the process and particularly of grinding wheel. In turn, they allow achieving high quality surfaces in a wide range of workpiece materials Figure 1.



Figure 1: Ground workpieces of different material for different field of application

Comparing with other machining processes, grinding has been characterized by low removal rates and low efficiency. However, the latest technological advances both in grinding machines Figure 2 and in abrasives make the possibility to be more competitive in a great variety of industrial sectors. There is a great diversity of grinding operations according to the kinematic of the process, such as surface grinding, internal and external grinding and centerless grinding. And also in terms of grinding wheel configuration and cutting parameters different operations can be defined, from roughing to super-finishing, using conventional abrasives or superabrasives.

Furthermore, in the last years, industrial requirements of removal rate and process efficiency increase and machining times decrease, have led processes, such as Creep Feed Grinding or High Efficiency Deep Grinding (HEDG) [1,2]. Creep feed grinding is characterized for a depth of cut until 1000 times the conventional ones. With this process, complex profiles in only a single pass or a few passes are possible to grind. The values of specific material removal rates for creep feed grinding are $Q'_w=0.1-15\text{mm}^2/\text{mm}\cdot\text{s}$. In HEDG reached cutting speed can achieve 200m/s [3], while conventional grinding is about 35m/s. Moreover, specific material removal rates are about $Q'_w=50-2000\text{mm}^2/\text{mm}\cdot\text{s}$, higher than for creep feed grinding and for conventional grinding. As it is shown before, grinding presents a great amount of alternatives for workpiece manufacturing.



Figure 2: Horizontal grinding machine [4]

II.2.2.Latest developments in grinding

The rapid evolution of technology has forced manufacturing processes to evolve at the same rate in order to satisfy industrial requirements. Therefore, research efforts in this field have to be constant. In this sense, grinding machines suffer great evolution in the last years to achieve required flexibility, productivity and accuracy reducing process costs. In general, the kinematic and accuracy of advanced grinding machines allow to obtain complex geometries with high removal rates [5]. On the one hand, the adaptation on grinding machines of tool exchangers, integrated workpiece automation and new dressing systems WireDress® [6] as it is shown in Figure 3, which leads to an increase of productivity of the process. Accuracy or geometric complexity is increased due to the development and integration of simulation tools and CAM tools in the process [7]. Moreover, monitoring of the process, on-machine measurements and thermal compensations in process [8] are a key to improve the quality of workpieces and to reduce process costs.

On the other hand, the sustainability of grinding is one of the handicaps of the process. The environmental impact has been addressed mainly from the point of view of the coolant and tool wear. Regarding the tool wear, embodied energy, emissions from tool use and waste regulations are the topics that affect to environmental sustainability [9]. With reference to cooling techniques, the oil-water coolant is being replaced in the latest years. Not only to address the environmental impact but also to enable the minimization of thermal problem in grinding. Cryogenic cooling or MQL and CO₂ combination are the latest advanced in grinding cooling techniques [10]. Grinding fluid is also a key factor in grinding wheels wear. If the fluid gets to the contact zone, the friction is reduced. However, the large contact length hinders the fluid penetration and its effect is reduced. In this field, researchers are worried about how guaranty contact lubrication and new techniques are continuously emerging [11].



Figure 3: (a) Wire Dress system developed by Studer company, integrated on grinding machines, (b) tool exchange of Studer S33 grinding machine [6]

Accordingly, the design of dressing process affects directly to wheel wear [12]. Dressing parameters define the topography and an adequate dressing frequency ensures not irreversible damages in the workpiece. Dressing does not minimize the wear but avoid the negative effects that it makes. However, grinding wheel recovery take up non-productive time, being the necessity of minimizes dressing times. Therefore, a great amount of studies are focused on the optimization of dressing process [13,14].

From the elements previously mentioned, grinding wheel topography is a key to achieve high quality surfaces because of the direct contact between workpiece and wheel. However, the quick evolution of workpiece materials and hence, of abrasive materials, hinder the characterization of grinding wheel wear. This problem is addressed in *Section II.5* and is the main issue of the present research work. Wheel wear is one of the most negative handicaps for the industry due to the damage that induces, both in process and in a final workpiece. The excessive wheel wear increases power consumption, decreasing the efficiency of the process. Furthermore, regarding the effects on a final workpiece, thermal damage, high roughness and vibration marks can be shown. All this leads to great economic losses for grinding process. Consequently, research effort is noticed for years in the characterization and minimization of grinding wheel wear [15,16], being the contribution of the present work in this line.

Textured grinding wheels are being trend in the last years. The texture geometries and texture dimensions (TD) are suitable for each grinding application and abrasive type [17,18]. In Figure 4 (a) different texture patterns can be shown and in Figure 4 (b) a real textured grinding wheel. Some research works reveals that circumferential grooved wheel improve grinding process both in terms of surface quality and in process time [19].

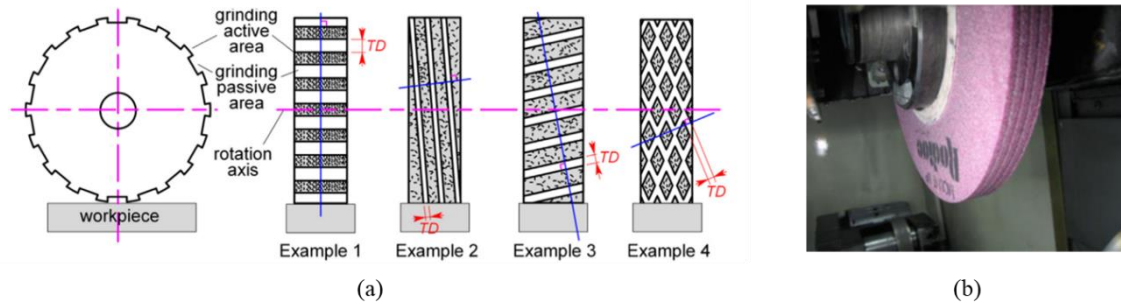


Figure 4: (a) Scheme of designs of textured grinding wheel with different TD [18], (b) Real circumferential textured grinding wheel [19]

Not only to improve wheel life but also new industrial requirements, force to grinding wheel manufacturers to achieve customized solutions for each specific grinding operation. In Figure 5 it is shown a new design of wheel for superfinishing for continuous grinding. In this wheel vitrified bond is used for rough and finishing operations and resinoid bond for the last step, superfinishing. This is only one of the thousands of specific designs that wheel manufacturers have to implement in the industry.

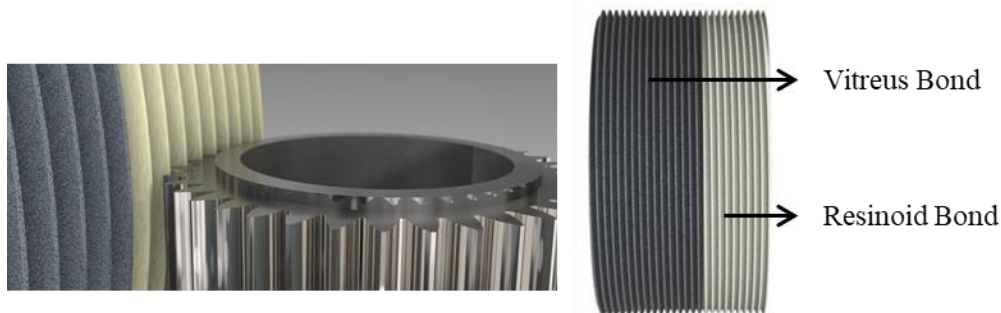


Figure 5: Design of 2 zone tool for gear grinding [20].

These industrial solutions can be successfully solved due to continuous research works that are developed for process enhancement. One of the fields that is booming is process monitoring, which is nowadays a requirement for grinding manufacturers. Not only from the industry to have an exhaustive control of each operation, but also, from a scientific point of view to study the parameters where improvements could be introduced. A great quantity of data, Big Data, allow to interpret the results with the aim of prevent workpiece damages or irregularities in the process, therefore, studies of multi-sensor data analysis are developed [21]. Power, force or temperature monitoring systems implemented on grinding machines are the most standard outputs of the process. However, best results of measurements are reached when sensors are closest to the origin of the signal. To measure the temperature in the contact, the research works are focused on sensor integrated wheels [22,23]. The implementation on a real process supposes a great complexity due to the rotation movement and high speed of the wheel. In the sense of

wheel wear monitoring, the latest research works are focused on acoustic emission technique [24], or on pneumatic sensors [25]. This issue is deeply addressed in *Section II.5.3* where wheel topography measurements and specifically, wear flat measurement is going to be deeply analyzed.

II.2.3. Basis of grinding process

In grinding, five main elements affect to the process: grinding machine, grinding wheel, workpiece material, grinding fluid and dressing process. All of them are carefully selected and designed to each grinding operation. Together with a correct design of cutting parameters, grinding is competent for achieving high accuracy and close tolerances machining hard material. In Figure 6 are shown the main elements that take part in grinding process and the definition of cutting parameters for surface grinding. The more detailed basis of the process can be found in [1,2].

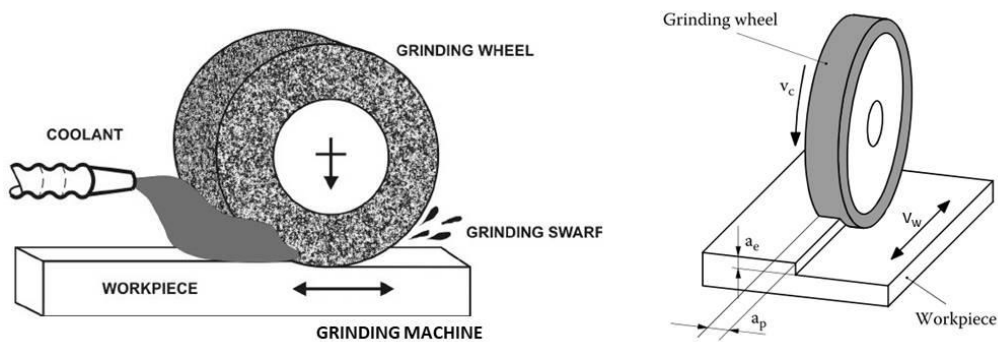


Figure 6: Grinding basis.(a) Main elements of grinding process [26],(b) Surface grinding cutting parameters [1]

As it is mentioned, non-defined cutting edges of grinding wheels hinder the study of the contact between a workpiece and abrasive grains. Furthermore, the characterization of the contact during grinding involves the study of wear, thermal problems and sliding friction, which are interconnected. High temperatures close to workpiece material melting point are reached between abrasive grains and the workpiece. Great proportion of generated heat is directed to the workpiece, between 25 % and 85 % depending on materials in contact and grinding conditions [2]. So, thermal damage could be generated on ground surfaces and hence final workpieces could be rejected. Furthermore, in the contact between abrasive grain and workpiece, high local pressures and high speed are achieved. As a consequence of this heavy contact conditions the wear of abrasive grains occurs, modifying contact conditions and also decreasing the efficiency of grinding process. Despite this topic have been addressed from scientific point of view for years, it still presents a lack of knowledge due to the difficulties of overlapping phenomena.

Therefore, a deep study of the contact and wear of abrasive grains is required and during the present research work the problem of abrasive grain wear is going to be addressed.

II.3. Grinding wheels

Grinding tools are defined by abrasive grains, bonding material and in some cases by the porosity. The properties of each element together with grinding wheel geometry lead to a custom design for each industrial application. In the same way, constant technological advances demand that grinding wheels meet the industrial requirements: increase the production of high quality surfaces increasing process efficiency, thus, increasing removal rates and cutting speed. However, one of the characteristic of new materials is its low machinability, arisen difficulties with the abrasive materials used, and decreasing grinding wheel life.

Firstly, to a better understanding of wheel behavior during grinding and before submit the latest studies to improve wheel life; a brief classification according to abrasive grains and bond material is done. Furthermore, other factor as grain size or porosity determinates the durability of each grinding wheel for the specific application.

II.3.1. General classification

General classification is done between conventional abrasives or superabrasives. On the one hand, aluminum oxides (Al_2O_3) and silicon carbide (SiC) are the conventional abrasive grains, presenting hexagonal crystal structure. Usually vitrified of resinoid bond is used to confine the wheel. On the other hand, diamond and cubic boron nitride (CBN) constitute the superabrasives, which are bonded with vitrified, resinoid or metallic material. There is no porosity in case of resin and metal bond. Therefore, to change wheel specification the formulation of the bond is modified. Each abrasive type, conventional or superabrasives, present standard marking system, in which abrasive material, grain size, grade (related to the hardness of the complete wheel), structure (related to the porosity) and bond material is defined.

Abrasive material is chosen depending on the ground material, taking into account its hardness and the chemical affinity between abrasive and workpiece material. In case of SiC, despite presenting good mechanical properties, its chemical affinity with ferrous metals limits its application field. SiC is commonly used to ground carbides, ceramics, casting and non-ferrous metals.

Superabrasives are harder and support higher temperatures than conventional ones. Furthermore, diamond is harder than CBN, but its hardness is fallen sharply when 700°C are achieved [1].

Moreover, diamond present high wear with ferrous metals and tungsten. Therefore its application field is mainly high speed grinding of ceramics and carbide metal. On the contrary, one of the most important characteristic of CBN is the thermal stability up to 1400°C. In addition, CBN do not present chemical affinity with ferrous materials. Therefore, it is used for high speed grinding of high hardness ferrous materials, tool steel as well as superalloys, normally used in aeronautic industry due to its heat-resistant characteristic.

Table 1: Properties of abrasive grain materials [27]

Grain Abrasive Material				
	Aluminum oxide (Al₂O₃)	Silicon Carbide (SiC)	Cubic Boron Nitride (CBN)	Diamond
Crystal structure	Hexagonal	Hexagonal	Cubic	Cubic
Melting Point (°C)	2040	2830	~3200 at 105kbar (triple point)	~3700 at 105kbar (triple point)
Knoop Hardness (GPa)	20.6	23.5	46.1	78.5

The main properties of abrasive material mentioned are built on Table 1. Both hardness and friability of abrasive grains have to be into account to design a grinding wheel. The hardness is related to the resistance to penetration, in contrast, friability with the tendency for the fracture. The hardest grain is not always the best choice. The friction increase promoting heat and vibrations. Therefore, increasing the friability of abrasive grains increase the tendency to fracture, leading to a new sharp cutting points.

Alumina and diamond are natural abrasives. However, all of used abrasive grains are synthetic. Physical properties of abrasive materials are modified with the aim of achieving the balance between hardness and friability among others. This fact leads to a continuous development on abrasives to enhance their properties and tool life. Generally, to improve the properties, chemical composition and crystalline structure are modified. This issue is deeply explained for alumina abrasive grains bellow.

Additionally, not only the characteristic of each abrasive have to be taken into account, but also the cost of each one. Conventional alumina is the most economic choice, so manufacturers selected it whenever possible. By contrast, there are some applications in which the use of superabrasive wheels is mandatory, such as when very hard materials are ground, high temperatures are expected or high speed is required.

II.3.2. Alumina: crystallographic structure

Bauxite is the raw material to get aluminum oxide abrasive grains. The first step to become bauxite in alumina is to purify by Bayer process. In this process 2500°C is reached to ensure the extraction of aluminum hydroxide. After that, three methods are distinguished according to the type of alumina. The different states of purity reached on the alumina, the added elements or the different crystallographic grades achieved during the processes lead to a great variety of alumina abrasive grains. Regarding the purity or added elements the following classification is done [27]:

- **Brown or regular alumina** is gotten adding titanium oxides (TiO_2) on the dehydration of alumina with coke and iron. These abrasive grains present low hardness and high toughness. Brown alumina is usually used for heavy-duty grinding due to its irregular shape. Depending on its purity, the friability of abrasive grains increase, becoming suitable for roughing or semi-roughing operations.
- **White alumina** is obtained by fusing pre-purified alumina. The absence of added elements during the treatment increases the purity of the alumina until 98-100 %. The abrasive grains present high hardness and low friability. This characteristic makes white alumina appropriate for finishing operation.
- **Modified alumina** by adding chrome, titanium or vanadium, around 3 %, during the fusion of pre-purified alumina. Depending on the element added, the properties of abrasive grains change. Chrome addition increases the hardness of the abrasive, and titanium the toughness. These abrasive grains are usually used for finishing operations.

In parallel with the above classification, depending mainly on the crystallization rate, monocrystalline, conventional or microcrystalline abrasive grains are obtained. The more rapid the cooling, the smaller the size of crystals achieved. Also the presence of impurities or addition of elements has influence on the crystal size. The classification takes into account the crystal size of abrasive grains, thus, the number of crystals that compose one abrasive grain, as it is shown in Figure 7.

The **conventional** abrasive grain, composed by three or four crystals is the most common on wheel manufacturing. The hardness of abrasive grains depends on the crystalline structure but also on the elements added during the manufacturing. Due to the elements added, the hardness of conventional alumina vary from 22.2 to 20.0 GPa. The value of white fused alumina (20.8 GPa) is taken to compare with other crystalline structures because is the conventional alumina that it is going to be studied during the present Research work. Furthermore the friability of white alumina is of 56.6. Besides that, not only complete wheels with conventional abrasive grains are manufactured but also this type of grains is required as base grain on almost every alumina grinding wheels. The values given for friability and hardness are achieved with a Ball Mill Test following the American National Standard B7418.

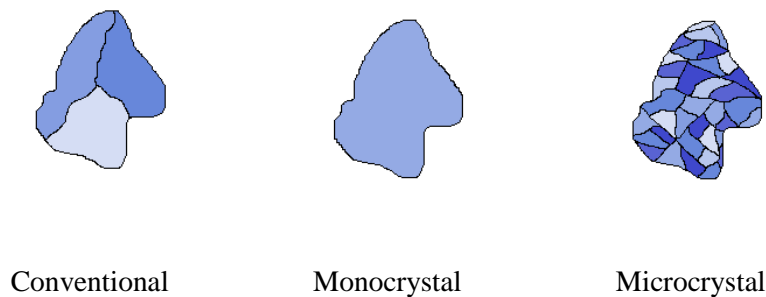


Figure 7: Crystalline structures of alumina abrasive grains

A unique crystal builds **monocrystalline** abrasive grain. To get this crystalline structure during the fusion of alumina alkaline compounds and iron sulphides are added to achieve a pure material. Both the fusion and the crystallization process are exhaustively controlled in order to achieve one crystal abrasive grain. The hardness of monocrystalline alumina is 22.4 GPa, higher than conventional ones. However, its friability is reduced until 47.7. Monocrystalline alumina is used on finishing operations in the industry.

Lastly, **microcrystalline** abrasive grains are composed by thousands of crystals. As well as in monocrystal structure, controlling the cooling of alumina, very small crystals are achieved. During this process second-phase inclusions of alumina are shown in the crystals. However, this is not the unique technique to obtain microcrystalline abrasive grains. Also sintering process is used to obtain sintered alumina with a crystal size between 1-5 μm . The raw material is extruded and chopped and sintered at a lower temperature than melting temperature.

But the most relevant development on abrasive grains is also related to the process for obtaining microcrystalline structure in alumina. This new generation of microcrystalline abrasive grains was developed by Leitheiser et al. US 1982/4,314,827 [28] in early 1980's. At the beginning the

patent belongs to 3M Company, and a year later to Norton Company. Microcrystalline alumina is obtained using a synthesis technology, in which an hydrosol or sol is converted into a gel or other physic stage and after drying and firing ceramic material is obtained. Due to the process this microcrystalline structure is named SGTM (Sol-Gel).

The main dissimilarity with the first explained process is that in this case the alumina is not fused. Besides, it presents a homogeneous microcrystalline structure of randomly oriented crystals, in which α -phase and second-phase of alumina are homogenously presented. Furthermore, the size of achieved microcrystals is usually lower than 1 μm . The process to obtain SGTM abrasive grains presents higher efficiency than the two others. Due to the absence of fusion of the material, the power required during the process is lower.

Through in those three processes microcrystalline structure of abrasive grains is achieved, it is characterized for high toughness and low hardness comparing with conventional alumina. The dissimilarities are higher on sintered abrasive grains. While microcrystalline structure achieved controlling the cooling and SG present hardness around 11 GPa and a friability index of 19, sintered alumina's hardness is of 6.5 GPa and its friability index of 13.4. Therefore, microcrystalline abrasive grains present higher tendency to fracture than conventional. Moreover, the microcrystalline structure is also shown on grain surface, presenting sharp edges, as it is shown in Figure 8. This characteristic makes microcrystalline grains suitable for heavy-duty grinding operations.

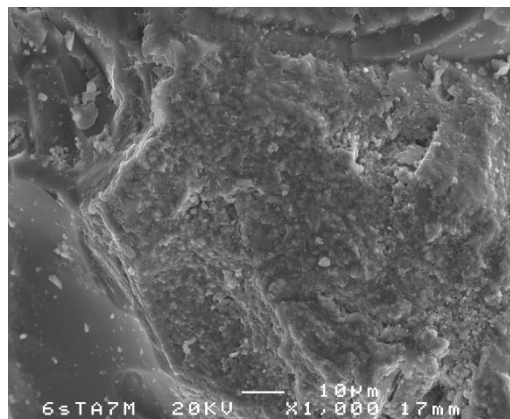


Figure 8: Detail of sharp edges on grain surface of microcrystalline structure of SG abrasive [29].

Due to their high friability, in the industrial applications, microcrystalline grains are mixed with conventional grains to ensure the toughness of the wheel. Therefore, if only microcrystalline wheels were manufactured, wheel life would be reduced because of the high tendency to fracture of abrasive grains. The percentage of SGTM abrasive grains regarding the total amount of abrasive material that compound the wheel is specified in the grinding wheel nomenclature.

The most habitual percentages are 10%, 30% and 50% of SG abrasive grains, named 1SG, 3SG and 5SG respectively.

Different shapes of abrasive grains and addition of chemical composition between other lead to a wide range of microcrystalline abrasive grains: SGATM, SGBTM, SGRTM or TGTM. The last one was developed after SGTM abrasive grains and it is gotten extruding. The shape of TGTM abrasive grains present high aspect ratio, until 8:1 approximately which are named ALTOSTM and are manufactured by Norton [30]. In Figure 9 are shown TGTM abrasive grains of aspect ratio 5:1. These abrasive grains are characterized by their low packing density, increasing material removal rates and decreasing specific cutting energy. Furthermore, the coolant effectiveness is increased. All these characteristics become suitable abrasive to ground high removal rates in superalloys, in the same way as CBN [31].

Finally, as it is mentioned before, one or other abrasive grain structure is used depending on the hardness of ground material and the surface quality required. Moreover, each crystalline structure present different tendency to wear, influenced also by cutting parameters. While on conventional abrasive grains, grain fracture supposes a volumetric wear on grinding wheel, for microcrystalline abrasive grain fracture leads to a self-sharpening of the wheel. It is commonly accepted that microcrystalline abrasive grains present self-sharpening during the process [1,32]. This affirmation it is correct if heavy-duty grinding operation is carried out, thus, if achieved grinding forces are high enough to break the microcrystals. However, during the present work, is demonstrated that this affirmation present some exceptions, for example changing cutting parameters. On the contrary, monocrystalline grains do not present grain fracture, only grain pull-out can be occurred.



Figure 9: TGTM with aspect ratio 5:1 manufactured by Norton [30]

As it is show, the crystalline structure of abrasive grains and their shapes present great influence on the wheel life and grinding efficiency. In this sense, the last trend on wheel manufacturers is to create a personalized grinding wheel for specific applications mixing different types of abrasive grains. Therefore, due to the industrial necessity of know the behavior of abrasive

grains under grinding conditions, the influence of crystalline structure on grinding wheel wear is deeply analyzed on *Section II.5.2* and it is going to be the main issue of the research.

II.3.3. Grinding wheel wear

In the last years research efforts has been constant to improve abrasive wheel life, due to the high cost that suppose for the overall grinding process. Wheel life is directly related to grinding wheel wear, thus, grinding wheel users are worried about the minimization of the wear and their effects on the process.

Before starting with a deeply analysis of the most relevant studies related to wheel wear, wear types are classified, emphasizing in the consequences that affect to wheel behavior. In these sense, special attention is paid in the characterization of wear flat, due to the negative and irreversible effects that this wear cause in the final workpieces.

In the bibliography several classifications of wear can be found, and the name assigned to each type of wear also differs depending on the author. In this case, it is considered appropriate to establish a first distinction between macrogeometric and microgeometric wear [1]. The first one is related to grinding wheel wear and the microgeometric wear with the abrasive grain wear.

The macrogeometric wear is promoted not only for the kinematic of the process but also in the set-up of grinding process. Three wear types are distinguished: profile deviation, roundness deviation and sharpness loss or cutting ability loss, as it is shown in Figure 10 On the one hand, profile deviation implies the loss of wheel shape, and hence dimensional and geometric variations on ground workpiece are achieved. In case of shape wheels, geometrical errors and on conventional wheels the final dimensions are not achieved. This wear is quantified as volumetric wheel wear, with G-ratio parameter, which is defined hereafter. This wheel wear happens if designed wheel is not enough hard to support large grinding forces. It is related to abrasive grain loss, microgeometric parameter which is defined in this section.

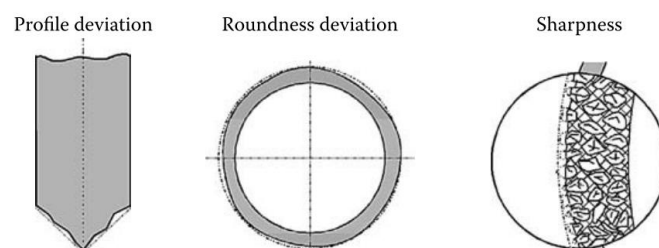


Figure 10: Macrogeometric grinding wheel wear [1]

On the other hand, due to grinding wheel assembly on the machine, radial run out is generated, which is corrected with a dressing before grinding. Machine eccentricities also affect to ground workpieces. Generally, these are also removed with a previous dressing. This wear produce wave marks on ground surfaces, modifying required surface quality. Furthermore, wave marks can be confused with vibrations, hindering the identification of the problem. Finally, the loss of cutting ability is considered macrogeometric wear from grinding wheel point of view. However, analyzing abrasive grain wear, also microgeometric wear is considered.

The main types of microgeometric wear are grain fracture, bond fracture and wear flat. In Figure 11 are represented three main types of abrasive grain wear. All wear types are generated at the same time in the wheel during grinding process. However, one wear type will be the predominant depending on the wheel design, the nature of abrasive, the crystalline structure of the grain and grinding condition.

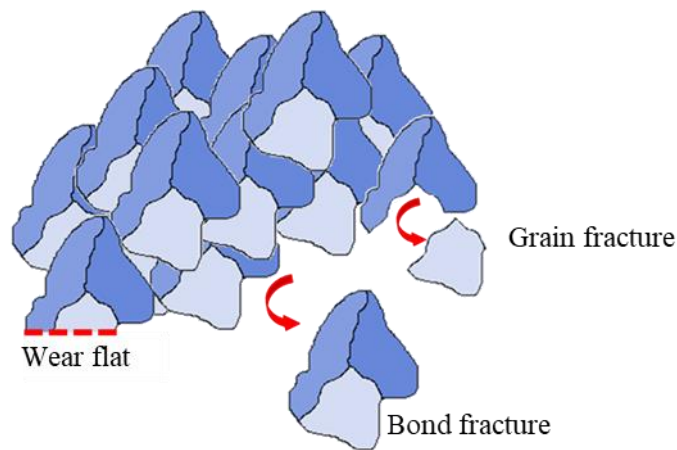


Figure 11: Microgeometric abrasive grain wear

Grain fracture is promoted by mechanical and thermal stress generated on abrasive grains intermittently. Transgranular or intragranular microcracks are generated inside the grains and their propagation leads to grain fracture. Transgranular cracks propagate through grain boundary, which makes easier the propagation comparing with intragranular cracks. Therefore, this type of fracture is more common than intragranular cracks, requiring higher stress. In the case of transgranular propagation, a complete crystal is lost. Depending on the size of crystals, the effect on wheel surface is negative or not for the process. If grain fracture take place on microcrystalline structure abrasive, self-sharpening of the grain is achieved, being a favorable effect for the process. However, if is emerged on conventional abrasive grains, much higher proportion of abrasive grain is lost, leading to a volumetric wear of grinding wheel. On the

contrary, this type of wear rarely occurs on monocrystalline structure, and if it occurs, it is due to intragranular microcracks.

Bond fracture, also named grain pull out, is the main wear if the forces generated during grinding are large enough to break bond bridges. The role of bond is to hold the grains, being strong enough under normal grinding conditions. However, if grains are too exposed the mechanical stress increases, leading to a bond fracture. The loss of a complete abrasive grain implies high volumetric wear on grinding wheel, which affect to final dimensions of the workpiece if it is not adequately quantified or identified. Furthermore, process temperatures promotes bond softening, decreasing its strength. In extreme situations, the bond softening can achieve values so high that flows through the wheel matrix. In this situation, the grains are too embedded on the bond leading to a cutting edge reduction [33].

The randomness of grinding wheel surface hinders wear measurement. The characterization of volumetric wear is done with G-ratio in the stable wear zone, zone 2 in Figure 12. This curve represents the wear pattern of grinding wheels.

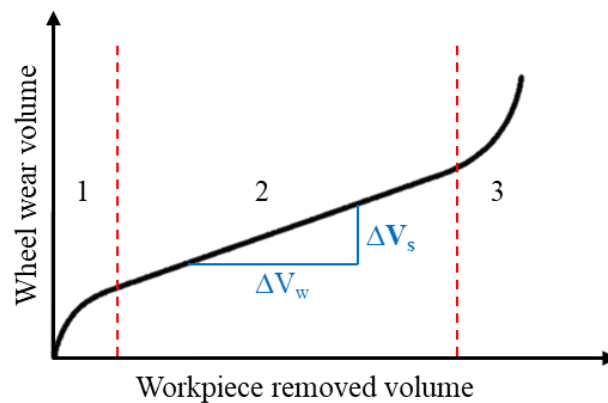


Figure 12: Wear pattern of grinding wheel [9]

Grinding ratio establishes wheel wear resistance and it is defined as the volume of material removed per unit of volume of wheel wear. In the Eq.1 G-ratio of steady stage of wear is represented, in which ΔV_w refers to removed workpiece material and ΔV_s to volume of wheel wear. G-ratio values vary in a wide range (from 1 to 60,000) depending on the wheel design and ground material.

$$G = \frac{\Delta V_w}{\Delta V_s} \quad \text{Eq.1}$$

Finally, **wear flat** is characterized by the flattening of abrasive grains. The volumetric wear in this case is negligible comparing with generated on grain and bond fracture. However, its consequences are too negative for the process. Wear flat results in thermal damage and loss of accuracy in the workpiece. Also affects to process efficiency, increasing both power and specific energy during grinding. Comparing with other types of wear, wear flat implies great economic losses for grinders. Consequently, wear flat is continuously studied, being Malkin the first author who shown the influence of the increase of flat areas on grinding forces and the burn generated because too large real contact areas generate higher temperatures in the contact [15]. The development of new generation of abrasive leads to a recent studies worried about the behavior of new abrasives, including the tendency of grain flattening [16,34].

However, one of the handicaps of grinding wheel wear characterization is that all types of wears take place at the same time, thus, to study the effect of each wear type in the process is nearly unable. The works carried out to study wheel wear [34] do not separate each type, and develop a complete study identifying each wear type in different abrasive grains. Other works, focused on measurement of wear flat [35–37] do not take care the other types of wear despite appear in the wheel. They accept that wear flat predominates in the wheel and that its effects dominate the contact.

As it is mentioned, both from industrial and scientific point of view, the study of the occurrence of wear flat on grinding wheel surface during the process is the key to understanding wear behavior in the contact. Accordingly, wear flat characterization is the issue addressed on the present work. Therefore, before starting with a deep analysis of wear flat, the study of the tribology of abrasive machining processes is required, in the next section is discussed.

II.4. Tribology of abrasive machining processes

As mentioned before, the contact between abrasive grains and workpiece material determinate the wear of grinding wheels. Therefore, to understand the phenomena that take place in the contact helps to improve grinding wheel life. Additionally, tribology is the science and engineering in which the interaction and hence, the friction and wear between two or more bodies in motion are analyzed [38]. In this sense, tribology provides a good approach and become in a right tool to analyze the contact between abrasive grains and workpiece material. Through tribological studies of grinding process, not only the relation between the parameters involved in grinding can be done but also the prediction of process outputs [2].

Regarding tribology, Archard [39] presented the first studies analyzing the contact and rubbing between two flat surfaces. Taking into account that the real contact area is smaller than apparent

contact area, the first assumption of the work carried out is that multiple contact conditions are considered to study the contact between two flat surfaces. On Archard's study the discontinuity on the contact is due to the roughness of two surfaces, on micro scale. Extrapolating this phenomenon to grinding process, on macro scale, the real contact corresponds to contact of abrasive grains embedded on a wheel matrix. Results show plastic and elastic deformation of contact area.

Tests were carried out on pin on ring wear machine and different combinations of steel-steel contact were analyzed. Furthermore, a linear wear patterns for different applied load were done from 1.5 to 124 KPa. Comparing with grinding contact conditions the contact is too mild and the materials in contact do not correspond to grinding. However, despite wear results, even wear patterns cannot be extrapolated to grinding, the multi-contact consideration of two flat surfaces are also assumed on grinding.

In general, the study of the contact between two bodies is not carried out with heavy contact conditions. One of the limitations is the device used for analyze the contact. One of the most common techniques is the sliding of a pin on a rotating disk, named pin-on-disk tests. The simplest set up of this device Figure 17 presents limitations both in maximum reached sliding speeds and on applied load. Therefore, different configurations of pin-on-disk devices are found on the bibliography depending on the required contact conditions [40,41]. In these studies, high sliding speeds are achieved and the pin moves radially to make non-overlapping spiral path and therefore allow the study of the wear pattern on the disk.

Montgomery developed high speed pin-on-disk tests in order to study **steel-steel** friction under heavy conditions. [40]. Sliding speeds from 40 to 183 m/s and apparent contact pressures of 140 MPa were tested. The high temperature achieved leads to a melting of pin just in contact with the disk and in the next step melted material is removed. Wear results of present study are applicable to wear resistance steels; in particular this study is directed to the study of the wear resistance of barrel guns. Concerning grinding process, sliding speeds are higher than achieved during a conventional grinding, only are suitable for superabrasive grinding wheels. Furthermore, contact pressures are far from achieved during grinding.

In tribology, the most common technique to study high normal pressure, from 100 MPa to 3 GPa is using plate impact pressure–shear friction experiments [42,43]. Dynamic conditions of this kind of tests present contact times in the order of μs and sliding distance of a few μm . Although the local contact pressures achieved are in the range of grinding conditions, the experiment does not present more analogies with grinding process, so, is not valid as approach of this machining process.

The more recent study analyzing friction under heavy contact conditions is carried out by Philipon [41]. On this work Philipon developed a new pin-on-disk set up to study dry friction between two metallic bodies under static and dynamic conditions. Steel-steel contact is studied in a wide range of sliding speeds, low speeds from 0 to 3 m/s and high sliding speeds from 13 to 60 m/s were analyzed. The pressure achieved with designed experimental set up is 230MPa and the studied sliding distance was 30mm.

This work concludes that friction coefficient decrease with sliding speed and with local pressure. Philipon attributes this phenomenon to thermal effects in the contact. The high temperature generates the oxidation of bodies in contact leading to a third body, which acts as a lubricant decreasing the friction in the contact. A deeper analysis of third body generation is carried out on following paragraphs in this section.

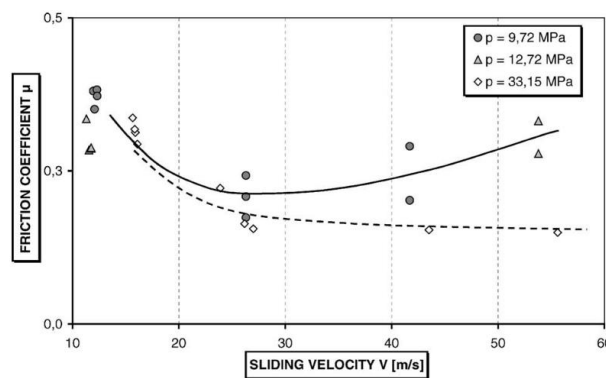


Figure 13: Friction coefficient evolution with sliding speed and contact pressure for steel-steel dry sliding [41]

Studied sliding speeds correspond to grinding cutting speeds as it is shown in Figure 13. Designed pin-on-disk is suitable to achieve high contact pressures. However, on plotted and analyzed results the maximum contact pressure is 33.15 MPa. In spite of mentioned differences, the results of this study are considered a first approach for a deeply analysis of the contact under grinding conditions.

The wear of alumina as ceramic material is widely studied from a tribological point of view. **Ceramic-ceramic** behavior has been long analyzed due to the importance in a wide range of applications, highlighting biomedical field for the manufacture of prosthesis [44–47]. Alumina is one of the materials to knee or hip prosthesis manufacturing. Therefore, alumina-alumina wear resistance is of interest to increase and ensure prosthesis life. All the works define different alumina wear zones. None of the mentioned authors agree on the limits of the zones neither on the number of states in which alumina wear is classified. However, on every works three regions can be differentiated: mild wear region, transition region and severe wear region. This last wear happens under the heaviest contact conditions.

Severe wear of alumina is characterized for high stress leading to high density of intragranular cracking and high dislocation density. It is also demonstrated that alumina undergo plastic deformation when suffer compressive and shear stresses [45]. Although the results obtained in these studies, firstly not correspond to steel-alumina contact and secondly the contact conditions are far from achieved during grinding, it is possible to affirm that alumina, during grinding, is going to work on severe wear region. Therefore, as a close approach, the above described phenomenon for severe wear is also expected on alumina abrasive grains.

II.4.1. Alumina-steel contact

As mentioned, ceramic-ceramic or metal-metal contact has been long studied and helps to understand the contact between bodies in general. However, few works refers to ceramic-metal contact, and particularly alumina-steel contact. In the manufacturing industry, alumina-steel contact is usual not only in grinding process, but also in turning or milling, being alumina a common coating for cutting tools. Also on machine elements, such as bearings or guides alumina-steel contact happens. Therefore, the necessity of minimize the wear of alumina or steel depending on the application, leads to the characterization of alumina-steel contact [48–56].

There are works focused mainly on the study of cutting tools wear. On one hand, the machining of ceramic workpiece material using metallic cutting tools is analyzed. In this case the wear metallic tool is characterize, passing alumina wear over [54–56]. On the other hand, if alumina is used as a coat of cutting tools to improve machining efficiency, the wear of alumina is studied. The contact conditions on these cases promotes friction, but the wear analysis is focused on tool wear characterization, identifying flank wear between other instead of analyze deeply the wear mechanisms at micro scale, tool wear is studied, such as flank wear [57].

In present research work, the wear of alumina abrasive grains are going to be characterized, so only the wear of alumina in contact with steel is going to be deeply analyzed. In this sense, Ravikiran presents a numerous works studying the behavior of alumina against steel [49,51–53,58,59]. His contributions are remarkable to understand the influence of contact conditions in alumina wear and derived results can be applied to alumina abrasive grains wear under grinding conditions.

Analyzing the behavior during dry sliding against hardened steel, zirconia-toughened alumina (ZTA) and pure alumina (99.5 %) is compared [52]. While pure alumina is harder than ZTA, ZTA is tougher and present higher resistance to wear. Furthermore, ZTA present better chemical behavior than pure alumina at high sliding speed [57]. Sliding tests were carried out at 15.5 MPa varying the sliding speed from 0.1 to 12 m/s. Both types of alumina behave similarly

until 7 m/s, friction coefficient is about 0.3-0.4 and decrease until 0.2 when sliding speed reach 12 m/s. Regarding the third body generated in the contact. At sliding speeds lower than 7 m/s Fe particles and iron oxides are the main components. However, for higher speeds, FeAlO₃ and Fe₃O₄ is the main composition of the third body.

Regarding wear, as of 8 m/s, ZTA presents higher wear rate than pure alumina due to the higher influence of chemical reactions. Furthermore, ZTA presents thermoelastic instability, leading to a higher contact pressures and temperature. Both types of studied alumina are used to abrasive grain manufacturing. Therefore, to know the behavior of each alumina under described contact conditions is useful to select a correct abrasive grain and hence grinding wheel for a concrete application.

A wider range of pressures were analyzed, from 3.3 to 30 MPa comparing 87 % Al₂O₃ and pure alumina (99.5 %) [60]. The studied speed range, steel and sliding condition, dry, correspond to previous study. The aim of this work is to link the influence of sliding speed (S), contact pressure (P) and apparent area (A) making an empirical relation between the three parameters as it is shown on Eq.2 Ravikiran established a critical value N=21 which separate the steady state from the friction thermoelastic instability. With regards to contact area, it is shown that smaller contact areas lead to less stable contact due to the discontinuous layer attached to worn surface.

$$N = S^2 P^{0.75} A^{0.5} \quad \text{Eq.2}$$

From works carried out by Nevelos [46] it is concluded that tribochemical reactions characterize mild wear region of alumina. Therefore, in the first attempt to characterize alumina wear under described conditions on Ravikiran studies, it could be concluded that mild wear is the predominant region. However, Ravikiran classified the studied wear on severe wear. This discrepancy with the alumina wear classification is due to the both regions are achieved and the outcomes of both regions are overlapped.

In general, the majority of studies are focused on dry sliding [54,58,61]. However, grinding process is usually carried out with lubrication in order to minimize the wear. Therefore, the influence of lubrication in the contact has to be taken into account. Additionally, some studies are attempted to tackle the problem of lubricated sliding. In one of his works Ravikiran deals with this issue carrying out pin-on-disk tests using water lubrication. On this study, the effect of the lubrication reduce the wear at low sliding speed, lower the 3 m/s [49]. However, water accelerates the oxidation and for high speed the wear increase. Regarding friction coefficient, at low sliding speeds wet contact present lower values, however, when wear rise, higher values of

friction coefficient are achieved for wet friction. The values of friction coefficient for higher sliding speeds are about 0.3-0.4 for wet friction and 0.2 for dry friction.

Moreover, He [62] carried out pin on plate tests using both wet air and water based lubricant. Achieved pressures are from 170 to 320 MPa, higher than used by Ravikiran. However, very low sliding speeds about 0.2 m/s are used. Results show the increase of real contact area with contact pressure, as happens with the evolution of wear flat areas during grinding. Regarding lubrication, in this work the oxidation effect due to the water lubrication is highlighted. At the beginning water present a lubrication effect, decreasing friction coefficient in ≈ 0.1 comparing with dry friction as it is shown in Figure 14. However, the oxidation of water lubricated contact leads to a higher friction coefficient.

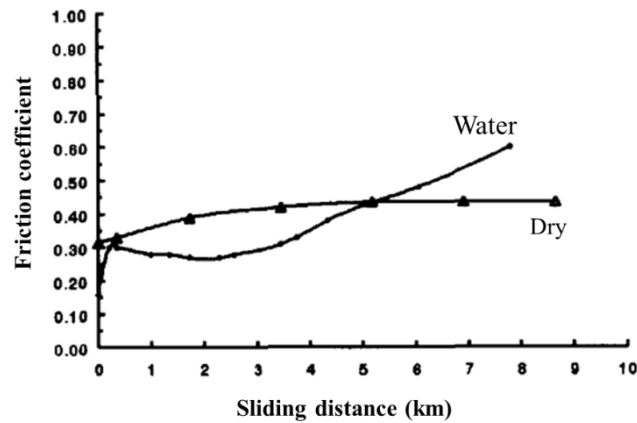


Figure 14: Friction coefficient evolution with sliding distance for alumina steel contact on dry and water lubricated conditions [62].

Comparing with friction coefficient during grinding, lower values of friction coefficient are shown on pin-on-disk tests for lubricated contact. However, friction coefficient behaves similarly on dry grinding reaching values from 0.18 to 0.25 [63]. For lubricated grinding, in this study values until 0.55 were achieved. The difference is that the main wear mechanism during pin-on-disk tests is sliding while during grinding have to be cutting. If grinding is efficient and the abrasive grains are not worn, sliding of abrasive grains present a minor influence in friction coefficient. However, if wear flat occurs, the main wear mechanism is rubbing and friction coefficient behaves as on pin-on-disk tests.

As a brief outline, a wide range of alumina is characterized (87 % Al_2O_3 , 99.5 % Al_2O_3 , ZTA). Studied alumina is also used to manufacturing abrasive grains, making easily the extrapolation of results to grinding process. Different kind of tribometer is used for the characterization, being pin-on-disk tribometer the most common. Thus, during the present study, an original design of pin-on-disk set up is going to use to characterize the alumina. The maximum achieved values

for sliding speed on tribological tests are 12 m/s. On the contrary, cutting speed on grinding is about 30 m/s for conventional process and much higher, until 120m/s on high speed operations. Similarly, maximum real contact pressure achieved during grinding are about 1-2 GPa. Instead, the maximum contact pressure achieved on analyzed studies is 320 MPa, furthermore at very conservative speed about 0.2 m/s. The combination of high speed and high pressure has not been analyzed from a tribological point of view. Therefore, this lack of knowledge is going to be tackled during the present study.

Furthermore, exhaustive analysis of tribochemical reactions in the contact is carried out. Third body is analyzed, being the composition different on each case of study. This third body modifies contact conditions, and it is adhered both to alumina and to steel. This issue is deeply analyzed in the following subsection, analyzing the effect of contact conditions and the materials in contact. Friction coefficient due to third body generation changes, as it is also mentioned for metal-metal contact [41]. The effect of dry or wet friction is also described. Dry friction decreases friction coefficient, which is detrimental effect for grinding process due to the loose of process efficiency. On the contrary, water lubrication sliding present higher values of friction coefficient but promotes the oxidation and accelerates the wear.

On the one hand, the characterization of alumina is carried out under heavy contact conditions from a tribological point of view. However, from a grinding point of view these parameters are very low and are not representative of grinding contact. On the other hand, only wear rate, friction coefficient and third body is analyzed to characterize the behavior of the alumina. However, a lack of information is found regarding other parameters such as normal and tangential force in the contact, wear types or a deeper analysis of worn surfaces.

As mentioned before, there are differences on the maximum achieved values in the contact regarding grinding. However, the tendencies of the behavior of the alumina are applicable to grinding process. Therefore, these contact studies are the basis to understand alumina wear behavior during grinding. More accurate results are going to be achieved if grinding contact conditions are implemented on pin-on-disk tribometer or even if the contact analysis is carried out during grinding. In the following subsections the contact during grinding is studied. Firstly the introduction of material removal mechanisms that occurs during grinding is done, analyzing also the approaches to characterize grinding process. After that, the study of the contact under grinding contact conditions from a tribological point of view is carried out, thus, the study of alumina-steel contact under grinding contact conditions is accomplished.

II.4.2. Material removal mechanisms in grinding process

Regarding real grinding process, material removal occurs when thousands of abrasive grains contact with a workpiece, which is mainly determinate for cutting parameter and wheel topography. However, in the paragraphs above the complexity of the contact in grinding is explained, being the sliding friction the phenomena which dominate the contact due to the kinematic of grinding [64]. During sliding friction the combination of adhesion, plastic deformation and grooves generation leads to a material removal. Therefore, the machining of material in grinding is defined by three material removal mechanisms and on each one different wear mechanisms take place.

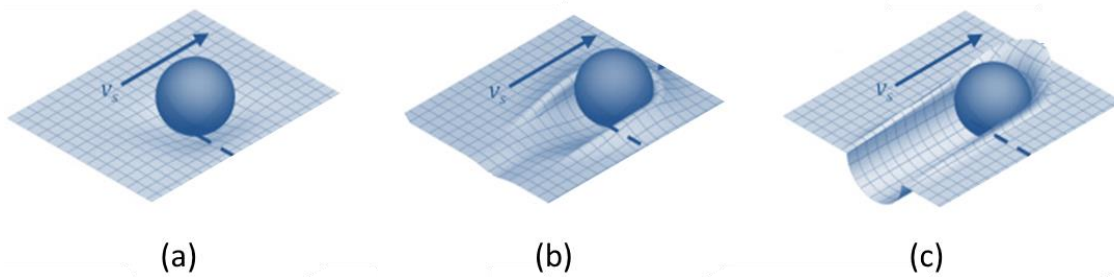


Figure 15: Material removal mechanisms in grinding [65]: (a) rubbing, (b) ploughing and (c) cutting [65]

The three material removal mechanisms are rubbing, ploughing and cutting [66]. Each abrasive grain suffers the three phases and depending on the abrasive grain penetration on the workpiece, and cutting speed one or other is the predominant. In Figure 15 are shown the material removal mechanisms. During grinding all stages take place at the same time on different abrasive grains and each abrasive grain reveals a different stage depending on the penetration on the workpiece. To a better understanding of the influence of material removal mechanisms in the efficiency of grinding, the interrelation with specific energy of the process is carried out.

Specific energy of grinding process is defined as the energy required removing a volumetric unit of material as it is represented on Eq.3. Furthermore, Kannapan presented the theory in which cutting specific energy is divided in three summand [67], corresponding to the three material removal mechanisms In Eq.4 the e_{cu} correspond to the energy involved in cutting, e_{pl} in ploughing and e_{sl} is the energy required for rubbing.

$$e_c = \frac{P}{Q_w} \quad \text{Eq.3}$$

$$e_c = e_{cu} + e_{pl} + e_{sl} \quad \text{Eq.4}$$

Rubbing Figure 15 (a), the first mechanism that occurs in the contact, is characterized for no chip formation and elastic deformation of workpiece material. Friction is the predominant phenomenon, becoming all the energy (e_{si}) in heat, and hence contributing to the increase of contact temperature. In Figure 16 (b) the evolution of specific energy with wear flat generation is plotted. This graphic shows the effect of rubbing on specific energy. At the beginning, when abrasive grains present cutting edge, the specific energy of the process correspond to cutting. However, with the increase of wear, the total specific energy increases. This e_c increase Eq.4 corresponds to rubbing, maintaining constant e_{cu} . Thus, the contact area increase and also the temperature in the contact and higher contact area leads to a less efficient process [67].

Consecutively, and in some cases overlapping to rubbing, ploughing occurs. The deformation suffered by the workpiece in this case presents higher values than for rubbing, corresponding to plastic deformation of workpiece material Figure 15 (b). The penetration of abrasive grains draws a scratch on the workpiece, the material is displaced but not material removal happens. Regarding the efficiency of the process, Figure 16 (a) shows the evolution of specific energy with equivalent chip thickness for a just dressed grinding wheel. So, it is assumed that rubbing specific energy is negligible [27] and a total specific energy correspond to ploughing and cutting. If h_{eq} present low value, the largest amount of energy correspond to ploughing. However, with the increase of equivalent chip thickness, e_{pl} is decreased exponentially, the process become more efficient for high h_{eq} .

In the last stage, cutting of material happen Figure 15 (c). Shearing is the predominant and more efficient material removal mechanisms. The consumed energy is used to remove material, and no energy is lost in deformation or friction. Therefore, the cutting parameters have to be designed to achieve large enough uncut chip thickness and hence, minimizing the effect of ploughing and the wheel wear, specially wear flat have to be characterized to early detection in order to reduce the rubbing between worn abrasive grains and the workpiece.

The predominant wear mechanism of abrasive grains affects directly to the process efficiency. Grinding process is designed to prevail cutting mechanism in the contact and hence, to maximize the efficiency of the process. However, the wear of abrasive grains modifies designed contact giving way to ploughing and rubbing as predominant mechanisms. Therefore, this issue worried both scientific and industrial communities. In this sense, from scientific point of view the problem have been addressed through single grain studies, which allows the easiest identification of wear mechanisms [65,68,69]. In following subsections, the most common tests carried out to the characterization of the contact in grinding are briefly outlined.

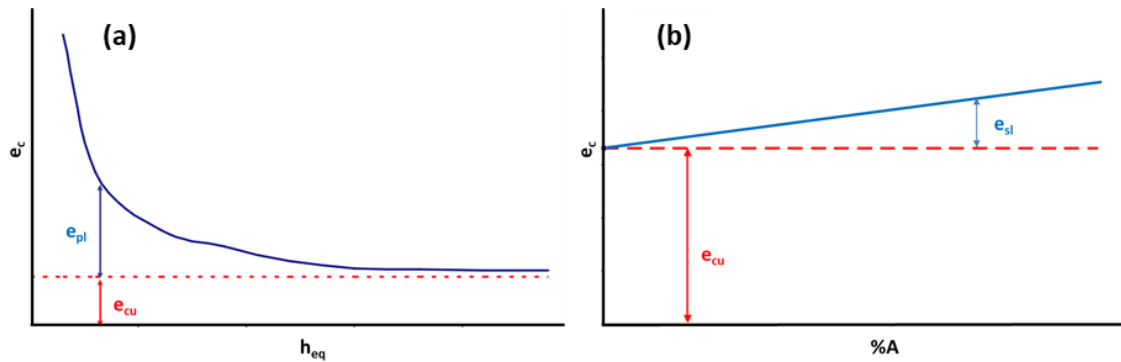


Figure 16: Evolution of grinding specific energy (a) with equivalent chip thickness and (b) wear flat area. The influence of wear mechanisms in specific energy is highlighted [27].

II.4.3. Approaches for the characterization of grinding process

As it is shown above, the efficiency of the process is determinate for predominant material removal mechanisms, for specific grinding process and for cutting conditions. Furthermore, the randomness of wheel surface and the interaction of surrounding abrasive grains hinder the characterization of the contact between abrasive grains and workpiece.

The experimental grinding tests have been the most popular for years to study the influence of grinding conditions on process efficiency and also to characterize the evolution of wear on grinding wheels. The main advantage of this kind of tests is that are carried out on a real grinding machine and hence the results are directly applicable to an industrial process. The influence of cutting speed, workpiece speed and even the apparent pressure can be easily analyzed using experimental tests. However, in many cases grinding tests present limitations related to control of real pressure, because when abrasive grains worn, the real contact area change. Wear flat area increases and hence local pressure of abrasive grain changes [34]. Also some limitations are found on monitoring of diverse process parameters [22,23,70,71], such as tool wear and temperature in contact zone, depending on grinding set up.

Therefore, to carry out the characterization of grinding process, instead of carrying out the study on a real process or with real grinding wheels, diverse tests have been developed during years in order to isolate described phenomena. So, to ensure the control of process in terms of temperature, real contact pressure even grinding surface wear tribological approaches are required.

On one hand, single grit scratch test is the more common technique to study material removal mechanism and chip formation [65,66,68]. The identification of material removal mechanisms is possible with this kind of test [66]. Furthermore, in the last years is also used for the validation of grinding force models for different grinding wheels [72,73]. Also high speed

scratch tests were carried out by Hadmi [74], showing the influence of the speed on the wear behavior. However, as it is previously mentioned the handicap of all these studies is the extrapolation of results to a complete grinding wheel. The randomness of wheel surface difficult the extrapolation of results achieved on a single grain tests.

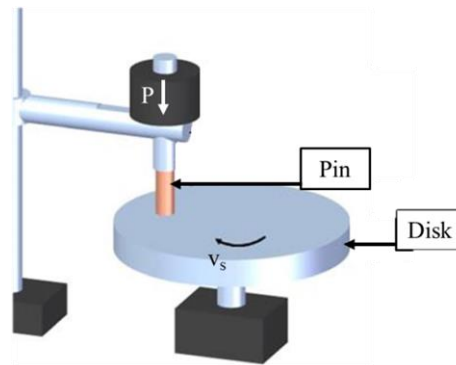


Figure 17: Pin-on-disk test set up [75]

On the other hand, pin-on-disk test are usually used for friction characterization [40,41,74]. On this studies pin loaded against a disk, this is rotating at slow speed Figure 17. Both normal pressure and sliding speed are exhaustively controlled. Pin-on-disk tests present high versatility, a widely range of material can be analyzed in a wide range of pressure and speed values. However, these values are far from values achieved during grinding, in which until 200m/s speed and about 1-2 GPa pressures can be achieved. The majority of works are oriented to study the friction between the two materials in contact. Likewise, Klocke use pin-on-disk test to analyze the behavior of abrasive material [16]. In the following subsection a deeper analysis of pin-on-disk approach to analyze the contact between steel and alumina under grinding contact conditions is carried out.

Despite the advantages named for mentioned tribological approaches, all of them present limitations for grinding process. On single grain tests and scratch tests, the influence of surrounding abrasive grains is not taken into account. Moreover, on pin-on-disk test the abrasive grains are not studied, only the tribochemical reaction between two materials in contact. So, the results obtained on these studies cannot be directly extrapolated to grinding process. However, these approaches are the basis to understand wear phenomena and allow the continuous improvements on grinding process.

As grinding process approach in this section also grinding process simulations are going to be considered. During years and also in the most recent research works, the thermal analysis in grinding [76] have been fundamental to understand the behavior of grinding process. Also, modeling of material removal mechanisms and grinding forces on new workpiece materials

helps to the characterization of grinding [77,78]. Additionally, wheel wear and abrasive grain wear models [79] are developed to know the influence of materials in contact on grinding wheel life between others [79,80]. These models are useful to a better understanding of the phenomena that take place during grinding. Meanwhile, these simulations have to be verified on a real grinding process to be accepted from an industrial point of view. Therefore, the main industrial problems such as tool wear and thermal damage on workpiece are the most relevant topics on grinding process simulation. Tool life prediction is one of the most important issues that concern to grinding manufacturer. In *Section II.6* modeling and simulation of grinding process and in particular abrasive grain wear behavior is going to be addressed.

II.4.4. Alumina-steel contact under grinding conditions: approaches

The grinding process kinematic is not taken into account when alumina steel contact is analyzed from a tribological point of view. Thus, one of the disadvantages of this kind of study is to extrapolate the results to real grinding process. On the contrary, the contact analysis during grinding present difficulties because of the great amount of parameters that take place. The identification of the influence of each parameter in the contact is too difficult during grinding process. The isolation of different phenomenon is required.

In this sense, Klocke [16,33] characterized microcrystalline alumina. The comparison of white alumina with 3 SG, 5 SG and 10 SG alumina were carried out. To perform a complete analysis of the contact, pin-on-disk test, single scratch test and grinding test were carried out. Regarding pin-on-disk tribometer, alumina pin and steel disk are used. Real contact pressure between 0.5-1.5 GPa are achieved during pin on disk tests. This real pressure is the highest seen in the bibliography. With a conventional pin-on-disk set up is too difficult to achieve so high real contact pressures. One of the handicaps analyzing the contact is to determinate real contact area and in this work there are no evidences of measuring real contact area. Furthermore, the implemented sliding speed is of 2 m/s, far from 30m/s, usual on conventional grinding. Likewise, the continuous contact of alumina with steel implies too high local temperatures in the contact, promoting the plastic flow of alumina. Contact surface presents very smooth appearance due to the deformation of the alumina. Furthermore, third body is adhered to deformed surface. FeO is the main component analyzed on adhered layer as it is shown in Figure 18 and also spinel (FeAl_2O_4) is attached between plastically deformed alumina and iron oxide. On this scheme are identified the more representative phenomena that occurs to alumina during sliding against steel. Subsurface cracks correspond to severe wear region. On the contrary, tribochemical reactions correspond to mild wear region. As it is previously affirm, alumina can be suffered mild and severe wear and its effects are overlapped.

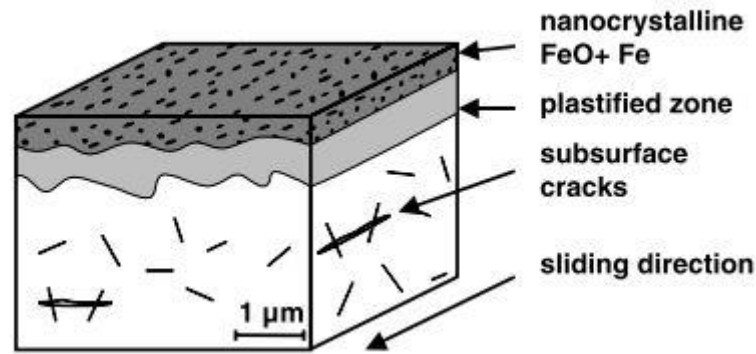


Figure 18: Main findings of TEM analysis of worn alumina [16]

Despite being the most complete study that it is found in the bibliography, the extrapolations of results cannot be done to a real grinding process because two critical factors are not taken into account. Firstly, effects of surrounding abrasive grains are not considered on single grain tests and on scratch tests. And secondly, on pin-on-disk tribometer a continuous contact of alumina with steel is studied. However, on real grinding process, the intermittent contact of abrasive grains occurs, the thermal cycles suffered by abrasive grains are not reproduced. Therefore, achieved temperature and hence the effect of temperature on alumina wear is not representative of a grinding process. This Study represents an attempt to tackle these two critical factors that affects to contact characterization.

Taking into account the difficulties involved in the analysis of the contact on pin-on-disk tribometer and its subsequent extrapolation of results, the analysis during grinding is done. The analysis of the contact of abrasive grains with alumina is required to better understanding of wear flat. In this sense, the attritious wear of alumina have been deeply studied by Malkin [15,81]. To study the wear of alumina abrasive grains, surface grinding tests were carried out. Thus, high local contact pressures were achieved at 30 m/s sliding speed. Malkin affirms that tribochemical reactions take place in the contact between abrasive grains and workpiece. Again, as it is mentioned on Klocke's analysis, despite contact parameters correspond to severe wear, the tribochemical reactions, typical of the mild wear regions also occurs. This fact is due to the alumina firstly suffer mild wear and if heavy contact conditions are imposed, after that also severe wear happens. Moreover, the effects of both regions are not isolated phenomena. Therefore, tribochemical reaction, adhesion, abrasion and plastic flow of alumina could appear together despite severe wear govern the contact.

It can be concluded that the control of the heavy contact between two surfaces and the analysis of the phenomena that take place in the contact is a complex task. However, it is of great importance to the characterization of wear flat during grinding process. Wear flat is

tribochemical nature wear, therefore, is of interest for the present study to know the chemical reactions that take place during the contact are.

II.4.5. Third body generation under grinding contact conditions

During the analysis of the contact carried out in this section, the third body is generated as a result of tribochemical reactions that take place in the contact. Depending on the materials in contact or contact conditions, the main composition of the third body changes. Moreover, Third body adhered to worn alumina is determinant for the value of friction coefficient achieved. As it is shown analyzing different works, sliding speed or contact pressure influence the friction coefficient evolution. But if third body becomes increasingly important, the friction coefficient decrease regardless contact parameters. Therefore, it is deeply analyzed hereafter due to the influence of third body in the contact characterization.

Table 2: Third body composition depending on contact conditions

	Contact Pressure	Sliding/cutting speed	Third body
Ravikiran [51,52,59]	15.5 MPa	< 7 m/s	Fe particles
		7 m/s < v_s < 12 m/s	FeAlO ₃ and Fe ₃ O ₄
Klocke [16,33]	0.5 1.5 GPa	2 m/s	External: Fe and FeO Internal: FeAl ₂ O ₄
Malkin [15,27,81]	1-2 GPa	30 m/s	FeAl ₂ O ₄

As it is mentioned different chemical reactions take place during alumina-steel contact. In Table 2 are summarized the main third body components and the contact conditions of the most representative studies. Despite on these studies a temperature in the contact is not measured, the analyzed components gives an idea of reached values. Heavier contact conditions leads to a higher temperature. The temperature is a decisive parameter in the chemical reaction imposing one or other final Figure 19 Fe₂O₃-Al₂O₃ phase diagram is represented. Fe₂O₃ is an iron oxide and on its mineral form is named hematite and the crystalline form of Al₂O₃ is corundum. Analyzing phase diagram, it is shown that until 1100 °C there are no chemical reactions. In this sense Ravikiran found Fe particles at a lower sliding speed and 15.5 MPa, the less aggressive contact condition. With the temperature increase first reactions lead to AlFeO₃, corresponding to

iron oxides, in purple is marked on phase diagram. Ravikiran at higher sliding speed found this component together with Fe_3O_4 , other iron oxide.

Despite on analyzed works the temperature in the contact is not measured, it is accepted that the temperature in the contact during grinding is close to the workpiece melting temperature. In this case steel is the workpiece material, therefore, it is going to be assumed that contact temperature on grinding is about 1375°C . This temperature is highlighted on phase diagram in red Figure 19. Above this temperature spinel appears. There are different composition for spinel being the FeAl_2O_4 the more predominant between these two materials in contact. The chemical reaction to generate FeAl_2O_4 needs higher temperature than the oxidation. On phase diagram the range of temperature that corresponds to spinel formation is marked in blue. Therefore, spinel only is generated if heavy contact conditions are imposed as on Malkin's works, on real grinding process.

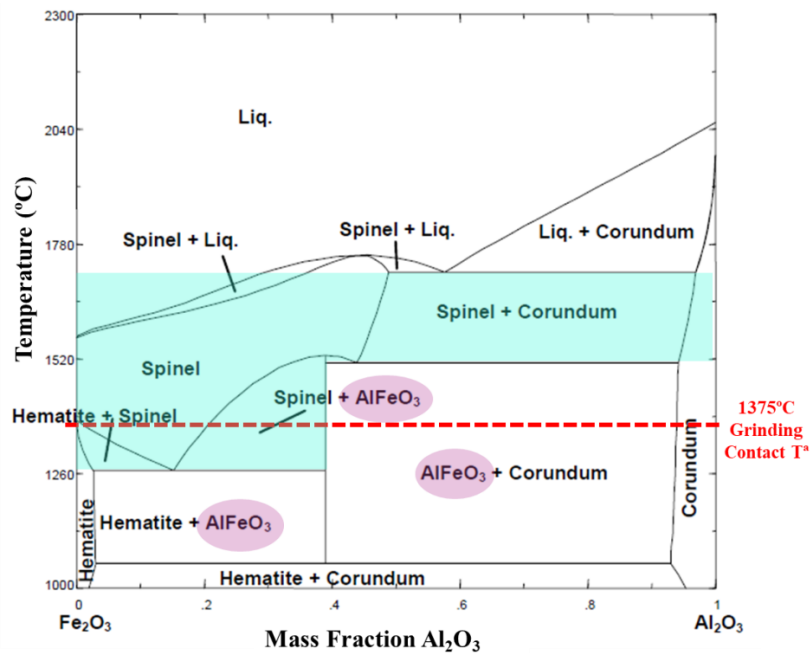


Figure 19: $\text{Fe}_2\text{O}_3\text{-Al}_2\text{O}_3$ phase diagram [82]

Besides that, Klocke found spinel, Fe particles and iron oxide. FeAl_2O_4 is formed in the interface between FeO and alumina and is only occasionally observed. Klocke affirm that FeO layer is melted and subsequently cristallization of the melted oxide occurs. Melting temperature of FeO is 1240°C [16]. At this temperature the plastic flow of alumina also occurs, as it is shown in paragraphs above. Comparing Malkin and Klocke results, differences on third body composition are found, however, the range of contact temperature in both cases is almost the same. So the dissimilarities found on the third body are due to the thermal cycle of the alumina. In the case of grinding, abrasive grains present intermitent contact. Therefore, the melting and

subsequent crystallization of FeO is not the predominant phenomena in the contact. On the contrary, on pin-on-disk test a continuous contact of alumina promotes mentioned chemical reactions and smooth layer formation.

As it is shown, third body governs the contact between alumina and steel under heavy contact conditions. In the present Research work the contact during grinding process is addressed, and in particular the wear flat evolution is going to be studied. Wear flat is a tribochemical nature wear, being third body generation directly linked to wear flat. So, to know how each parameter affects to third body generation to a better understanding of wear flat evolution is required. In *Section II.5* a deep analysis of wear flat is carried out.

II.5. Wear Flat of alumina grinding wheels

II.5.1. Wear Mechanisms involves in wear flat generation

In the paragraphs above, wear types are described, related not only to abrasive grain wear but also to whole grinding wheel wear. Abrasive grain flattening occurs due to the overlapping of wear mechanism between abrasive grains and workpiece, changing contact conditions and promoting wear of abrasive grains. Therefore, deeply mention to wear mechanisms which leads to wear flat is done hereafter.

Heavy contact conditions are achieved during grinding, pressure values are in the order of 1-2 GPa, promoting very high local temperatures, close to workpieces melting point [27] and high tribological stress. Furthermore, the small depth of cut and high cutting speed of the process, comparing with other machining processes, promotes sliding friction. This phenomenon dominates the contact between abrasive grains and workpiece [63]. Henceforth, to analyze the contact of abrasive grain, the cutting material is not taken into account, only the phenomena that affect to abrasive grains is considered.

Wear flat is a tribochemical type of wear [27]. Mechanical effects are related to abrasion, adhesion and plastic flow of abrasive grains. Chemical reactions depend on materials in contact and the temperature on the contact leads to a different compound. All the mechanisms appear at the same time being impossible to isolate each one and study its consequences separately during grinding process. Abrasion of material occurs due to the differences of hardness between grains and workpiece. The grains are harder than the workpiece; however, abrasive grains also suffer the friction effect.

Adhesion is characterized by micro-welding between materials in contact and the breakage of generated bridges. It is promoted by high temperatures and the absence of coolant in the contact. Plastic flow of abrasive material is encouraged by forces supported by the grain. Due to the plastic flow, peaks on abrasive surface disappear, decreasing the friction in the contact. Finally, chemical affinity of materials in contact accelerates wear process and leads to a new components in the contact, composing the third body. The concept of the third body is previously explained in *Section II.4.3*. In general, described wear mechanisms increases their effects with high temperatures reached during grinding and their influence on the wear is reduced if the contact is adequately lubricated.

From the wear mechanisms described, chemical affinity of materials in contact is the predominant phenomena. One of the factors to take into account when an abrasive material is chosen for specific application is its chemical affinity with the workpiece material. For example, to ground steels, SiC abrasives are avoided. In this sense, alumina is the most widely used abrasive for steel grinding. Its chemical affinity is not as high as SiC material, however also chemical reactions take place during grinding, related to the oxidation of iron and the reaction with the abrasive. The following chemical reaction Eq.5 governs the contact between ferrous materials and alumina [27].



Spinel (FeAl_2O_4) is the main component generated between steel and alumina contact under grinding conditions as it is previously explained on the third body analysis. This component is attached to the flat abrasive grains with the formation of very strong links, changing the contact conditions [83]. Wear flat of abrasive grains and the third body adhered to flat surfaces decrease friction coefficient. Coolant also influences in chemical reaction. On one hand, if water lubricant is used, reached temperatures are lower, so the stimulation of chemical reaction is less aggressive. On the other hand, water accelerates the oxidation of iron, and hence the third body generation [49]. However, lubricate the process presents more beneficial effects, so there are only few applications in which dry grinding is applied.

II.5.2. Wear Flat characterization during grinding

Wear flat occurrence is conditioned by contact conditions. Its evolution during grinding affects to process efficiency, increasing the temperature in the contact, normal forces and power consumption. However, if adequate characterization of wear flat is carried out, the damaging effects of wear could be reduced or even detached. Thus, if the occurrence and evolution of

wear flat is decisive for a particular grinding process, dressing could be adequately design to avoid achieving large flat areas. In this sense, the first step is to measure the areas corresponding to flat grains using %A parameter, which is widely used to characterize this type of wear. The %A is the percentage of flat surface compared to the apparent area of grinding wheel.

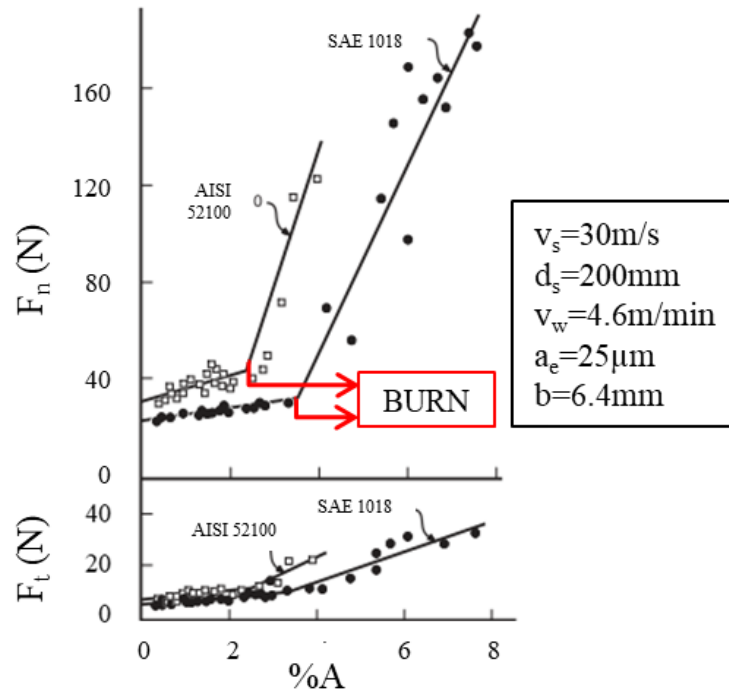


Figure 20: Evolution of grinding forces with wear flat [27]

Malkin studied the influence of %A on grinding forces as it is shown in Figure 20. The two analyzed steels present the same behavior. At the beginning, to low values of %A, forces increase slowly showing efficiency grinding. However, a critical %A is reached and forces present a high increase. This critical value establish the burn in the workpiece and the decrease of process efficiency [81]. In the same way, as %A increase, friction coefficient decrease, promoting the sliding friction in the contact. The loose of cutting edges of abrasive grains occurs, being ploughing and rubbing the material removal mechanisms.

Malkin study deeply grinding wheel wear and its influence during grinding process [81,84]. This works evolve not only wear flat, but also fracture wear using monocrystalline alumina to ground steel. Using monocrystalline alumina transgranular grain fracture is avoided, but wheel may suffer bond fracture. One of the handicaps of these works is that wear flat is not isolated from the other type of wear. If abrasive grain flattening occurs, grinding forces increase. So, bond fracture could take place, losing a flat abrasive grain. For the process, these consecutive events present advantages. However, the evaluation of wear flat generation is not possible and after the loose, starting again grain flattening on a new abrasive grains.

In the same way, these studies reveal that wear flat area increases with the wheel hardness. The hardness of grinding wheels is referred to the resistance of the bond to maintain abrasive grains embedded on a wheel matrix. So, harder wheels require higher tangential forces to break a bond. If forces are not higher enough to break the bond bridges, the flattening of abrasive grains is growing steadily and hence achieved %A is higher. Regarding dressing influence, fine dressing promotes a faster evolution of wear flat. The flatness of just fine dressed abrasive grains is higher than if coarse dressing is done. The topography achieved on both cases is different. With coarse dressing more distance between contact areas are obtained. Larger cutting edges are achieved. On the contrary, closer contact areas related to fine dressing promotes the increase of the temperature, and the evolution of wear flat is faster than for coarse dressing. Third body is also generated in the contact, corresponding to spinel $FeAl_2O_4$. An extensive analysis of third body analyzed by Malkin has been presented in *Section II.3* on this chapter.

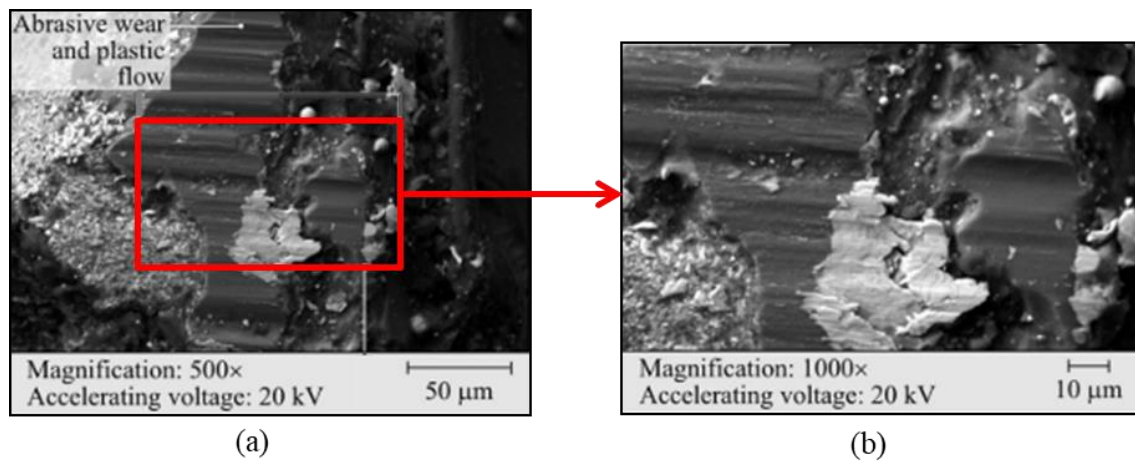


Figure 21: Plastic flow of SG abrasive grains and third body adhesion (a) a complete worn abrasive grain and (b) detailed flat grain and third body adhesion [34]

More recent work related to wear flat occurrence on alumina during grinding process is carried out by Nadolny [34]. In this case, microcrystalline alumina is characterized, due to the popularity and the extensively use in the industry. The experimental work is carried out for internal cylindrical grinding using SG grinding wheels, analyzing wheel life, wheel topography and the predominant wear phenomena. Nadolny confirms that abrasive wear, plastic flow, thermo-fatigue wear and micro chipping happen in the contact between SG alumina and steel. Furthermore, to high percentage of bond in the wheel, plastic flow and abrasive wear predominates the contact. In this case, wear flat is the main wear type. The higher amount of bond is in contact with abrasive grains. If grain temperature increases, the bond around the grain is also heated. Consequently, tribochemical reactions and plastic flow of alumina is promoted. In Figure 21 both phenomena are shown. On this work the effect of each wear type is not individually analyzed. Nadolny is not concerned about the influence of wear flat as isolated

phenomena, but in the different type of wear that SG alumina grinding wheel can be suffered. In this sense, despite the study is focused on internal cylindrical grinding, obtained results can be directly extrapolated to other industrial cases.

As it is shown on Klocke's tribological tests [16], Nadolny confirms that during grinding tests plastic deformation of alumina also occurs. Described plastic deformation is generated because of the sliding of microcrystals promoted by high temperatures in the contact and subsequent adhesion. On the contrary, monocrystalline alumina is analyzed by Malkin, being the plastic flow of alumina not mentioned during all the studies. The reason is that on monocrystalline alumina there are not crystals inside the grains, a complete grain is formed by an only crystal. So, the effects that lead to plastic flow of alumina cannot take place on monocrystalline abrasive grains. Meanwhile, plastic deformation of alumina depends not only on the size of microcrystals but also in the strain level in the contact.

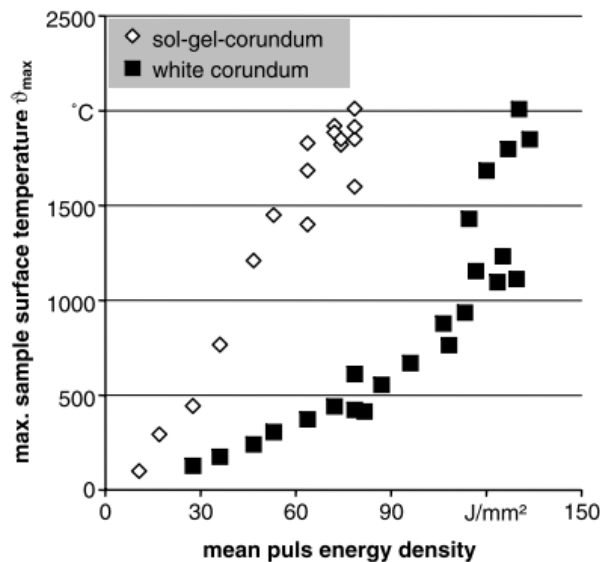


Figure 22: Thermal cycle experiment on conventional and SG alumina carried out by Klocke [16]

Klocke [16] compare the behavior of white alumina, which is conventional alumina, with SG alumina. Firstly, thermal cycle experiment was carried out showing a lower heat conductivity of SG alumina comparing to white alumina as it is shown in Figure 22. This difference is attributed to a higher grain boundary in SG alumina as well as to the presence of pores. Lower heat conductivity leads to a higher plastic deformation of alumina and also promotes tribochemical reactions. Therefore, during pin-on-disk a smooth surface of SG abrasive grains is shown due to the plastic flow and third body generation as it is previously mentioned Figure 18.

Accordingly, the crystalline structure of abrasive grains have an influence on plastic flow of alumina and hence of wear flat occurrence. In this sense, there are not works comparing the

behavior of the three crystalline structures under real contact conditions. To ensure an exhaustive control of contact conditions a tribological approach together with real grinding tests are required. Therefore, in the present research work the comparison of crystalline structure of abrasive grain on the wear flat generation is going to be addressed. Hereupon, Klocke's work, provide good approaches of the behavior of the alumina against steel from a tribological point of view. However, the contact conditions reproduced on the tribometer do not reach real cutting speed of grinding process. This study has been deeply analyzed in *Section II.4.3*.

II.5.3. Wear Flat and wheel topography measurement techniques

One of the handicaps of grinding process analysis is to measure grinding wheel topography. Numerous techniques have been developed for the characterization of grinding wheel topography in general, and of wear flat in particular. Nature of abrasive grains and randomness of wheel surface make difficult the measurement of wheel topography. There is not established a commonly accepted methodology to characterize wheel topography and hence wheel wear. From scientific point of view different techniques have been developed during years. However the specific preparation of specimens or wheel surface and high time consuming methods hinder the application on industrial environments.

In general, the technique to measure wheel topography is divided in two steps. Firstly the topography is obtained. The methods are divided on contact or non-contact and can be carried out during grinding, which are known as online methods, or once the grinding process has finished, offline methods. The tendency in the last research works is to develop online methods because from an industrial point of view only these are suitable. Subsequently, achieved topography have to be analyzed, thus, the data have to be assessed to quantify the wear. In the following paragraphs the most used methodologies are presented, pointing out its advantages and limitations.

Contact methods are basically referred to profilometer technique [85,86] and usually are not implemented on a grinding machines. In this case, depending on the size of the stily, surface information can be lost. Nowadays, they are rarely used for wheel surface characterization due to their limitations. Therefore, in the last years a great amount of works based on non-contact methods are developed to characterize wheel topography. Great diversity of methods are undertake depending on the needs. One of these is based on grinding sound and it was implemented to determinate the necessity of dressing [87]. This monitoring system was developed using neural network technique. From the dressing sound is taken the reference frequency and wheel surface is discriminated depending on the frequency of grinding signals. Moreover, acoustic emission (AE) methods are developed to wheel topography characterization

of alumina grinding wheels [24]. The measurement is carried out at 30 m/s, being an advantage regarding optical scanning methods. However, the study is focused on roughness parameters of wheel topography and the relation with process parameters and wear flat study is not addressed using AE quick method.



Figure 23: Automatic image processing device implemented on surface grinding machine [88]

As it is described, in general these sensors are not available for practical applications or are not able to analyze wear flat. However, optical methods do not attempt to all these limitations. The low time consuming and wheel or workpiece material independence becomes optical methods on an optimal solution to wheel topography characterization. Therefore, optical method is going to be used to characterize wear flat evolution on the present Study. In general, optical methods are performed on grinding machine, so are classified as online methods. However, online term leads to discrepancies in the bibliography. If wheel measurement is carried out during grinding, online methods are considered. However, the majority of devices are not able to get the surface topography at cutting speed and the wheel has to be decelerated even stopped during the measurement. Both software and hardware limitations and also the presence of cooling during grinding do not allow online measurement. To achieve an accurate topography, wheel surface has to be dry, otherwise, the water disperse light or laser rays.

Different works related to wheel loading measurement [89,90] or wear flat characterization [35–37] are carried out by optical methods. CCD camera is used to get 2D images of wheel surface, and confocal technique is implemented to analyze 3D topography. This last measurement is usually conducted outside the grinding machine, due to the complexity of the microscopes, and on the contrary is usually undertaken to complement the grinding surface analysis [34,91]. 3D

roughness surface parameters are taken from these measurements, being Abbot Firestone curve a useful parameter to determinate both loading or abrasive grain sharpness loose.

The characterization of wear flat is usually done through the analysis of 2D images taken using CCD camera implemented on surface grinding machine as it is shown in Figure 23. Some works are focused on the development of an automatic image processing device [35,37,88]. Despite this method is classified as online method, the images are taken with the wheel stopped and the position of the image is servo controlled to ensure the analysis of wear flat on the same abrasive grains. However, due to the randomness of the abrasive surface, it is not mandatory to analyze the same abrasive grain during a complete study. It is enough to take a high number of samples and take the mean value of wear flat for each wear state.

The particularity of wear flat is that a flat surface is generated on abrasive grains. To measure the area corresponding to flat surfaces this property is seized. The technique of coaxial light is widely used to measure wear flat [35,88]. Once images are taken, 2D images have to be analyzed. A great variety of methodologies are developed. The most common and the least time consuming image processing technique is related to the binary segmentation of images. The difficulty is to determinate the threshold value which divided flat area from rough surface. In general, the images are analyzed on gray scale, establishing the threshold values to determinate flat or not flat surface. Mathematically, the binarization is defined as it is shown on Eq.6, where t is the threshold value established and g_q is the grey level of the corresponding pixel.

$$P(g_q) = \begin{cases} 0 & (g_q < t) \\ 255 & (g_q \geq t) \end{cases} \quad \text{Eq.6}$$

Likewise, diverse filters are developed to differentiate the real wear flat areas from other measured points that do not correspond to flat grains. One of the technique is based on the detection of pixels that are on the focus plane, which correspond to wear flat [35]. The region growing method was also developed to characterize wear flat evolution [36]. The limitation of this method is that the same abrasive grain has to be analyzed, so angular encoder and wheel position servo control is required. In Figure 24 previously detailed steps to wheel topography characterization or schematically plotted.

Additionally, depending on the wheel surface and abrasive grains nature, wear flat characterization becomes on a challenging task. While the identification of wear flat on CBN or diamond abrasive grains is fairly straightforward, on alumina grinding wheels the abrasive grains and bond present difficulties to be differentiated. Furthermore, the translucent

characteristic both of alumina and vitreous bond hinder this identification. In these sense, the analysis of alumina grinding wheel on a vitreous matrix is going to be analyzed. To carry out the characterization of wear flat evolution on this wheels, the image collecting are done using binary segmentation technique to quantify the %A on wheel topography.

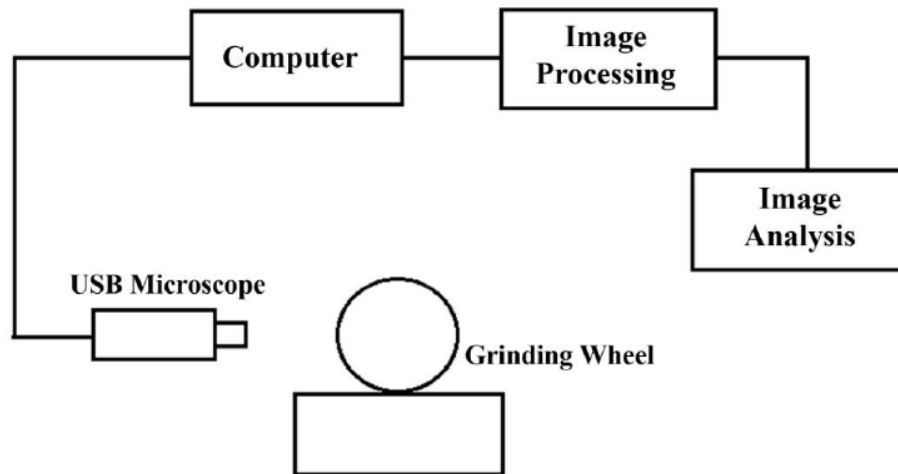


Figure 24: Schematic diagram of wheel surface analysis [88]

II.6. Simulation of grinding process

Simulation and modeling of grinding process is an excellent tool to select the optimum combination and process strategy in order to achieve minimum process time and maximum workpiece quality and process efficiency. An adequate combination between process and machining parameters and grinding results makes process simulation almost essential both for industrial production and for research community. Therefore, modeling and simulation of process has become on a critical predictive analysis for grinding.

Parameters such as, grinding forces, grinding temperature, abrasive wheel topography, thus wheel wear, or even surface integrity are predicted using grinding models and simulations. Some models are more suitable for grinding design while others for control the process. There are different categories of models with different application areas as it is represented in Figure 25 [92]. Physical, empirical and heuristic models are the three main types. Physical models involve regression, finite element, fundamental analytical, kinematic and molecular dynamic models, which are described for macroscopic to microscopic studies. Regression and artificial neuronal net are referred to empirical models and rule based model correspond to heuristic

model. One of each model category presents advantages and limitations, so a brief gathering of this kind of models is accomplished hereafter.

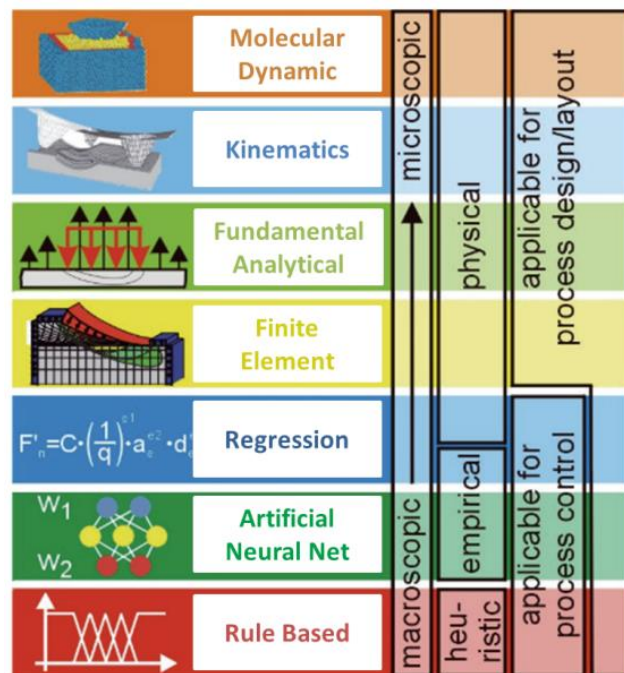


Figure 25: Application and classification of different types of grinding models [92].

Fundamental analytical methods are based on mathematical formulations, providing a good understanding of grinding. These methods are widely used to model grinding forces, process energy or contact temperature [73,93]. However, the accuracy of the process relies on input parameters, which are obtained experimentally. Kinematic models reproduce in detail grinding, being the results too close to real process. On the contrary, kinematic models are high time consuming and it is very complex to reproduce realistic grinding wheel topography. Therefore, single grain approaches are reproduced and only the tendency of forces or other parameters can be obtained, moreover, material removal mechanisms are analyzed [14,65,94].

Finite element analysis enable the simulation of the complete grinding process, however the computational requirements is very high. This type of method needs an experimental result to be verified and in some cases there is not possible to measure required parameters with accuracy, such as temperature in the contact. However, are widely used to removal mechanism simulation [95] or grinding temperature simulation [96] between others, being focused on macroscopic behavior of grinding. As on kinematic methods, instead of simulate a complete process, the approach of single grain is broadly used.

On the contrary, molecular dynamic models are developed to the understanding of microscopic material behavior and material properties at atomic level. Three dimensional simulations of

single grain studying the interaction with a workpiece are carried out as it is shown on Figure 26. Material anisotropy and atom-atom interaction is modeling, being simulations of very high CPU and time consuming. The most studies are focused on micro cutting, no specially in grinding [97]. The simulation of grinding process is limited to initial states of the contact, being contact length in the order of nm and contact time in ps [98,99]. Analyzing scratching models or even grinding, the largest work achieve 120 000 atoms [100,101]. Moreover, on molecular dynamic studies the abrasive grain is not being studied, the attention is focused on material removal mechanisms.

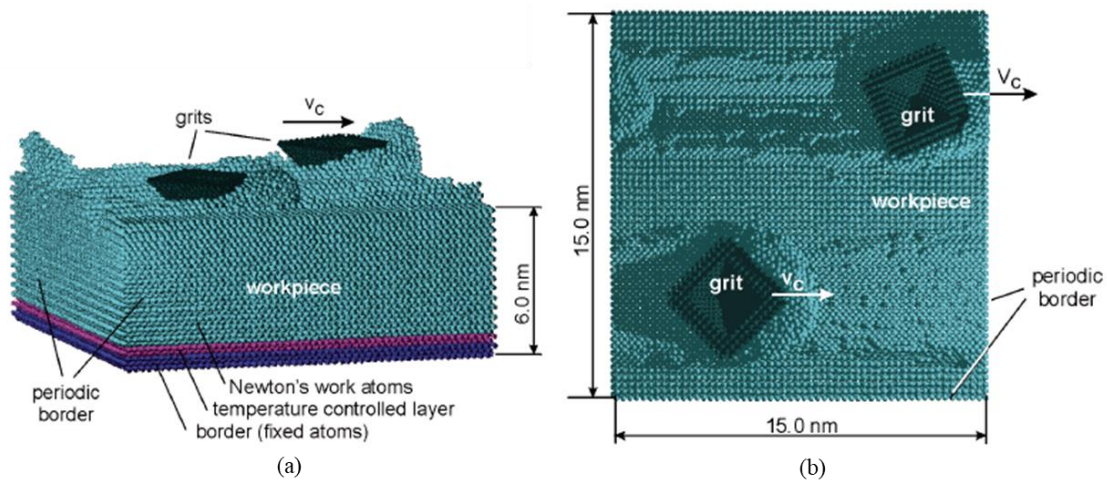


Figure 26: Groove scratching tests with 2 grains 360 000 time steps, 144ps. (a) side view, (b) top view [92].

The main reason to develop a regression analysis method, mathematical statistical method, is the low computational power. Results obtained from this method are highly dependent of number of experiments and their quality. The majority of the works are focused on grinding forces modeling for different workpiece and abrasive materials in order to optimize both grinding and dressing processes [102]. Additionally, wheel wear is also analyzed basically using G-ratio parameter. Comparing with artificial neural net (ANN) models, both present an equality on the quality of simulations. As well as on regression methods, a great amount of data is required, in this case for training. The design of an adequate ANN is very complex. Meanwhile, these two methods are promising if they are combined with physics models. In grinding, ANN are useful to predict both output and input parameters and also to monitoring of grinding. The prediction of wheel life is possible using ANN models [103]. Finally, ruled based methods are developed in order to help human reasoning when difficult problems have to be addressed. A sophisticated knowledge base helps to achieve high quality prediction of output parameters. Different algorithms are developed to learning and reasoning of grinding behavior. In general, rule based methods are designed for give recommendation of grinding to users, combining the design of grinding wheel and the election of grinding parameters [104].

As it is described, to accurate process modeling, wheel topography, workpiece characteristics as well as kinematic of the process has to be taken into account, being a complex relationship between all of them. Force models are developed to predict grinding wheel wear, so it is also necessary to consider wheel topography. Moreover, force models also predict grinding energy, allowing the determination of contact temperature and its effect on workpiece surface integrity. Therefore, workpiece characteristics have to be taken into account too. Thus, there are difficulties to develop accurate simulations and there are wide varieties of models focusing on the design and control of grinding process. Meanwhile, the first grinding simulation correspond to 2D models [105], while the most recent studies are referred to 3D models [106–108], because of the computational power increase. Furthermore, there are not many works referred to abrasive grain wear. Temperature, forces and material removal mechanism are topics which concern to researchers in this field, leaving out the wear of abrasive grains. The present research work is focused on wheel wear, particularly on wear flat, therefore, in the following paragraphs a deeply analysis of wheel topography and abrasive grain wear modeling is tackled.

II.6.1. Modeling of grinding wheel topography

The randomness of wheel surface and diverse shapes of abrasive grains hinder wheel workpiece contact modeling. Single grain tests have been the most popular to understand the contact in grinding. To simulate single grain contact finite element methods or analytical methods are used [109]. However, the main objective of these works is usually the characterization of material removal mechanisms, without considering the wear suffered by the abrasive grain. Moreover, the shape of the abrasive grains is widely discussed in the bibliography. Conical, spherical ellipsoidal, pyramidal even irregular shapes of abrasive grains are analyzed in order to achieve more realistic contact modeling [110–112].

Nevertheless, carrying out a single grain tests the influence of surrounding abrasive grains is not taken into account. In this sense, high efforts to modeling wheel topography have been done. 2D and 3D topography models were developed using physical approaches [113] and stochastically approaches [114]. These models take into account abrasive grain shape and size, random distribution of wheel matrix and dressing mechanics accounting for fracture and deformation leading to a dressed surface. In Figure 27 is presented a general 3D wheel surface approach.

Moreover, volumetric composition of grinding wheel is considered to simulate 3D wheel structure using a numerical method [112]. The shape and position of the grains, the pores even the bond are simulated, leading to a realistic wheel matrix. However, this work do not take into account the effect of dressing process on wheel surface neither the wear suffered by abrasive grains. Osa [115] simulates the wheel-workpiece contact and to reproduce 3D structure of

grinding wheel discrete element model (DEM) is used, showing that DEM is a useful tool to grinding wheel modeling. In the same way, this study reproduces the wheel topography but the wheel wear is not addressed.

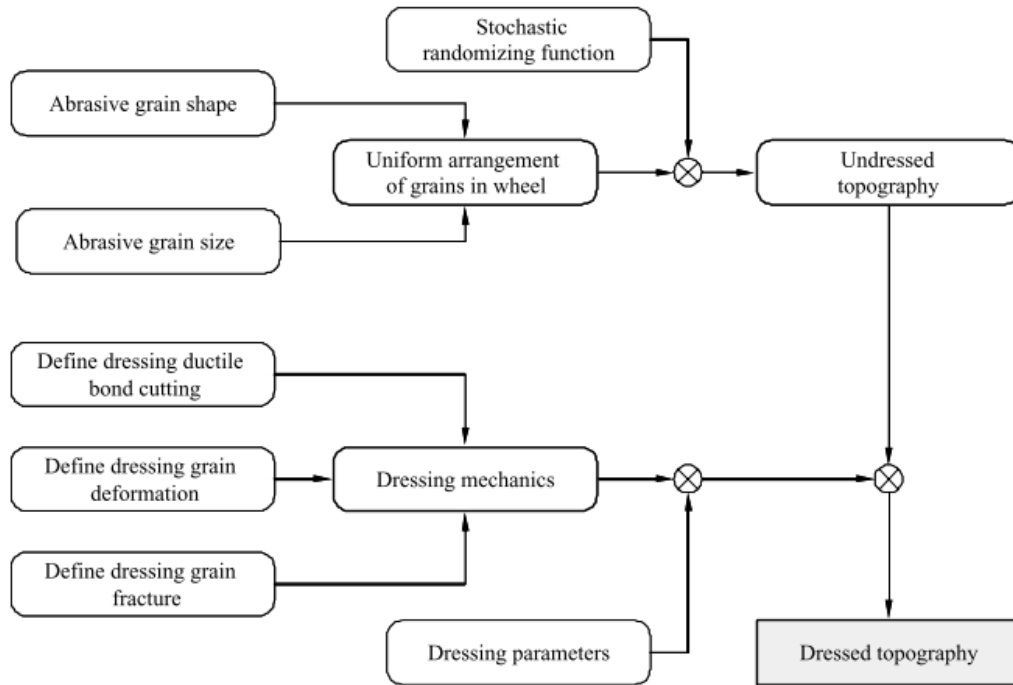


Figure 27: Scheme of 3D topography physical approach [110]

Regarding workpiece ground roughness and wheel topography prediction, mathematical models are developed taking into account wheel topography dressing effect and also wear effect [116]. The wear is introduced in the model as a height (0-3 μm) from the highest peak obtained with dressing modeling. These wear values are suitable to reduce the roughness, however, high wear values leads to thermal problems.

On the one hand, there are some works in which the attritious wear and grain fracture is taken into account to determinate real grinding forces [117]. From this analytical model grinding forces, power consumption, workpieces burn identification even workpiece roundness are obtained, being the wear an input parameter to the simulation. On the other hand, works which refer to abrasive wear are focused on the wear of steel, without model the wear suffered by abrasive grains [111]. Blunting of abrasive grains is also modeling on this research work achieving an empirical expression for blunting. However, this simulation cannot be directly extrapolated to grinding process due to the contact conditions and because in this modeling pin steel against abrasive paper has been analyzed. Moreover, this work concludes that the wear of brittle materials is proportional to the hardness, therefore abrasive grains present higher wear resistance than steels. Additionally, regarding grinding process, Torrance affirms that the rake

angle of abrasive grains also affect to the wear rate between abrasive grains and workpiece material [111].

II.6.2. Modeling of grinding wheel wear

With concern to abrasive grains wear, this is mainly modeling taking into account the flattening of abrasive grains, being the height value of wear the parameter of interest in the majority of cases, because determinates the penetration of abrasive grain in the materials. In this sense, probabilistic method is developed [118] in order to predict the state of wheel surface during grinding, which is determined for the number of contacts of each abrasive grain with the workpiece.

More specific model is developed to characterize the wear and wheel life expectancy of CBN abrasive grains taking into account two different phases [119]. In the first phase grain pull out is considered and in the second phase grain wear, involving wear flat and grain fracture together. To model the first phase, grinding kinematic, grain-workpiece thermal shock and Paris-law approach is considered, showing that the thermal stress affects until 5 times more than mechanical stress to grain pull out. Additionally, second phase is modeling with Preston approach, showing that the grain wear rate is highly dependent of workpiece feed rate.

Regarding wheel loading, analytical model is developed [120] based on the adhesion of workpiece material to CBN abrasive grains. The abrasive grain size and number of cutting edges are known. However, wheel loading have to be quantified with the workpiece material embedded on wheel pores and not only taking into account the material adhered to abrasive grains. In fact, this analytical model predicts a high dependence of wheel loading with depth of cut and with cutting speed.

Finally, wear flat have been simulated through an statistical analysis allowing the determination both of active grain density and wear flat area [121]. In this work a pyramidal grain shape is assumed for diamond abrasive grains, becoming on square flat areas with wear. Linear relation between grinding forces and wear flat area is achieved for the different tests carried out as it is shown in Figure 28. The advantage of simulate CBN or diamond abrasive grains is the ease of real measurement real of wear flat values to validate the simulation and the ease to determinate the active grains of the surface. On the contrary, using a conventional abrasive grains, this two aspect hinder the characterization.

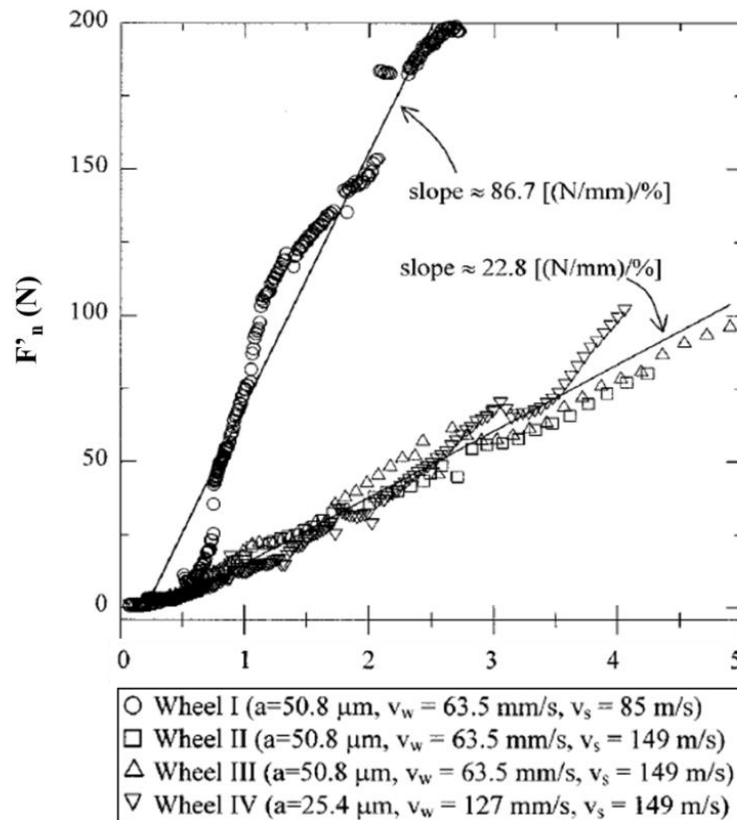


Figure 28: Evolution of normal specific grinding force with wear flat increase. 4 simulated cases are represented varying cutting parameters [121].

In this sense, a mathematical model for flat area determination taking into account mechanical and physicochemical reactions is developed [122]. In this study conical shape of alumina abrasive grains is modeled. The formulation is done regarding the grain weight loss due to the mechanical interaction and the grain weight loss because of chemical affinity of material in contact. However, this approach does not take into account the adhesion of third body to flat areas. The third body changes the contact conditions, the materials in contact change and hence, the physicochemical defined interactions are different once third body is adhered to flat grains.

Briefly summarizing, works focused on the prediction of wheel wear are mainly focused on analytical approaches. Finite element model or discrete element models are not developed to predict grinding wheel wear. Meanwhile, almost all analyzed wear models are validated with CBN or diamond grinding wheels, due to their easy characterization. However, conventional abrasives are the most used in the industry and in fact the less characterized. Furthermore, the majority of works analyzed are focused on wheel loading, grain pull out even on wear rate, which can be generated due to attritious wear and grain fracture. Wear flat is a very few simulated wear. The tribochemical reactions that lead to wear flat and the continuous changing contact conditions hinder contact modeling. Third body generation is one of the factors which have not been taken into account for wear flat simulation and on the contrary present great

influence on the contact. In this sense, the present research work is focused on the simulation of tribochemical reactions that leads to a wear flat occurrence taking into account the adhesion of third body to flat surfaces. Therefore, the contact between abrasive grains and workpiece is going to be tackled from a tribological point of view. Hereafter the simulation of the contact using DEM is assessed.

II.6.3. Application of DEM to tribological studies

Discrete element method (DEM) is a numerical method for modeling different physical states such as movement, temperature, and position, for a great number of elements. The model takes into account all the interactions between two particles or between a particle and geometries. DEM is commonly used to model discrete media, heterogeneous material, being a very useful for composite modeling [123] between others. However, the development of cohesive beam model allows the simulation of continuous materials using DEM [122], without miss the particularity of its discontinuities. This fact becomes a discrete element method on a suitable approach for the wear and fracture simulation.

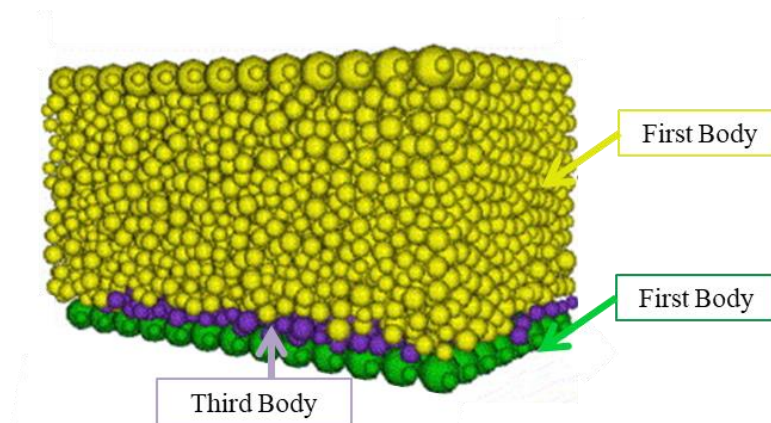


Figure 29: DEM simulation of the contact between two bodies and third body generation [124]

The contact between two bodies has been studied using both FEM and DEM. The models developed using FEM are generally based on Archard wear law [39]. However, one of the handicaps of FEM is that once the material is detached from one of the bodies, is no longer taken into account. However, in a real contact, once the material is detached the third body generated is retained between the first two bodies in contact. The adhesion force is the responsible of maintain the third body in the contact. Moreover, DEM allows maintaining also the third body in the contact as it is shown in Figure 29, being the adhesion forces well represented. In this sense, several studies were carried out modeling the contact between two bodies and the third body generation [124,125].

In parallel, abrasive processes, from polishing to grinding, are studied using DEM. The discrete abrasive particles used on polishing [126] are well modeled using discrete media, furthermore wear occurs in the contact. Grinding wheels present heterogeneous matrix, composed by pores, grains and bond. Moreover in the contact between abrasive grains and workpiece, adhesion, abrasion and fracture occur, so DEM is an adequate approach to simulate the process [115]. In this work discrete elements simulate the abrasive grains and beams properties correspond to bond properties.

Taking into account on the one hand the suitability of DEM for wear and third body characterization and on the other hand the discontinuous attribute of grinding process, in the present research work DEM is going to be used to simulate the contact between abrasive grains and the workpiece. Moreover, this model is going to be capable to reproduce the third body and its influence on the contact.

II.7. Conclusions

After a deep analysis of the state of the art relating to the wear of abrasive grinding wheels and in particular the characterization of wear flat on alumina grinding wheels, the following conclusions can be drawn:

- One of the most generalized problem in the study of wheel wear during grinding process is the overlapping of different type of wear. This fact hinders the analysis of each type of wear separately and the effect of each occurrence on the process. The isolation of each type of wear is not addressed on real grinding tests.
- The values of %A obtained in grinding tests is not very large due to the presence of grain pull out or grain breakage at the same time of wear flat increase. Therefore, the real evolution of wear flat cannot be analyzed. In order to address this problem, in the present work the isolation of wear flat from the other type of wear is going to be addressed.
- Malkin carry out a real grinding tests analyzing monocrystalline grinding wheels and varying wheel hardness, showing maximum values of wear flat about 8% for $500 \text{ mm}^3/\text{mm}$. Also the influence of dressing parameters has been studied, concluding that fine dressing promotes a more rapid evolution of wear flat than coarse dressing. Therefore, the flatness of just fine dressed abrasive grains is higher than if coarse dressing is done. However, obtained values are not too large due to the occurrence of the other type of wear at the same time.

- Form the different works analyzed, can be shown the dissimilarities between analyzing wear flat on CBN or diamond grinding wheels and on alumina grinding wheels. Almost all methodologies to characterize or quantify wear flat are developed on CBN or diamond grinding wheels. However, the characteristics of alumina abrasive grains and the corresponding bond hinder the extrapolation of CBN methodologies to alumina grinding wheels.
- Likewise, there is the necessity of characterizing wear flat in alumina grinding wheels because are the abrasive type used in the industry. Therefore, in the present work the evolution of wear flat on alumina grinding wheels is going to be studied. Moreover, from the analyzed methodologies to quantify wear flat, the technique of coaxial light is going to be applied.
- In order to study the effect of wear individually, single grain tests or tribological tests are developed. However, the extrapolation of achieved results under controlled parameters on these specific test benches to real grinding process is not immediate.
- The most relevant works to analyze the contact between alumina and steel are developed using pin-on-disk tribometer. However, one of the limitations of this kind of test bench is the contact conditions which can be reproduced.
- While on conventional grinding tests 30 m/s sliding speeds and 1-2 GPa contact pressure are achieved, the heaviest contact conditions achieved on pin-on-disk are 12 m/s and 320 MPa, but not achieved at the same time.
- Despite Klocke develops the most complete study of alumina-steel applied to grinding process, two shortcomings are detected. On the one hand, Klocke develops pin-on-disk test analyzing SG alumina, in which $s=2\text{m/s}$ and $p_r=0.5\text{-}1.5\text{ GPa}$. However, the contact conditions are not clearly exposed in this study. Thus, in the present work a new design of pin-on-disk tribometer is going to be developed and it is going to be mounted on a real grinding machine in order to achieve $s=30\text{ m/s}$.
- On the other hand, in the same study, the extrapolation of SG wear results from the tribometer to grinding process is performed, without consider the differences in the thermal cycle suffered by the alumina. In the present work, this limitation is going to be tackled using real grinding wheel as a disk in contrast with pin of raw alumina used by Klocke.
- On the analyzed experimental works, grinding and tribological tests, the influence of third body generation and its adhesion to worn alumina is observed. The third body reduces friction coefficient changing contact conditions between alumina and steel, promoting sliding friction.

- Likewise, depending on the crystalline structure analyzed the composition of third body present variations. Malkin on grinding tests study wear flat of monocrystalline alumina, showing FeAl_2O_4 the main component of the third body. In contrast, Klocke on tribological tests found iron oxide as the main composition of the third body.
- Regarding wear modeling, wear flat have not been deeply analyzed. The few works referred to wear flat are based on analytical models, without taking into account the influence of third body in contact conditions variations.

Finally, once the shortcomings in the state of the art are identified, in the present work the wear flat of alumina is going to be deeply analyzed. Firstly, the occurrence of wear flat and its quantification is going to be addressed on alumina grinding wheels. Likewise, the influence of crystalline alumina and of grinding parameters is going to take into account. The worn alumina is going to be deeply analyzed in order to better understanding of third body generation in the contact. Moreover, tribological tests are going to be carried out in order to control contact conditions during alumina wear. And after that, the wear of alumina abrasive grain is going to be modeled in order to study the influence of temperature in the contact and wear evolution and to model the third body adhered to the flat abrasive grain and its influence in the contact.

Chapter III: On the development of
wear flat occurrence on alumina
grinding wheels during grinding

III. ON THE DEVELOPMENT OF WEAR FLAT OCCURRENCE ON ALUMINA GRINDING WHEEL DURING GRINDING

III.1. Introduction

In the review of the state of the art it is shown the difficulties of grinding process and wheel wear characterization mainly for the randomness of grinding wheel and also for the heavy contact conditions between abrasive grains and the workpiece. In this chapter specific grinding experimental tests are developed in order to achieve the closest conditions to real grinding process, implementing real sliding speed and using a real grinding wheel. Therefore, the present experimental work primarily is focused on the analysis of the occurrence of wear flat in grinding wheel during grinding.

Hereafter it is detailed the experimental work and worn abrasive surface analysis. To this end, a designed methodology is decisive to isolate wear flat phenomena from other type of wears, while the typical contact conditions of real grinding operations are reproduced. Extremely hard wheel is used so that the development of wear flat emerges as the predominant effect. Experimental tests are implemented on three different crystalline structures of alumina, comparing the development of wear flat and its influence on grinding parameters. Additionally, a deep analysis of worn wheel surface is carried out. As it is known, wear flat is a tribochemical nature wear [27], therefore the analysis of worn surface and third body is of interest in order to understand the main wear mechanisms that leads to wear flat. Showing attention on the look of flat grains and on the quantity and composition of third body adhered to flat abrasive grains it is also possible to know the influence of crystalline structure of abrasive grains in the wear flat occurrence.

III.2. Experimental set up for grinding tests

As mentioned before, the main objective of these experimental grinding tests is to isolate the wear flat from other type of wears that take place in the grinding wheel. Both, grain pull out and grain fracture, are prevented on these tests to ensure the analysis of wear flat with grinding wheel and grinding parameters design. On the one hand, to avoid grain pull out, thus bond breakage, a very hard grinding wheel, grade R, and hard workpiece material are proposed. On the other hand finishing grinding parameters are chosen, but always in the range of industrial

parameters. Thus, the minimization of forces on each abrasive grain during grinding and hence the minimization of grain fracture are achieved.

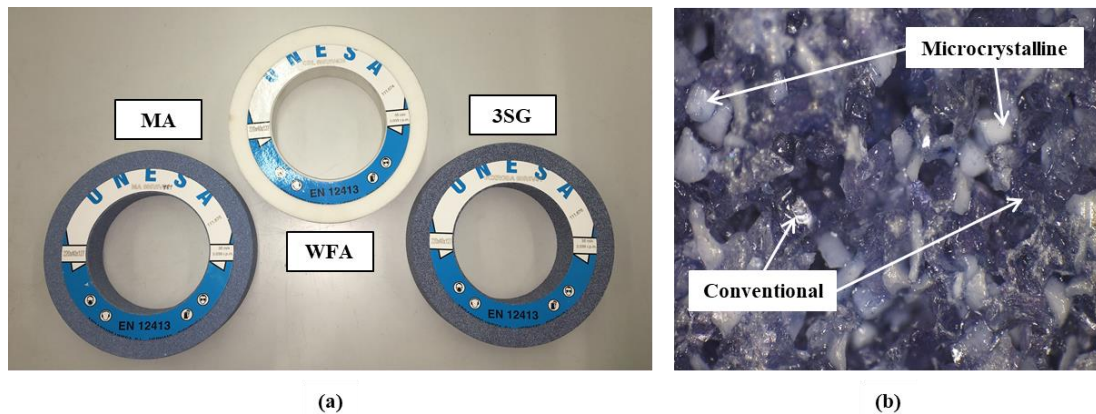


Figure 30: (a) The 3 grinding wheels used during tests, (b) dressed 3SG grinding wheel surface combining conventional an microcrystalline abrasive grains.

Regarding grinding wheel, further to observe wear flat in more detail close structure is chosen. Therefore, abrasive grains of 250 μm of diameter are embedded on a vitreous bond matrix leading to a close and hard grinding wheel with the following nomenclature 60R6V89. The dimension of grinding wheels is 220x40x127 mm, and they are manufactured by UNESA. S.A. Alumina abrasive grains are studied, being the most common abrasive in the industry due to its versatility and low cost comparing with superabrasives.

Table 3: Chemical composition of AISI D2

C	Si	Mn	Cr	Mo	V
1.55	0.3	0.4	11.3	0.8	0.8

Moreover, to analyze the influence of crystalline structure on wear flat generation, conventional alumina, also called white fused alumina (WFA), monocrystalline alumina (MA) and microcrystalline alumina (3SG) are studied; in Figure 30 (a) the three grinding wheels are shown. In the case of microcrystalline alumina, the 30% of abrasive grains are SG grains, they are mixed with conventional grains in order to decrease the friability of the wheel, as shown in Figure 30 (b), when microcrystalline and conventional grains can be differentiate on a just dressed 3SG wheel surface.

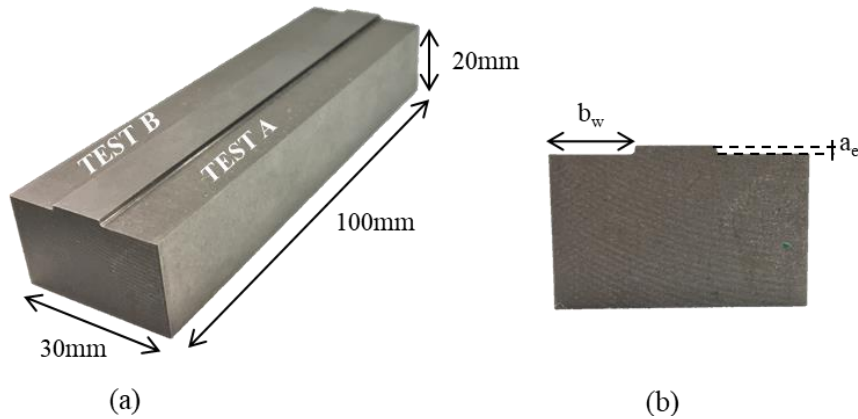


Figure 31: Workpiece (a) dimensions and two tests carried out, test A and test B and (b) side view of the workpiece highlighting grinding width and depth of cut of the grinding tests.

In addition to the grinding wheel configuration, workpiece material is also of relevance. Hard grinding wheel together with hard workpiece material promotes the occurrence of wear flat on the grinding wheel surface. Tempered AISI D2 of hardness of 60 ± 2 HRC is chosen to carry out grinding tests. AISI D2 is a high carbon and high chromium tool steel characterized by high wear resistance, high compressive strength and high stability in hardening.

Table 4: Surface grinding machine main characteristics

SURFACE GRINDING MACHINE ORBIT CNC 36

Spindle speed	6500 rpm
Power	8.5 KW
X axis max. speed	40000 mm/min
Y axis max. speed	3750 mm/min
Z axis max. speed	4000 mm/min
Work area	300x1000x600 mm
Ø max. wheel	400 mm



In Table 3 the composition of this tool steel is summarized. These properties make AISI D2 suitable for the manufacture of applications when cutting thicker and harder materials; when forming and where high impact loads are involved, such as metal forming operations, die forming, rolling or forging. The test workpiece dimensions are 30x100x20 mm as shown on Figure 31 (a).

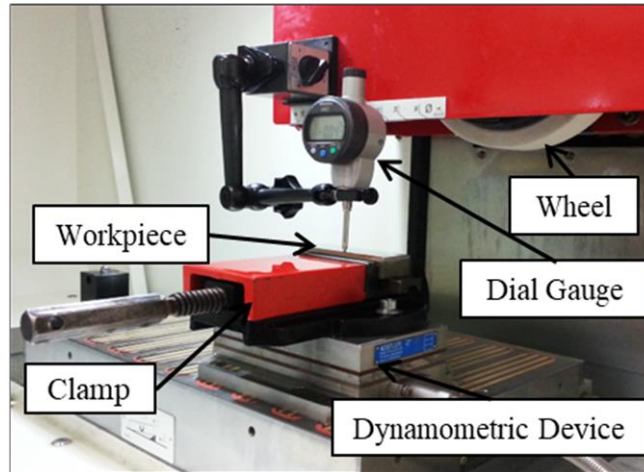
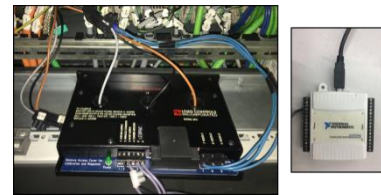


Figure 32: Set up of wheel, workpiece on a clamp, dynamometric device and dial gauge on grinding machine

Table 5: Devices used for real parameter measurement during the tests




Parameter	Instrument
Power consumption	Power meter: <i>Load Control Incorporated UPC</i> Acquisition card: <i>National Instruments</i>
Grinding forces	Dynamometric device: <i>Kistler 9257B</i>
Real depth of cut	Dial gauge <i>Mitutoyo</i>



The experiments are carried out on a universal surface grinder *Blohm Orbit CNC 36*, its main characteristics are summarized in Table 4. The grinding machine is equipped with a static diamond. For these tests a single point diamond is used for dressing of grinding wheel surface in order to achieve the same surface reference in every case of study. The grinding tests are carried out on a wet atmosphere; using 5% oil water based cooling with a flow rate of 45 l/min.

During tests, power consumption and grinding forces are measured; data acquisition devices are described on Table 5. Required software for data acquisition is *LabView* for power consumption acquisition, being 100 Hz sampling frequency, and *DynoWare* for grinding forces acquisition with a sampling frequency of 500 Hz. Furthermore, real depth of cut is measured for every grinding passes using a dial gauge, taking as a reference plane the part of the workpiece which have not been ground. The set-up of the workpiece, clamp and dynamometric device mounted on the grinding machine work area and dial gauge on measurement position can be shown in Figure 32.

Table 6: Main equipment used for wear flat characterization and surface analysis.

NAME	CHARACTERISTICS	
<i>Optical microscope</i> PCE MM200	<ul style="list-style-type: none"> • Resolution:1280 x 1024 pixels • Magnification: 10x-200x • Light source:4 white LEDs 	
<i>Confocal microscope</i> Leica DCM 3D	<ul style="list-style-type: none"> • Z range: 0.1nm-17mm • XY scanning by Microdisplay (stiching) • Magnification: 5x-150x • FOV 2500-80 μm, X/Y resolution 3-0.3 μm) 	
<i>Scanning Electron microscope (SEM)</i> JOEL JSM-7000F	<ul style="list-style-type: none"> • Resolution: 1nm(15KV)-1.4nm(1KV) • Magnification: 25x-1,000,000x • Accelerating voltage: 0.1KV-30KV 	

Wheel surface analysis is addressed using three different microscopes: optical microscope, confocal microscope and scanning electron microscope (SEM) as shown in Table 6. This table gathers the name of used microscopes and their main characteristics and limitations. 2D images

taken with optical microscope are processed using a specific module, *Image Analysis module*, which is implemented on *Leica Map* software. This software is used to detect wear flat areas and to quantify the %A applying different filters, which are going to be detailed in *Section III.3.1*. Moreover, test pieces to carry out SEM and EDXA analysis have to be exhaustively conditioned, firstly test pieces dimensions have to be 10x10x10 mm, and analyzed surfaces have to be conductor, the metallization of wheel surface is required.

III.3. Grinding tests methodology

Methodology is divided in wear flat generation and its quantification and on wheel surface analysis. Firstly, wear tests are presented, tests parameters and the steps to generate and measure wear flat areas are explained. Secondly, once tests are finished the analysis of *worn* surface is carried out, comparing *new* and *worn* states of abrasive grains and also getting surface roughness parameters in order to identify differences between both states.

III.3.1. Methodology for wear flat generation and quantification during grinding

The current experimental work involves four grinding tests for the three abrasive grinding wheels previously described. During the test wheel speed (v_s) is maintained constant at value of 30 m/s, the speed usually used on conventional grinding. However, workpiece speed (v_w) and programmed depth of cut (a_e) are varied in order to study their influence on wear flat occurrence. The selected values of a_e are suitable due to the extremely hard wheel used. Programmed parameters of the four tests are built in Table 7. Apart from the mentioned parameters, specific material removal rate obtained from programmed a_e Eq.7 and speed ratio Eq.8 are shown in the table. Q'_w is in the range of conventional grinding for the four designed tests, however, tests 1 and 2 present $q_s=120$, just in the limit of thermal damage in the workpiece. At time of tests design, wear flat occurrence is considered but workpiece burn is not taken into account.

$$Q'_w = a_e v_w \quad \text{Eq.7}$$

$$q_s = \frac{v_w}{v_s} \quad \text{Eq.8}$$

Tests are carried out with b_w of 10 mm, on the one hand allowing the measurement of real a_e and on the other hand corroborating that the volumetric wear of grinding wheel is negligible. The scheme of tests is shown in Figure 33, differentiating worn part of the wheel, marked in red in Figure 33 (b) and just dressed wheel, which is not going to contact with the workpiece during the tests (marked in green). For wheel analysis, wheel surface is used as a reference.

Table 7: Grinding tests real parameters

Test	v_s [m/s]	v_w [mm/min]	a_e Prog. [μm]	Q'_w Prog. [$\text{mm}^3/\text{mm}\cdot\text{s}$]	q_s
1	30	15000	10	2.5	120
2	30	15000	15	3.8	120
3	30	25000	10	4.2	72
4	30	25000	15	6.3	72

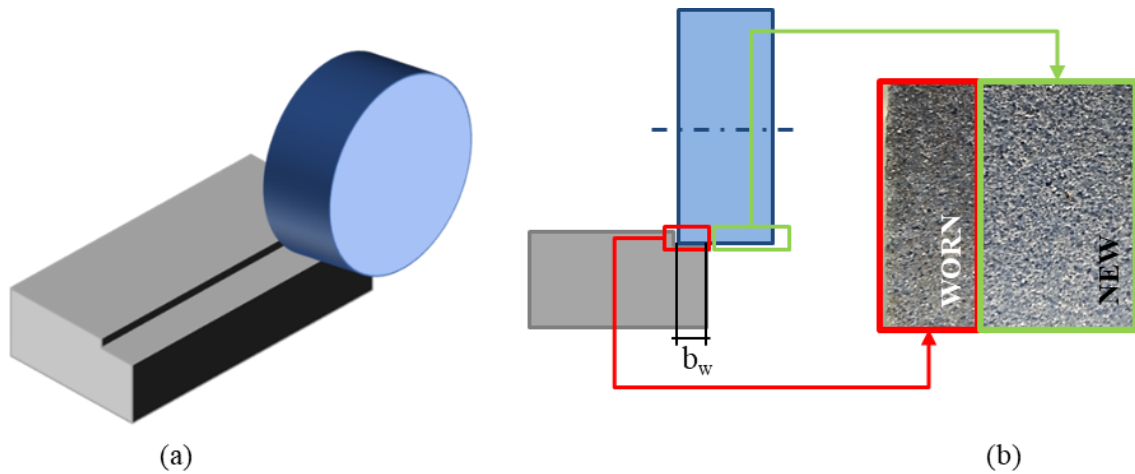


Figure 33: (a) Wheel-workpiece positioning during tests and (b) tests scheme in order to analyze just dressed and worn surfaces

Accumulative grinding tests were carried out in order to study the evolution of wear flat during grinding. Thus, grinding wheel is only dressed at the beginning of the tests in order to have information for initial surface and allowing the later comparison with *worn* surface. Meanwhile, the starting wheel surface for the three studied wheels is the same, dressed with the same parameters, which are built in Table 8. Small dressing depth (a_d) is selected to wheel conditioning, as the wear flat occurrence is higher using fine dressing parameters than coarse dressing parameters [81].

Table 8: Dressing parameters

v_s [m/s]	v_d [mm/min]	a_d [μm]
30	250	10

Therefore, the first step to carry out grinding tests is dressing wheel surface, being the only time which is going to be dressed during a complete tests. During a complete tests a total of $100 \text{ mm}^3/\text{mm}$ are removed, thus the wear flat evolution is studied from 0 to $100 \text{ mm}^3/\text{mm}$. Comparing with other studies which are focused on wear flat evolution, the final of the tests regarding removed material happens quickly. On works carried out by Malkin workpiece removed specific volume is 5 times higher [27]. This fact is due to the hardness of grinding wheel, leading to a higher wear flat occurrence than on Malkin set up.

In order to an adequate evaluation of wear flat generation, the surface images are taken every $10 \text{ mm}^3/\text{mm}$, so, for each test the wear flat is measured in 10 different states. Furthermore, to minimize the measurement error, on each state worn wheel surface is measured in 6 different zones. Regarding real depth of cut, it is measured at every pass, and after the measurement spark out is done until achieve programmed a_e . Meanwhile, the surface is conditioned for the next grinding pass providing a control of real a_e . To carry out the spark out on every grinding passes allows the correct correlation between grinding forces and real a_e . In Figure 34 the methodology to carry out accumulative grinding tests is schematically represented. The block in red represents one of the 10 blocks of $10 \text{ mm}^3/\text{mm}$ in which is divided a complete test. As said, the surface measurement is done after each one. In green is represented a real depth of cut, inside of one block. Depending on the test, thus if a_e is 10 or $15 \mu\text{m}$, the number of passes to achieve a complete bock varies.

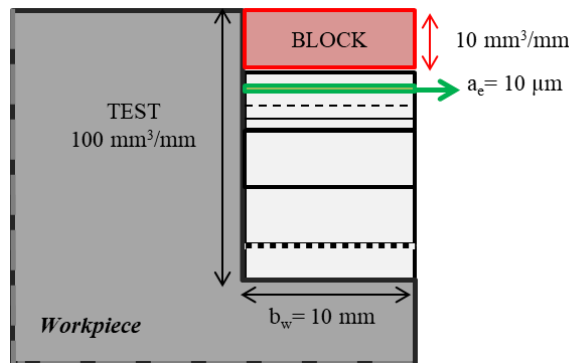


Figure 34: Methodology of accumulative grinding tests

Quantification of wear flat is conducted by analyzing 2D images taken during the test on grinding machine using an optical microscope as shown in Figure 35. The images present a total of 192,000 pixels on an area of $2.5 \times 1.9 \text{ mm}$. In the first row of Table 9 the image resolution and magnification are detailed. The image acquisition corresponds to the first step of the quantification. Images of just dressed (from now on *new*) and worn wheel surface at 10 different states of wear are taken during the experiments in order to analyze the complete evolution of

wear flat with workpiece material removal. The last state of wear is going to be named *worn*, referring to the state at which $100 \text{ mm}^3/\text{mm}$ has been removed.

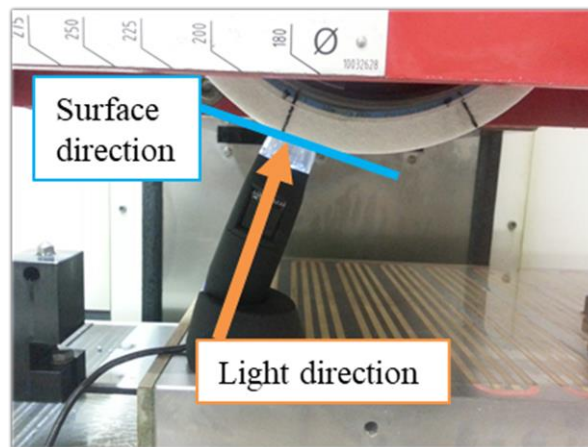


Figure 35: Optical microscope set on grinding machine. Light direction is perpendicular to wheel surface in order to apply coaxial light technique.

The images during grinding tests are taken using the coaxial light technique. As it is analyzed on *Section II.5.3*, this technique is the most used for researchers [35] to wear flat detection on alumina. It is based on a light reflection on wheel surface. The light underscore perpendicularly to wheel surface, as shown in Figure 35. If the light shines on no flat surface the light reflects on any direction as Figure 36 (a) shows and the real color of the 2D image is achieved. On the contrary, if the light shines on flat surface Figure 36 (b), it reflects perpendicularly to flat area, the microscope receives the light rays and on the image white or light and bright color is gathered. The light reflects on flat surface, both if third body is adhered to flat grains or not, therefore wear flat are easily identifiable as brightest area of the images. In the case of third body adhered on the flat grains, the color tends to be yellow instead of being white shine area. However, the identification is possible in both, if third body is adhered or if it is not.

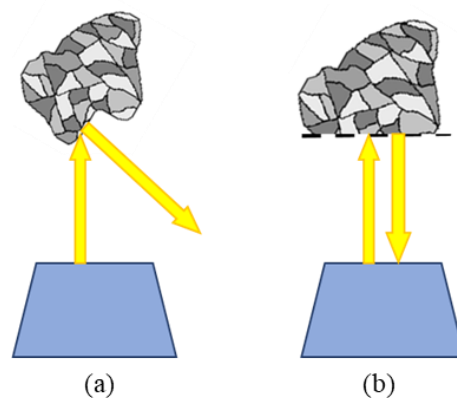


Figure 36: Coaxial light of microscope (a) light hitting a rough surface (b) light hitting flat surface

The last step to quantify wear flat areas is processing raw 2D images taken, which is shown in Figure 37 (a). Specific module for image analysis of Leica Map software is used. For this analysis a binary segmentation technique is used in order to quantify flat areas. Pixel sets are identified and extracted as area corresponds to flat abrasive grains. The identification of pixels that correspond to flat abrasive grains or to third body adhered is carried out selecting adequate range of colors. Leica software allows the detection of more relevant colors of the image selecting the range of colors that correspond to flat areas. In this sense, wear flat areas presenting a white yellow color are well detected as revealed in Figure 37 (b), when wear flat is marked in red.

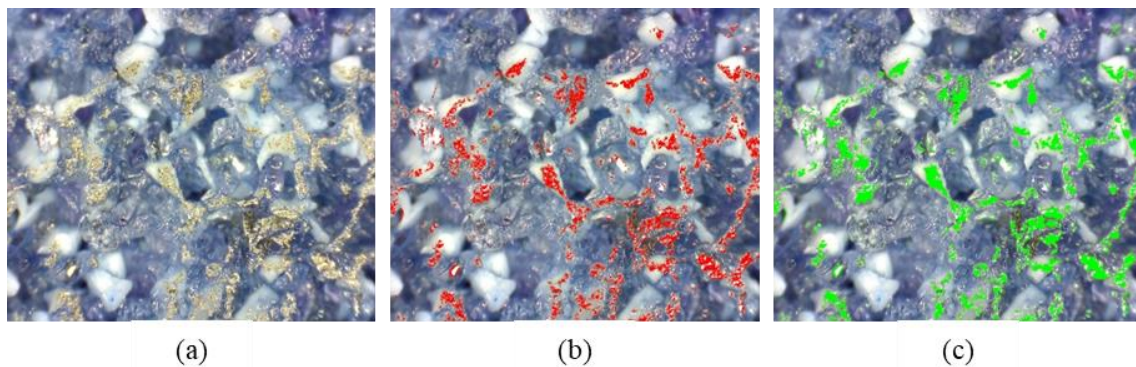


Figure 37: Steps for wear flat quantification (a) raw 2D image, (b) automatically flat areas detection and (c) filtered image.

Meanwhile, to achieve good results of %A quantification, the images were treated through the implementation of two filters. The aim of the first filter is to avoid brightness that does not correspond to wear flat areas. This filter deletes areas smaller than a set of 8 pixels, which are considered to have a brightness that is due to the light reflection on surfaces that are not flat. Areas of 8 pixels corresponding to $62.72 \mu\text{m}^2$ are negligible comparing with abrasive grain size of $250 \mu\text{m}$ in diameter. The second filter fills in the gaps inside one area due to measurement or brightness identification errors, that is, it adds a pixel to the wear flat area if all pixels around it correspond to a wear flat area. In Figure 37 (c) a filtered image is presented, green areas correspond to wear flat. Therefore, the quantification of %A is done with the number of pixels marked in green regarding the total of pixels in the image.

III.3.2. Methodology for wheel surface analysis

Once grinding tests are finished and the wear flat is quantified, in order to enhance the study of the surface analysis, it is worth analyzing the wheel surface topography. In this case wheel surface is analyzed in two states, *new* and *worn*, being not analyzed the intermediate states, because of the impossibility to measure the wheel surface without destructing the wheel. The

dimension of working area of used microscopes is much smaller than the dimensions of grinding wheel, particularly in the case of SEM analysis.

On the one hand, grinding wheel surface is measured using 3D confocal microscopy, obtaining wheel topography and 3D functional roughness parameters. The measurements are carried out with x10 magnification and a height resolution of 2 μm as it is gathered in Table 9. The studied area is of 3.6x4.75 mm, it is achieved using stitching function on the confocal microscope, taking 3x5 images with 10% of overlapping area. On the other hand, SEM and EDXA analysis complement the surface study. Images at two different magnifications are taken. In Table 9 the main parameters used for obtaining the images are built. At magnification of 50x with analyzed area of 1.83x2.26 mm, which permit comparing *new* and *worn* surface and the detection of third body deposition on flat surface. Complementarily, at magnification of 500x and analyzed area of 183x226 μm the details are shown, such as the microcrystal on SG abrasive grains and the flatness of the worn grains. Moreover, EDXA analysis of the third body is applied to determinate its main components. This analysis also allows the identification of materials that composed flat surface, which can be third body, abrasive grain and also bond material.

Table 9: Parameters used to wear flat characterization and wheel surface analysis on the three microscopes.

UTILITY	PARAMETERS	STUDIED AREA (XY)
On machine wheel surface images to measure %A	Magnification x200 Resolution 2.8 $\mu\text{m}/\text{pix}$	2.5x1.9 mm
Wheel topography and 3D functional roughness parameters	Magnification 10x Z resolution 2 μm	3.6x4.75 mm
High magnification and EDXA analysis to characterize 3rd Body	Magnification x50-x500-x1000 at 20 KV	1.83x2.26 mm (x50) 183x226 μm (x500)

III.4. Experimental results

In this section, firstly, the influence of grinding parameters on wear flat generation and occurrence is discussed. For the three types of abrasive grinding wheels, an analysis is presented regarding wear flat evolution with specific material removed, showing the influence of crystalline structure of abrasive grains in wear flat evolution. Furthermore, the influence of wear flat on grinding forces and the friction coefficient is analyzed, showing the conditions changes.

Finally, an in-depth evaluation of wheel topography is presented. 3D roughness surface parameters, mainly Abbott-Firestone curve, and S_k , S_{pk} and S_{vk} , are analyzed in order to see dissimilarities between *new* and *worn* surfaces. However, this study is not enough to understand tribochemical phenomenon that leads to attritious wear and it is completed with more detailed but qualitative analysis of grinding wheel surface, obtaining also the composition of third body.

III.4.1. Grinding analysis

III.4.1.1. The importance of measuring real depth of cut

In Section III.2 it is continuously remarking the real and programmed depth of cut due to programmed a_e . It is rarely achieved during grinding process despite carrying out the tests on a high quality grinding machine. Therefore, before starting with the discussion about the influence of grinding parameters, it is of interest to justify the differences obtained between programmed and real depth of cut. Specific removal rates from 2.5 to 6.3 mm³/mm s are achieved with programmed grinding parameters. On the contrary, after measuring real a_e , specific removal rates are reduced for every test around 70 % regarding programmed ones. Now the highest Q'_w is of 2.08 mm³/mm s instead of 6.3 mm³/mm s as it is shown on Table 10. The main reason for this behavior is probably to be found in the elastic deflection suffered by the machine spindle during grinding. In the grinding process, this effect is widely known. However the discrepancies between real and programmed values are not so large. Therefore, in the case of study, this effect is encouraged by the considerable hardness of the grinding wheel and the characteristics of the tests. So, for now on, the results and conclusions are going to be referred to real cutting parameters, thus to real a_e .

Table 10: Differences between real and measured depth of cut and specific material removal rate.

Test	a_e Prog. [μm]	a_e Real [μm]	Q'_w Prog. [$\text{mm}^3/\text{mm}\cdot\text{s}$]	Q'_w Real [$\text{mm}^3/\text{mm}\cdot\text{s}$]
1	10	3	2.5	0.75
2	15	5	3.8	1.25
3	10	3	4.2	1.25
4	15	5	6.3	2.08

III.4.1.2. Error in wear flat quantification

Regarding wear flat quantification, and in order to determinate the error in the measurements, 2D images corresponding to *Tests 1* are measured three times by different people. Thereby, the human factor when selecting the range of color that corresponds to wear flat is also taken into account. The images of all studied crystalline structure are represented as shown in Figure 38. The error of each type of grinding wheel presents different values, from 11.7% of error to WFA for 3.37% of error for MA. The main reason is the color of each abrasive wheel and of the abrasive grains. Studied WFA wheel is white, hindering the detection of wear flat areas. In contrast, 3SG wheel combine white opaque and blue translucent grains and MA only is composed of blue translucent grains, helping wear flat identification.

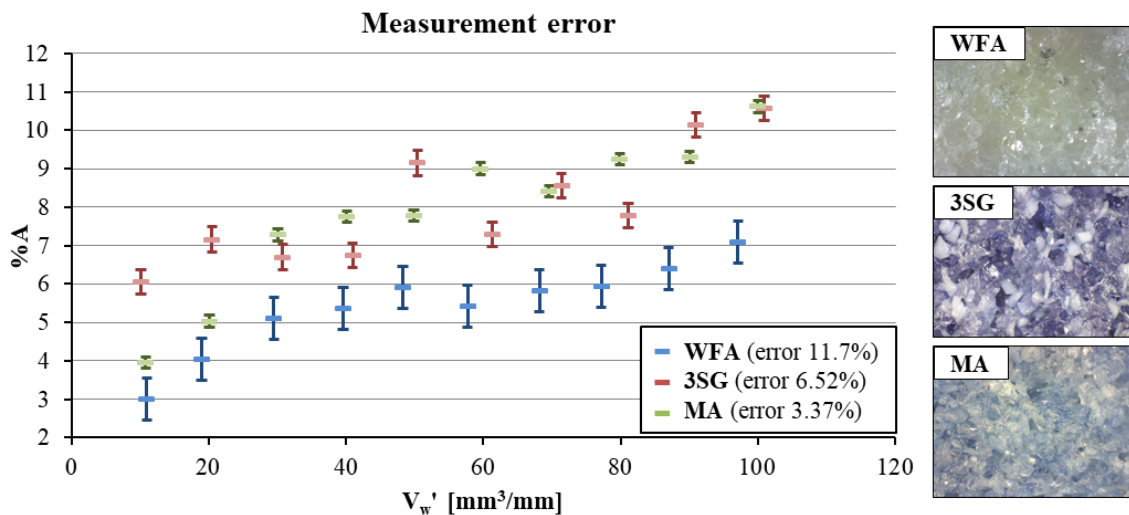


Figure 38: Evolution of wear flat with specific material removal representing the error of wear flat measurement corresponding to *Test 1* and the differences of studied *new* wheel surfaces

III.4.1.3. Influence of crystalline structure of abrasive grains on wear flat evolution

Once the error is determined, the effect of both crystalline structure and grinding parameters are going to be deeply analyzed in the following paragraphs. It is noteworthy that in all the cases studied here an almost linear trend of wear flat growth can be seen, which is entirely compatible with the results obtained by Malkin [27,81]. On the contrary, regarding the initial value of % A achieved in every case, on each test this value for the first measurement at 10 mm³/mm was observed to be between 4 and 6 %. Previous studies report values of around 2-3 % of wear flat for the same V_w' . Therefore, here achieved values are relatively high in comparison with previous ones. The differences could be explained primarily in terms of the stringent conditions used to promote wear flat. The high hardness and closed structure of designed grinding wheels, together with the fine dressing parameters described in *Section III.3.1* lead to a smooth surface.

Consequently, initial surfaces do not present very sharp appearance due to the dressing and wheel conditions. Moreover, in the initial phase of testing the most sharpened grains lose their cutting ability, as in the typical wear pattern of cutting tools, presenting rapid wear at the beginning of the tool life. Accordingly, just in $10 \text{ mm}^3/\text{mm}$ of specific removed material, the %A value was already as high as 6%.

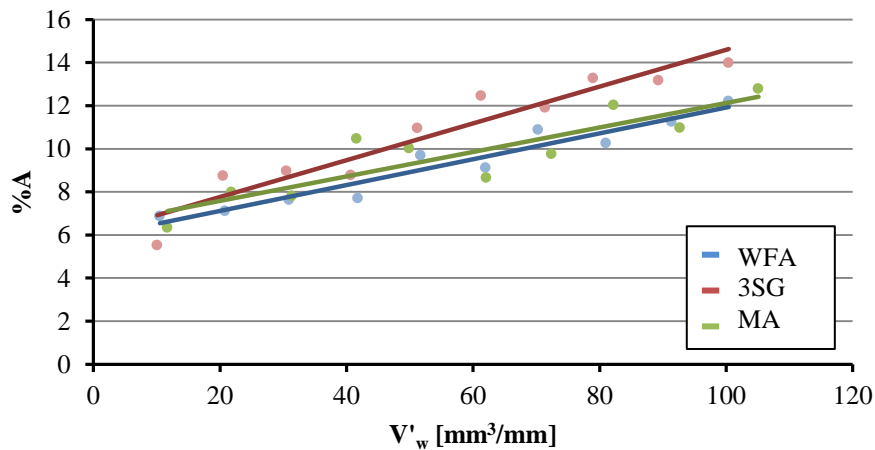


Figure 39: Influence of crystalline structure of abrasive grains on wear flat evolution whit specific material removal for $v_w=15000\text{mm}/\text{min}$ and $a_e=5\mu\text{m}$ (*Test 2*).

In Figure 39 the evolution of wear flat with specific material removal is represented for *Test 2*, being real a_e of $5 \mu\text{m}$ and v_w of $15000 \text{ mm}/\text{min}$. Only *Test 2* is represented in order to study the influence of crystalline structure on wear flat evolution because the %A increase behaves similarly for every studied case. Regarding the maximum value of %A achieved, 3SG wheel shows higher values than WFA and MA. For instance, on *Test 2*, maintaining constant grinding parameters, the maximum %A for WFA and MA is approximately 11 % whilst for 3SG grinding wheel this value is about 14 %. This result indicates that 3SG wheel present higher tendency to become flat than the other two studied crystalline structures when other types of abrasive wear are isolated.

These findings are also in accordance with the work of Klocke [16]. In this study the author pointed out that thermal conductivity of the SG abrasive grains was smaller than that of WFA grains due to the greater amount of crystal edges in the first case. Monocrystalline alumina is not taken into account on his study. However, following the same reasoning of amount of crystal edges, MA does not present any crystal edges and hence the thermal conductivity has to be closer to WFA thermal conductivity than to SG. This fact is extremely important in wear flat generation. The temperatures in the grain-workpiece contact will be higher in SG grains than in the case of WFA and MA grains because of the smaller heat conductivity. Taking into account

that the generation of wear flat is a tribochemical issue, the higher temperature will promote wear flat occurrence.

Moreover, it is generally accepted, particularly in the industry, that SG abrasive grains present the ability of self-sharpening. This affirmation is true if the cutting parameters are adequate to each specific grinding operation. Thus, if roughing parameters are established using SG grinding wheel self-sharpening occurs due to the grinding forces on each abrasive grain are big enough to break the grain. However, as occurs in the present work, under the same grinding conditions, finishing conditions, low values of a_e generate forces that are not sufficiently strong to produce breakage of microcrystals and self-sharpening of 3SG wheel is avoided. It can be concluded that, due mainly to the rubbing phase in the grinding process, SG alumina presents a higher tendency to develop wear flat than WFA and MA.

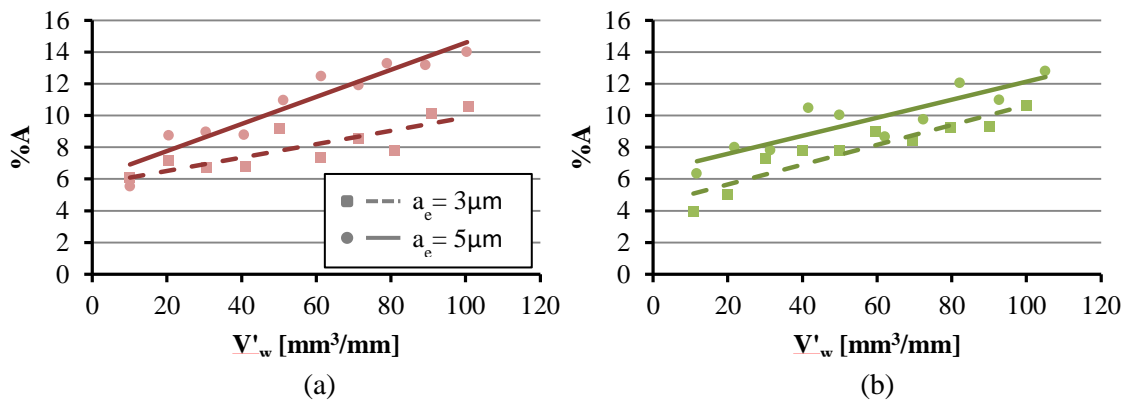


Figure 40: Influence of real depth of cut on wear flat evolution with specific removed material. (a) Results of 3SG grinding wheel and (b) results of MA grinding wheel.

III.4.1.4. Influence of grinding parameters of abrasive grains on wear flat evolution

Regarding the influence of grinding parameters, both real a_e and v_w are deeply analyzed. In order to analyze the influence of real depth of cut, workpiece speed is maintained constant. In Figure 40 the results corresponding to *Tests 1* and *Tests 2* are plotted for 3SG grinding wheel Figure 40 (a) and for MA wheel Figure 40 (b), being $v_w=15000$ mm/min constant. It is shown that regardless the crystalline structure of abrasive grains, generation of wear flat increase with real a_e . In the case of 3SG grinding wheel, wear flat starts for both depth of cut at 6 % reaching in the case of $a_e=3\mu\text{m}$ 10.5 % of flat areas and for $a_e=5\mu\text{m}$ maximum wear flat is of 14 % Figure 40. Therefore, an increase of 25 % of wear flat at the end of the tests is observed with an increase of a_e from $3\mu\text{m}$ to $5\mu\text{m}$. Similarly, on MA grinding wheel an increase of 20 % is achieved at the end of the tests, being the 13 % the maximum flat area for MA and $a_e=5\mu\text{m}$. Moreover, it is observed that the starting value for flat area for MA wheel is different depending

on the real depth of cut, being of 4 % for $a_e=3 \mu\text{m}$ and 6 % for $a_e=5 \mu\text{m}$. Higher depth of cut implies for MA higher %A not only at the final of the test, but also at the beginning, showing almost the same slope regardless real a_e .

For all type of abrasive grains studied, it is necessary to take into account that the correlation between %A and a_e will only occur when the grinding forces are lower than the retaining forces of the grains. The high hardness of the grinding wheel (R) and small real depth of cut implies that in the present study the correlation of %A and a_e is valid. For other cases in which grinding forces are higher than retaining forces, when using, for instance, a very soft grinding wheel, grain pull out will be the predominant source of wear, and the %A measured would decrease with a_e .

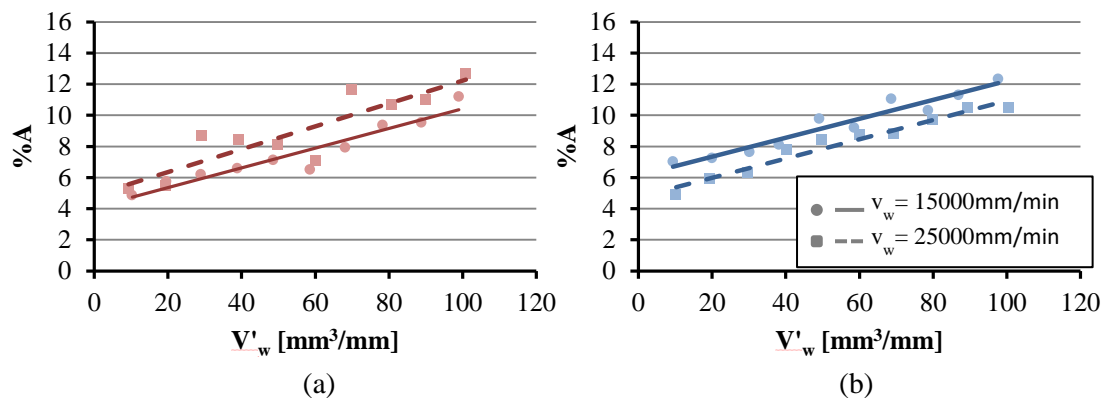


Figure 41: Influence of workpiece speed on wear flat evolution with specific removed material. (a) Results of 3SG grinding wheel and (b) results of WFA grinding wheel.

With concerns to workpiece speed, in Figure 41 it is plotted the evolution of wear flat with specific removed material maintaining constant $a_e=5 \mu\text{m}$. Thus, *Test 3* corresponding to $v_w=15000 \text{ mm/min}$ and *Test 4* $v_w=25000 \text{ mm/min}$ are represented. In the case of 3SG wheel (Figure 41 (a)) higher %A is reached for higher workpiece speed. In contrast, for WFA (Figure 41 (b)) grinding wheel higher values of %A correspond to lower v_w , and for MA wheel the behavior of workpiece speed corresponds to WFA behavior. The slope of represented tests is similar, however, if the representation for $a_e=3 \mu\text{m}$ of 3SG grinding wheel had been chosen, differences in the trends depending on v_w have been shown. The pattern of wear flat evolution presents a higher slope for higher workpiece speed in this case of study. In view of presented discrepancies in the tendencies of workpiece speed on wear flat occurrence, there is not possible to undertake a clear influence of v_w in wear flat generation.

In the tests carried out, values achieved in the first measurements at $10 \text{ mm}^3/\text{mm}$ vary from 4 % to 7 % while the values corresponding to the last worn state are from 10 % to the maximum of

14 %. These values are significantly higher than those described in the study by Malkin [27], where values of approximately 6 % were found for $100 \text{ mm}^3/\text{mm}$. However, this difference can be explained mainly in terms of the grinding wheel hardness, in the present work R, and the aim to promote wear flat in the current study. Even so, the results presented here are in agreement with the findings confirmed in the study by Malkin, verifying that the %A increases with wheel hardness.

III.4.1.5. Wear flat influence on grinding forces and friction coefficient

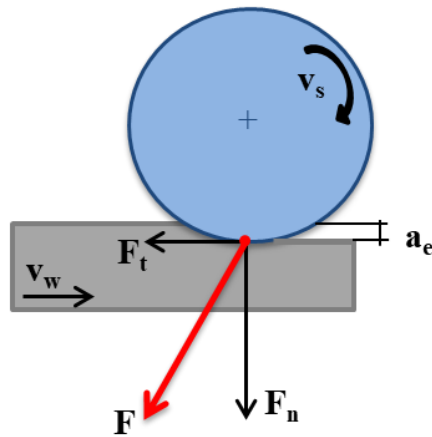


Figure 42: Grinding kinematic, force directions representation.

In Figure 42 grinding kinematic is represented, showing the directions which are taken into account in order to analyze the influence of wear flat on forces involved in the process. In Figure 43 normal and tangential specific grinding forces are plotted for every crystalline structure. The results of this graphic correspond to *Test 2* with $a_e=5 \mu\text{m}$ and $v_w=15000 \text{ mm/min}$. Hereafter, the results presented from *Test 2* are representative of each of the tests carried out. Thus, given forces for WFA, MA and 3SG show the similar evolution for the four grinding tests carried out.

Regarding specific force values, about 30 % higher normal and tangential values are achieved on *Test 2* and *Test 4* comparing with *Test 1* and *Test 3* respectively, due to the increase of depth of cut from $3 \mu\text{m}$ to $5 \mu\text{m}$. Therefore, higher depth of cut leads to higher specific normal and tangential forces. However, the increase of grinding forces due to workpiece speed is less significant than due to real a_e . Specific force values present an increase lower than 10 % if v_w increase from 15000 to 25000 mm/min.

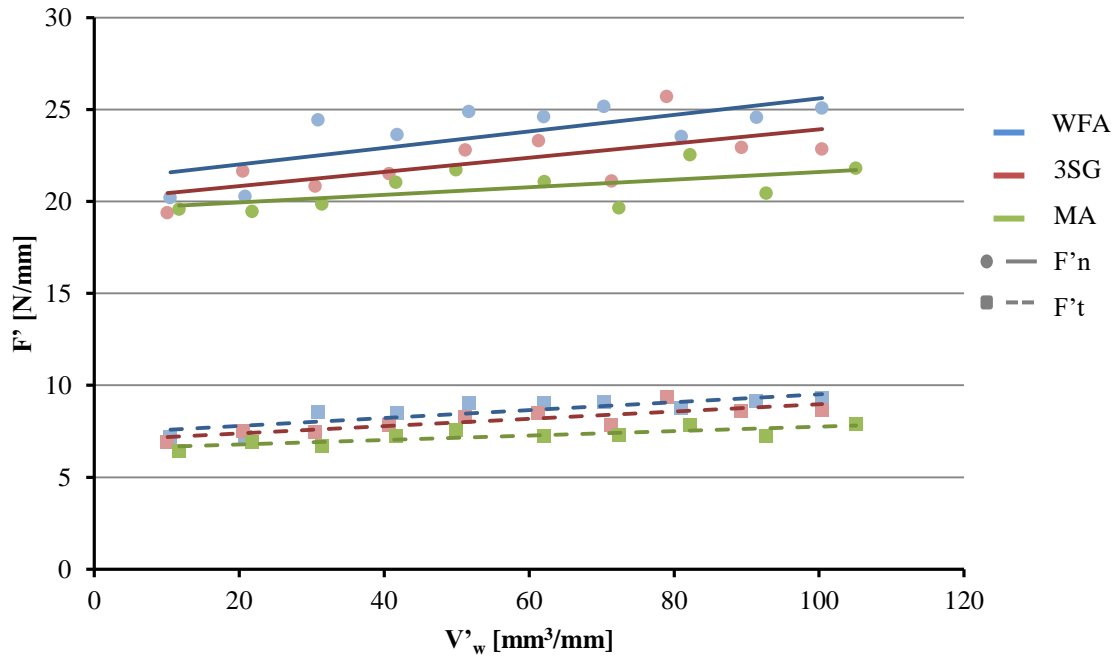


Figure 43: Specific grinding forces evolution with specific removed material (*Test 2*)

With regards to the evolution with specific removed material, both normal and tangential forces present a very slight increase as the grinding wheel is worn. A value of around 25 N/mm for normal specific force and around 9 N/mm for tangential specific force is reached in case of WFA. In spite of the different values of %A found between WFA, MA and specially 3SG worn grinding wheels and the increasing tendency to observe wear flat, grinding forces present very similar values for the three types of crystalline structures and increase very slightly, showing a quasi-constant increase. This observation is primarily due to the initial wheel surface, along with the small depth of cut achieved.

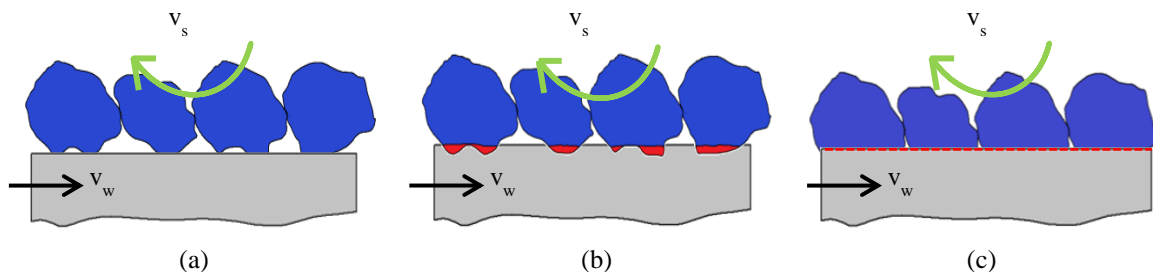


Figure 44: Contact evolution between abrasive grains and workpiece. (a) Initial contact of *new* surface, (b) abrasive grain wear just in the beginning of the contact and (c) the contact of *worn* surface.

Figure 44(a) represents the first state, the initial contact between abrasive grains and workpiece. This *new* surface, just dressed, is characterized by sharp edges and represents the smallest contact area. In Figure 44 (b) the second state represents grain wear for the first grinding passes. This state is immediately achieved and the sharpness of abrasive grains is lost. Finally, Figure 44 (c) shows the last state, representing the *worn* surface, at $100 \text{ mm}^3/\text{mm}$. Grain flatness, together with the closed structure leads to a high contact area. Heat evacuation is hardly affected for the high contact area achieved for designed tests. This effect is the responsible for the high values of %A measured in the first $10 \text{ mm}^3/\text{mm}$ and a fast increase in %A during the studied specific removed material. Therefore, grinding surface is continuously modified, and hence, contact conditions.

To better understanding of surface modifications and its effect on the grinding force, in the following subsection the wheel surface roughness is deeply analyzed. Furthermore, due to the high temperatures in the contact, chemical reactions are promoted, leading to a third body generation. This third body changes the contact between abrasive grains and workpiece material, becoming sliding in the predominant phenomenon. Therefore, grinding forces do not suffer a notable increase with %A.

The sliding phenomenon which governs the contact is promoted with designed grinding parameters. A small depth of cut was chosen to avoid grain breakage. Therefore, rubbing and ploughing are the main material removal mechanisms, whereas, the relevance of cutting is almost negligible. Again, due to the absence of the cutting mechanism the value of the grinding force is quasi-constant.

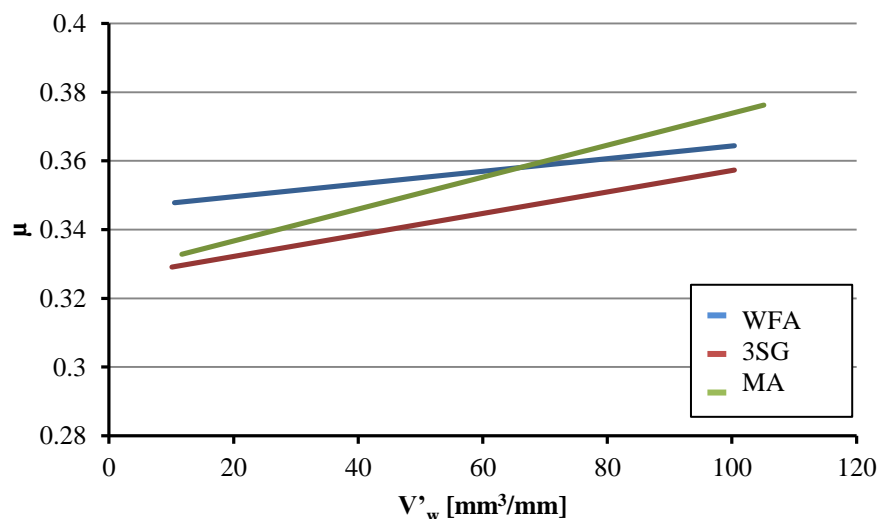


Figure 45: Friction coefficient evolution with specific removed material for Test 2

Friction coefficient is analyzed in order to complete the grinding analysis. In Figure 45 the evolution of friction coefficient with specific removed material corresponding to *Test 2* is represented. Taking into account that the maximum variation of friction coefficient regardless crystalline structure is from 0.33 to 0.38, it can be affirmed that friction coefficient grows slightly with specific removal material, and hence with an increase of wear flat. 3SG grinding wheel presents the lowest friction coefficient values, from 0.3 to 0.36 approximately. This is due to the higher %A achieved and also higher quantity of third body adhered, as it is shown in the following section. On the contrary, MA grinding wheel presents the highest friction coefficient value, being the increase during the test more marked than in the other two cases. The main reason is because of the designed tests are adequate to finishing process and the monocrystalline alumina too. Therefore, working conditions are more suitable in this case and the wheel behaves better.

In general, these values of friction coefficient are in accord with results obtained from the pin-on-disk tribometer test used to study the wear of SG alumina [16,33]. Malkin, using monocrystalline alumina grinding wheels also confirmed that as the hardness of the grinding wheel increases, the friction coefficient decreases in experiments carried out with wheel grade R [27,67]. Moreover, the adherence of third body to flat abrasive grains leads to quasi-constant values of friction coefficient. Once the third body is adhered, the contact behaves as a metal-metal contact as opposed to ceramic-metal contact. Meanwhile, a low value for specific removal rates of $1.25 \text{ mm}^3/\text{mm s}$ is achieved during this test, and according to [1], this fact together with quasi-constant values of friction coefficient supports the notion that rubbing and ploughing are predominant during grinding tests carried out.

The differences in %A reached on the three crystalline structures together with similar values reached on force and friction coefficient prompted the microscopic study of the wheel surface in order to confirm the differences found on %A values for both type of alumina.

Summarizing, %A increases with specific removal material, however, grinding force is maintained quasi-constant all studied grinding wheels: WFA, MA and 3SG. Both facts, this initial wheel surface and designed grinding parameters lead to this behavior. In the first $10 \text{ mm}^3/\text{mm}$, flat surface is achieved, losing the sharp edges. Additionally, the %A reached in 3SG wheel is higher than on WFA and MA alumina. The dissimilarities in thermal conductivity corroborate achieved values of %A, being higher contact temperature achieved in the case of 3SG grinding wheel, and hence, promoting wear flat occurrence. A deeply a microscopic and 3D roughness study of the grinding wheel surface is carried out in the following section in order to clarify mentioned differences.

III.4.2. Microscopic analysis of wheel surface

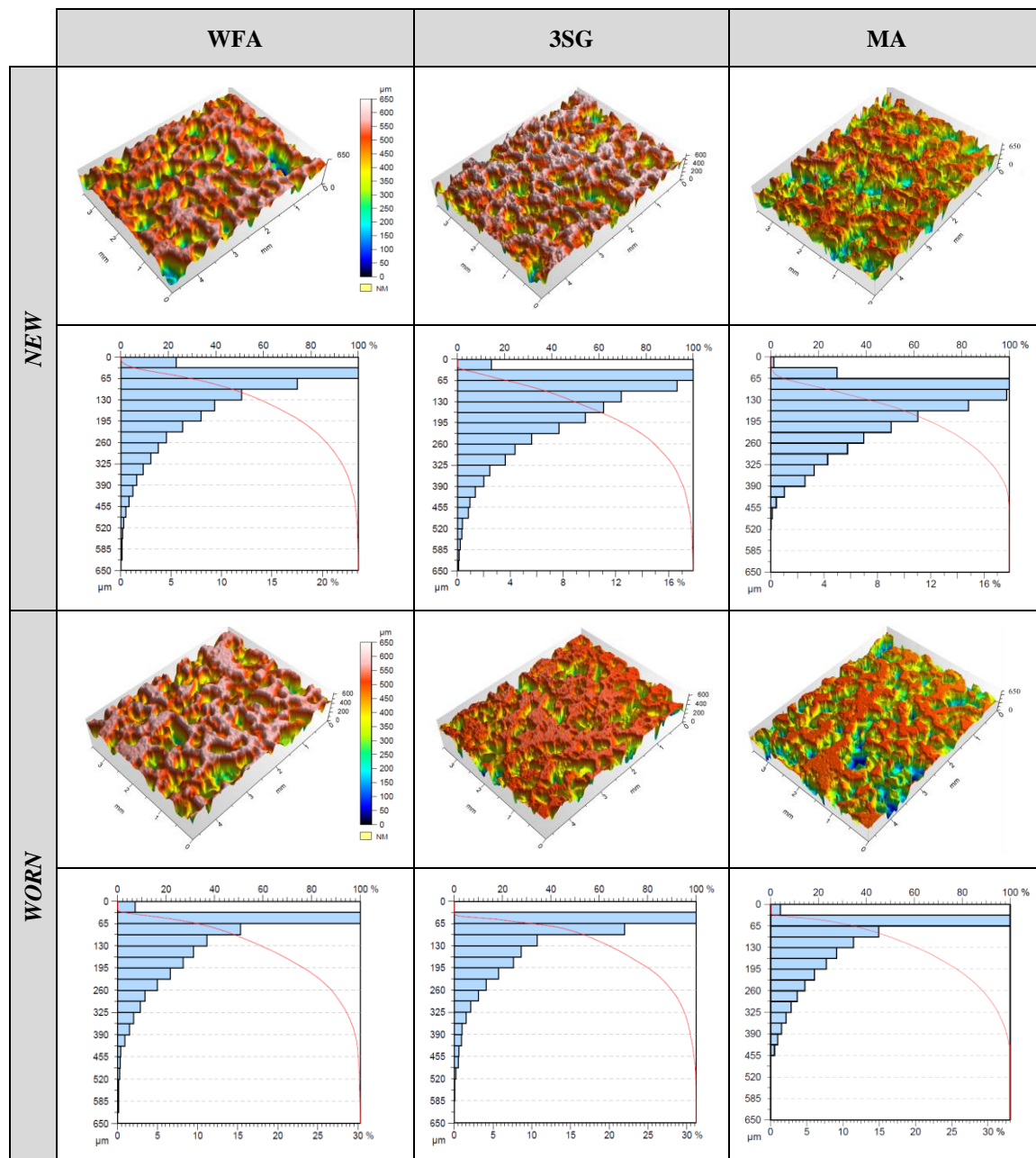
Wear flat characterization by measuring % A is not enough to understand the influence of its evolution during grinding, so, a deeper analysis of the wheel surface is needed. Regarding % A, remarkably differences were found in wear flat maximum values and on its evolution with specific removal rate. On the contrary, friction coefficient, but primarily grinding forces do not present appreciable differences depending on the crystalline structure of tested abrasive wheel. Therefore, a detailed wheel surface analysis is required to look into tribochemical phenomena occurring on the abrasive grains during grinding. The surface study is divided in a 3D functional roughness parameters analysis, obtaining the most representative parameters to determinate the worn surface and in a SEM and EDXA analysis, allowing the identification of third body from the grains or bond.

III.4.2.1. 3D functional roughness parameters analysis

As it is described in Sections III.2 and III.3.2, *new* and *worn* wheel surface topography with dimensions of 3.6 x 4.75 mm² is measured using 3D confocal microscopy with parameters described above. Table 11 shows the 3D topography and Abbott-Firestone curve of *new* and *worn* surface for WFA, 3SG and MA grinding wheels. Focusing attention on 3D surface representation, 3SG and MA alumina clearly present a greater degree of wear than WFA, since the *worn* 3SG and *worn* MA appearance is smoother than *worn* WFA.

Additionally, analyzing Abbott-Firestone curve, the distribution of material confirms that the *new* surfaces are sharper than *worn* surfaces. In *new* graphics, in the first 30 µm of height until 5% of total volume is built and the next 30 µm about 20 % of a total volume is presented. However, for *worn* surfaces, in the first 30 µm, almost no volume appeared, and in the second 30 µm, between 30 and 35 % of total volume is built. This fact corroborates the loose of sharpness of abrasive grains. Moreover, it is confirmed that only attritious wear occurs, since the depth of wear in both cases is approximately 30 µm, and the abrasive grain diameter is 250 µm.

Table 11: 3D topography and Abbott-Firestone curve of *new* and *worn* topography for WFA, 3SG and MA.



From Abbott-Firestone curve the height 3D functional parameters of S_k , S_{kp} and S_{vk} are taken as it is shown in Figure 46. Furthermore, in Table 12 the values of the main functional roughness parameters for studying surface changes are included. S_{pk} refers to surface peaks that are above the core roughness depth. From the three studied crystalline structures S_{pk} varies from 21.8 to 3.7 for *new* surfaces, however, for worn state, the values are too close, varying from 2.13 to 3.11. For every reduced peak height decrease from *new* to *worn* surface, corresponding to the sharpness loss, the initial peaks of the surface are removed. Likewise, the variation of S_{pk} parameter depending on the crystalline structure analyzed is negligible in comparison with a

measurement range of 650 μm . Therefore, the value of removed peaks is not sufficiently large to confirm volumetric wear on the wheels.

Table 12: Wheel surface representative functional roughness parameters.

	<i>New WFA</i>	<i>Worn WFA</i>	<i>New MA</i>	<i>Worn MA</i>	<i>New 3SG</i>	<i>Worn 3SG</i>
S_{pk} [μm]	10.8	2.13	21.8	2.88	3.7	3.11
S_k [μm]	155	125	181.9	127.8	195	79.8
S_{vk} [μm]	205	192	139.3	115.6	200	202

In contrast, the S_{vk} value does not present significantly changes from *new* to *worn* surfaces and thus dull material does not remain on deep holds, which is confirmed in the following paragraphs analyzing SEM images. However, comparing crystalline structures, while WFA and 3SG present almost the same values, MA reduced valley height is smaller. The differences are not due to the dullness. Despite the structure of designed grinding wheel is the same for the three crystalline structures (9), the characteristic shape of each abrasive grain leads to differences on the wheel structure due to the positioning of abrasives with the bond. Therefore, S_{pk} allows the identification of sharpness loss and S_{vk} shows the absence of dullness in grinding wheel, however, these parameters are not useful for comparing wear flat.

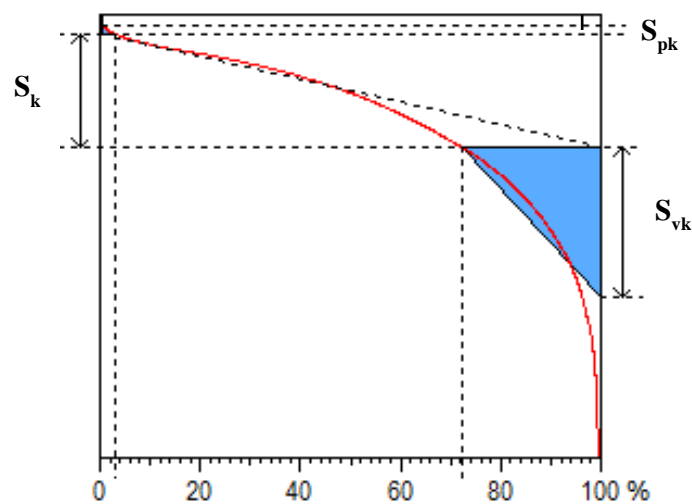


Figure 46: Representation of S_k , S_{pk} and S_{vk} parameters obtained from Abbott-Firestone curve for *new* WFA.

From studied parameters, S_k is the parameter that shows the greatest variation. For WFA, S_k decreases by 30 μm with wear flat and for MA by 54.1 μm while for SG the decrease is 115.2 μm , indicating greater wear for SG than for WFA and MA grinding wheel, being WFA the less affected wheel surface. Regarding the Abbott-Firestone curve for SG wear the absence of material in the first 32.5 μm together with the 3D topography confirms the wear flat of SG alumina. MA wheel also presents less material quantity in the first 32.5 μm , but not the absence of it. Accordingly, comparing 3D topography, more flat appearance is shown for both 3SG and MA than for WFA.

However, it is necessary to point out that the S_k parameter is not a quantitative parameter. The value of S_k depends directly on the distribution of the material on the wheel surface, and if changes are presented in the distribution, the value of S_k also will change despite wear flat occurs. But the differences between *new* and *worn* surfaces are shown through core roughness depth, allowing the identification of changes in the surface and therefore identification of surface flatness. This parameter confirms the %A measured using an optical microscope mainly for 3SG and WFA. However, %A of MA is closer for WFA than for 3SG and surface analysis does not show the same results, being MA worn surface more similar to 3SG grinding wheel. Therefore, a deeper analysis is required to draw firmer conclusions and to understand tribochemical phenomena with affects to surface appearance and to the %A. Moreover, with this measurement technique it is not possible to distinguish between abrasive grains and dullness, therefore EDXA analysis provides the main chemical elements of analyzed surfaces.

III.4.2.2. SEM and EDXA analysis

To complete surface analysis, wheel surface topography is deeply analyzed through the images taken by SEM. This qualitative analysis compares both *new* and *worn* surfaces in order to determinate the differences due to attritious wear. The *new* surface shown in this section is the same for all the tests carried out, but the worn surface corresponds to *Test 2* for every crystalline structures. However, obtained conclusions can be extrapolated to every studied case.

In Table 14 *transition* images of wheel surface are gathered. These images of wheel topography are taken at magnification of 50x, with an analyzed area of 1.83 x 2.26 mm². *Transition zone* is referred to the part of the wheel in which the test is carried out and the part which is only dressed as it is shown in blue in Figure 47.

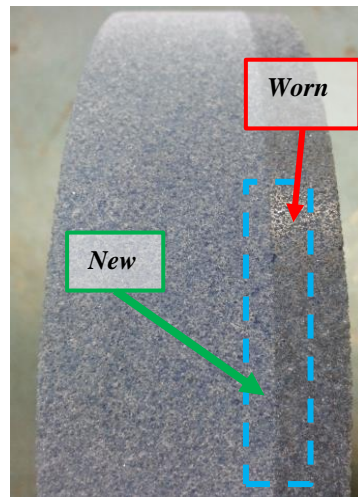


Figure 47: Wheel surface after grinding tests highlighting transition zone between *new* and worn surface.

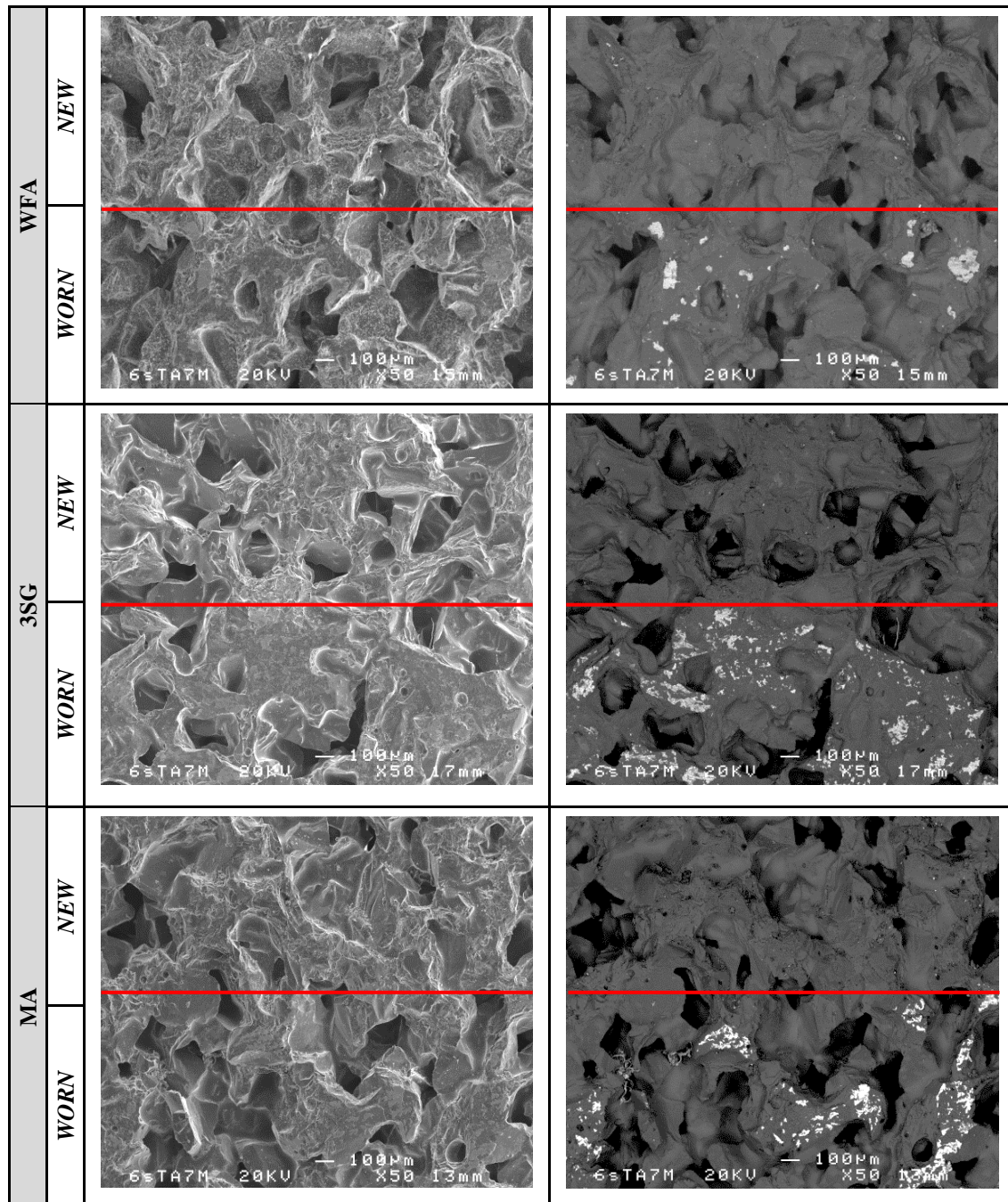
In Table 14 the upper part of the images corresponds to *new* wheel surface and the down part of the images to worn abrasive grains; both parts are delimited by a red line. Moreover, the images in the right are taken using high contrast in SEM, which allows the differentiation of chemical elements and hence between abrasive grains, bond or adhered third body to flat grains. The elements with higher atomic weight present light colors, such as iron (Fe) and with low atomic weight the colors are darker, for example aluminum (Al). Therefore in the upper part of the images in the right the absence of iron or chromium particles is observed while in the down part, which correspond to worn surface white particles are shown. A deeply analysis of composition of worn surface is carried out hereafter. In Table 13 the atomic weights of the main elements that are found on analyzed surface are built.

Table 13: Atomic weight of the main chemical elements found in the wheel surfaces.

Chemical element	Al	Si	Cr	Fe
Atomic weight	13	14	24	26

Comparing the *new* surface for the three crystalline structures, WFA and MA grinding wheels present a less uniform surface than 3SG grinding wheel. Furthermore, in the case of WFA different layers could be observed. Despite this difference in the initial surface after dressing, the starting wheel surfaces are considered sufficiently comparable for analyzing the evolution of %A. Moreover, in the first 10 mm³/mm of specific material removed the three crystalline structures present very similar values for the same grinding conditions, about 7% for the *Test 2*.

Table 14: SEM analysis of the transition between *new* and *worn* surface. for the three types of crystalline structure. The images in the right are taken with contrast.



Once the tests had been conducted, the down part of the images clearly shows the wear of abrasive grains, revealing the differences between the WFA, MA and 3SG surfaces. At a magnification of 50x, the topography of 3SG wheel represents a more continuous and homogeneous surface than the WFA grinding wheel. The MA worn surface corresponds to an intermediate surface, thus it is smoother than WFA but it does not present as homogenous appearance as 3SG wheel surface. In addition, the grinding direction can be observed in worn

surface of both MA and 3SG flat areas, from left to right in the images in Table 15. Although the WFA surface is flat, it is possible to distinguish abrasive grains in worn surface. Even in MA surface, although with more difficulties than on WFA surface, the shape of abrasive grains are identified. However, this distinction is not possible to do in 3SG wheel. The homogeneous appearance hinders the identification.

Table 15: Worn surface at 50x magnification and flat areas remarked

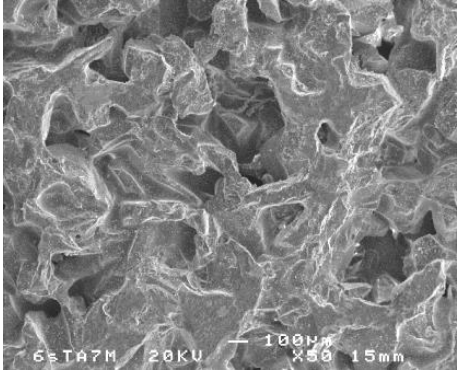
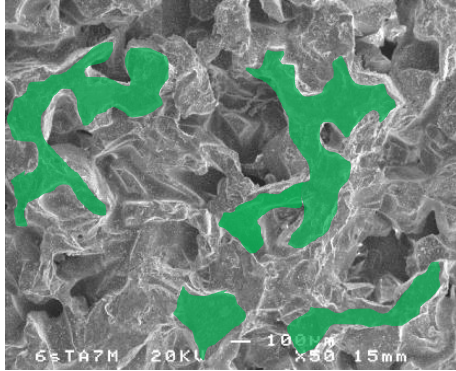
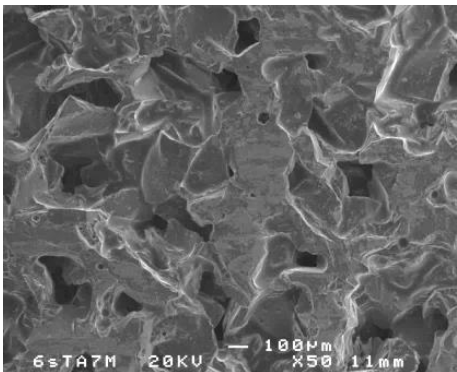
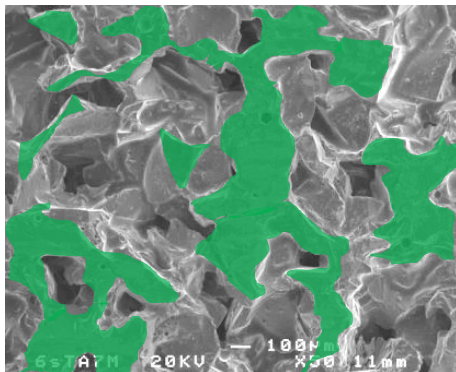
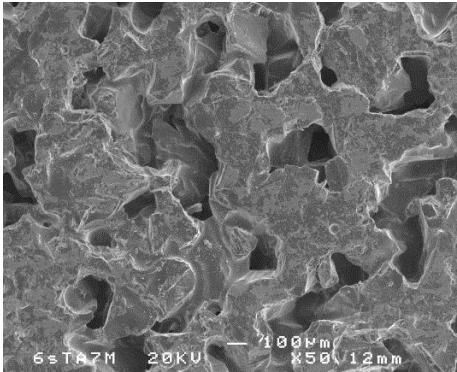
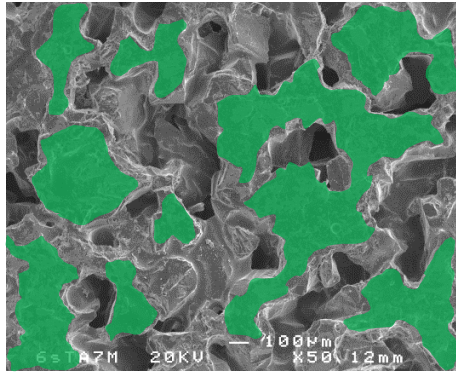
WFA		
3SG		
MA		

Table 16: SEM images taken at magnification of 500x. Detailed *new* and flat abrasive grins

	NEW DETAILED GRAIN	FLAT DETAILED GRAIN
WFA		
3SG		
MA		

Regarding the flat area of worn surface, in Table 15 the flat parts of the surface after a complete test are highlighted in green. The areas on the 3SG and MA wheels are larger than those of the WFA. Moreover, the areas corresponding to 3SG surface are more connected than the areas of WFA. Again, MA surface presents large areas but they are not completely connected like in 3SG surface. Accordingly with the %A values shown in Figure 39, 3SG grinding wheel achieves 14% of wear flat, higher value than WFA and MA which achieves a maximum value

of 11%. Therefore, the results for WFA and 3SG alumina are in agreement but the large flat areas shown in SEM analysis are not represented with the %A.

In order to detect the reason of the differences found on both studies, a further analysis was conducted with a magnification of 500x on Table 16. The analyzed surface is of $183 \times 226 \mu\text{m}^2$, allowing for a detailed inspection of one abrasive grain. These images verified grain flatness after grinding. The grain surface before and after the tests was also compared taking into account roughness of flat grains, since this is one of the parameters that influences third body adhesion.

In the left row of Table 16 the *new* abrasive grains are shown. On this images the grain appears together with the bond. Also free white particles can be differentiated. These particles have been analyzed by EDXA, resulting in diamond particles from the initial grinding wheel dressing. Moreover, on MA and WFA abrasive grain smooth plains can be seen. In Figure 48 (b) WFA detailed abrasive grain is shown at magnification of 1000x, being the studied area of $91.5 \times 113 \mu\text{m}$. In Figure 48 (a) the surface corresponding to SG abrasive grain is show. Comparing both surfaces, WFA grains present smoother surface than SG. The rough surface of SG abrasive grains corresponds to its microcrystalline structure. The size of microcrystals will be lower than $1 \mu\text{m}$ as it is said in previous Chapter, and in this image it can be corroborated.

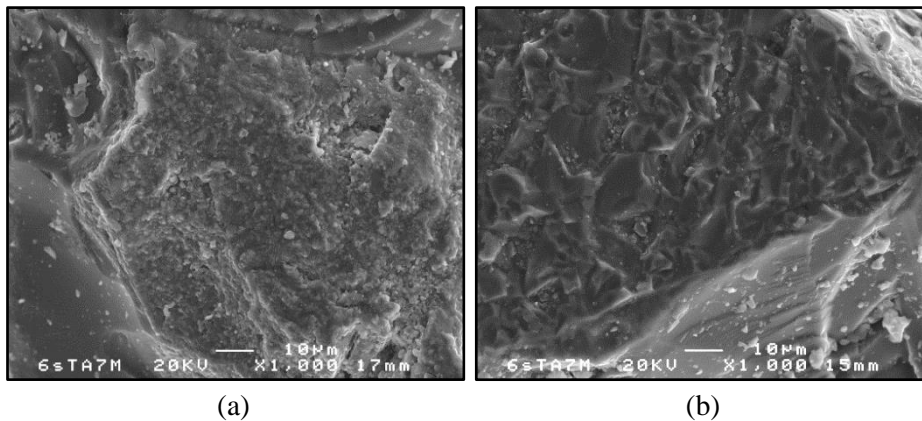


Figure 48: Detailed grain surface (a) SG *new* abrasive grain and (b) WFA *new* abrasive grain.

The right row of Table 16 shows the worn grains in detail. The three crystalline structures show the flat face of the grain. The appearance of flat grain is rougher than the *new* grain mainly in MA surface. However, for SG abrasive grains the microcrystalline appearance do not change. The characteristic of flat surfaces together with other factors as the temperature in the contact makes easier the adhesion of third body to the flat surface. In the case of SG abrasive grains, the adhesion is easier than for WFA even for MA due to the rough surface. In this sense, on the three images corresponding to worn abrasive grains in Table 16 and also in Table 14 and Table

15 a higher quantity of third body adhered for 3SG grinding wheel than for WFA can be shown. The MA worn surface also presents great quantity of third body adhered, although it is less than 3SG surface. This difference is largely due to the discrepancies in the temperature reached, and the characteristic of flat surfaces provided by the crystalline structure of alumina. High temperatures accelerate chemical reactions, which generate a higher quantity of third body. Furthermore, the roughness of the SG abrasive grains promotes the adhesion of the third body to flat surfaces, causing it to remain on the grains.

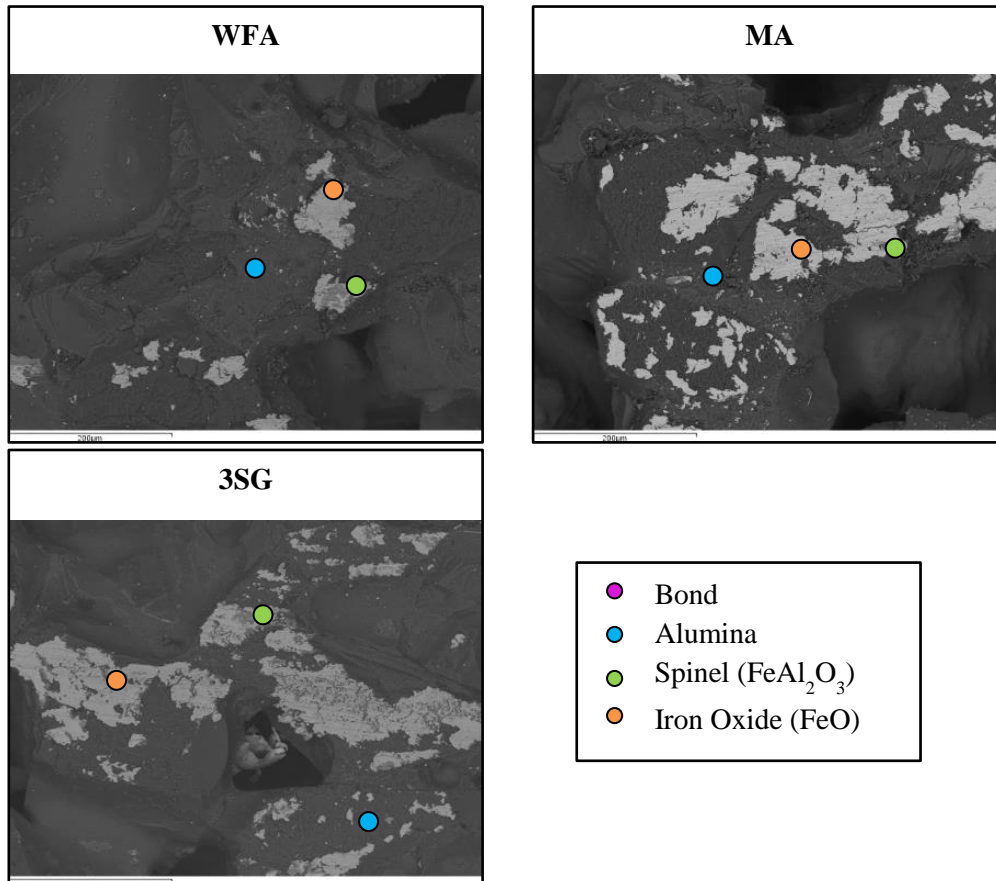


Figure 49: EDXA analysis for third body analysis

In Table 16 third body is easily identified. Its appearance is similar on WFA and MA worn surfaces, being the attached layer thicker than for 3SG surface and generating a continuous body. However, for 3SG surface, the third body is more distributed for all the surface and two different colors are interlayer corresponding to two different compositions of the third body as it is described hereafter. Moreover, in every case third body is presented as a flat irregular shape with grinding direction marks. The third body changes the contact conditions, becoming increasingly important in the case of contact between steel and third body in comparison with steel and alumina contact. The scratch marks due to friction demonstrate that the third body is in contact with the workpiece, keeping friction coefficient at a quasi-constant value of around 0.35.

This quantity of third body is obtained thanks to the fact that during the test there is a lack of grain loss, and hence third body loss. However, on a real grinding process the third body found is highly reduced.

To continue studying the third body, an EDXA analysis was carried out. In Figure 49 the main elements of worn wheel surface are shown for the three crystalline structures. And in Figure 50 the distinction between abrasive grain and bond is done. Vitreous bond is marked in purple in the image and its correspondent EDXA analysis is shown in the upper part, with Si being the principal element. The vitreous bond is coating the abrasive grain, which is highlighted in blue in the image, likewise its EDXA analysis in the down part of the figure shows Al as the main element.

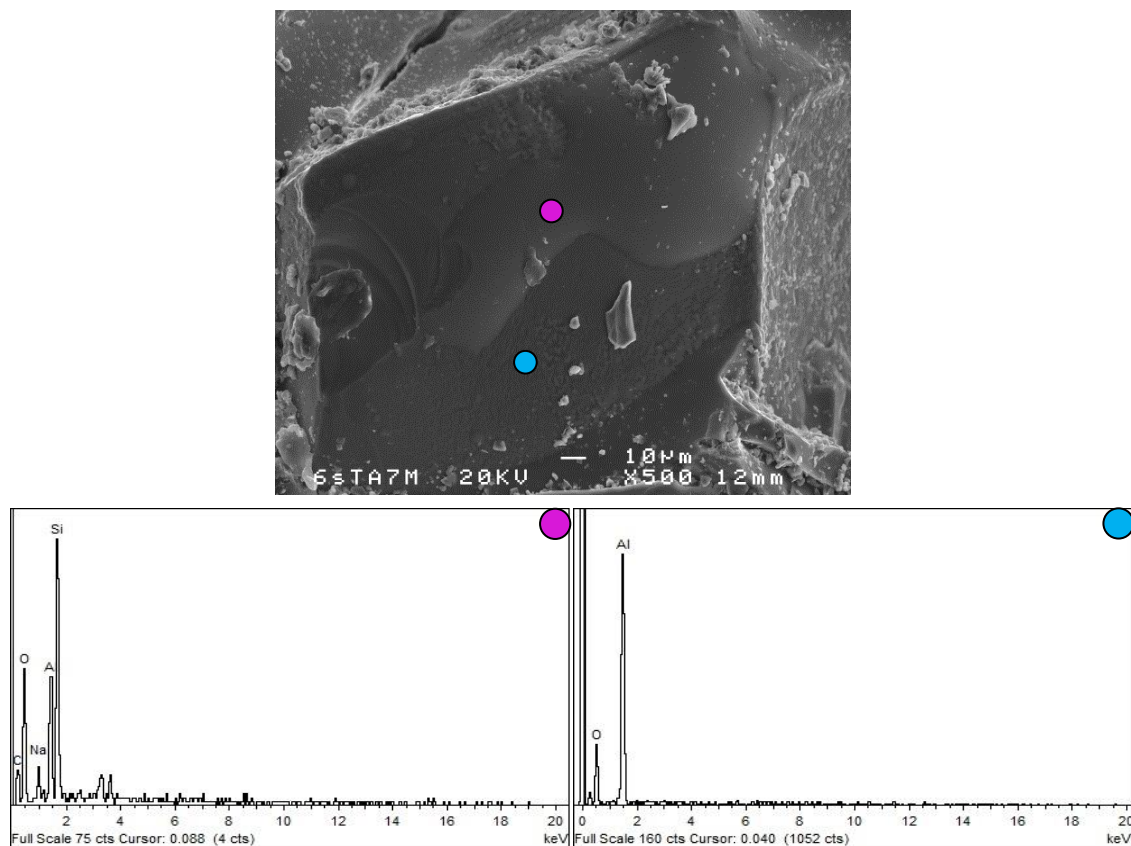


Figure 50: EDXA analysis for the distinction between abrasive grain and bond

As it is mentioned, EDXA analysis allows the detection of third body, remarked in green and orange in the three images in Figure 49. Third body is generated due to chemical reactions and abrasion between the workpiece and abrasive grains. Not only workpiece material but also contact conditions have an influence on third body composition. Iron oxides are predominant in the whitest zones, marked in orange in Figure 49. Furthermore, iron spinels (FeAl_2O_4) appear attached to the abrasive grain as a grey color, highlighted in green. This grey color is due to the presence of Al in addition to Fe. The presence of spinel is higher for 3SG worn surface than for

WFA and MA. Furthermore, it is possible to affirm that spinel corresponds to thinner layers that are only attached to abrasive grains, whilst iron oxide corresponds to thicker layers that generally cover the spinel. The results obtained by Klocke on pin-on-disk tribometer studying sol gel sintered alumina against steel disk [16] could be applied to the grinding tests employed in the present work.

As it is shown on analyzed images, the wear flat measured during current experimental work not only corresponds to abrasive grains but also to vitreous bond. High temperatures are reached on contact and these high temperatures remain both on abrasive grains and on vitreous bond. In three studied grinding wheels, abrasive grains are in a vitreous bond environment, and thus the temperature reached for abrasive grains is conducted from grains to bond. However, as previously mentioned, the 3SG wheel reaches a higher temperature than the WFA and MA. Therefore, the bond evolving SG grains heat up more than the others, presenting smooth appearance and large flat areas. In the case of WFA this large areas are not achieved and flat areas correspond mainly to abrasive grains. The heat conductivity of SG alumina and WFA has been analyzed by Klocke [16], achieving significantly lower heat conductivity for SG alumina than for WFA due to the imperfections, high number of pores and great quantity of boundaries due to the microcrystals.

Moreover, the fusion temperature of silica is lower than the alumina's one. The melting temperature of vitreous bond is around 1200°C [14], while SG abrasive grains are melted at around 2000°C. Despite the temperature reached on contact between surface grinding wheel and workpiece is not measured in the current experimental work, the literature reports values are close to workpiece temperature melting point [81], around 1300°C for tempered steel used in this work. As it is shown in SEM images, the bond of the 3SG grinding wheel is modified due to the high temperature and the contact with the workpiece due to the achieved temperature is in the order of vitreous bond melting temperature. Therefore, melted vitreous bond flows through the abrasive grains forming smooth flat. In the case of WFA this phenomenon does not take place. In contrast, for the MA grinding wheel thermal conductivity has not been analyzed and the behavior is less controlled. However, taken into account SEM images, smoother surface than for WFA is achieved, which implies that achieved temperature is also close to melting temperature of vitreous bond.

The melting of bond is observed in the present work due to the extreme achieved contact conditions and the high %A generated. However, in habitual grinding, the bond is lost with abrasive grains, and it is not in contact for long during a complete grinding operation. Moreover, in the present study, due to wheel hardness (R) this loss does not occur, and the third body remains on both the abrasive grains and the modified bond.

These facts explain why the look of worn 3SG and MA wheel is more homogenous and continuous than worn WFA. This also accounts for the maximum values of 14 % of wear flat observed during experimental work on the 3SG wheels. However, the value achieved for MA is not so high, being 11% measured wear flat. These differences on achieved wear flat values, despite presenting a similar flat surface are due to the transparent color of bond. Therefore, the value of %A measured is not affected by bond modification, since light reflection occurs on flat abrasive grains and the third body, but not on the bond (whether raw or modified). However, if third body will be attached to the bond, this area would be taken into account in the total %A. This phenomenon explains the similarities on smooth flat surfaces between 3SG and MA grinding wheel but not in %A measured and also similarities between %A of MA and WFA, about 11%.

Moreover, the similar values of friction and grinding forces found between the three types of wheels are due to the initial surface designed to promote wear flat, along with the grinding parameters. Grinding wheels are without cutting ability almost from the beginning of the test. The sharpness presented on the 3SG wheel is quickly lost and the flatness and third body leads to a quasi-constant force.

III.5. Preliminary conclusions

The present chapter examined the evolution of wear flat in alumina grinding wheels by isolating and promoting this effect. Three crystalline structures of alumina are studied, comparing its influence on wear flat generation. The influence of the crystalline structure is observed on both the look of the grinding wheel surface and on the %A reached. Moreover, wear flat is strongly affected for the grinding parameters. The conclusions that derive from these results are the following ones:

- Wear flat presents a linear increase the three crystalline structures, with a similar slope observed for WFA, 3SG and MA grinding wheels. These results are broadly consistent with the results obtained by Malkin [27] and they appear to point to the possibility that the pattern of wear flat growth depends mainly on the abrasive crystalline structure.
- In the case of 3SG grinding wheel, the value of the total wear flat area is around 23% higher than that of WFA and MA grains. The WFA and MA grinding wheels behave very similarly for studied grinding parameters. These results confirm the influence of the crystalline structure on the occurrence of wear flat, and this effect is quantified for grinding wheels.

- Concerning to grinding parameters, workpiece speed presents different patterns depending on the studied case. Therefore, it is not possible to undertake a clear tendency of wear flat generation with v_w . On the contrary, %A increases with a depth of cut between 3 and 5 μm from 10% to 14% respectively in the case of 3SG grinding wheel. This increase is not so pronounced for the case of WFA and MA grinding wheels.
- The maximum %A reached is 14 % for SG alumina at $v_w=15000$ mm/min and $a_e=5$ μm after 100 mm³/mm of workpiece material has been removed.
- Both tangential and normal grinding forces remain practically constant independently of depth of cut and crystalline structure. A very few increase is shown with specific material removal. Friction coefficient also shows the same pattern, a quasi-constant value is drawn between 0.33-0.38 This phenomenon is because of the initial wheel surface, along with the grinding parameters designed to promote wear flat, ensuring that sliding is the main phenomenon that occurs during grinding.
- The correlation between grinding wheel wear and 3D functional roughness parameters is established: S_{pk} allows the identification of sharpness loss, S_{vk} shows the absence of dullness in grinding wheel and S_k together with S_{pk} helps to the identification of abrasive grain flatness and abrasive grain height loss which is related to wear flat.
- Moreover, 3D roughness analysis revealed differences between *new* surfaces of different crystalline structures, with the 3SG surface being sharper than WFA and MA *new* wheel surface. However, after testing, the 3SG and MA surface was found to be flatter than WFA. SG accumulates 32.5 % of material from 32.5 μm to 65 μm , while WFA accumulates the same quantity of material in the first 65 μm , being the MA surface in the intermediate wear state.
- Analysis of the three crystalline structures wheel surface revealed differences on just dressed and worn topography. For *new* surfaces at a magnification of 50x, 3SG surface presented a smoother appearance than WFA and MA *new* surface. Furthermore, WFA seems as it is composed by a different layer in the *new* abrasive grains. However, at a magnification of 500x the microcrystals of the 3SG wheel are noticeable, leading to a rougher surface and promoting third body adhesion.
- Once the tests had been completed, it was found that 3SG and MA *worn* surfaces presented a very homogenous appearance. Moreover, 3SG wheel presents a bit more quantity of third body adhered than MA and the difference in the third body adhered is increased with WFA, being the surface with less third body adhered to flat surface. This phenomenon is due to the

fact that the thermal conductivity is lower in SG alumina and hence the temperature is higher on contact, accelerating chemical reactions and modifying the bond on contact. Third body adheres to both flat abrasive grains and the transformed bond.

- These experimental tests have demonstrated that in conditions where the most important material removal mechanisms are ploughing and rubbing (e.g. finishing operations), the main problem of SG abrasive grains when compared with the WFA grains is the excessive wear flat generated during the process. Moreover, MA grinding wheels, despite presenting the appearance as smooth as 3SG grinding wheel, the %A achieved is not so high. This fact is due to the influence of bond in the flat appearance and also because at finishing parameters monocrystalline alumina behaves better than SG abrasive grains. As the presented analysis show, the reason for this behavior is the crystallographic structure of the abrasive grain. This idea is in accord with what is found in industrial practice and will help wheel manufacturers to better understand the grinding process and to base their selection of abrasive grains not only on experience but also on scientific knowledge.

Chapter IV: New design of a
Pin-On-Disk tribometer for alumina
abrasive grain wear analysis

IV. NEW DESIGN OF A PIN-ON-DISK TRIBOMETER FOR ALUMINA ABRASIVE GRAIN WEAR ANALYSIS

IV.1. Introduction

Chapter II presents the difficulties of alumina wheel wear characterization, particularly, the wear flat. Its tribochemical nature raises the need to address this issue. In *Chapter III*, the wear flat occurrence on alumina grinding wheels is addressed from the perspective of studying the grinding process. The results obtained from the experimental work, described in previous chapter, indicates the importance of the tribochemical effect on the generation of wear flat. This issue requires a deeper analysis, with the need for an exhaustive control of contact conditions despite the randomness of wheel topography. In this sense, the present chapter studies the alumina abrasive grain wear implementing tribological tests. A new design of pin-on-disk tests is developed in order to reproduce grinding contact conditions. As it is deeply analyzed in the state of the art, alumina-steel contact has been widely studied from a tribological point of view using a wide range of contact conditions [16, 60]. However, both sliding speed and contact pressure close to grinding conditions are not achieved in the same time. Therefore, contact time and reached temperatures cannot be extrapolated to grinding tests.

The aim of present chapter is to address the lack of knowledge by applying real grinding conditions to a new design of pin-on-disk tribometer. The main purpose of this new design is to reproduce a discontinuous contact between alumina and steel using real alumina grinding wheel as a disk. Following the study of the influence of crystalline alumina of abrasive grains in the wear, a comparison of the wear behavior of WFA and 3SG grinding wheels is conducted. Using these grinding wheels as disks, real randomness of the topography is evaluated, reproducing the thermal cycle that is suffered by the alumina during grinding. Furthermore, the simulated contact conditions are close to the grinding parameters, using a sliding speed of 30 m/s and controlling real contact area (A_r) in order to reach contact pressures close that achieved during grinding. Finally, a deep analysis of worn alumina is carried out through a 3D parametrical study of disk topography. This study complements the grinding wheel analysis carried out in *Chapter III* in order to acquire a deeper knowledge of the wear flat phenomenon and the wear mechanisms that take place during contact of abrasive grains and workpiece. After taking into account the two facts, wear results obtained on pin-on-disk tribometer can be extrapolated to real grinding process.

IV.2. New design of a pin-on-disk tribometer

In general, the main challenge of studying a specific type of wear is the isolation from the other types. In the present work this fact is addressed designing hard grinding wheel, avoiding grain breakage and grain pull out. Moreover, the other issue that have detected on works carried out is the difficulties to reproduce grinding contact conditions on a test bench under them exhaustively control. Therefore, the second issue to deal with is the design of the pin-on-disk tribometer that allows to reproduce grinding conditions and to control the real contact. These contact conditions involves not only sliding speed (s) and real contact pressure (p_r) of grinding process but also the thermal cycle suffered by abrasive grains.

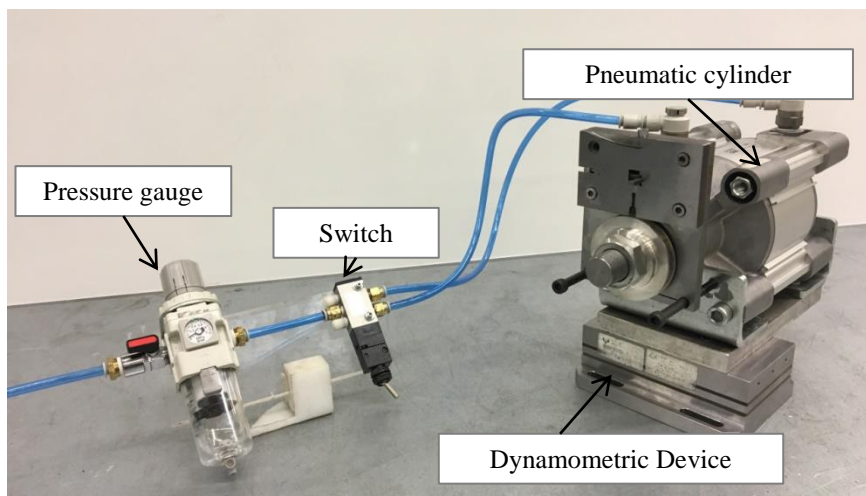


Figure 51: Set up of pneumatic control of pin-on-disk

On the one hand the classical pin-on-disk test bench are designed to study less aggressive contact conditions between two materials, as it is detailed in *Chapter II Section II.4*. When high speed or high pressure had been analyzed, specific designs of pin-on-disk set up had been carried out. In the present study in order to achieve the same sliding speed that it is used in real grinding process, the test bench is assemblage on a surface grinding machine. Likewise, the objective of this design is to achieve real contact pressures close to achieved during grinding.

Table 17: Specification of pneumatic elements

Pressure gauge	AW30-F03BE-B, 0.05-0.85 MPa
Selector valve	Valve ¼ EVZM550-F01-00 0.15-0.8 MPa
Pneumatic cylinder	Double action pneumatic cylinder CP96SDB125-50 Cylinder: Ø125 mm, Stroke: 50 mm Max. Pressure: 1MPa, $F_{max}=12000$ N

In this sense, a pneumatic system is designed consisted of a double-acting pneumatic cylinder activated by a selector valve, a switch, and a pressure gauge that allows flow regulation. The specifications of pneumatic elements are detailed in Table 17. In Figure 51 the pneumatic control set up is schematized. The theoretical maximum force of the double action cylinder is 12000 N. However, the maximum force that is going to be achieved in the present work is 8500 N with a pneumatic pressure of 7 bar, which is the pneumatic pressure of the workshop installation. The designed pneumatic device allows the reduction of pneumatic pressure with the pressure gauge, but not to increase it. On the cylinder plunger, a pin holder with a guide system is assembled to avoid rotation of the pin due to the tangential force imposed during tests as it is shown in Figure 52

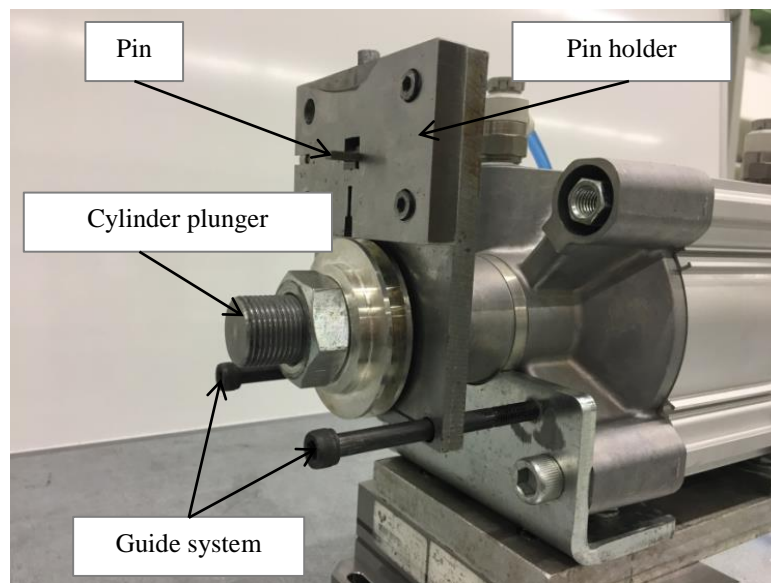


Figure 52: Pin holder and guide system of pneumatic cylinder to avoid pin rotation during tests

On the other hand, with the purpose of achieving a discontinuous contact of alumina and thus, reproducing the thermal cycle of abrasive grains, two requisites are taken into account. First, pin and disk roles are changed. Generally, pin material is the material under examination. However, in this study, alumina is analyzed and an alumina disk is employed. However, if the wear of alumina is analyzed on this kind of test bench, being alumina pin, a continuous contact between alumina and steel is achieved. Therefore, in the present work steel pin and alumina disk is used.

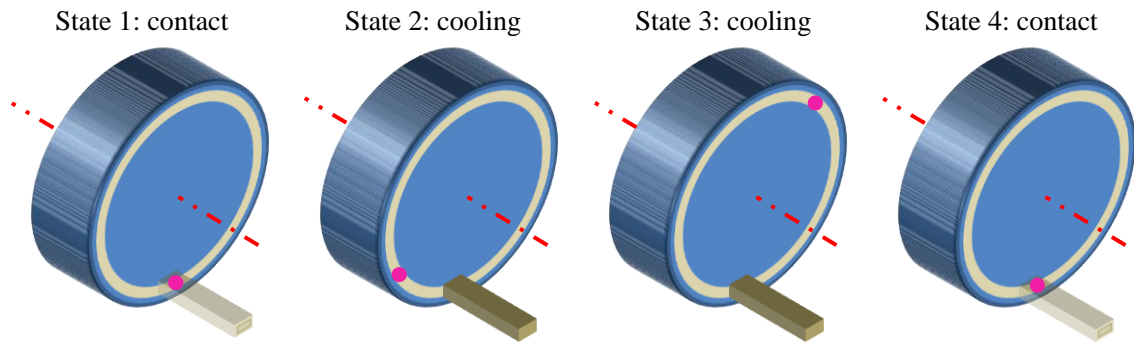


Figure 53: Reproduction of thermal cycle of one abrasive grain (in pink) with designed pin-on-disk set up.

With this configuration the material of abrasive grains, alumina, is studied. However, the shape of abrasive grains, the effect of wheel configuration, bond and matrix structure are not taken into account if alumina pin is used. So, in the present design of pin-on-disk tests a real grinding wheel is used as disk, allowing the study of different crystalline structure of abrasive grains also. Finally, in order to control better the real contact area, the tests are carried out on the frontal flat face of the grinding wheel, which is conditioned as is explained hereafter. In Figure 53, the path of one abrasive grain is represented from the first state in which the abrasive grain is in contact with the pin. Following the intermediate states in which the abrasive grain is cooling due to the absence of contact and finally the grain contacts again with the pin, closing the thermal cycle.



Figure 54: Set up of tribometer mounted on a surface grinding machine.

Therefore, considering all the requisites, the designed pin-on-disk tribometer allows the close reproduction of grinding contact conditions and its control. In Figure 54 set up of designed tribometer mounted on a surface grinding machine is shown.

IV.3. Experimental set up for pin-on-disk tests

The present tribological study characterizes the wear of alumina abrasive grains working against steel under grinding conditions. As it has been deeply described in the paragraphs above, a particular design of pin-on-disk tribometer is required in order to achieve grinding contact conditions. This tribometer is mounted on a surface grinding machine, the same that it is used in grinding experimental work. The specifications of grinding machine are detailed in table 2 of *Chapter III*. Furthermore, dynamometric device is also used to measure grinding forces during the tribological tests. Table 18 specifies the name of the device and the software used to acquire grinding forces. Likewise, the tests are carried out with cooling, being the coolant and the flow the same of the previous experimental work, detailed in Table 18.

Table 18: Set up of Pin-on-disk tests

Surface grinding machine	Blohm Orbit CNC 36
Coolant	5% oil water based Flow rate: 45 l/min.
Wheel specification	54R6V89, grain size 300 μm
Wheel dimensions	400x20x127mm
Workpiece Material	Tempered AISI D2 60 \pm 2 HRC
Pin Dimensions	3x5x25mm
Dynamometric Device	Kistler 9257B DynoWare software
Microscope	Confocal microscope Leica DCM3D magnification 10x Leica Map software

Moreover, real grinding wheels are used as a disk to achieve results as close to grinding process as possible. Aiming to develop previous experimental grinding work, *Chapter III*, in this tribological study the influence of crystalline structure of abrasive grains is also taken into account. In this case only white fused alumina (WFA) and microcrystalline alumina (3SG, composed by 30% of SG abrasive grains) grinding wheels are analyzed due to a higher use on industrial applications. Hard grinding wheels are designed, grade R, with the same purpose of the previous grinding tests, isolate wear flat. Likewise, the abrasive grain diameter is about 300 μm , so the evaluation of the grain flatness is easier. The grain size also helps to differentiate

grain pull out, if occurs. The wheel is the closest wheel that can be manufacture in order to avoid high porosity, which could lead to problems in the tests due to the small size of the pin. Finally, the abrasive grains are embedded on a vitreous bond matrix, as they have been on the grinding experimental tests. The nomenclature of a complete wheel and the dimensions are specified in Table 18. Moreover, Erickson [50] affirms that the wear of the materials is determined by contact geometry and the conditions of lubrications. Therefore, in the present study both items are taken into account in the tribometer test, using a real grinding wheel as a disk.

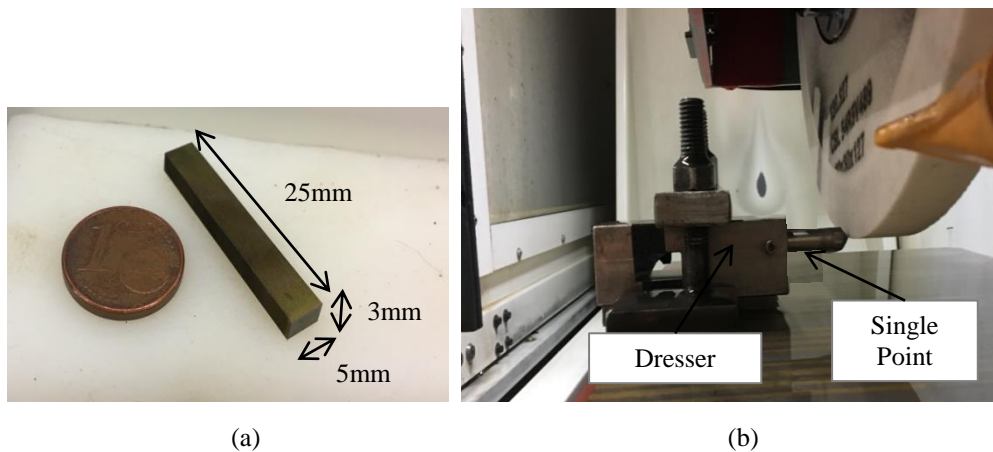


Figure 55: (a) Pin dimensions, (b) dressing set up of vertical surface of the wheel.

Regarding the pin material, hardened steel is also studied, detailed in Table 18. In order to control real contact pressure and achieve contact pressure values as close to those that occur during the grinding process as possible, small pin section is designed. Hardened steel pins are set by wire electrical discharge machining (WEDM) due to their small size. The pin section is 3x5 mm and 25 mm long as it is shown in Figure 55. The area must be sufficiently large to avoid pin breakage and small enough to increase the contact pressure, being 15 mm² the most suitable pin contact area. The close structure of the wheels and fine dressing parameters allow the control and the increase of the real contact area. In Figure 55 (b) the dressing set up is shown being dresser tool of a single point diamond assembled to dress the vertical surface of the disk.

Finally, the characterization of wear alumina is done. Confocal microscopy is used to determinate the real contact area and to analyze the wear generated on the disk after carrying out the tests. The specifications of Leica DCM3D confocal microscopy are detailed in Table 4 of *Chapter III*. Obtained topographies are analyzed using Leica Map software, allowing the analysis of a functional surface of disks. 3D parametrical study based on ISO 25178 standards is addressed.

IV.4. Methodology for tribological tests to characterize abrasive grain wear

The contact between alumina and steel is studied in order to characterize alumina wear under grinding conditions. One of the handicaps of this study is accurately known the real contact conditions. In this sense, the quantification of real contact is necessary before starting tribological tests. After that, contact tests are conducted and finally the characterization of wear of alumina abrasive grains is attempted. Hereafter is detailed a complete methodology to develop the study of abrasive grain wear under controlled contact conditions.

IV.4.1. Real contact area quantification

Before starting the quantification of real contact area, both pin and disk have to be conditioned. Pins are manufactured by WEDM not only due to the small size of pin dimensions but also to ensure a complete contact with the disk. Roughness lower than $2\mu\text{m Ra}$ is achieved on the surface of 15 mm^2 which contacts with the disk. Regarding the disk, in these tests, a real grinding wheel is used but a different operation surface is applied. Dressing is carried out to vertical surface of the grinding wheel as it is shown in Figure 55 (b). Specific holder is manufacture for the assembly of the dresser-tool on the horizontal position. A dresser speed of $v_d= 60\text{ mm/min}$ and dressing depth $a_d= 5\ \mu\text{m}$ are used to vertical wheel surface conditioning. In Table 19 dressing parameters are built.

Table 19: Dressing parameters of vertical surface

v_s [m/s]	v_d [mm/min]	a_d [μm]
30	60	5

Despite the fact that this parameters correspond to fine dressing parameters, the random wheel surface and its structure leads to A_r smaller than apparent contact area (A_a), which in this case is 15 mm^2 . These differences between A_r and A_a are also found on grinding process. Therefore, after pin and disk conditioning the next step is to quantify the real contact area between pin and disk. The quantification of A_r is performed measuring the just dressed wheel topography using confocal microscopy. Images are taken at magnification of 10x and stitching technique is implemented in order to analyze a higher area. 2x2 images are overlapped in order to study an area of $1.6 \times 1.8\text{ mm}^2$. Moreover, the analyzed height range is $600\ \mu\text{m}$ or $300\ \mu\text{m}$.

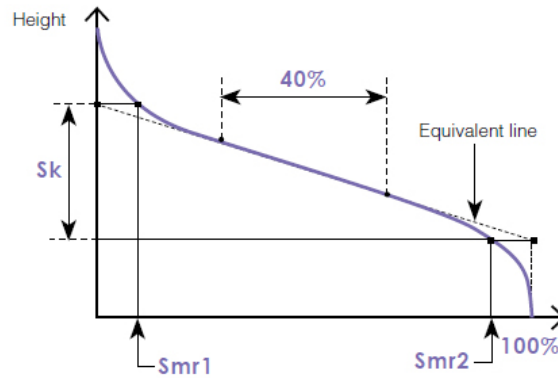


Figure 56: Abbot Firestone curve and the attainment of functional parameters.

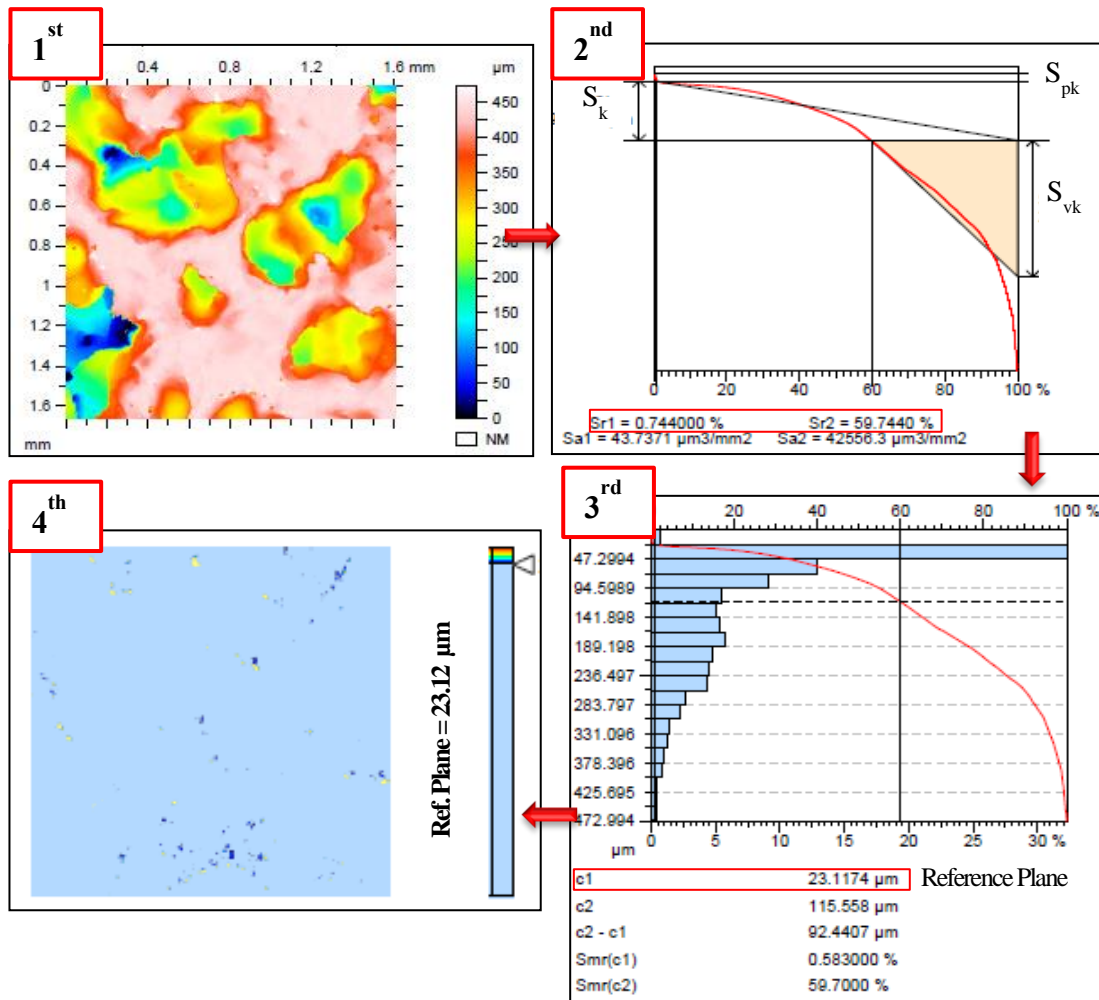


Figure 57: Steps to achieve reference plane of dressed disk surface using 3D functional parameters.

Once the topography of the just dressed surface is obtained, the Abbot-Firestone curve and particularly 3D functional parameters are used in order to determinate the reference plane. From

functional study, S_{mr1} and S_{mr2} values corresponding to areal material ratio that divides the reduced peaks and valleys respectively from core roughness (S_k) are obtained following the ISO 25178 standards as it is shown in Figure 56. From represented case of dressed WFA, in the second step of Figure 57, $S_{mr1}= 0.74\%$ and $S_{mr2}= 59.74\%$ values are obtained. These values are inserted in the dynamic Abbot-Firestone curve, represented in the third step of Figure 57, where the corresponding material distribution is also represented. To determinate the reference plane, S_{mr1} is an useful parameter, which delimitates the core roughness with reduced peaks. Therefore, from this step, the value of cI is achieved, which is the height from the top of the topography to S_k parameter. This height sets the reference plane that it is going to be used to determinate the A_r between pin and disk. For the represented case, the reference plane is established at $23.12\ \mu\text{m}$ from the top of the topography. In the fourth step of Figure 57 the slice of dressed topography at this height is revealed. As it is shown, the material accumulated up to this slice corresponds only to the peaks.

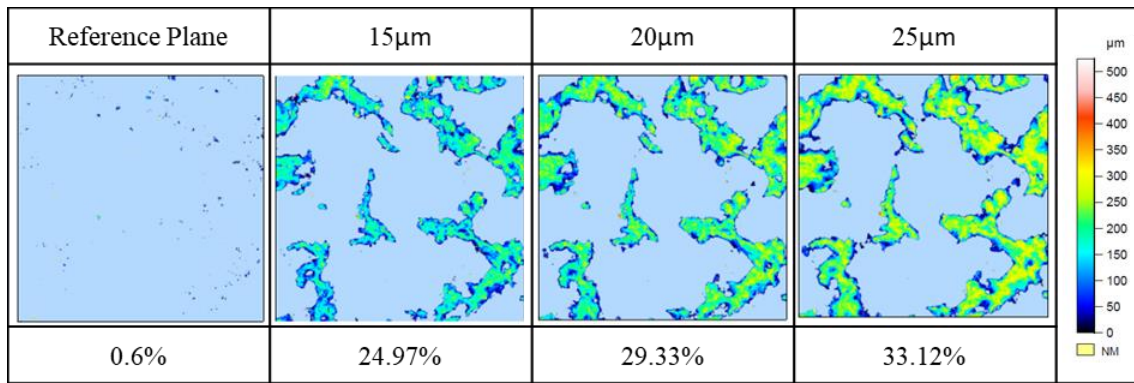


Figure 58: Parallel slice to reference plane sets in order to quantify real contact area depending on wear depth.

Once the reference plane is defined; parallel planes are conducted at different depths of the analyzed 3D surface. Furthermore, after conducting the pin-on-disk tests, the worn alumina is measured. The depth of worn alumina establishes the plane at which the contact area is quantified, which allows to obtain the A_r value for each studied surface, and hence, the real contact pressure. In Figure 58 are represented the slice planes at distance of $15\ \mu\text{m}$, $20\ \mu\text{m}$ and $25\ \mu\text{m}$ measured from the reference plane with its corresponding real contact area quantification. These values correspond to WFA measurements. Therefore, once the tests are conducted and worn depth is measured the correlation with A_r can be done.

IV.4.2. Methodology for Pin-on-disk tests

Following wheel and pin conditioning, and dressed surface measurement to real contact area quantification, the pin-on-disk tests are carried out. Sliding speed, pneumatic pressure and theoretical force are varied in order to observe the influence of each parameter. Table 20

displays the complete battery of experimental tests. Sliding speed is varied from 20 to 30 m/s, values corresponding to conventional grinding, and theoretical grinding forces achieve values of 7200 N, 8400 N and 9600 N. A total of 9 tests are conducted for each grinding wheel in order to evaluate not only the influence of contact parameters in the wear of abrasive grains but also the influence of crystalline structure. In Figure 59 schematic and real set up of tribological tests are represented. Also, the force directions are highlighted. The theoretical force applied to the pin corresponds to the direction of F_n .

Table 20: Pin-on-disk parameters

		Pneumatic Pressure [MPa] / Theoretical Force [N]		
		0.6 / 7200	0.7 / 8400	0.8 / 9600
Sliding speed [m/s]	20	1a	2a	3a
	25	1b	2b	3b
	30	1c	2c	3c

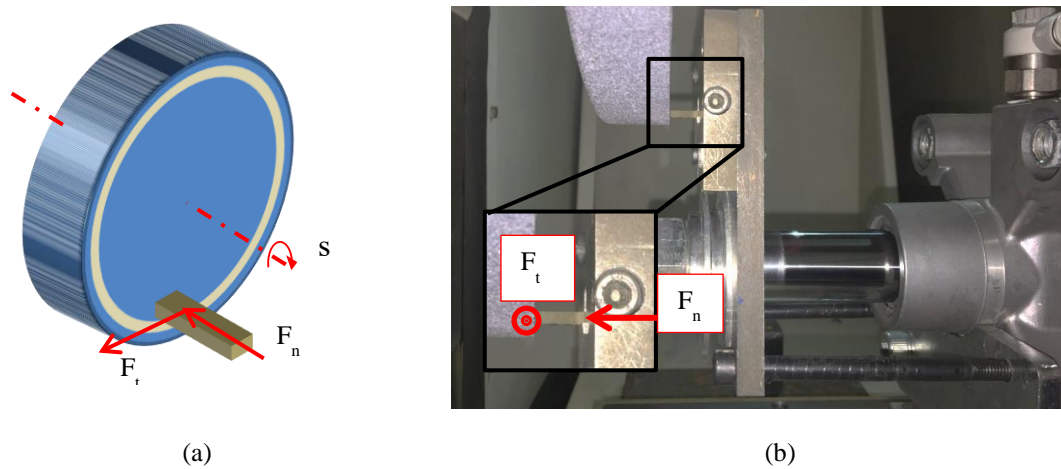


Figure 59: Set up of the first contact between pin and disk (a) schematic representation of the set up and (b) real tribological tests set up. In both cases force directions are represented.

Furthermore, the pneumatic pressure is established and due to the characteristic of the designed pneumatic system, the corresponding theoretical force is achieved. During the tests forces are measured using a dynamometric device, described in Section IV.3. Short contact time between pin and disk is achieved during tribological tests comparing to grinding process. The contact time of these tests is limited by the length of the pins, 25 mm. Due to the slenderness of the pins, it is not possible to increase the length within the designed area. Moreover, the small

contact area of the pin leads to high and continuous temperatures in the contact for steel pin, enhancing a faster wear of the steel.

The first contact between pin and disk is a critical point of these tests. To ensure a more realistic contact comparing to grinding tests, firstly, the rotation of the wheel is set and secondly the linear movement of pneumatic cylinder is activated and the pin contact with the disk. This way, the initial interlock of the pin in the irregular disk surface is avoided. Likewise, before starting the tests, the pneumatic cylinder stroke is restricted to a certain pin length in order to avoid the contact between pin holder and the disk. Despite 25 mm pins are manufactured, work length of the pins are about 11 mm and the other 14 mm are meant to be held to the pneumatic cylinder and to establish a security distance with the pin holder. In Figure 60 (b) in the left the new and the worn pin are shown, in which the generated burr is marked. In the right part of the image the sliding direction is highlighted in red and also pin dimensions can be differentiate. Moreover, in Figure 60 (a) the groove generated for three tests on the disk are shown.

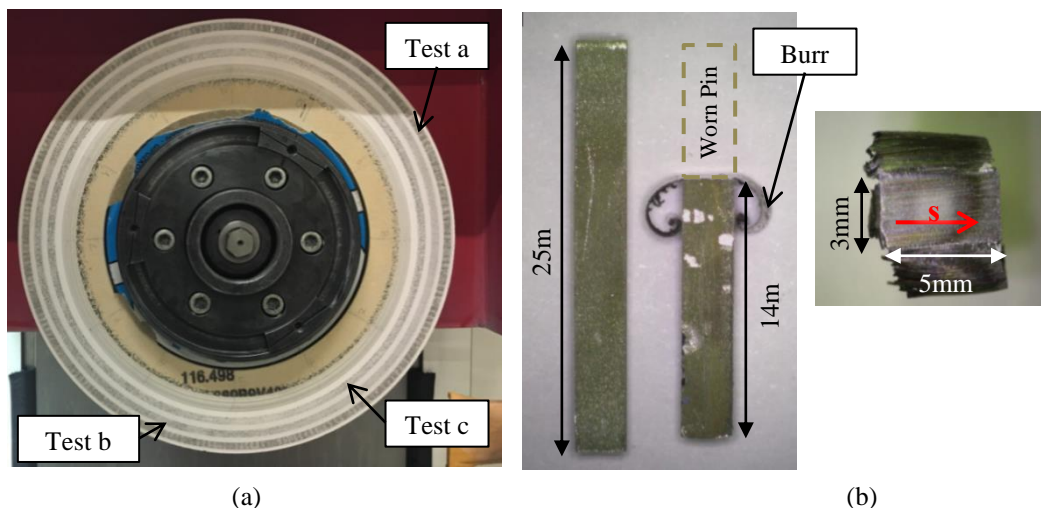


Figure 60: (a) 3 tests conducted on flat vertical surface of the disk. (b) Comparison between new and worn pins, generated burr and the marks of sliding direction in pin surface.

IV.4.3. Methodology for abrasive grain wear measurement

Subsequent to the pin-on-disk tests, alumina wear is characterized. Confocal microscopy is used to analyze the wear generated on the disk, to quantify the groove generated in the flat surface of the disk. The measured area (x, y) is $6.69 \times 1.77 \text{ mm}^2$ and z scan range of $600 \mu\text{m}$, with a resolution of $4 \mu\text{m}$. In addition, monochromatic light is used and the disk is covered with graphite in order to minimize the brightness of the images. As it is shown in Figure 61 (a) the measured area involves both worn and just dressed alumina. This is necessary in order to measure the depth of the groove. The just dressed surface is the height reference to establish

worn depth. From now on, to show the methodology to characterize the wear of alumina abrasive grain the *Test 1a* for WFA is chosen. Therefore, Figure 61 and Figure 63 correspond to this case of study. However, the methodology is the same for every tests whatever the type of alumina.

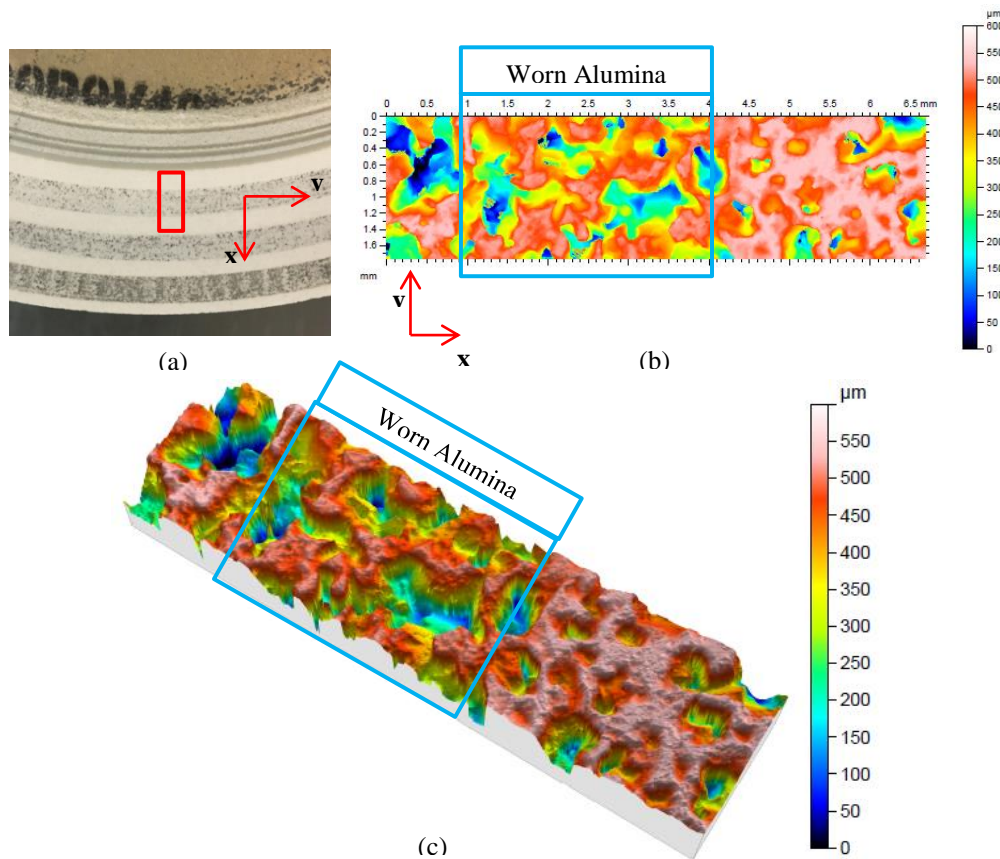


Figure 61: (a) WFA disk highlighted measured area, (b) 2D representation of digitalized area and (c) 3D surface digitalization

In order to characterize alumina wear not only is the depth of groove generated in the disk surface measured, but also 3D functional parameters are analyzed. In Figure 61 (c) 3D surface topography reveals the generated groove in the dressed surface. Each test is measured in six different sections equally spaced along the wheel toward avoid point surface defects and thus to minimize measurement errors. Therefore, the mean value of the depth of groove is obtained for each test.

In order to quantify the wear depth, for each digitalization 100 profiles are extracted and superimposed, as shown in the 1st step of Figure 63. The upper line limiting all the profiles shows the shape of the groove. In the 2nd step of this figure the upper line involving all superimposed profiles is extracted in order to quantify the depth of the groove. However, the quantification on this raw profile is not possible because of the brightness of abrasive grains,

which generates the distortion of the profile. Therefore, this upper profile is filtered using morphological filters as it is shown in the 3rd step of Figure 63.

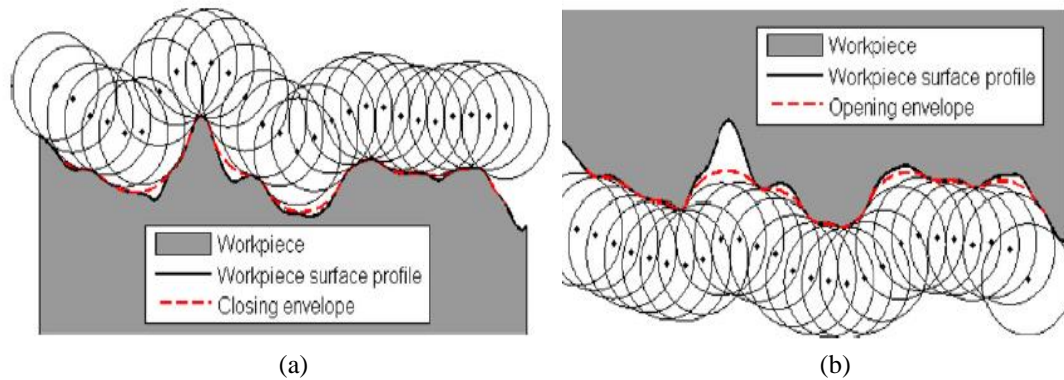


Figure 62: Representation of (a) closing and (b) opening morphological filters [127]

Morphological filters are widely used to analyze engineering surfaces, and they are suitable for extracting geometrical features of surfaces such as the shape [127]. In Figure 62 the operation of closing and opening filter are shown being a disk the structuring element. In this study, an alternate opening-closing sequence of filters is used for eliminating high and thin peaks and valleys. The structuring element employed to apply the morphological filter is a circular disk of 0.5 mm diameter.

In Figure 63 the profile of the 3rd step corresponds to the enveloping line after the sequence of morphological filters application. On this profile the depth of groove can be measured without being disturbed due to the brightness of the disk surface. Finally, in order to enable wear quantification, the profile after morphological filters application is leveled using *Matlab* software. In purple is delimited the depth and the width of the groove. For this particular case, the measured depth is about 20 μm . Likewise, the generated groove is about 3 mm width, which is approximately the same for all the tests carried out due to the correspond to pin dimensions.

Finally, following groove depth measurement, a functional disk surface characterization is carried out. Following the nomenclature of *Chapter III*, worn and just dressed, new, alumina are studied. For the previous digitalized areas a sample of 2x1.5 mm² is extracted from new and worn alumina. 3D functional study based on ISO 25178 standard is used to compare the behavior of both WFA and 3SG wheels under grinding conditions with an exhaustive control of the contact and to find differences between new and worn states of each type of alumina.

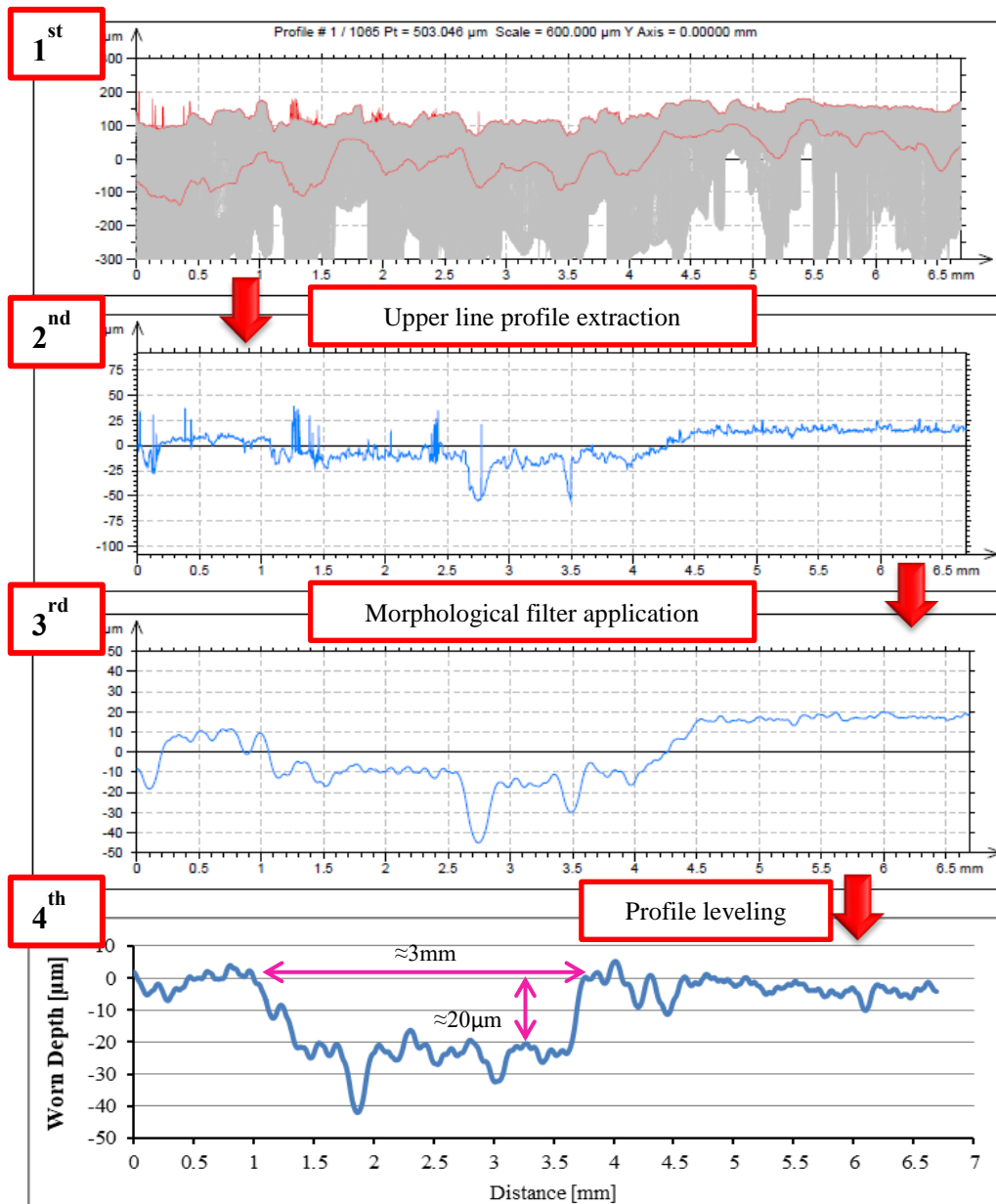


Figure 63: Depth of worn alumina quantification: 1st step, profiles superimposition, 2nd step, upper line profile, 3rd step, profile after morphological filter application and 4th step, leveled profile and depth quantification

IV.5. Pin-on-disk experimental results

Pin-on-disk tests are conducted varying the pneumatic pressure of the cylinder, thus, the normal force imposed, and the sliding speed for both WFA and 3SG alumina disks. In Table 20 the parameter variation is built, being their influence on alumina wear analyzed hereafter. Likewise, the influence of crystalline structure on the abrasive grains wear is also studied in this section. In order to perform an accurate analysis, it must be considered the real contact area between alumina and steel, accordingly, the quantification of A_r is the starting point for the next study.

IV.5.1. Real contact area quantification

The main objective of this original design of pin-on-disk tribometer is to control the real contact pressure, which requires the determination of the real contact area between the alumina disk and steel pin. Therefore, once the tests have been conducted, the first step before starting with the analysis of the results is to quantify the A_r through disk surface characterization. It is established the hypothesis that the contact between pin and disk occurs at the depth of disk wear. So, before obtaining the real contact area, the groove generated in the alumina must be quantified.

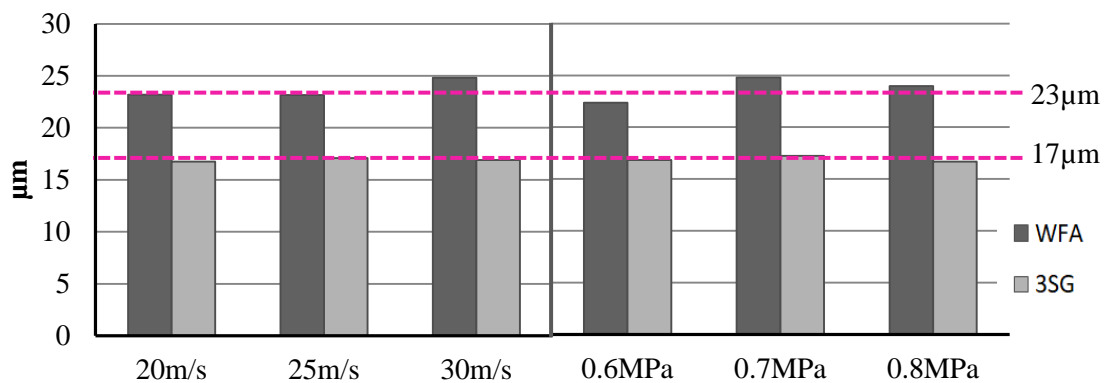


Figure 64: Quantification of groove depth generated on WFA and 3SG alumina disks. Variation with sliding speed, pneumatic pressure and the mean value is represented.

The quantification of wear depth is carried out for each test following the steps shown in Figure 63. The mean value of the groove depth for each abrasive grain structure, for each sliding speed and for each pneumatic pressure is represented in Figure 64. This graphic show that the influence of sliding speed and pneumatic pressure is almost negligible for the studied range. A deeper analysis is addressed in the following section, when the influence of contact parameters in the wear of abrasive grains is analyzed. Related to the abrasive grain structure, a greater depth of groove is measured for WFA than for 3SG alumina disk. Therefore, in order to determinate the A_r , the mean value of worn depth is used for each crystalline structure. WFA presents a mean depth of 23 μm while 3SG has a mean depth of 17 μm .

Once the groove depth is quantified A_r can be determined. For each abrasive grain structure, different depths are measured. Thus, the depth at which the real contact area is obtained is different for each disk. As it was previously explained, a reference plane is defined for each just dressed surface, new surface. In Figure 58 slices parallel to the topography at different depths are represented in order to show the differences in real contact area depending on the contact depth. Now, to determinate A_r , from the reference plane, slices are made at a wear depth of 23 μm for WFA new topography and at 17 μm for 3SG.

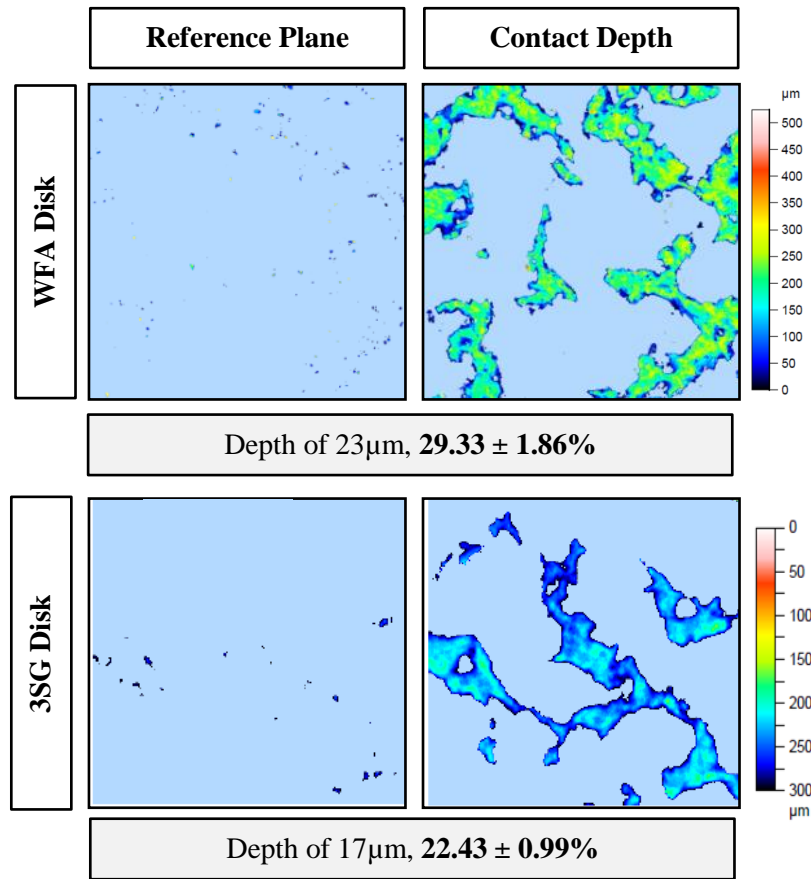


Figure 65: Real contact area quantification from wear depth. Reference plane and contact depth slices for WFA and 3SG disk.

Three different measurements are done for each crystalline structure. The mean value and the error of each one is obtained. In Figure 65 one of the studied cases is represented, showing both the reference plane and the slice plane at the corresponding contact depth for WFA and 3SG surfaces. Measured *new* surface area is 2.88 mm² and the apparent pin area is 15 mm². In the case of WFA, with a A_r 29.33 ± 1.86%, 4.4 mm² and for 3SG alumina this is 22.43 ± 0.99%, 3.36 mm². The A_r of 3SG alumina is slightly lower than WFA due to the sharper surface. Furthermore, the wear depth of 3SG disk is smaller than WFA disk, this fact also has an influence on the differences in the contact area.

From now on, the real contact area is used to analyze the wear of alumina abrasive grains and particularly to obtain real contact pressure between alumina disk and steel pin, being one of the limitations in order to reproduce grinding contact conditions using the pin-on-disk tribometer. To develop these pin-on-disk tests, works carried out by Klocke [16,128] are taken as reference. However, on these works the phenomenon of real contact area is not described, despite the use of A_r to achieve p_r . The reduction from A_a to A_r values leads to higher contact pressures from 0.5 to 1.5GPa. This fact is one of the most relevant achievements of these works and on the

contrary, how to quantify the real contact area is not detailed. Therefore, in the present work great importance has been given to the quantification of A_r .

IV.5.2. Influence of the contact conditions in the wear of the abrasive grains

Once the real contact area is quantified for both WFA and 3SG alumina disks, a deep analysis is carried out in order to determinate the influence of sliding speed and real contact pressure on alumina wear. As it has been previously mentioned, real forces, both normal and tangential, are measured during the tests. The directions of these forces are shown in Figure 59.

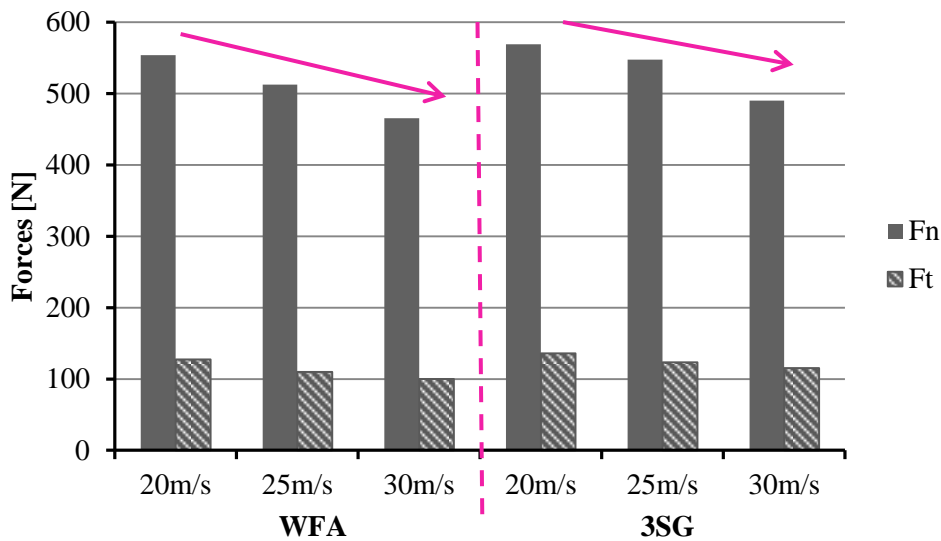


Figure 66: Normal and tangential forces evolution with sliding speed for 0.6MPa (test1a, test1b and test1c)

Both normal and tangential forces are plotted. In Figure 66 the evolution of the forces versus the sliding speed is shown. Despite being represented for 0.6MPa, the behavior is the same regardless of the pneumatic pressure. Higher normal and tangential forces are achieved to lower sliding speed. For WFA tests and a sliding speed of 20m/s, the mean value of F_n is 514 N. However, for 30 m/s, a value of 455 N was reached. In contrast, there is no clear tendency of the variation of the forces with pneumatic pressure as it is shown in Figure 67, where results for 30m/s are plotted. For WFA almost a constant value of about 450N is achieved regardless the pneumatic pressure of the test. For 3SG disk a higher variation is appreciated, increasing from 490 N to 580 N with the increase of pneumatic pressure. Likewise, the behavior of tangential forces are comparable with the corresponding normal forces. These slightly variations are due to the materials in contact and the heavy conditions of the tests.

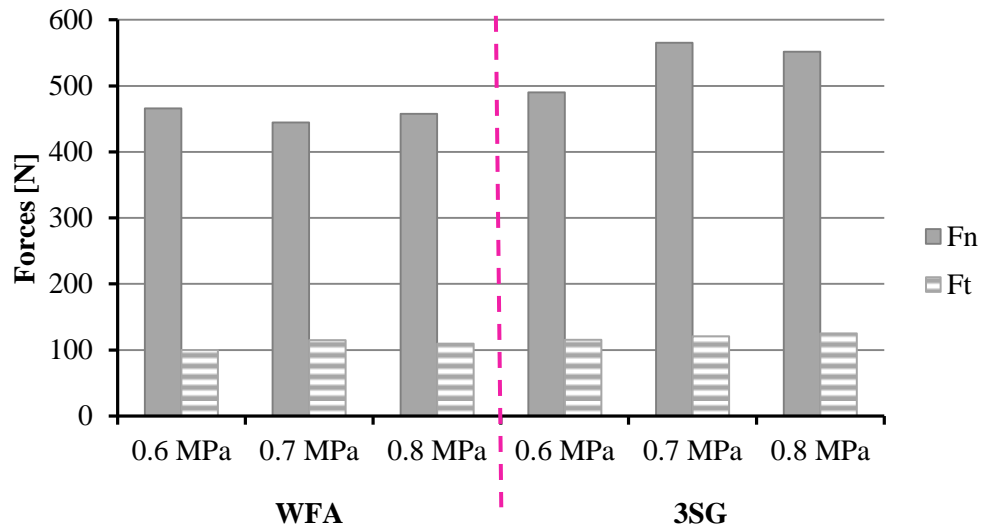


Figure 67: Normal and tangential force evolution with pneumatic pressure for 30m/s (*Test1c*, *Test2c* and *Test3c*)

Regarding the contact time of the tribological tests, it can be obtained analyzing the forces. Therefore, in Figure 68 the normal and tangential force of *Test 1a* are plotted, whilst the alumina steel contact time is also shown. The small $A_a=15 \text{ mm}^2$ together with high sliding speed enhances high temperatures on the contact, softening hardened steel and increasing abrasive grain wear. Therefore, the contact time is very short, $t_c \approx 1.15 \text{ s}$, which denies reaching the theoretical forces. This is the main reason why the studied cases do not present significant variations with pneumatic pressure. Similarly, the wear that occurs in 1.15 s is too high compared to the wear suffered during a real grinding process. This fact is due to the heavy initial wear and then the wear increases slower.

From now, only sliding speed variation is considered on the pin-on-disk tests, therefore, results are analyzed according to s and abrasive grain crystalline structure variation. The values shown for each sliding speed correspond to the mean value of the three pneumatic pressures studied. Regarding the influence of sliding speed on wear, very similar values of wear depth are shown in Figure 64 for the three speeds tested, about $23 \mu\text{m}$ for WFA disk and $17 \mu\text{m}$ in the case of 3SG disk, as it has been previously mentioned. Therefore, for the s range studied, there is no significant variation of the depth of wear.

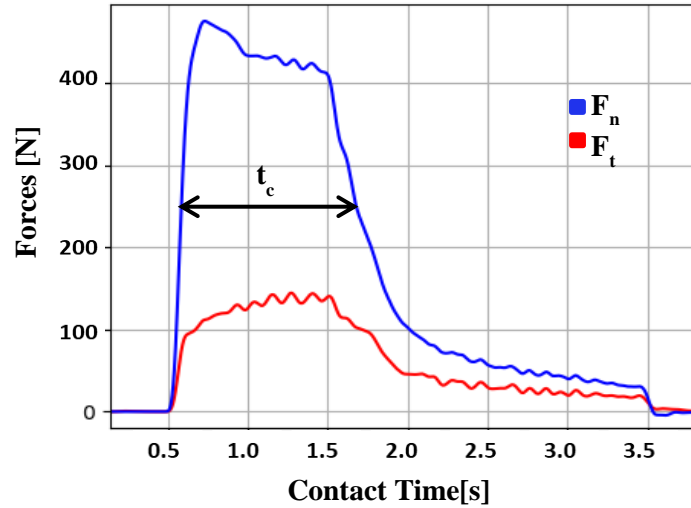


Figure 68: Normal and tangential force signals and contact time for *Test 1a* on WFA

On the contrary, the studied range of sliding speed presents differences on achieved grinding forces and hence, on the real contact pressure as it is shown in Figure 69. Real contact area is defined as follow in Eq.9. Here the importance of quantify real contact area. For the studied range of sliding speed, higher s leads to lower real contact pressures, varying from 190MPa for $s=20$ m/s and 160 MPa for $s=30$ m/s in the case of 3SG alumina disk. The p_r is reduced about 15% for 3SG alumina disk while for WFA the reduction is of 11%. In this regard, Klocke [16] obtained pressures of approximately 0.5-1.5 GPa at a sliding speed of 2m/s. In the case of this study, the sliding speed is at least 10 times higher, and close to the observed during the grinding process, whilst high values of real pressure values are obtained. Therefore, the obtained results on pin-on-disk tribometer can be readily extrapolated to the grinding process, and are useful for characterizing abrasive grain behavior under controlled real contact conditions. Likewise, p_r presents higher variations with abrasive grain structure than with sliding speed. Therefore, in *Section IV.5.3* is addressed a deeper analysis of the real contact pressure with crystalline structure of alumina.

$$p_r = \frac{F_n}{A_r} \quad \text{Eq.9}$$

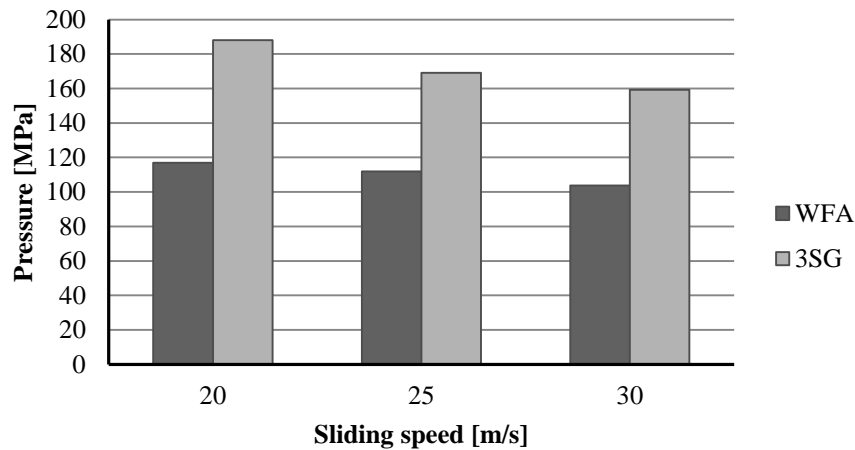


Figure 69: Variation of real contact pressure with sliding speed and crystalline structure.

Concerning to the friction coefficient, values between 0.21 and 0.25 are maintained. On grinding tests carried out in previous chapter, the obtained friction coefficient range is 0.33-0.38 (*Section III.4.1.5 of Chapter III*). This difference is primarily due to the wear mechanisms that occur during contact. In the case of the grinding process, cutting, ploughing, and rubbing are involved in the contact. In contrast, in the case of pin-on-disk tests, the effect of cutting is minimized and ploughing and rubbing are the main wear types. This behavior is deeply analyzed in the following section, comparing the contact of 3SG and WFA disks due to the dissimilarities measured on the two disk surfaces.

IV.5.3. Influence of crystalline structure of abrasive grains in the wear.

Related to the influence of crystalline structure of abrasive grains, the differences on wear depth, disk topography and also on real contact pressure achieved between the pin and the disk are discussed in this section. As it has been mentioned during the analysis of the results, greater depth of groove is measured for WFA than for 3SG alumina disk. WFA presents a mean depth of 23 μm while SG has a mean depth of 17 μm as it is shown in Figure 64. Both disks have been designed with abrasive grain size of 300 μm , therefore, measured wear depth represents 7.67% of a total abrasive grain for WFA and 5.67% in the case of SG abrasive grains. In this sense, linking the wear suffered by grinding wheel during a real grinding process to the wear of alumina disk on pin-on-disk tribometer can be verified due to the lack of abrasive grain pull out.

Furthermore, in the case of WFA abrasive grains, it can also be confirmed the no existence of grain breakage on WFA abrasive grains. This affirmation can be done because if one crystal of a complete abrasive grain is broken, approximately 1/3 of abrasive grain size, thus 100 μm would be lost. However, the measured wear is about 23 μm . Therefore, the unique type of wear that

can occur is flatness of abrasive grains due to tribochemical reactions. Similarly to grinding wheel wear on a real process, this type of wear represents wear flat. In contrast, this is not the case for 3SG alumina disk, because of the size of the microcrystals of SG abrasive grains, approximately 0.1-5 μm . Therefore, the distinction between grain breakage and grain flatness cannot be done only with wear depth quantification.

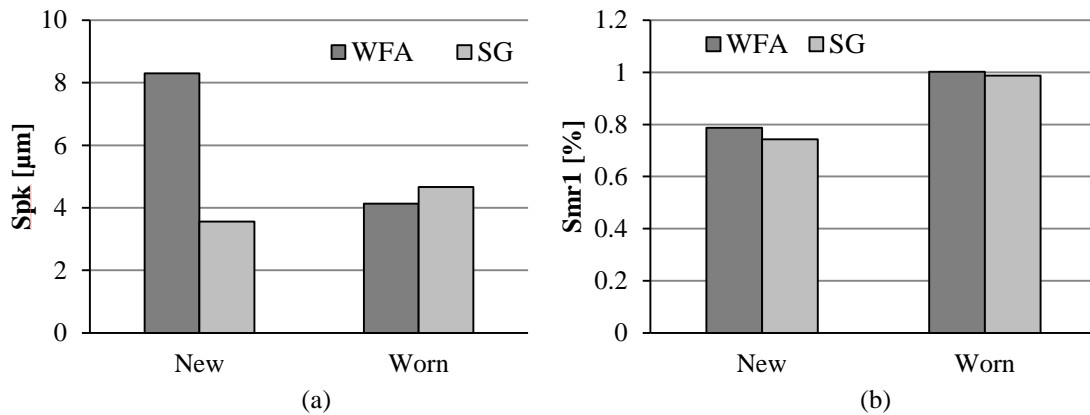


Figure 70: Comparison between *new* and *worn* states of WFA and 3SG alumina disk (a) reduced peak height and (b) peak material proportion

To identify each type of abrasive grain wear, particularly the 3SG alumina disk, in tribological wear tests, 3D functional parameters are used. Reduced peak height (S_{pk}) and peak material proportion (S_{mr1}) parameters are the most significant parameters to determinate the differences between *new* and *worn* states of alumina disk for both WFA and 3SG. The values of these states are represented in Figure 70 respectively. Regarding WFA, if *new* and *worn* states are compared, higher values of S_{pk} are achieved for *new* alumina. Just dressed state is rougher than worn alumina; a sharper surface due to dressing is achieved on the disk. As it is shown in Figure 70 (a) the height of the peaks is halved for worn alumina. Additionally, in worn WFA surface an increase of 20% is shown on material proportion in the peaks in Figure 70 (b). These two facts lead to a loss of sharpness of the worn surface, being higher the quantity of material accumulated in lower height. Therefore, it is confirmed that wear flat is the wear type that occurs in WFA disk studied under controlled contact conditions.

Regarding 3SG alumina disk, and in contrast to WFA behavior, S_{pk} increases from *new* to *worn* by less than 25%, showing a sharper surface on *worn* alumina. With respect to S_{mr1} , the same increase of 25% in the peak material proportion is shown, maintaining the relation between peaks and material increase and hence maintaining the surface characteristic. Both *new* and *worn* 3SG alumina disk present a very similar sharpness. Therefore, the main wear type of 3SG alumina disk during pin-on-disk tests is the microfracture of abrasive grains, leading to self-

sharpening. Likewise, analyzing valley material proportion S_{mr2} , Figure 71, for both WFA and 3SG disk there are no differences shown between *new* and *worn* states. Therefore, it can be confirmed the absence of dulling of abrasive surfaces.

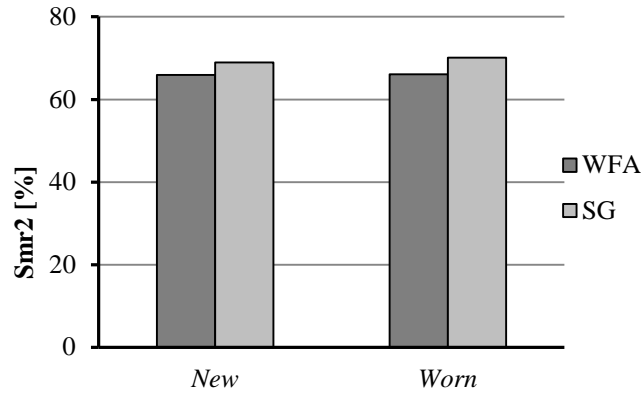


Figure 71: Valley material proportion to compare of *new* and *worn* states of WFA and 3SG disk

The conclusions reached regarding mainly to S_{pk} and S_{mr1} functional parameters, are corroborated on the surfaces shown in Figure 72, 3D digitalized topographies show dissimilarities on the worn alumina which can be clearly appreciated on the envelope line of profiles after applying morphological filter, in the down part of the figure. The groove generated after the tribological test is marked in red both in 3D topography and in the envelope line. A flatter surface is shown on *worn* WFA disk compared to *worn* 3SG alumina disk, and greater peaks are plotted on the 3SG *worn* profile, corresponding to the effect of self-sharpening of SG abrasive grains.

Regarding the real contact pressure achieved between the alumina disk and the steel pin, the crystalline structure of alumina abrasive grains is the parameter which presents higher influence on it. The real contact pressure, p_r , achieved for 3SG disk is approximately 35% higher than for WFA regardless of the sliding speed as it is shown in Figure 69. Two effects are responsible for these dissimilarities regarding crystalline structure of abrasive grains. On the one hand, higher real contact area values are measured on WFA, due to the abrasive grain shape and surface. Likewise, *new* 3SG surface is sharper than that of the WFA. While A_r is about 30% of A_a for WFA disk, for 3SG is of 25%. Furthermore, as it is shown in Figure 72 not only *new* but also *worn* 3SG alumina presents a sharper surface. On the other hand, normal forces reached during the tests are approximately 16% lower for the WFA than for the 3SG alumina disk. Therefore, following the Eq.9 higher real contact pressures are achieved for the 3SG alumina disk, reaching a maximum of 190 MPa for 20 m/s.

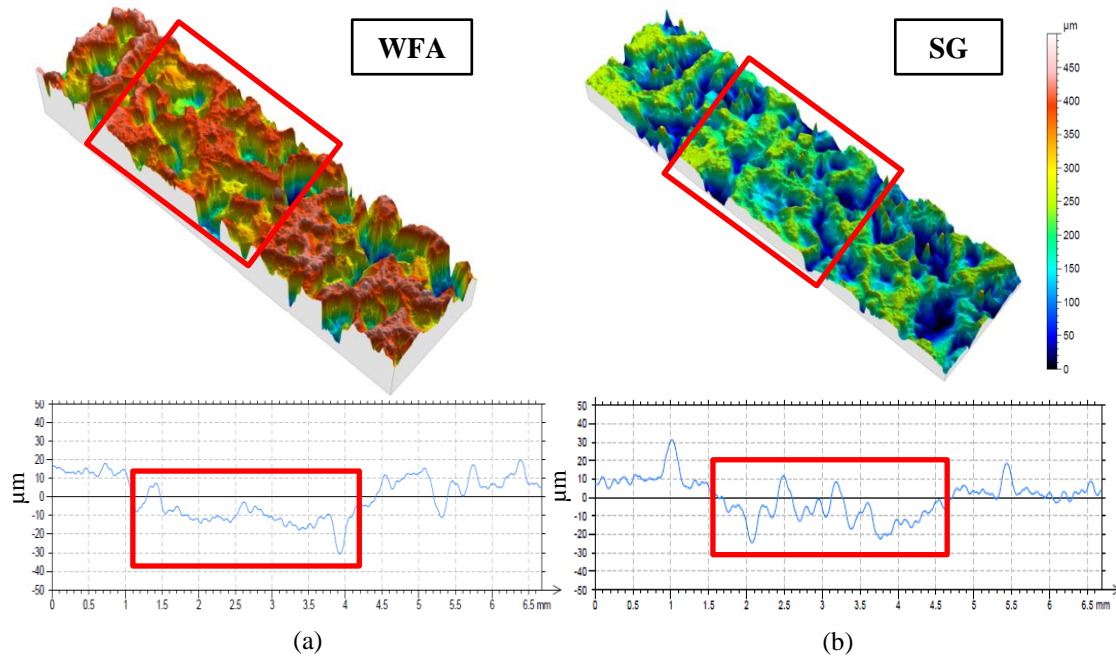


Figure 72: 3D wheel surface digitalization and envelope of filtered superimposed profiles for (a) WFA and (b) 3SG alumina.

Making a similarity to the grinding process, during the pin-on-disk tests, of the three wear mechanisms that take place during grinding contact, rubbing and ploughing are the most relevant. However, for 3SG disk topography, due to the sharper surface comparing with WFA disk surface, cutting also takes place, but to a lesser extent than real grinding tests values. The rubbing mechanism in WFA has a higher importance, which is confirmed with the S_{pk} parameter comparing the effect of the wear. Therefore, rubbing phenomenon increases the contact temperature and hence, the pin temperature. The hardened steel pin becomes soft and it is worn quicker than the case of 3SG alumina disk. As it is shown in Figure 73, SG abrasive grains contact more times with the pin than the WFA ones. Thus, the contact time of 3SG tests is slightly higher and pin wear is not as quick as the WFA tests. The theoretical force is imposed for the pneumatic cylinder but the short contact time enhanced the material softening due to high temperatures in the contact leads to a lower contact force than the programmed ones. Furthermore, the fact that high temperatures are reached in the contact also explain the high wear values reached on both alumina disks in a very short contact time.

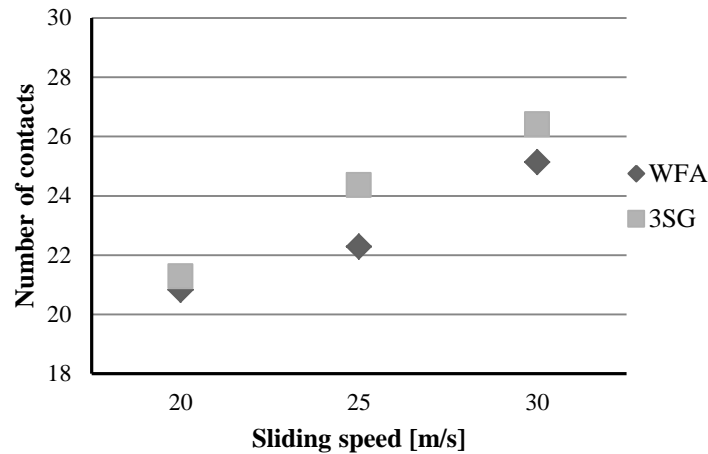


Figure 73: Number of contacts of each type of abrasive grain with the steel pin on a complete test.

IV.6. Preliminary conclusions

On the basis of the designed pin-on-disk and the tests carried out using contact conditions close to grinding process, the following conclusions can be drawn:

- An original design of a pin-on-disk tribometer is presented for the analysis of the behavior of abrasive grains in the grinding processes conditions. The achieved contact conditions are close to those of the real grinding process. This consideration allows the extrapolation of results obtained on the pin-on-disk tribometer to the design of industrial grinding wheels for a specific grinding operation.
- With the designed pin-on-disk tribometer not only are sliding speeds and real contact pressures close to those achieved in grinding process reproduced but also the thermal cycle suffered by abrasive grains is considered. Regarding sliding speeds, 20-25-30 m/s are studied. In contrast, the maximum real contact pressure achieved is about 190MPa, being the pressure of grinding process about 1-2 GPa. Despite this difference, this work is the closest approach to real grinding process.
- Grinding contact conditions are imposed and thoroughly controlled on the tests carried out in the pin-on-disk tribometer with the aim of differentiate wear behavior of two types of alumina crystalline structure: WFA and SG abrasive grains.
- The real contact area is quantified once the abrasive surface of the disk is dressed. In the case of WFA, the real contact area is $29.33 \pm 1.86\%$ of apparent area and for 3SG alumina surface this is $22.43 \pm 0.99\%$. These values shown a sharper 3SG alumina disk compared to WFA.

- Due to the heavy contact conditions and the small pin area, high temperatures are reached in the contact, leading to a very short contact times of about 1.1 s. Therefore, the theoretical forces could not be achieved. Likewise, the influence of imposed pneumatic pressure is negligible in the obtained results. Only the influence of sliding speed on the test results is taken into account.
- Lower sliding speed leads to higher contact forces regardless of the alumina studied. Moreover, a lower real contact area is measured on SG alumina. Therefore, the real contact pressure decrease with sliding speed, from 20 m/s to 30 m/s a decrease of 15% is measured. Extrapolating the influence of s to the grinding process, it can be concluded that higher cutting speed implies lower real contact pressure on abrasive grains.
- For the studied sliding speed range, s does not present a significant influence on abrasive grain wear. However, the influence of the crystalline structure of abrasive grains is appreciable both on the depth of wear and the appearance of the *worn* surface. WFA presents a 23 μm wear depth whilst 3SG disk presents a wear depth of 17 μm . Moreover, the 3SG *worn* surface is sharper than the WFA *worn* part.
- Regarding the friction coefficient, the values reached on the pin-on -disk tests vary from 0.22 to 0.25. However, on grinding tests these values are higher, from 0.33 to 0.38. These differences are due to the predominant wear mechanisms on contact. In the case of grinding tests, cutting, rubbing and ploughing appear. In contrast, during the tribological tests rubbing and ploughing are predominant although for WFA its influence is heavier, leading to a flatter *worn* surface.
- The presented device appears to be suitable for the analysis of the behavior of abrasive grains in the grinding process, suggesting that this could be a useful industrial tool for the design of grinding wheels for specific application. The materials in contact, grinding wheel characteristics (grain crystalline structure, material, size...), contact conditions even the cooling of grinding process are considered in the design of the pin-on-disk tribometer.

Chapter V: First approach to modeling
the wear of alumina abrasive grains

V. FIRST APPROACH TO MODELING THE WEAR OF ALUMINA ABRASIVE GRAINS

V.1. Introduction

As pointed out in *Chapter III* and *Chapter IV*, the wear of grinding wheels is a handicap in the design and implementation of the grinding process. Furthermore, in *Chapter II* it is addressed the randomness of abrasive wheels and the difficulties of modeling the grinding process, particularly grinding wheel wear. In this sense, and following the tribological study carried out in *Chapter IV*, the main contribution of the present chapter is to reproduce the contact between a single abrasive grain and the workpiece under real conditions in order to understand the phenomenon which leads to grain wear. Discrete element method (DEM) is used to develop the model of wear of an alumina abrasive grain. As on a whole research work, from the different type of wears, the characterization of wear flat is addressed. In *Chapter III* it is determined the importance of tribochemical reactions on wear flat generation. Third body adhered to worn abrasive grains changes contact conditions during grinding. Likewise, in *Chapter II Section II.6.3* tribological studies using DEM are shown, being the main advantage the consideration of detached elements of the main bodies as a third body. Using DEM, the third body is maintained in contact with the other bodies even if it is adhered to the bodies.

Therefore, due to the importance of the tribological behavior and the third body influence on the contact during grinding and wear generation, DEM is used to model the wear of an abrasive grain under grinding contact conditions. GranOO is a free C++/Python discrete element workbench used for the development of the model. In this sense, the present work was performed in the facilities of the department of i2M dept. DUMAS of the ENSAM in Talence, supervised by Prof. Ivan Jordanoff.

This chapter is distributed as follows. Firstly, the basis of wear modeling is presented, so the main objective of the wear model is clarified. After that, the definition of two different behavior of alumina are justified, showing the variation of alumina properties with the temperature. Likewise, 2D finite element thermal model is carried out in order to determinate the height of the isotherm at which the alumina presents the higher variations on its behavior. This height is an important requisite to develop the discrete element model to predict wear of a single abrasive grain. DEM is the last issue that is going to be addressed in the present chapter.

V.2. Alumina abrasive grain wear model

V.2.1. Objectives of the wear model

The work developed in previous chapters is focused in the study of abrasive grain wear from an experimental point of view. On the one part, the wear flat occurrence in alumina abrasive grains during real grinding is analyzed. On the other part, tribological experiments are carried out in order to quantify the wear of alumina abrasive grain under controlled contact conditions. The results obtained from both experimental works are representative of real grinding process behavior. In contrast, as it is known, the experimental work presents limitations. For this case of study, the two main limitations are related to the temperature reached in the contact and to the tribochemical behavior that leads to third body generation and grain wear.

Regarding the contact temperature, the short contact time and the difficulties to access to contact zone make almost impossible the measurement of the temperature during tests. However, to know this temperature is of interest because of the changes in the behavior of the alumina. Properties of alumina change with temperature, presenting a behavior closer to a ductile material near the contact and to brittle material, as at room temperature. Likewise, experimentally is not possible to know the proportion of the abrasive grain affected by the temperature. To this end, a thermal model is required to analyze the thermal field of the abrasive grain.

Concerning to the third body and tribochemical wear, on grinding tests is observed the presence of the third body adhered to the flat abrasive grains. Moreover, on tribological test only final wear of the alumina is quantified. Initial and final states of the alumina can be analyzed, but the intermediate states of the wear and the third body evolution cannot be known. Likewise, it is of interest to know how the third body is generated and how contact conditions affect to the third body generation and hence, to the wear of the abrasive grain. In this sense, wear simulation helps to reach a better understanding of the generation of the third body and grain wear from the beginning of the contact to the last state.

Therefore, the general objective of this chapter is to understand the behavior of the wear of the abrasive grains under real contact conditions during grinding process. To this end, the following two intermediate goals are set. Firstly, the temperature in the contact and inside abrasive grain is determinate using a thermal analysis. The distribution of the isotherms inside the abrasive grain is of interest. Secondly, the generation of third body in the contact and its influence on the wear of thee abrasive grains is evaluated developing a discrete element model in which real contact conditions are imposed.

V.2.2. Basis of the wear model

As it is known, a grinding wheel is composed of abrasive grains randomly embedded on a bonding matrix, presenting also a certain porosity. Therefore, the reproduction of the behavior of a complete grinding wheel is a difficult task, and vast majority of works are focused on the single grain models [65,78,107]. Likewise, to reproduce the mechanical properties of an heterogeneous body is one of the handicaps to model grinding wheels under process real conditions. In this sense, the use of DEM is the most appropriate method to reproduce an heterogeneous bodies [115,129]. Moreover, the generation of both grinding wheel structure and its surface with accuracy is also a tedious task. For simplicity, a single abrasive grain model is developed as a first approach to model the wear of alumina abrasive grains under real contact conditions. This abrasive grain slides against a hardened steel workpiece.

Regarding the shape of the abrasive grain, real abrasive grains present random shape with a numerous cutting edges. In the bibliography a wide range of simple shapes are chosen by different researchers. Abrasive grains can be assumed spherical [130], conical [131] or pyramidal [132] in shape. The sharpness of cutting edges is usually defined by the radius and the slope of each cutting edge. While conical and pyramidal shapes reproduce well the slope of the cutting edges, in the case of the sphere, the radius is well reproduce but also the slope because the inclination changes depending on the depth of the abrasive grains. Therefore, it is concluded that the best shape to reproduce an abrasive grain is sphere. So, for the present wear model a spherical abrasive grain is going to be modeled. Moreover, the size of this abrasive grain is 300 μm of diameter, like the abrasive grain size of grinding wheels used for the tribological tests in *Chapter IV*. For the implementation of the wear model, the loads applied to the abrasive grain are also obtained from the tribological test data. These parameters are going to be detailed in the next paragraphs.

The abrasive grain is embedded on a wheel matrix, being more than 50% of the abrasive grain inside the wheel, surrounded by the bond. At worst, for the case of study, 150 μm are subject to be worn. This fact allows to model a semi-sphere instead of a complete sphere. This hypothesis has also the advantage of the reduction of the model computational cost. However, this reduction is not the unique advantage of modeling a semi-sphere, the presence of a flat surface enable the application of model inputs as is detailed in following paragraph.

With concern to the model inputs, as on tribological tests carried out in *Chapter IV*, sliding speed (s) and real contact pressure (p_r) are implemented. In Figure 74 the two bodies in contact are shown, abrasive grain and workpiece and the two model inputs. The values of sliding speed and contact pressure are going to be the same that the ones used in the tribological tests in order

to compare the results obtained from the simulations with the experimentally achieved values. As it is mentioned above, only a semi-sphere is modeled. Thus, in the upper part of the abrasive grain a flat surface is generated. This surface allows the homogeneous application of the pressure on all the abrasive grain, being therefore another advantage of simulating only a half of a sphere.

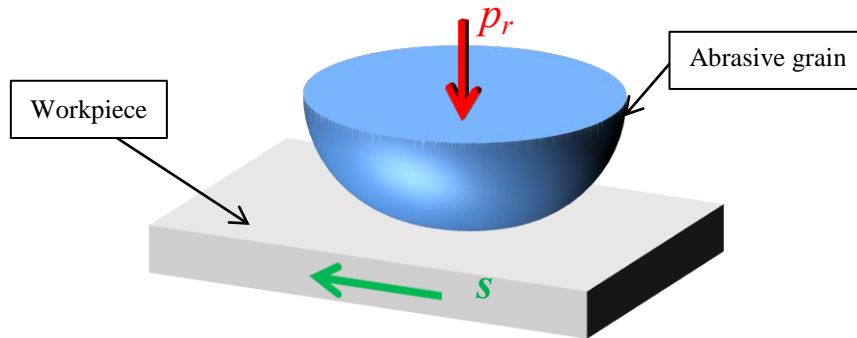


Figure 74: Scheme of contact modeling, two bodies in contact and the model solicitations.

The few numerical works referred to the study of the wear of grinding wheels are based on probabilistic methods or statistical analysis between others, simulating a complete topography of grinding wheel. These methods do not differentiate the type of wear or the phenomenon that leads to the wear as it is deeply analyze in *Chapter II*. On the contrary, the aim of the present model is to determinate the tribochemical wear of the abrasive grain. This wear is mainly represented by the generation of the third body, both attached to the worn abrasive grain and removed from the contact. Due to the suitability of discrete elements to modeling the third body generation and to the faculty of reproduce the wear. A single abrasive grain is modeled using discrete element method.

When two bodies are in contact and external forces are applied the third body is generated. In a real contact this third body consist of detached particles from the two first bodies in contact, in this case particles of alumina and particles of steel and also of other compounds generated due to the chemical reactions. However, for simplicity, from the two initial bodies in contact, alumina abrasive grain and hardened steel workpiece, the hypothesis of consider a non-degradable body to workpiece is assumed. Therefore, the third body is going to be composed of alumina detached particles. As the third body generates, alumina abrasive grain wears down.

DEM is usually suitable to model discontinuous material. However, in this case alumina is considered a continuous material. The reason, as it is previously mentioned, is that DEM is well adapted to simulate wear because discrete elements are easily detached from the initial body. In

this sense, the discretization of the body is useful to model the wear and third body generation, as it behaves as a discontinuous material. Likewise, in order to simulate continuous material using DEM a 3D cohesive beam model was created [133], which is implemented in order to model the alumina abrasive grain. The basis of this cohesive beam model is deeply detailed in *Section V.4.4* hereafter.

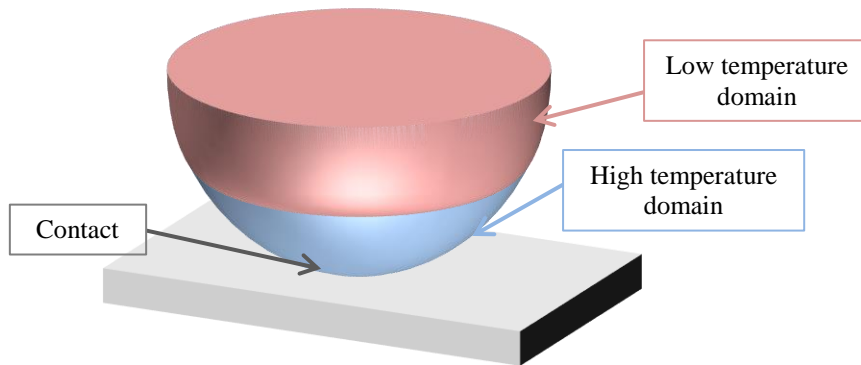


Figure 75: Domains division regarding the temperature in the contact.

One of the most important parameter that affects the wear of the abrasive grain is the temperature reached in the contact. In *Chapters III and IV* it is remarked the importance of the temperature in wear flat development and in the acceleration of chemical reactions. Therefore, it is necessary to consider the effect of temperature to model the wear of the abrasive grain. A thermal discrete element model is not accomplished. In contrast, a higher temperature of the contact part comparing to the inner part of the abrasive grain is considered. To this end, the semi-sphere, which models the abrasive grain, is divided in two different domains as it is shown in Figure 75. The *down domain* (in blue) is in contact with the workpiece and the temperatures reached in this domain are higher than temperatures in the *up domain*, in red. This differentiation allows to consider the temperature in the discrete element model without the necessity to develop a thermal DEM.

Finally, the wear of both WFA and SG abrasive grains are simulated. Properties of conventional and microcrystalline alumina are quite different. However, in the bibliography, are not clearly defined the crystalline structure of the alumina when mechanical or thermal properties are defined. Therefore, the dissimilarities between two crystalline structures are taken into account both in thermal and wear model with the following assumptions. For the thermal model, the heat source of WFA or SG abrasive grain is calculated using the tribometer data. Therefore, each

case of study is calculated with a real heat generated in the tribometer, being higher for SG alumina abrasive grain. To bear in mind the different behavior of alumina in wear model, different beam failure criteria is defined. These two hypothesis to consider the crystalline structure in the thermal and finally in wear model are deeply analyze during this chapter.

V.3. Determination of 2 domains in the abrasive grain

Once the necessity of differentiate two domains in the abrasive grain is established, the next step is to quantify the height of the abrasive grain corresponding to the *down domain* and to *up domain*. Moreover, it is of importance to bear in mind the variations of mechanical and thermal properties of alumina with temperature. Hereafter, the variations of these properties are analyzed and the alumina properties are shown. Likewise, in order to determinate with accuracy the height of *down domain*, a 2D thermal analysis is carried out to alumina abrasive grain.

V.3.1. Variation of Al₂O₃ properties with temperature

Thermal, mechanical and physical properties of alumina are a key input for the model in order to simulate the wear of the abrasive grain. On the one hand, depending on the porosity, crystalline structure and even the purity of alumina, the properties of alumina may be different, in some cases in a wide range of values. On the other hand, properties of alumina vary with the temperature. Therefore, in the bibliography a great discrepancy of alumina properties is found. To carry out the simulation of the wear of the alumina abrasive grain, the following alumina properties are considered, taking into account the changes with temperature. In Figure 76 the evolution with temperature of thermal conductivity (K), specific heat capacity (c_p) and Young's modulus (E) is plotted [134]. As it is shown, the increase of temperature varies the properties of alumina, being necessary to take into account this variation in the behavior of the alumina during wear simulation.

As it is previously mentioned, the influence of temperature in the wear of alumina is considered establishing two different domains in the abrasive grain. *Down domain* corresponds to high temperature domain because it is the part of the abrasive grain in contact or close to the contact, in which high temperatures are achieved. The behavior of this part is affected by high temperatures and presents a more ductile behavior than if room temperature governs. In contrast, *up domain* correspond to room temperature domain. The alumina, a ceramic material, presents low thermal conductivity, therefore, the increase of the temperature in the alumina is negligible comparing to the temperature reached in the contact. This fact it is corroborated in the thermal analysis carried out on a single abrasive grain in *Section V.3.2*.

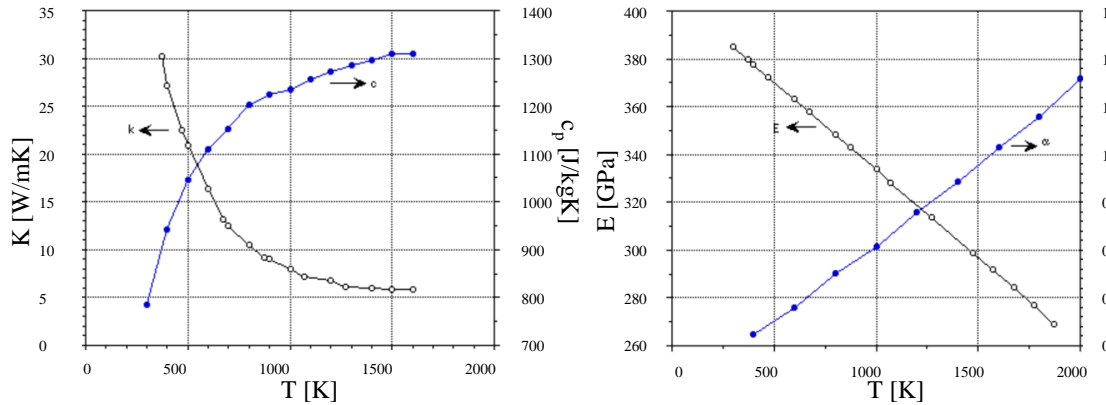


Figure 76: Variation of alumina properties with temperature [134]

Once the necessity to define two different domains in the abrasive grain is established, the next step is to determinate the proportion of the abrasive grain which corresponds to the *down domain* and to the *up domain*. To this end, thermal model of a single alumina abrasive grain is developed in the following section, with the aim of obtaining the height corresponding to the *down domain*.

V.3.2.2D finite element thermal model of alumina abrasive grain

The 2D thermal model is developed using a finite element method (FEM). The software used to carry out the simulation is ANSYS[®] Mechanical APDL. This software is a powerful scripting language that allows to automate common tasks and to parameterize the model. For simplicity, the model consists of a single abrasive grain with a heat source in the contact area. The aim of this thermal model is simply the determination of the height of the isotherm at which the behavior of alumina is different due to the changes on its properties.

Thermal conductivity is continuously decreasing and specific heat capacity continuously increasing with temperature. The steady properties of alumina are reached at temperatures higher than 1300°C. However, the changing values of properties at lower temperatures have also an effect on the wear of the alumina, not only when temperature of 1300°C is reached. Therefore, for the present thermal model and also for the wear model, the hypothesis of establishing differences in the behavior at a temperature of 200°C is assumed. Therefore, the height corresponding to 200°C isotherm is determined in the abrasive grain, and this value of height defines the 2 domains.

With this hypothesis, it is considered that alumina behaves similarly from room temperature up to 200°C but from this temperature the changes of alumina properties lead to changes in the behavior of the alumina, even behaving as a ductile material just in the contact, when the

highest temperatures are reached [16]. In the experimental grinding tests explained in *Chapter III*, the effect of high temperature in worn alumina is discussed, showing also the plastic deformation in the most superficial layers of the grinding wheel, confirming the high temperatures reached in the contact. Based on the previous affirmation, in which the behavior of the alumina is different depending on the temperature and assuming the isotherm of 200°C as a temperature at which the behavior of alumina changes, the development of the thermal model is deeply explained hereafter.

V.3.2.1. Simplifications for the finite element thermal model

As it is previously mentioned, the aim of this thermal model is to establish the height from the contact at which the behavior of alumina changes due to the temperature. To this end, a single abrasive grain is modeled. The shape of the abrasive grain is shown in Figure 77, being the equivalent diameter of the abrasive grain of 350 μm . Moreover, the contact distance of the abrasive grain is calculated following the approach doing by Malkin [27], being in this case 35 μm , as it is marked in red in Figure 79. This length is considered to generate the shape of the abrasive grain and is the part of the grain in which heat source is applied.

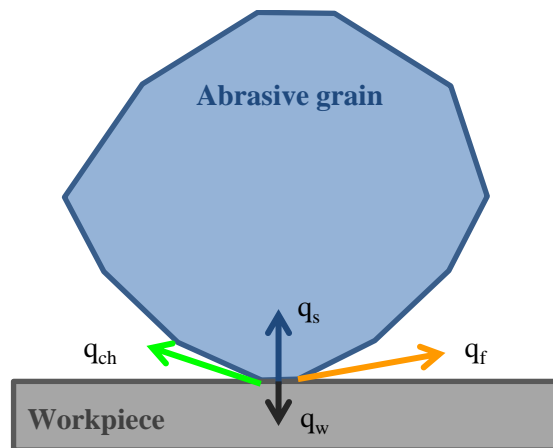


Figure 77: Heat distribution in grinding

To calculate the heat source, results obtained in tribological tests in *Chapter IV* are used. As on tribological tests, three different cases are simulated for each type of crystalline structure of alumina, WFA and SG, at three different sliding speeds of 20-25-30 m/s. The data acquired from the tribometer is the real contact area (A_r), tangential force (F_t) and real contact time (t_c) for each case of study. Total heat flux on the contact is calculated using the tribometer data following Eq.10. Moreover, in Figure 77 and Eq.11 the distribution of total heat flux is shown. The heat flux of the grain and of the workpiece is at least two orders of magnitude bigger than the heat flux of the chip or of the grinding fluid. Therefore, the heat flux corresponding to the

chip and the fluid is negligible comparing to heat flux of the grain and the heat flux of the workpiece. From now on, it is going to assume that the total heat flux is the summation of grain and workpiece heat flux as it is described in Eq.12.

$$q_t = \frac{P}{A_r} = \frac{F_t s}{A_r} \quad \text{Eq.10}$$

$$q_t = q_w + q_g + q_{ch} + q_f \quad \text{Eq.11}$$

$$q_t = q_w + q_g \quad \text{Eq.12}$$

Likewise, the heat flux of the workpiece is also expressed as in Eq.13. The partition of heat that is directed to the workpiece, R_w , is of maximum interest in thermal aspects of grinding. While R_w is mainly studied due to the thermal damage generated in the workpiece, for the case of study is of interest to determinate the heat flux directed to the abrasive grain in order to analyze the wear of the grain. Nevertheless, the value of R_w is widely studied by different authors [27,32,63,135], showing a wide range of values varying from 0.25 to 0.9 depending on the wheel, workpiece materials and grinding kinematics. As it is mentioned, for the present thermal model, the heat flux of the grain is required, which it can be directly calculated if the total heat flux and partition of heat of the workpiece is known as it is shown in Eq.14.

$$q_w = R_w q_t \quad \text{Eq.13}$$

$$q_g = (1 - R_w) q_t \quad \text{Eq.14}$$

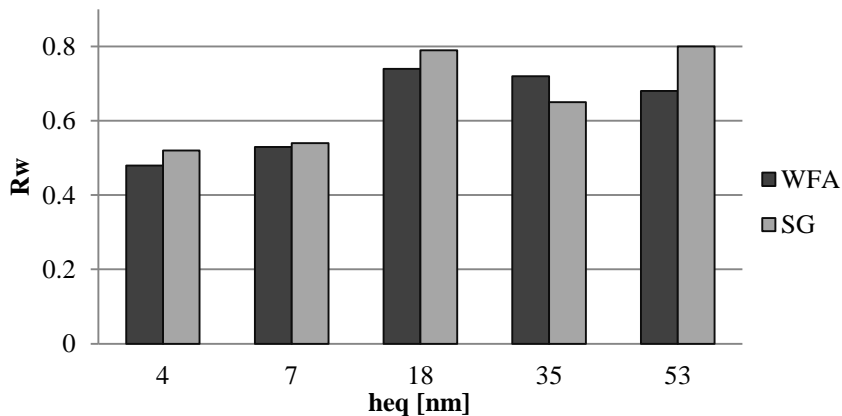


Figure 78: Values of heat partitioning ratio to workpiece depending on equivalent chip thickness and crystalline structure of alumina abrasive grains [63]

For the case of study, a single abrasive grain sliding against hardened steel is evaluated, being ploughing and rubbing the wear mechanisms that take place. Moreover, Garcia [63] analyze R_w depending on the equivalent chip thickness and on the crystalline structure of the alumina abrasive grains as it is shown in Figure 78. He concludes that for low equivalent chip thickness ($h_{eq}=4-7$ nm), where ploughing and rubbing are the predominant wear mechanisms, also low values of R_w are reached. This means that the heat to the abrasive grain is higher if ploughing and rubbing are the predominant wear mechanisms. So, to calculate the heat source of the 2D thermal model, $R_w=0.48$ for WFA abrasive grains and $R_w=0.54$ for SG alumina are used.

V.3.2.2. Thermal model definition

Once the simplifications and hypothesis to develop a thermal model of a single abrasive grain are established, the next step is to define boundary conditions. Heat source and the environment temperature are the boundary conditions that are considered in the thermal model as it is shown in Figure 79. With the aim of reproducing the tribological tests but modeling a single abrasive grain, the use of coolant is also taken into account. Thus, on grain free areas heat losses by convection for the fluid. A constant heat transfer by convection is used for fluid $h_f=10000$ W/m²K.

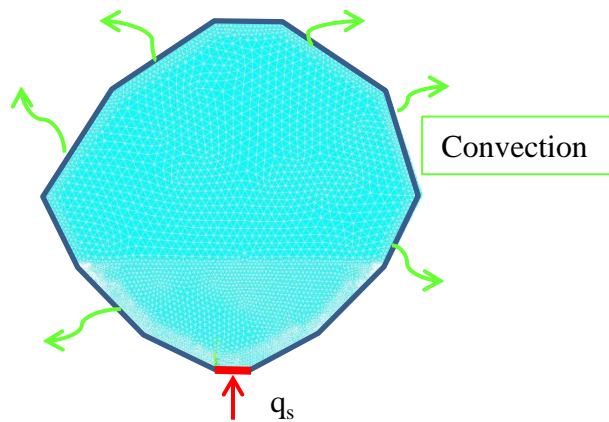


Figure 79: Abrasive grain boundary conditions and mesh density

Moreover, with R_w established in the previous section and the total heat flux obtained from the tribometer results of Chapter IV (F_t and A_r) the heat flux to the abrasive grain is calculated. In Table 21 the heat source for each case of study are built, which is one of the input parameter for 2D thermal model. The contact time is also a very important input for the thermal model. In this case, to get the contact time (t_c), the length of the pin, the sliding speed (s) and the number of contacts on each tribological test are taken into account. Due to the short t_c and the high s , the intermittent contact of each abrasive grain is not considered in the thermal model. In Table 21 t_c for each test are built.

Table 21: Input parameters for 2D thermal model.

Sliding speed [m/s]	20	25	30
Contact Time [s]	0.00525	0.00092	0.000858
q_g [W/m ²] WFA	304624 450	337743356	384326196
q_g [W/m ²] SG	386785714	413917411	483455357

Apart from the heat flux to the grain and the contact time, alumina properties are also determinants in order to develop a 2D thermal model. In the bibliography a wide range of values are found depending on the temperature of alumina, its purity even the crystalline structure of alumina, as it is mentioned in *Section V.3.1*. Therefore, for this particular model, in which the aim is to get the height of 200°C isotherm, the properties of alumina at 200°C are chosen as it is shown in Table 22. Finally, the model is meshed using triangular elements. The density of the mesh is higher in the down part of the abrasive grain and also in all the edge of the grain as it is shown in Figure 79.

Table 22: Alumina properties at 200°C [134]

Density ρ [kg/m ³]	3900
Thermal Conductivity K [W/mK]	20
Specific heat capacity c_p [J/kgK]	1046

V.3.2.3. Results of 2D thermal simulations

A total of six simulations are carried out in order to determinate the height of the isotherm corresponding to 200°C. Three for each alumina crystalline structure, at different sliding speeds as it is shown in Table 21. The results of each simulation are plotted in Figure 81, showing very similar results for 25 and 30 m/s tests and a higher heat for 20 m/s sliding speed. While for 20 m/s the isotherm height is higher than 100 μm , for 25 and 30 m/s is lower than 50 μm , as it is shown in Figure 80 (b). Likewise, comparing the influence of crystalline structure, upper height is achieved for SG abrasive grain comparing with WFA, as it is also shown in Figure 81 and Figure 80 (b).

Concerning to the maximum temperature, in Figure 81 the distribution of temperature through the abrasive grain are shown and in Figure 80 (a) the maximum temperature reached near the contact is summarized. In general, the maximum temperature is 900°C for 20 m/s and between 550 and 700°C for 25 and 30 m/s. Comparing the influence of crystalline structure, higher temperatures are reached in the contact for SG abrasive grain, about 100°C higher. In this thermal model the heat source is different for SG and WFA abrasive grains because is directly obtained from the results of tribological tests. However the results shown the initial hypothesis done to calculate the heat flux is correct owing to the temperatures reached are in concordance with thermal conductivity results obtained by Klocke [16].

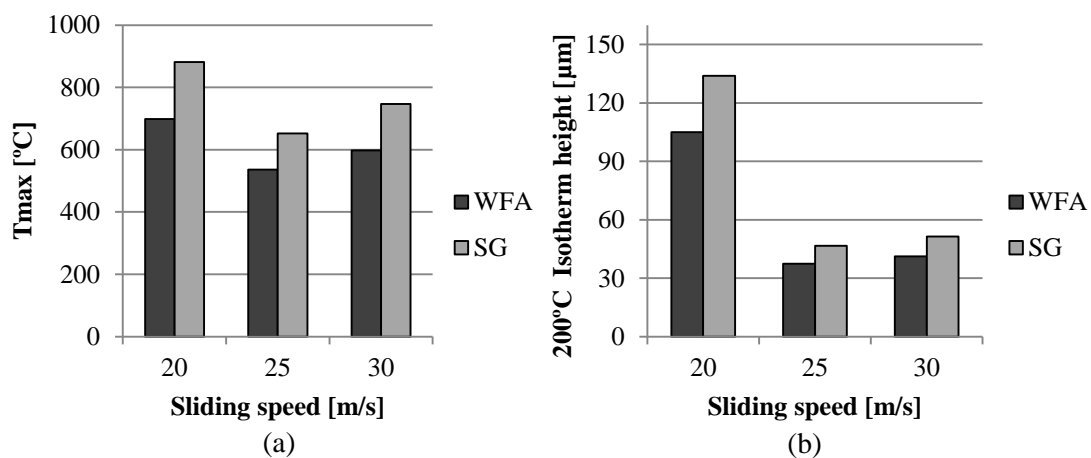


Figure 80: (a) Temperature maxima reached in the abrasive grain and (b) the height of 200°C isotherm.

Regarding the maximum values of temperature reached in the contact, in *Chapter III* it is mentioned that the temperature in the contact is close to melting temperature of workpiece material, about 1300°C for hardened steel. In contrast, thermal analysis of single abrasive grain shows a maximum value of 900°C. This dissimilarity is due to the short contact time comparing to the grinding process. Therefore, there is not enough time to achieve such high temperatures. Comparing different tests, a higher temperature is reached for the case of 20 m/s. So, the sliding speed has an influence on temperature reached in the alumina abrasive grain. In this sense, Klocke's results show great regions of alumina affected by plastic flow, however, in the actual grinding experimental tests, this phenomenon is not so relevant. This differences, apart from due to the thermal cycle suffered by the abrasive grains are also due to the differences in sliding speed, being 2 m/s in Klocke's tests and from 20 to 30 in the tests of the present work. Therefore, this finite element model brings out the influence of sliding speed in the achieved temperature and hence on the wear of the abrasive grain.

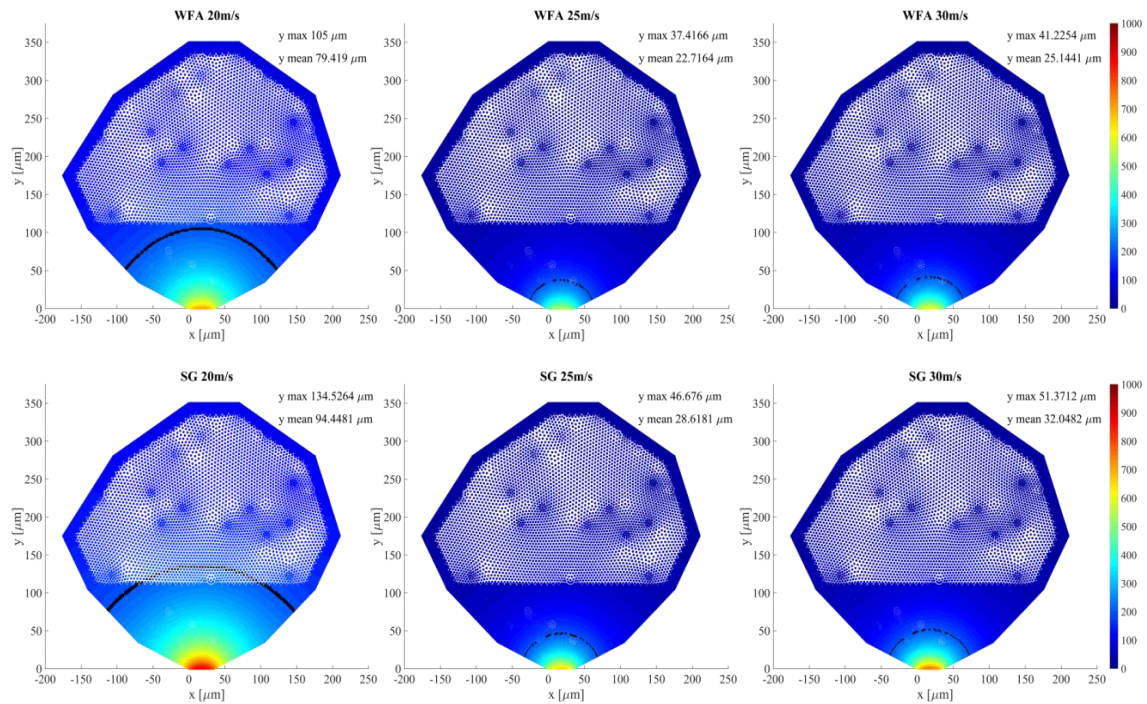


Figure 81: 2D thermal simulations results for the six cases of study.

Finally, to develop a discrete element model, the same height is going to be used for 25 and 30 m/s tests because the difference in height is lower than 10%. The sliding speed 20 m/s is not considered to carry out wear model. In contrast, differences due to the crystalline structure are bearded in mind to analyze the wear of WFA and SG abrasive grains. In Table 23 the heights that are going to be used in discrete element abrasive grain wear model are built and also, the height corresponding to 20 m/s.

Table 23: Mean values of 200°C isotherm height to define DEM

	20 m/s	25-30 m/s
WFA	105 μm	38 μm
SG	134 μm	47 μm

V.4. Abrasive grain wear simulation model

V.4.1. DEM for alumina abrasive grain wear simulation: GranOO

Discrete element methods are numerical methods generated by a large number of small particles, which demands high computational cost. DEM presents the capacity to describe a granular medium, therefore, is commonly used to study the damage of heterogeneous media. Thus, DEM is suitable to model discontinuous materials [133]. The discrete nature of this method leads to accurate results for a numerous applications. On the contrary, not only can heterogeneous solids be modeled using DEM, but also the behavior of homogeneous materials such as machining of ceramics are also analyzed [136]. Moreover, the problems of wear or fracture are not well adapted to continuous simulations using FEM because wear is a discontinuous phenomenon. Therefore, in order to consider a discontinuous phenomenon the use of DEM is a well adapted alternative.

In this sense, to develop the simulation of wear of alumina abrasive grain, DEM is chosen. Despite being alumina a continuous material, the discretization of the body is useful to model the wear of the abrasive grain, presenting discontinuous behavior. One of the main reasons to implement a DEM to simulate the wear of abrasive grain is the easiness to detach DEs corresponding to worn alumina. However, the main difficulty of DEM is the simulation of continuous material. To this end a 3D cohesive beam model is implemented [133]. The basis of this model is deeply explained in *Section V.4.4* hereafter.

From the different software or DEM workbenches that are available, GranOO C++ Workbench is used to carry out the abrasive grain wear model [137]. Its modularity together with its explicit DEM code specialized in modeling continuous materials allows the simulation of alumina abrasive grain. From the different choices of GranOO, only mechanical model is going to be implemented. Moreover, the regular contact laws implemented on GranOO enable to tackle the discontinuous dynamic problem of wear.

V.4.2. Main algorithm of the abrasive grain wear model

Figure 82 shows the flowchart that summarizes the simulation of the wear of the alumina abrasive grain using discrete element model. The simulation time is the real contact time, t_c , defined in Table 21, varying from 5 to 0.85 ms depending on the case of study. The most important variables to adjust in the model are the failure stress of the beams ($\sigma_{f\mu}$) and the adhesion parameter (γ), related to the third body adhesion both on abrasive grain and between

third body particles. These two parameters and all issues that have to be considered to develop the wear model are deeply described hereafter.

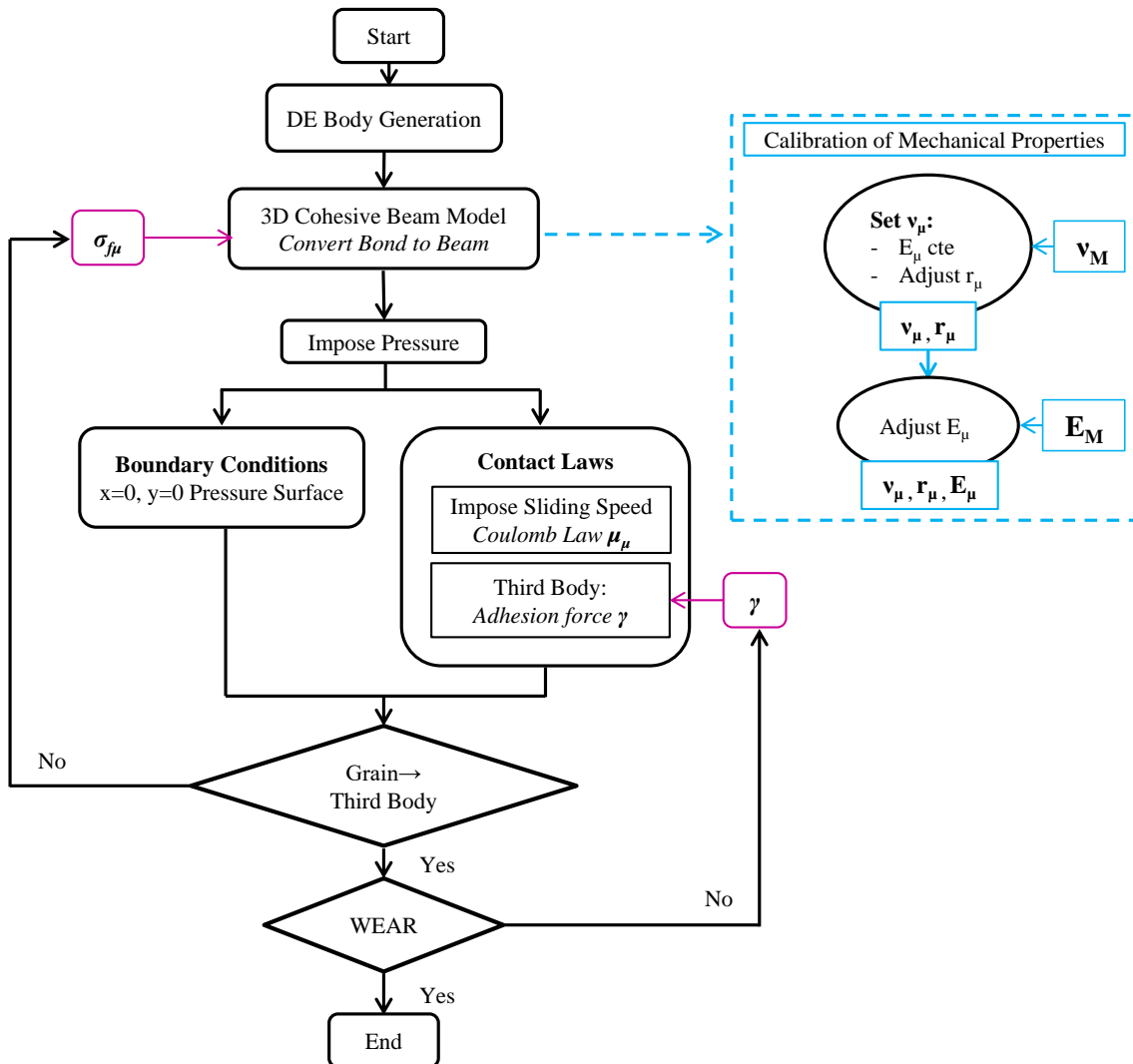


Figure 82: Flowchart to predict alumina abrasive grain wear

V.4.3. Discrete element model definition

Following the hypothesis of wear model detailed above in Section V.2 the contact between single alumina abrasive grain and the workpiece is studied using DEM. In this first approach of modeling of the wear of the abrasive grain only the differences in crystalline structure are considered. In this sense, the first model is developed for WFA abrasive grain. Once the model for WFA reproduces the wear, $\sigma_{f\mu}$ is adjusted until reproduce SG abrasive grains wear.

The sliding speed presents a great influence in the temperature reached in the abrasive grain and hence, on its wear. However, different sliding speeds are not considered in the model. The results of thermal analysis have shown similar isotherm height for 25 and 30 m/s, so the same

height is evaluated for both cases as shown in Table 23. In contrast, the case of 20 m/s is not analyzed in this first approach.

The contact behavior between the abrasive grain and the workpiece is determined by the contact laws defined for the grain, the workpiece and the generated third body. The correct definition of these contact laws allows to reproduce the real contact behavior and to generate the wear as on the real process. In the following paragraphs the contact laws are deeply analyzed. As it is previously detailed, from the two initial bodies in contact, the abrasive grain is a degradable first body while workpiece is a non-degradable first body. Therefore, in the model third body is only composed of detached grain particles. Even so, implementing an adequate contact law between third body and surrounding elements, the real behavior of third body in the contact can be simulated.

Regarding the workpiece, this body is modeled as non-degradable and non-deformable first body, a plane. The dimensions of this plane are 600x600 μm , positioned in the down part, just in contact with the abrasive grain as it is shown in Figure 83. The role of the workpiece in the model is to establish contact with the abrasive grain, with the purpose of impose the sliding speed.

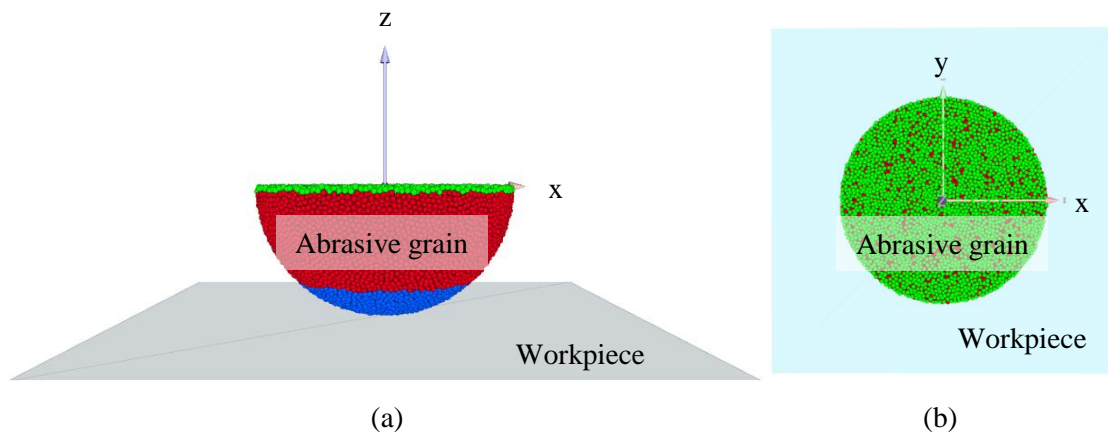


Figure 83: (a) Front view of model disposition and (b) upper view

In contrast, the abrasive grain is modeled as degradable and deformable first body being a semi-sphere $\text{Ø}300 \mu\text{m}$. The discretization of the abrasive grain is carried out using spherical DEs. In order to reproduce the continuous behavior of alumina material, 3D cohesive beam model is imposed. Thus, the DEs composing the abrasive grain are joined by beams. This issue is addressed in the next paragraph. For the grain generation, the radius of spheres are randomly chosen within a range of 25% around a mean value of the programmed radius 3 μm , a complete sphere of $\text{Ø}300 \mu\text{m}$ is built. The complete sphere is composed by a total of 85196 DEs.

However, in order to reduce the simulation time, between others, only a half of the sphere is modeled as it is previously justified in *Section V.2*.

As it is mentioned, two domains are defined in the abrasive grain in order to consider the effect of temperature in the wear simulation. Depending on the crystalline structure of the abrasive grain, the height corresponding to the *down domain*, affected by the temperature, is different. In Figure 84 the differences in *down domain* height are shown on WFA, 38 μm , and SG, 47 μm .

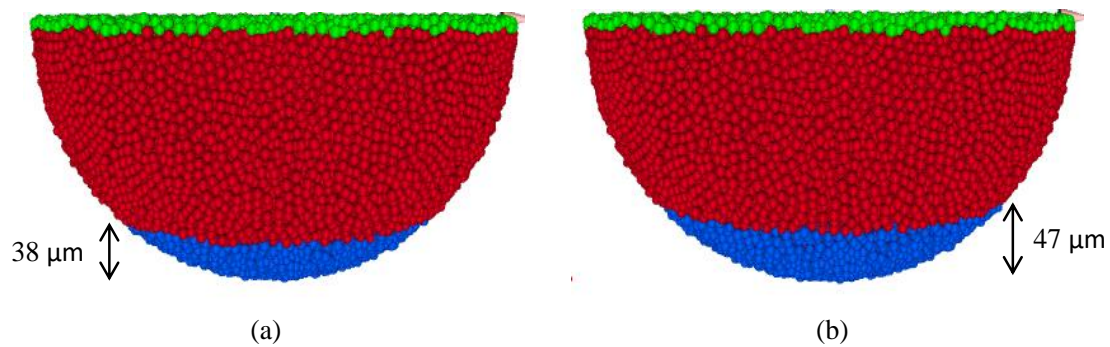


Figure 84: Domains and pressure surface definition on (a) WFA and (b) SG abrasive grains.

In the abrasive grain different sets of DEs and beams are defined in order to impose to each set different properties. For the case of study, four sets are distinguished: *down domain*, *up domain*, *Pressure Surface* and *third body*. *Down* and *up domains* are required to implement different behavior on beams. Therefore, *up domain* beams present the properties of alumina at room temperature. In Figure 84 *up domain* correspond to red+green DEs, while blue DEs represent *down domain*.

Table 24: Alumina macro properties for the different domains.

	Down domain (650°C)	Up domain (Room T ^a)
Density [kg/m ³]	3900	3900
Young's modulus [GPa]	343	385
Poisson's ratio	0.22	0.22

Alumina properties at 650°C are imposed to *down domain* beams. In Table 24 the properties of alumina at room temperature and at 650°C are built. Moreover, pressure surface is needed in

order to apply pressure to the model. Flat and homogeneous surface just in the upper part of the semi-sphere is generated halving the initial sphere. Finally, third body set allows implementing contact law between DEs corresponding to third body and the rest of the abrasive grain, with the workpiece and even between third body DEs. It is to be mentioned that DEs corresponding to third body are not connected by beams. In contrast, the adhesion force maintains third body attached to the abrasive grain or to other third body DEs.

V.4.4.3D cohesive beam model to alumina modeling

As it is previously mentioned, DEM is suitable to model discontinuous materials, however, because of the development of 3D cohesive beam model a continuous material can be modeled [133]. Cylindrical beams are defined by geometrical and mechanical properties. The length L_μ and a r_μ , the ratio between cohesive beam radius and the average DE radius are geometrical properties. Figure 85 shows the scheme of the cohesive beam configuration. Young's modulus E_μ and micro Poisson's coefficient ν_μ are mechanical properties which define the behavior of the beams. It is important to point that the micro properties of the beams are not the same as those mechanical properties of the alumina. These micro properties have to be calibrated as it is described hereafter.

The ends of the beams are fixed to DE centers and the beam is represented by the median line. Initially the beams are relaxed, but when the DEs moves, load is applied in the beams. Bending moment, axial force and torque are different type of load in the beam. The formulation describing forces and force reactions in the cohesive beam model are developed in [133].

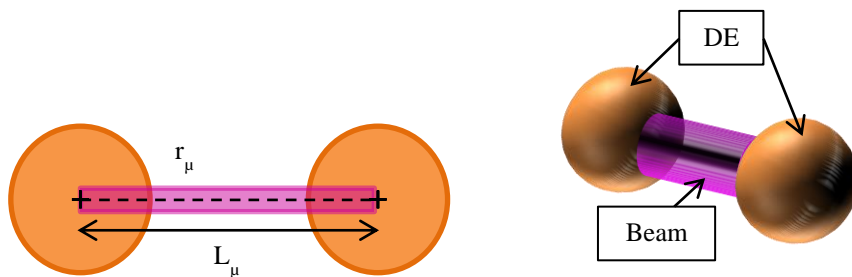


Figure 85: Cohesive beam bond [133]

Unlike the mechanical and geometrical properties, the beams do not have a mass. In DEM the mass is imposed to the discrete elements. This mass has to be calibrated and depend on the discrete element volume and density. The discrete element volume is known once the body of the abrasive grain is built. However, micro density of DEs has to be calculated from macro properties of a continuous domain following the Eq.15 [133].

$$\rho_{\mu} = \frac{\rho_M V_M}{\sum_{i=1}^N V_{\mu i}} \quad \text{Eq.15}$$

For the case of study, a semi-sphere is modeled as the abrasive grain. The density of the alumina is the same at room temperature and at 650°C. So, to calculate the micro density the two domains in the semi-sphere are not differentiated. The total volume corresponding to 41671 DEs which build the semi-sphere (V_{μ}) is $4.71 \times 10^{-12} \text{ m}^3$. To calculate the density of the model not only has the mass of the real abrasive grain to be considered, but also the mass of the complete system, thus, the mass of the grinding wheel. This consideration is required due to the pressure applied as a force in the wear model, this fact is deeply analyze in *Section V.4.5*. Therefore, to obtain the micro density of the model, the equivalent macro density of the abrasive grain has to be calculated first. This equivalent macro density corresponds to the total wheel mass in the semi-abrasive grain. The wheel mass is 10 kg and the macro volume of a semi abrasive grain (V_M) is $7.07 \times 10^{-12} \text{ m}^3$, so, the equivalent macro density (ρ_M) is $1.41 \times 10^{12} \text{ kg/m}^3$. Applying the Eq.15, micro density (ρ_{μ}) which corresponds to the semi-sphere is $2.12 \times 10^{12} \text{ kg/m}^3$. It is important to note that this ρ_{μ} has to be recalculated if the shape or the size of the modeled DE body changes.

V.4.4.1. Calibration of mechanical properties of the abrasive grain

From the four parameters that define the cohesive beams, L_{μ} , r_{μ} , E_{μ} and ν_{μ} , beam length depends on the distance between the discrete elements and it is imposed by built discrete domain but the other three are free parameters, so, they have to be calibrated. The calibration is carried out using a numerical uniaxial tensile test on cylindrical body following the procedure set by André et al. [133]. In this work is affirmed that macro Young's modulus is influenced by E_{μ} and r_{μ} and macro Poisson's ratio only by r_{μ} . Likewise, micro Poisson's ratio does not present influence in macro properties. Moreover, 10000 DEs cylinder is built to carry out the tensile test, which is considered a domain with acceptable precision.

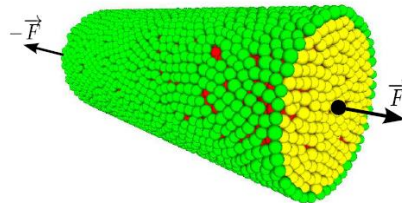


Figure 86: Force applied in tensile tests on a cylinder generated with 10000 DEs [133]

For the case of study, two different domains are defined in the semi-sphere. The *up domain* corresponds to alumina at room temperature and *down domain* to 650°C. Properties of alumina

change with temperature as shown Table 24. Therefore, the calibration of beams is carried out for both domains. In the following paragraphs calibration steps are described showing the results for room temperature case. Nevertheless, in Table 25 the results of the calibration for *down* and *up domain* are summarized.

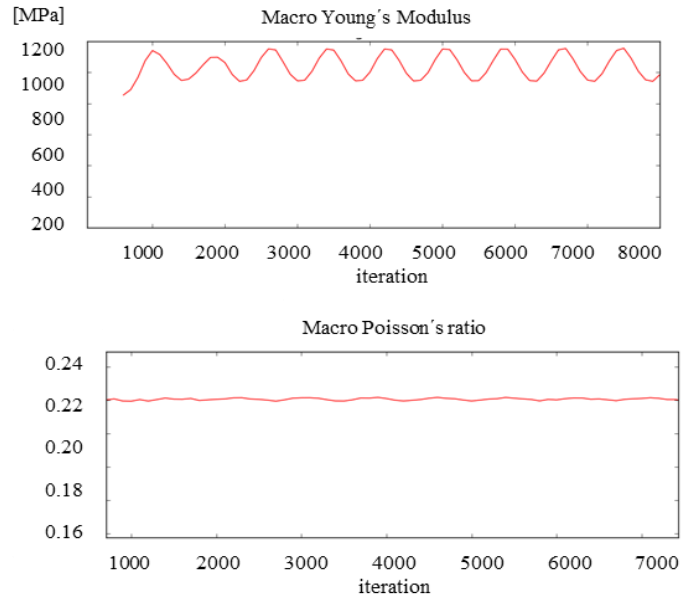


Figure 87: Results of the first tensile test. r_{μ} calibration obtaining stable and constant macro Poisson ratio.

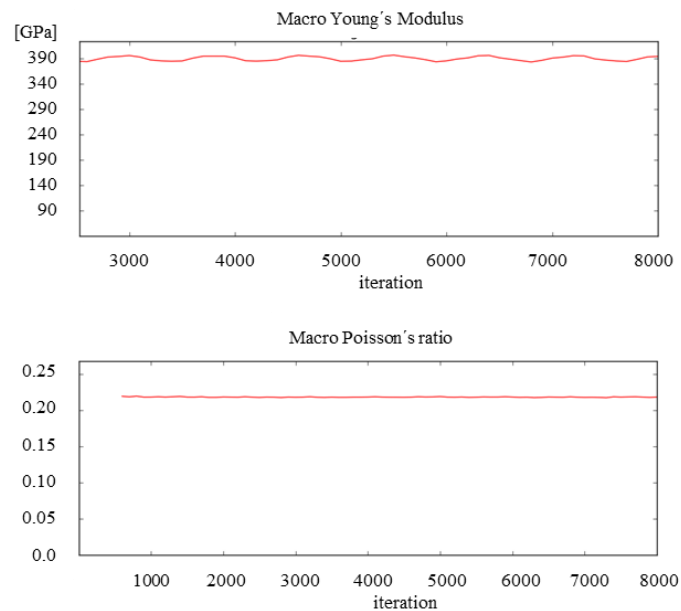


Figure 88: Results of the last tensile test. E_{μ} calibration obtaining stable and constant macro Poisson ratio and macro Young's modulus.

Loading force is applied to the tensile tests as a linear ramp and axial and transversal strain are measured. Due to the lack of influence of micro Poisson's ratio in macro parameters, an

arbitrary value can be established. So, in the present study $\nu_\mu=0.3$ is set, as it is usual. The calibration of the other two parameters is carried out in two steps: first the calibration of r_μ is done because ν_M only depends on this parameter and then E_μ is obtained. Micro parameters that are introduced in the model have to be iterated until achieve real macro parameters. In Figure 87 and Figure 88 the results of micro properties calibration at room temperature are shown.

In the first tensile test, the iteration of micro parameters is done until achieve stable and constant value for $\nu_M=0.22$. In this case, Figure 87 shows that the value obtained for E_M is not taken into account. In the first step $r_\mu=0.445$ is fixed. In the second test, both E_M and ν_M have to be constant and stable as shown in Figure 88. The value of $E_\mu=4015$ GPa is obtained in the last test, completing the calibration of the cohesive beams. As Table 25 shows, only macro and micro Young's modulus are affected by the temperature for the case of study.

Table 25: Micro properties of alumina for down and up domains

	Down domain (650°C)	Up domain (Room T ^a)
Density semi-sphere [kg/m³]	2.12x10 ¹²	2.12x10 ¹²
Radius ratio	0.445	0.445
Young's modulus [GPa]	3575	4015
Poisson's ratio	0.3	0.3

V.4.4.2. Failure criteria calibration and wear criteria definition.

The third body, wear, is generated when discrete elements are removed from the degradable first body, the abrasive grain. It is established that one DE is detached from the first body if every beams connected to this DE with the rest of the body breaks. In Figure 89 (a) beams breakage is represented. The failure criterion that it is imposed is the maximum failure stress on beams, which is detailed in the following paragraphs. Therefore, the behavior of alumina is modeled with the failure stress of the beams. In this sense, differences on the behavior depending on the crystalline structure of alumina are modeled imposing different failure stress. For the case of study, firstly the failure stress for WFA abrasive grains is achieved and then this value is adjusted to reproduce the wear of SG abrasive grains.

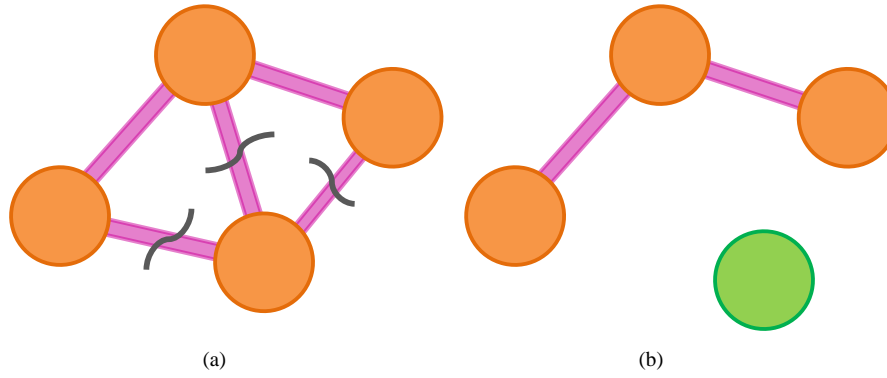


Figure 89: (a) First body set of DE pointing the break of beams (b) detached element in green due to the break of beams supporting it

In Figure 89 (b) the generation of the third body is shown. The adhesion force is imposed to detached DEs in order to simulate the effect of the third body adhered to the worn abrasive grain. Related to the failure stress, it is assumed that beams corresponding to *up domain* are unbreakable beams. This assumption is done owing to the absence of the influence of temperature in this part of the abrasive grain. In contrast, *down domain* is affected by the temperature. Moreover, the high temperature reached just in the contact leads to modifications in the behavior of alumina. Thus, it is considered that *down domain* behaves as a ductile material instead of a brittle material. To implement this hypothesis in the model Von Mises yield criterion is used. Applying Von Mises criterion on a beam, the stress is defined in Eq.16, where σ is the normal tension of the beam and τ is the tangential tension. Therefore, the failure criterion is defined using Von Mises stress (σ_{vm}) as follow in Eq.17. The beam breaks if micro failure stress ($\sigma_{f\mu}$) reaches σ_{vm} .

$$\sigma_{vm} = \sqrt{\sigma^2 + 3\tau^2} \quad \text{Eq.16}$$

$$\text{If } \sigma_{vm} > \sigma_{f\mu} \text{ the beam breaks} \quad \text{Eq.17}$$

The micro failure stress of beams ($\sigma_{f\mu}$) has to be also calibrated to complete the calibration of a cohesive beam model. The usual way to calibrate the micro failure stress is implementing tensile failure tests using macro failure stress values, as it is done for r_μ , E_μ and ν_μ calibration. However, it is much more difficult to obtain the macro failure stress value of alumina abrasive grains. Therefore, an alternative for the calibration of micro failure stress is developed without the necessity of quantify macro failure stress.

In tribology, it is accepted that generated third body between two first bodies in contact corresponds to the wear. Therefore, in this wear model it is assumed that generated third body is

equivalent to the wear suffered by alumina on pin-on-disk tests. So, for the present wear model, $\sigma_{f\mu}$ is calibrated comparing the third body generated in numerical model with the wear measured on pin-on—disk tribometer tests.

Wear height about 23 μm for WFA and 17 μm for SG is measured in tribological tests. The correlation of these values with the correspondent discrete volume is done, as Table 26 shows. Therefore, the value of $\sigma_{f\mu}$ which provides the same volume third body generated as wear in the real tests is the value for micro failure stress. The micro failure stress have to be adjusted until achieve the optimal behavior of the model.

Table 26: Discrete volume of abrasive grains wear obtained on pin-on-disk tests

	WFA	SG
Wear Height [μm]	23	17
Wear Discrete Volume [m^3]	2.02×10^{-13}	1.23×10^{-13}

V.4.5. Model inuts

V.4.5.1. Sliding speed

The sliding speeds used on pin-on-disk tribometer (20-25-30 m/s) are higher than habitual sliding speeds evaluated on tribological tests. This fact allows implementing of a simplification of the sliding speed in the wear model. As it is previously detailed, for both sliding speeds of 25 and 30 m/s almost the same wear is achieved and also the height of the isotherm is the same. Therefore, from now on, the wear model is carried out with $s=30$ m/s.

This simplification is based on Coulomb Law. This law, to low sliding speeds, presents initial static part, in which friction coefficient increases with speed. After that, stable friction coefficient is reached; this corresponds to dynamic friction coefficient. The static friction coefficient does not affect the contact for the case of study because of high sliding speed of tests. Therefore, a constant dynamic friction coefficient is assumed during a complete contact. In Figure 90 the evolution of friction coefficient on static and dynamic states is plotted pointing the sliding speed for the case of study.

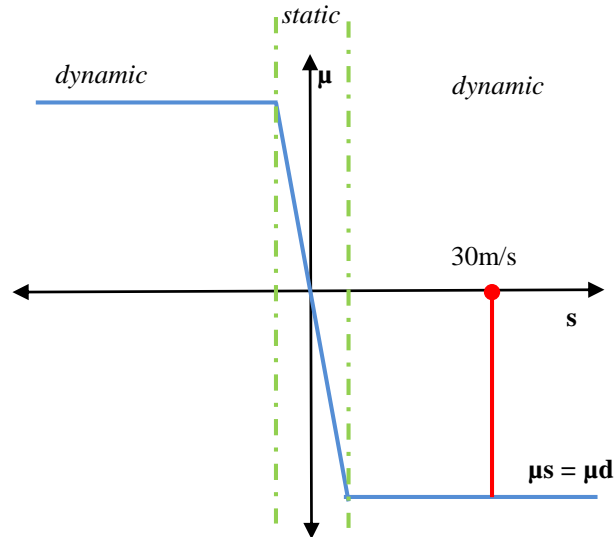


Figure 90: Regularized Coulomb Law

$$F_{t\mu} = \mu_{\mu} F_{n\mu}$$

Eq.18

The sliding speed generates a tangential force on the contact, which is the force responsible of the friction. This force is applied to each DE as it is shown Figure 91 (a), being different to the global force in the wear model. This tangential force is defined in Eq.18. On this way, it is not required to introduce the sliding speed on the model, but it is necessary to achieve the optimal micro friction coefficient (μ_{μ}) representative of 30 m/s sliding speed. Micro friction coefficient is different from a macro friction coefficient that it is achieved during tribometer tests. This friction coefficient has to be adjusted to simulate the wear of the abrasive grain.

V.4.5.2. Pressure

To impose the pressure in the abrasive grain the simplification of the force application is imposed. When applying force, the most influent parameter in the model is the mass. As it is previously mentioned the mass of the complete system affects to the behavior of the model. The abrasive grain is embedded on a matrix composed by abrasive grains and bond. Thus, for the case of study, in the abrasive grain $\varnothing 300 \mu\text{m}$, being a very small part of a complete grinding wheel, the total mass about 10 kg have to be taken into account, as it is previously detailed. To implement this mass the correspondent density is calculated in the abrasive grain in *section V.4.4.*

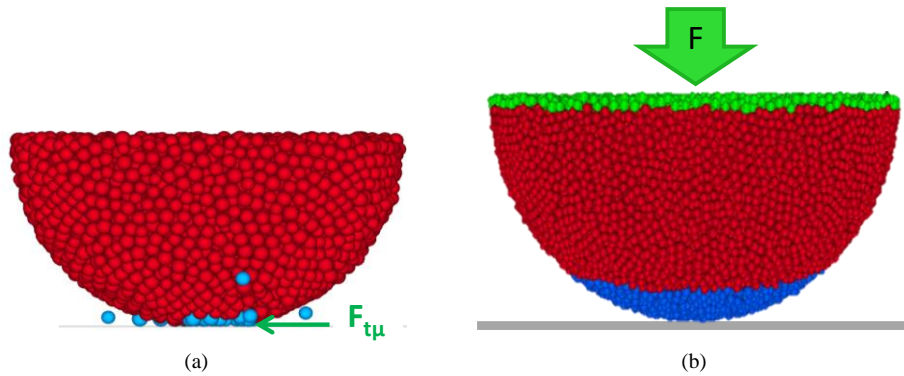


Figure 91: Model solicitations: (a) Micro tangential force applied in the contact to impose the sliding speed and (b) force imposed in the *Pressure Surface* to impose the real contact pressure

In order to apply the force homogeneously on the abrasive grain, a set of DEs denominated *Pressure Surface* is generated. Figure 91 (b) shows in green the set of DEs corresponding to *Pressure Surface* and the force applied in this surface. The force is applied in all the DEs that composed the *Pressure Surface*. The value of the applied force is calculated with the real pressure obtained on pin-on-disk tribometer tests. As it is previously established for sliding speed, the values corresponding to 30 m/s are used on the wear model. Thus, the real contact pressure is about 105 MPa for WFA and 160 MPa for SG abrasive grains.

V.4.6. Boundary conditions

The abrasive grain is embedded in a wheel matrix; therefore, the abrasive grain cannot oscillate as Figure 92 shows. In order to avoid the free movements of the abrasive grain mainly due to the micro tangential force applied, the movement of DEs of pressure surface on X and Y directions are restricted. Likewise, rotation in directions, X, Y and Z are also restricted. With these boundary conditions the real behavior of the abrasive grain inserted on a very rigid body is simulated.

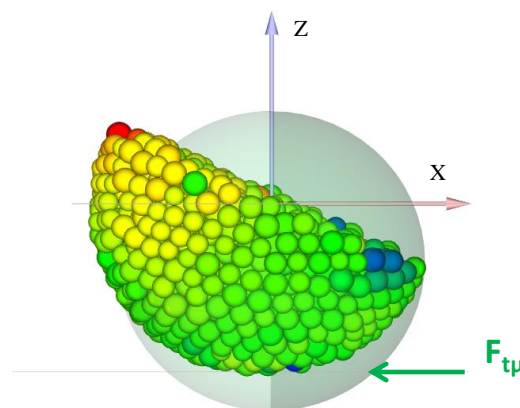


Figure 92: Abrasive grain oscillation due to micro tangential force effect

V.4.7. Contact problem: definition of contact laws

Once the two bodies are defined, model inputs are described and the boundary conditions are taken into account, the next step is to define the contact between the bodies and the different sets of DEs, which are mentioned in the previous sections. In Table 27 are summarized the sets of DEs and their correspondents sets of bonds for the abrasive grain wear simulation.

Contacts between different sets are defined using contact laws. The adequate definition of contact laws is a trivial issue to model the wear of abrasive grain. Detection method, contact law and the parameters needed to calculate the force on each DE have to be defined. The parameters could be physical or mathematical, and both of them have an influence on the behavior of the wear.

Table 27: Set of DE and bond used on the model

Set of DE	Set of bond
Up domain	Up Grain + bond on interface between down and up
Down domain	Down Grain
Pressure Surface (belongs to up)	Pressure Surface
Semi-sphere (Up + Down)	Semi-sphere
Third Body	No Bonded

- *Mathematical parameters:* stiffness (κ), coefficient of restitution (COR). The stiffness is calculated with properties and dimensions of the beams, and its value is the same to every contact laws $\kappa=1 \times 10^6$. The restitution coefficient is related to the damping effect, for the case of study also a constant value COR=0.8 is used.
- *Physical parameters:* adhesion (γ), micro friction coefficient (μ_μ) and micro failure criterion ($\sigma_{f\mu}$). These three parameters have to be adjusted in order to achieve the abrasive wear as close to real wear as possible. μ_μ and $\sigma_{f\mu}$ are defined in the paragraphs above. γ is the parameter that characterizes the third body and it is detailed hereafter.

Regarding the third body, DEs forming this set are not joined by beams. Once beams are broken, adhesion force is the unique force responsible to maintain the particles of the third body in contact with the abrasive grain, adhered between them. This parameter is adjusted to obtain an optimal behavior of the third body. If very high γ is chosen, the third body maintains adhered to the grain but the particles do not leave the contact and the abrasive grain wear does not occur.

On the contrary, if γ is too low the third body is generated and consecutively leaves the contact [124].

The adhesion between two particles is higher if both particles are third body or third body and grain, and slower if the adhesion is between third body and the workpiece. Following with the effect of the third body in the contact, due to its low viscosity, the presence of third body reduces the effect of friction. So, a very low value of friction coefficient is established when third body participate in the contact.

Regarding the sliding speed, a new contact law named *Tangential Friction* is created. The objective of this contact law is to impose the sliding speed in the contact between abrasive grain and the workpiece. This law applies the tangential force on DEs which are in contact with the workpiece. On this law the dynamic friction coefficient, micro friction coefficient is the main parameter and it has to be adjusted.

V.5. Validation of the abrasive grain wear DEM model

This section presents the results obtained from the DEM wear model. The first issue is to compare the behavior between modeling the semi-sphere or only *down domain* of the abrasive grain. Once the verification of the reduction of computing time is accomplished, the result of wear of the WFA abrasive grain is done. Finally, to achieve the modeling of SG abrasive grain wear some modifications have to be implemented.

V.5.1. Verification of only *down domain* simulation

To reduce the computational cost of the wear model is of interest. Therefore, the first issue that it is addressed is the minimization of this computational cost. To this end, the simulation of semi-sphere and only *down domain* of the abrasive grain is simulated. This verification is carried out for WFA abrasive grain. The number of DEs is reduced from 41671 to 5448 as Figure 93 shows; therefore, the reduction about 85% is achieved modeling only the down part of the grain.

In previous sections it is detailed the procedure to obtain the equivalent micro density of the discrete domain for the semi-sphere. Now, the micro density of *down domain* has to be calculated in order to generate equivalent bodies. Moreover, the pressure applied to WFA abrasive grain is 105MPa, being the corresponding force applied on *Pressure Surface* different in the both cases. This fact is due to the radius of the *Pressure Surface* (R') is different for semi-sphere and *down domain*. In Table 28 recalculated parameters are built.

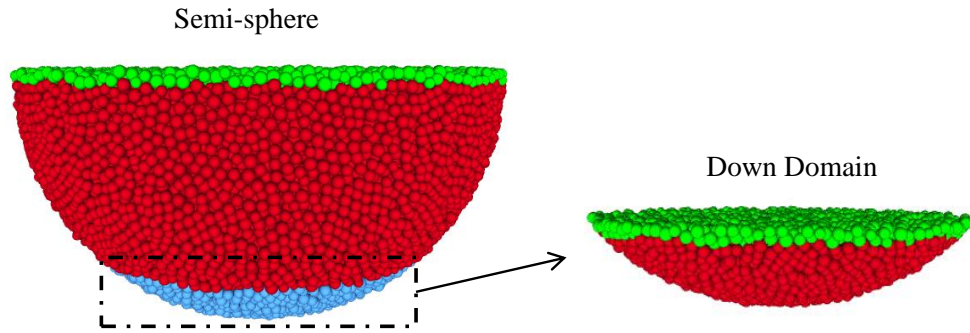


Figure 93: Discretization of semi-sphere and only the *down domain* of WFA abrasive grain

Table 28: Micro properties and model solicitations for semi-sphere and *down domain*

	ρ_{μ} [kg/m ³]	p_r [MPa]	R' [μm]	F [N]
SEMI-SPHERE WFA	2.12×10^{12}	105	150	7.42
DOWN DOMAIN WFA	1.62×10^{13}	105	106	3.71
DOWN DOMAIN SG	1.18×10^{13}	160	114	6.58

Once the models are equivalent, the model inputs are imposed. The same behavior of both models is achieved imposing on the *Pressure Surface* 7.42 N for semi-sphere and 3.71 N for *down domain*. Moreover the micro friction coefficient which reproduce the effect of sliding speed in the model is $\mu_{\mu}=0.7$. The contact time of the wear simulation is 0.85ms, as on real tribological tests.

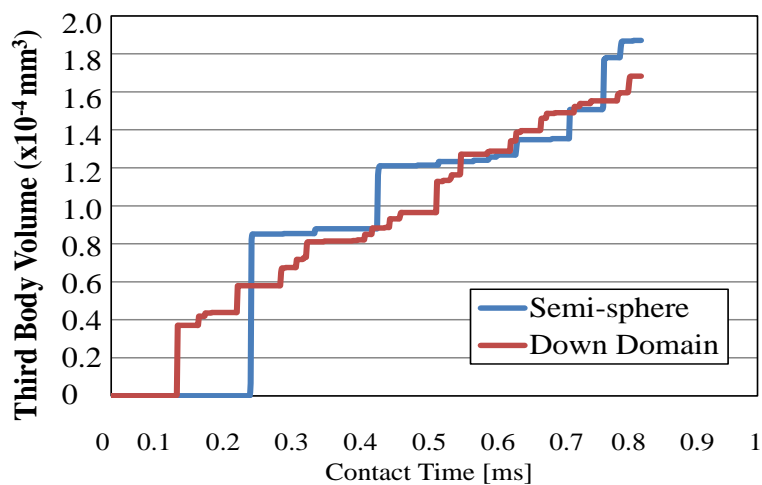


Figure 94: Third body generation on semi-sphere and only *down domain*

In Figure 94 the third body volume generation during the contact time is plotted. The third body increase similarly for the semi-sphere and for the *down domain*. Focusing the attention in the tendencies, it can be concluded that the behavior of both models are equivalents. The value achieved for the third body is analyzed in the following section. Additionally, the reduction of the total computational time proves the hypothesis of modeling *down domain*. Therefore, this results justifies the use of only *down domain* to model the abrasive grain.

V.5.2. Wear model for WFA abrasive grains

As it is demonstrated above, the wear model is developed modeling only the down part of the abrasive grain. The first model is developed for WFA abrasive grain. To simulate the contact conditions between WFA abrasive grain and the workpiece the model inputs are calculated and adjusted to behaves as on real experimental tests. On the one hand, the micro friction coefficient that reproduces better 30 m/s sliding speed is $\mu_\mu=0.7$, and the normal force equivalent to 105 MPa imposed on the *Pressure Surface* is 3.71 N, as it is built in Table 28. On the other hand, adhesion and micro-failure stress values are adjusted in order to reproduce wear behavior.

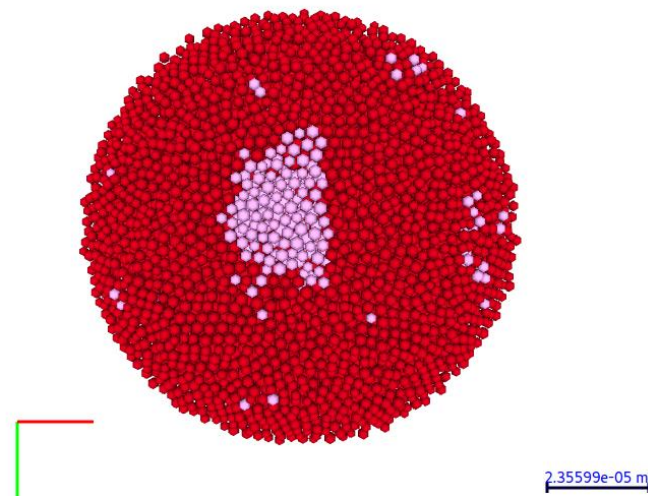


Figure 95: Incorrect micro failure stress (0.8GPa) of WFA abrasive grain, down view

For WFA abrasive grain the adhesion value that reproduces better the contact is $\gamma=0.001$. This adhesion corresponds to the contact between two third body particles or grain-third body particles. The adhesion between workpiece and third body is one order of magnitude lower than $\gamma=0.0001$. The last parameter to adjust is the failure stress. High values lead to no wear generation and low values tends to break the beams in the upper part of the grain, as it is shown in Figure 95, in which 0.8 GPa is used. Therefore, the optimal value of micro failure stress is $\sigma_{fi}=1$ GPa.

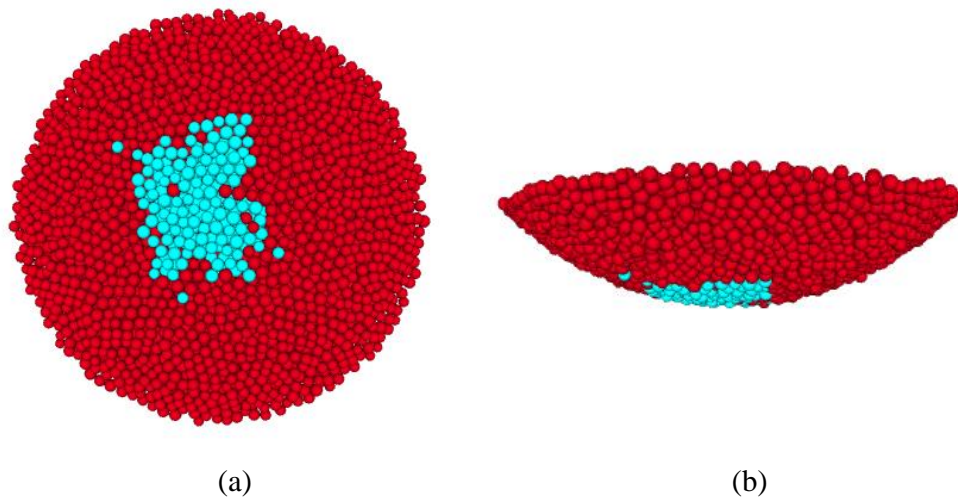


Figure 96: Third body generation in WFA abrasive grain

In Figure 96 the third body (in blue) generated in the contact between abrasive grain and workpiece is shown. The third body is accumulated in the left part of the abrasive grain instead of accumulate on the center of the grain due to the effect of the sliding speed. Moreover, in Figure 98 the maximum stress of the beams is plotted, showing in yellow 1 GPa. For WFA abrasive grain the beams which have reached failure stress, are represented by yellow beams in the contact, corresponding to break beams due to the failure criteria imposed. In the *Pressure Surface* yellow and also red color (corresponding to 2.2 GPa) appears. However, these beams are unbreakable and do not become third body.

Third body evolution during a contact of 0.85 ms is shown in Figure 97. As it is highlighted, three different parts can be differentiated in the evolution of the wear. During the first 0.18 ms there is not wear. After that, until 0.38 ms approximately, the third body occurs but the increase is slow. In the last step, the slope increases and the wear grows faster, reaching a value of $2.18 \times 10^{-4} \text{ mm}^3$.

The wear achieved on WFA tribological test is built in Table 26, being $2.02 \times 10^{-4} \text{ mm}^3$. Comparing the wear obtained in experimental tests with the wear of numerical model. The error of the experimental result is about 8%, being the wear model a good approach to reproduce the wear of the abrasive grain.

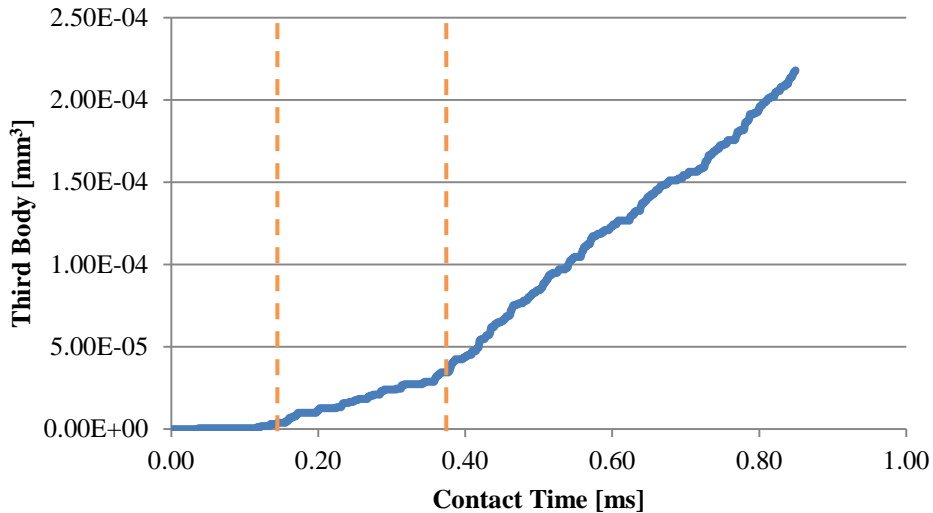


Figure 97: Third body evolution with contact time for WFA

V.5.3. Model variations to reproduce SG abrasive grain wear

Once the behavior of WFA is reproduced, the behavior of SG alumina abrasive grain is modeled. The differences in the crystalline structure are considered in the thermal model when the heat flux is imposed to the abrasive grain, and thus, in the proportion of the domain affected by the temperature. Moreover, the density of the discrete elements also differs in both cases. Finally, micro failure stress of beams also varies from WFA to SG wear model.

Table 29: Parameters in which the effect of the crystalline structure of abrasive grains is considered

	Down domain height	Micro density	Normal Force
WFA	38 μm	$1.62 \times 10^{13} \text{kg/m}^3$	3.71 N
SG	47 μm	$1.18 \times 10^{13} \text{kg/m}^3$	6.58 N

The SG suffers less wear than WFA, therefore, the failure stress of beams have to be higher than the WFA ones. All the other parameters adjusted for WFA are also valid for SG wear model. In Table 29 the parameters which are inputs of the wear model and are affected by the influence of crystalline structure are built.

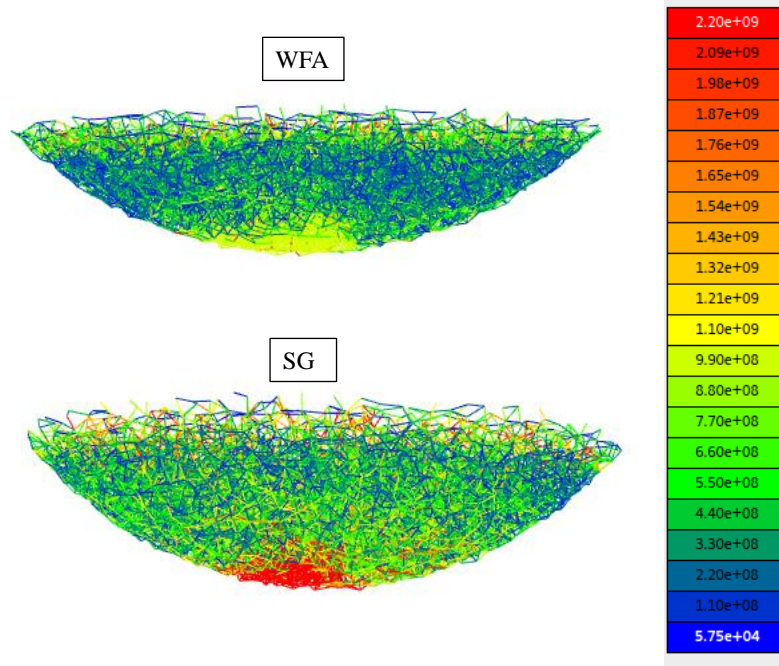


Figure 98: Beams stress of WFA and SG abrasive grains

Therefore, if the micro friction coefficient $\mu_\mu=0.7$ and adhesion $\gamma=0.001$ are maintained, just the failure stress have to be adjusted to reproduce the wear of SG abrasive grains. The beams are broken if Von Mises stress is higher than the failure stress, as it is shown in Eq.19. Failure constant, C , multiplies to micro failure stress. For the case of WFA $C=1$. However, for SG abrasive grains C has to be adjusted to reproduce the wear of SG alumina.

$$\sigma_{vm} > C \sigma_{f\mu} \tag{Eq.19}$$

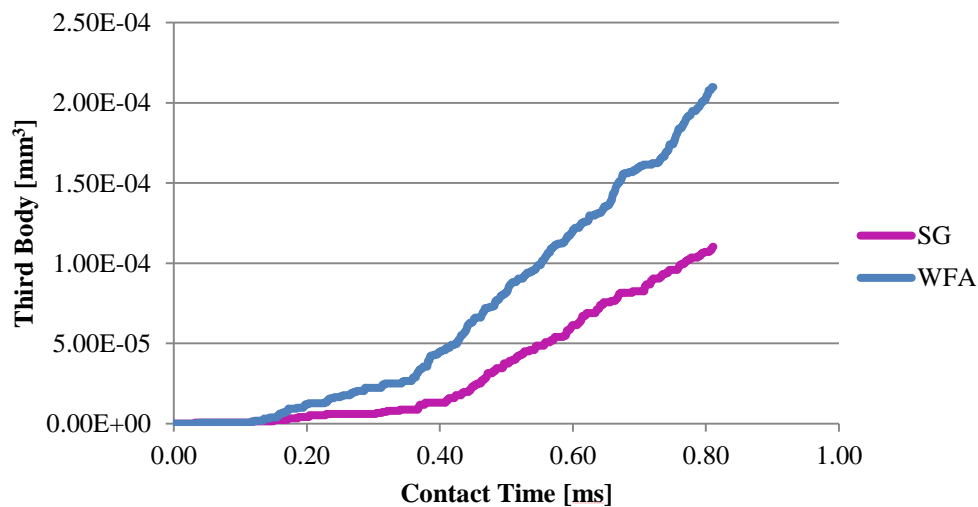


Figure 99: Comparison of the third body generation on WFA and SG abrasive grains

The best behavior of SG abrasive grain is achieved for $C=2.2$, thus, the failure stress for SG abrasive grains is 2.2 GPa while for WFA is 1 GPa. In Figure 98 the differences of the maximum stress reached in both cases are shown, WFA and SG abrasive grains. Furthermore, it can be observe the concentration of beams that reach the highest stress just in the contact.

In Figure 99 the wear generated on WFA and SG abrasive grains is compared. As it is explained for Figure 97, SG wear also present three parts, matching with WFA parts even in the time of each part. In contrast, WFA present higher wear than SG abrasive grains, as occur in experimental tribological tests. Moreover, SG abrasive grains suffer a discrete volumetric wear of $1.23 \times 10^{-4} \text{ mm}^3$ on pin-on-disk tribometer. For numerical model the maximum wear achieved after 0.85 ms is $1.04 \times 10^{-4} \text{ mm}^3$. The error between experimental and numerical results is about 15%. The error on SG wear model is higher than on WFA model, however the evolution of the wear is very similar in both cases.

V.6. Preliminary conclusions

The present chapter proposes a discrete element wear model for alumina abrasive grains. To this end, before implement the wear model, 2D finite element thermal model of a single abrasive grain is carried out. From the thermal model of the abrasive grain the following conclusions can be drawn:

- The two domains inside the abrasive grain are established with the hypothesis that the alumina, from room temperature to 200°C behaves with the properties at room temperature and from 200°C to the contact temperature acquire the properties of the contact temperature.
- The height of the isotherm at 200°C is higher than 100 μm to 20 m/s and lower than 50 μm for 25 m/s and 30 m/s, which present a very similar value. Likewise, the contact temperature reached for the case of 20 m/s is 900°C, about 23% higher than the other two cases.
- Regarding the influence of crystalline structure in the temperature, SG abrasive grain reaches about 720°C in the contact while WFA 600°C for 30 m/s. This dissimilarity is shown for the three studied sliding speeds. The 200°C isotherm height is about 19% higher for SG abrasive grain. This result is in concordance with experimental tests, in which the appearance of worn surface for SG alumina is smoother than WFA worn alumina. Moreover the transformed bond shown on SG experimental tests are justified for the higher temperature reached in the contact for SG alumina. Thus, lower thermal conductivity of SG abrasive grains is represented.

- The thermal behavior at 25 and 30 m/s is similar in both SG and WFA abrasive grains. However, at lower sliding speed, 20 m/s, the thermal behavior changes and the abrasive grain heat increases faster, reaching higher temperatures in the contact. Therefore, it can be affirmed that lower sliding speeds leads to higher temperatures in the contact and therefore the probability of thermal damage in the workpiece increase.
- Therefore, the wear at a sliding speed of 20 m/s is not analyzed for the wear model. Only the mean value of 200°C isotherm height is used for 25 and 30 m/s. For WFA the height of the isotherm which separates thermal affected alumina and no affected alumina is about 38 μm and for SG abrasive grain about 47 μm .

Once the thermal model is accomplished, 3D cohesive beam wear model is carried out. The aim of this model is to understand the phenomenon that enhances abrasive grain wear under real grinding contact conditions. Wear model allows the study not only of the wear but also, of the third body evolution during the contact time. The conclusions taken from this work are shown hereafter:

- In order to analyze the behavior of the alumina at high temperatures, it is assumed that the alumina behaves as a ductile material in the part of the alumina affected by the temperature, close to the contact. Therefore, Von Mises failure criterion is implemented in 3D cohesive beam model.
- The sliding speed is introduced in the model as a tangential force imposed on DEs in the contact. Due to the high sliding speed of tribological tests, 30 m/s, a constant dynamic friction coefficient is established, micro friction coefficient, μ_μ . The value corresponding to sliding speed of 30 m/s is $\mu_\mu=0.7$.
- To impose the pressure in the contact, a force is imposed in the abrasive grain. In order to reproduce the behavior of the abrasive grain embedded in the grinding wheel, the total mass of the system (10 kg) is imposed to the modeled abrasive grain.
- The hypothesis of simulating only the *down domain* of the abrasive grain in order to analyze the wear and the behavior of the third body in the contact is verified, showing the similar tendencies in wear and the third body generation. With this assumption the computational cost is reduced 85% comparing to the simulation of a semi-sphere.
- The adhesion coefficient of $\gamma=0.001$ and failure stress coefficient of $\sigma_{f\mu}=1$ GPa are the parameters that best reproduce the wear of alumina abrasive grains. Moreover, for WFA failure constant present the value $C=1$ and for SG abrasive grain $C=2.2$.

- The error obtained comparing experimental and numerical tests is about 8% for WFA and 15% for SG abrasive grains.
- Finally, the evolution of the third body generation, wear, can be shown from the beginning to the end of the contact. The first wear occurs at 0.18 ms approximately, increasing slowly in the next 0.2 ms at after that presenting a higher increase, until 0.85 ms when the contact is finished.

Chapter VI: Conclusions and future works

VI. CONCLUSIONS AND FUTURE WORKS

In the present chapter the main conclusions and the future works are gathered.

VI.1. Conclusions

This section summarizes the main conclusions drawn from developed research work. The complete study involves experimental and numerical parts. The experimental analysis is referred to the real grinding tests and the tribological tests carried out in the pin-on-disk tribometer and the main conclusions are presented as follow:

- The evolution of wear flat in alumina grinding wheels is deeply analyzed isolating and promoting this effect during real grinding tests. This isolation allows the study of the influence of crystalline structure of abrasive grains and the influence of grinding parameters in wear flat evolution.
 - The wear flat presents a linear increase with similar slope regardless of the crystalline structure of abrasive grains. However, 3SG grinding wheel shows a %A 23% higher than WFA and MA.
 - Regarding the influence of grinding parameters, the workpiece speed does not present clear tendency in the wear flat occurrence. In contrast, increasing depth of cut from 3 to 5 μm , the %A increases from 10% to 14% for 3SG grinding wheel.
 - The maximum value of measured wear flat is 14% for 3SG grinding wheel after 100 mm^3/mm material removed at $v_w=15000$ mm/min and $a_e=5$ μm .
- The initial wheel surface is designed to promote wear flat, ensuring the sliding as the predominant phenomenon. Therefore, normal and tangential forces and friction coefficient are quasi-constant during grinding. Friction coefficient varies from 0.33 to 0.38 regardless of the crystalline structure and grinding parameters. These values are obtained due to the presence of the third body in the contact.
- The analysis of the wheel surface is essential to evaluate the influence of crystalline structure in wear flat occurrence, showing the importance of not only %A value but also, the surface appearance on both *new* and *worn* states.

- 3D functional roughness parameters allow to identify wheel wear: S_{pk} is related to sharpness loss, S_{vk} shows the absence of dullness and S_k and S_{pk} identify the flatness of abrasive grains. *New* 3SG wheel is sharper than WFA and MA. In contrast *worn* 3SG and MA are smoother than *worn* WFA.
- SEM analysis of the three crystalline structures show smoother surface for *new* 3SG grinding wheel at lower magnification. *New* WFA abrasive grains are composed by different layers. However, the microcrystals of the *new* 3SG wheel are detected at higher magnification, leading to a rougher surface and promoting the adhesion of the third body.
- In contrast, 3SG and MA *worn* surfaces present a very homogenous appearance. Moreover, *worn* 3SG wheel presents more quantity of the third body adhered, being WFA the surface with less third body adhered to flat surface. The lower thermal conductivity of SG alumina accelerates chemical reactions, modifying the bond on the contact.
- Each crystalline structure presents different behavior with grinding parameters. The main problem of SG abrasive grains is the excessive wear flat generated during the process owing to the finishing parameters. With this parameters MA grinding wheels achieve lower %A. This idea is in accord with what is found in industrial practice and will help wheel manufacturers to select the most suitable abrasive grain basing, not only on the experience but also, on scientific knowledge.
- One of the handicaps of real grinding tests is the impossibility of control real contact conditions. To this end, an original design of pin-on-disk tribometer is developed in order to evaluate the wear of abrasive grains.
 - Contact conditions, close to the real grinding contact, are reproduced and thoroughly controlled. The sliding speeds between 20 and 30 m/s are tested and maximum real contact pressure of 190MPa is obtained.
 - The thermal cycle suffered by the abrasive grains is reproduced, changing the role of pin and disk in the tribometer. All these conditions are the closest approach to reproduce the real grinding contact.
- Short contact time about 1.1 s is measured during the tribological tests. Therefore, the theoretical force is not reached and the real contact pressure is lower that designed ones.

- The methodology to quantify real contact area on grinding wheels is established. About 29.33% for WFA and 22.43% for 3SG of apparent contact area is measured. This quantification is required to know real contact pressure, which is one of the most important parameter in the wear generation.
- The real contact pressure decreases with sliding speed, from 20 m/s to 30 m/s a decrease of 15% is measured. Extrapolating to grinding process, it is concluded that a higher cutting speed implies a lower real contact pressure on abrasive grains.
- The range of studied sliding speed does not present influence on the wear of the abrasive grains. However, the influence of the crystalline structure is appreciable both on the depth of wear and on the appearance of the *worn* surface. WFA presents a wear depth of 23 μm while 3SG disk 17 μm . Moreover, the 3SG *worn* surface is sharper than the WFA.
- The pin-on -disk friction coefficient varies from 0.22 to 0.25. In contrast, values between 0.33 and 0.38 are obtained in the grinding tests. These differences are due to the predominant wear mechanisms in the contact. In the case of the grinding tests, cutting, rubbing and ploughing occurs but during the tribological tests only rubbing and ploughing take place.
- On designed pin-on-disk tribometer the materials in contact, grinding wheel characteristics, contact conditions even the cooling of grinding process are taken into account. Therefore, it is suggested as useful industrial tool for the design of grinding wheels for specific application.

Due to the limitations of the experimental work, two numerical models are developed to a better understanding of the real phenomena. The first model is related to the temperature reached in the contact between the abrasive grain and the workpiece and the influence of the temperature inside the abrasive grain. The other model is a wear model, developed in order to understand the influence of the tribochemical nature of the wear flat in the complete contact. The main conclusions obtained from these two numerical models are summarized:

- 2D FEM thermal model is developed imposing the heat flux obtained from the tribometer data to the contact zone on the abrasive grain. The main conclusions of the thermal model are gathered:

- Contact temperatures about 900°C for 20m/s tests and about 720°C for 30 m/s are achieved, being about 17% lower for WFA than for SG alumina.
- Moreover, two domains inside the abrasive grains have been established in order to differentiate the alumina affected by a high temperature and alumina that works at room temperature. The 200°C isotherm is used to delimitate the two domains. For WFA the isotherm height is 38 μm and for SG is 47 μm .
- One of the handicaps of the pin-on-disk tests is that only initial and final states of grinding wheel surface can be analyzed. Moreover, in the grinding tests the influence of third body in the wear flat generation and the influence in the contact are shown. Therefore, 3D wear model of a single abrasive grain is developed using DEM. The main findings derived from the discrete element wear model are as follow:
 - Discrete element method is used to develop 3D the wear model of alumina abrasive grain. Cohesive beam model is implemented in order to represent continuous material using DEM. Moreover, Von Mises stress is imposed as beam failure criteria due to the high temperature in the contact. Likewise, DEM present the ability of reproduce the wear of the abrasive grain through the third body generation.
 - The real sliding speed of 30 m/s, and the contact pressure about 160MPa for SG and 105MPa for WFA are imposed to the wear model. The sliding speed is modeled imposing tangential force on DEs in contact with the workpiece being the value corresponding to 30 m/s represented with $\mu_t=0.7$. The real contact pressure is achieved applying a normal force to the abrasive grain, which has the mass of the complete grinding wheel.
 - The hypothesis of simulate only the *down domain* of the abrasive grain in order to analyze the wear and third body behavior in the contact is verified, showing the similar tendencies in the wear evolution. With this assumption the computational cost is reduced 85% comparing to the simulation of a semi-sphere.
 - The adhesion coefficient of $\gamma=0.001$ and failure stress coefficient of $\sigma_{f\mu}=1$ GPa are the parameters that best reproduce the wear of the abrasive grains of the alumina. The failure constant is established in order to differentiate the influence of crystalline structure in the modeled abrasive grains. For WFA failure constant present the value $C=1$ and for SG abrasive grain $C=2.2$.

- The main advantage of simulate the wear of the abrasive grain of the alumina is to know the evolution of the third body generation in the contact between the abrasive grain and the workpiece. Using the pin-on-disk tribometer only the final state of the alumina can be analyzed. In contrast, the wear model allows to study the evolution of wear from the beginning to the end of the contact. The numerical simulation shows the first wear at 0.18 ms approximately for both WFA and SG abrasive grains, increasing slowly in the next 0.2 ms and presenting a higher increase, until 0.85 ms. Likewise, the error achieved comparing the experimental and the numerical tests is about 8% for WFA and 15% for SG abrasive grains at the end of the contact.

VI.2. Future works

From the conclusions derived from presented research work the necessity of a constant research in grinding wheel wear is shown. The identified future research lines are summarized as follow:

- To develop a software to detect and quantify the wear flat in alumina grinding wheels automatically. The range values of the filters applied to the raw images have to be set in order to automate wear flat measurements. Moreover, this software can be implemented on an industrial tool in order to increase the outputs to analyze after grinding operation.
- To characterize the behavior of abrasive grains with different shapes. In the present research work only the crystalline structure of abrasive grains is tested. However, in the industry the use of microcrystalline abrasive grains with different shapes is booming, TG or TGX, between others. Therefore, it is of interest to analyze wear behavior of abrasive grains depending on its shape.
 - From experimental point of view, designed pin-on-disk tribometer can be used in order to characterize the behavior of the abrasive grains with different shapes. The unique change is to use a grinding wheel with this type of abrasive grains.
 - From numerical point of view, the new version of *GranOO 2.0* allows to detect the contact between DEs with different shape. In *1.0* version DEs are spheres. Therefore, wear modeling of grinding wheels using the same shape on the real process and on the numerical simulation can be done.
- To improve the simulation of the wear flat on a single abrasive grain. To this end, the third body generation and the wear of the abrasive grains is going to differentiate. The force

balance in the DE is used to differentiate between them. If the adhesion force in the DE is higher than the repulsive force on it, the DE will be adhered to the grain and third body is generated. On the contrary, if repulsive force is higher, the DE leaves the contact, being considered wear, loss of volume occurs.

- To develop a more realistic wear model. In the present work only the first approach of wear model is accomplished. In this model the wear of the abrasive grain due to tribochemical reactions is simulated without taking into account the other type of wears. Thus, only the wear flat is modeled. In a new wear model grain fracture could be included in order to develop more realistic wear model of abrasive grain. To this end, groups of DEs could be defined, in the abrasive grains. The behavior of beams inside the defined groups would be different to the behavior between groups, simulating the wear flat or grains fracture respectively.

References

REFERENCES

- [1] Marinescu ID, Hitchiner M, Uhlmann E, Rowe WB, Inasaki I. Handbook of machining with grinding wheels. 2006.
- [2] Marinescu ID, Rowe WB, Dimitrov B, Inasaki I. Tribology of abrasive machining processes. 2004.
- [3] Jackson MJ, Davis CJ, Hitchiner MP, Mills B. High-speed grinding with CBN grinding wheels - applications and future technology. *J Mater Process Technol* 2001;110:78–88. doi:10.1016/S0924-0136(00)00869-4.
- [4] Danobat Group. www.danobatgroup.com (Last access 01/2019) 2018.
- [5] Neugebauer R, Denkena B, Wegener K. Mechatronic Systems for Machine Tools. *CIRP Ann - Manuf Technol* 2007;56:657–86. doi:10.1016/j.cirp.2007.10.007.
- [6] Studer United Grinding. www.studer.com (Last access 11/2018) 2018.
- [7] Wegener K, Bleicher F, Krajnik P, Hoffmeister H, Brecher C. Recent developments in grinding machines. *CIRP Ann - Manuf Technol* 2017;66:779–802. doi:10.1016/j.cirp.2017.05.006.
- [8] Chen GS, Mei XS, Li HL. Geometric error modeling and compensation for large-scale grinding machine tools with multi-axes. *Int J Adv Manuf Technol* 2013;69:2583–92. doi:10.1007/s00170-013-5203-7.
- [9] Linke BS. Review on Grinding Tool Wear With Regard to Sustainability. *J Manuf Sci Eng* 2015;137:060801. doi:10.1115/1.4029399.
- [10] Sanchez JA, Pombo I, Alberdi R, Izquierdo B, Ortega N, Plaza S, et al. Machining evaluation of a hybrid MQL-CO₂ grinding technology. *J Clean Prod* 2010;18:1840–9. doi:10.1016/j.jclepro.2010.07.002.
- [11] Li HN, Axinte D. On a stochastically grain-discretised model for 2D/3D temperature mapping prediction in grinding. *Int J Mach Tools Manuf* 2017;116:60–76. doi:10.1016/j.ijmachtools.2017.01.004.
- [12] Pombo I. Estudio teórico- experimental de una nueva tecnología de rectificado ecológico. University of Basque Country, 2010.
- [13] Badger J, Murphy S, O'Donnell GE. Acoustic emission in dressing of grinding wheels: AE intensity, dressing energy, and quantification of dressing sharpness and increase in diamond wear-flat size. *Int J Mach Tools Manuf* 2018;125:11–9. doi:10.1016/j.ijmachtools.2017.11.007.
- [14] Pombo I, Cearsolo X, Sánchez JA, Cabanes I. Experimental and numerical analysis of thermal phenomena in the wear of single point diamond dressing tools. *J Manuf Process* 2017;27:145–57. doi:10.1016/j.jmapro.2017.04.001.
- [15] Malkin S. The attritious and fracture wear of grinding wheels. Massachusetts Institute of Technology, 1968.

- [16] Mayer J, Engelhorn R, Bot R, Weirich T, Herwartz C, Klocke F. Wear characteristics of second-phase-reinforced sol-gel corundum abrasives. *Acta Mater* 2006;54:3605–15. doi:10.1016/j.actamat.2006.03.049.
- [17] Denkena B, Grove T, Götttsching T, da Silva EJ, Coelho RT, Filleti R. Enhanced grinding performance by means of patterned grinding wheels. *Int J Adv Manuf Technol* 2015;77:1935–41. doi:10.1007/s00170-014-6579-8.
- [18] Nan H, Axinte D. Textured grinding wheels : A review. *Int J Mach Tools Manuf* 2016;109:8–35.
- [19] Mohamed AMO, Bauer R, Warkentin A. Application of shallow circumferential grooved wheels to creep-feed grinding. *J Mater Process Technol* 2013;213:700–6. doi:10.1016/j.jmatprotec.2012.11.029.
- [20] Tyrolit n.d. <https://www.tyrolit.co.uk/divisions/metal-precision/product-news-2018.html>.
- [21] Kannan K, Arunachalam N, Chawla A, Natarajan S. Multi-Sensor Data Analytics for Grinding Wheel Redress Life Estimation- An Approach towards Industry 4.0. *Procedia Manuf* 2018;26:1230–41. doi:10.1016/j.promfg.2018.07.160.
- [22] Varghese B, Pathare S, Gao R, Guo C, Malkin S. Development of a sensor-integrated 'intelligent' grinding wheel for in-process monitoring. *CIRP Ann - Manuf Technol* 2000;49:231–4. doi:10.1016/S0007-8506(07)62935-7.
- [23] Tönshoff HK, Friemuth T, Becker JC. Process monitoring in grinding. *CIRP Ann - Manuf Technol* 2002;51:551–71. doi:10.1016/S0007-8506(07)61700-4.
- [24] Boaron A, Weingaertner WL. Dynamic in-process characterization method based on acoustic emission for topographic assessment of conventional grinding wheels. *Wear* 2018;406–407:218–29. doi:10.1016/j.wear.2018.04.009.
- [25] Cui C, Xu X, Huang H, Hu J, Ye R, Zhou L, et al. Extraction of the grains topography from grinding wheels. *Measurement* 2013;46:484–90. doi:10.1016/j.measurement.2012.08.005.
- [26] Rubio E, Jáuregui-Correa JC. A wavelet approach to estimate the quality of ground parts. *J Appl Res Technol* 2012;10:28–37.
- [27] Malkin S, Guo C. *Grinding technology. Theory and Applications of machining with abrasives*. 2008. doi:10.1063/1.2717084.
- [28] Leitherser MA, Sowman HG. Non fused aluminium oxides-based abrasive mineral US 1982/4,314,827, 1982.
- [29] Godino L, Pombo I, Sanchez JA, Alvarez J. On the development and evolution of wear flats in microcrystalline sintered alumina grinding wheels. *J Manuf Process* 2018;32. doi:10.1016/j.jmapro.2018.03.023.
- [30] Norton Saint-Gobain. www.nortonabrasives.com (Last seen 11/2018) 2018.
- [31] Nadolny K. State of the art in production, properties and applications of the microcrystalline sintered corundum abrasive grains. *Int J Adv Manuf Technol* 2014;74:1445–57. doi:10.1007/s00170-014-6090-2.

-
- [32] Rowe WB. Principles of Modern Grinding Technology. 978-0-8155-2018-4, 2009, p. 40–2, 82–7. doi:10.1016/B978-1-4160-5009-4.50004-2.
- [33] Klocke F, Engelhorn R, Mayer J, Weirich T. Micro-Analysis of the Contact Zone of Tribologically Loaded Second-Phase Reinforced Sol-Gel-Abrasives. *CIRP Ann - Manuf Technol* 2002;51:245–50. doi:10.1016/S0007-8506(07)61509-1.
- [34] Nadolny K. Wear phenomena of grinding wheels with sol–gel alumina abrasive grains and glass–ceramic vitrified bond during internal cylindrical traverse grinding of 100Cr6 steel. *Int J Adv Manuf Technol* 2015;77:83–98. doi:10.1007/s00170-014-6432-0.
- [35] Oliveira JFG, Coelho RT, Neto CK. Development of an Optical Scanner To Study Wear on the Working Surface of Grinding Wheels. *Mach Sci Technol* 1999;3:239–53. doi:10.1080/10940349908945692.
- [36] Lachance S, Bauer R, Warkentin A. Application of region growing method to evaluate the surface condition of grinding wheels. *Int J Mach Tools Manuf* 2004;44:823–9. doi:10.1016/j.ijmachtools.2004.01.006.
- [37] Lachance S, Warkentin A, Bauer R. Development of an automated system for measuring grinding wheel wear flats. *J Manuf Syst* 2003;22:130–5. doi:10.1016/S0278-6125(03)90010-0.
- [38] Bruce RW. Handbook lubrication tribology. vol. II. 2012.
- [39] Archard JF. Contact and rubbing of flat surfaces. *J Appl Phys* 1953;24:981–8. doi:10.1063/1.1721448.
- [40] Montgomery RS. Friction and wear at high sliding speed. *Wear* 1976;36:275–98.
- [41] Philippon S, Sutter G, Molinari A. An experimental study of friction at high sliding velocities. *Wear* 2004;257:777–84. doi:10.1016/j.wear.2004.03.017.
- [42] Irfan MA, Prakash V. Time resolved friction during dry sliding of metal on metal. *Int J Solids Struct* 2000;37:2859–82. doi:10.1016/S0020-7683(99)00112-2.
- [43] Prakash V. A pressure-shear plate impact experiment for investigating transient friction. *Exp Mech* 1995;35:329–36. doi:10.1007/BF02317542.
- [44] Yamamoto T, Saito M, Ueno M, Hananouchi T, Tokugawa Y, Yonenobu KJ. Wear analysis of retrieved ceramic-on-ceramic articulations in total hip arthroplasty: Femoral head makes contact with the rim of the socket outside of the bearing surface. *J Biomed Mater Res B Appl Biomater* 2005.
- [45] Zeng P, Rainforth WM, Inkson BJ, Stewart TD. Transmission electron microscopy analysis of worn alumina hip replacement prostheses. *Acta Mater* 2012;60:2061–72. doi:10.1016/j.actamat.2012.01.009.
- [46] Nevelos JE, Prudhommeaux F, Hamadouche M, Doyle C, Ingham E, Meunier A, et al. Comparative analysis of two different types of alumina-alumina hip prosthesis retrieved for aseptic loosening. *J Bone Jt Surg* 2001.
- [47] Nevelos JE, Ingham E, Doyle C, Fisher J, Nevelos AB. Analysis of retrieved alumina ceramic components from Mittelmeier total hip prostheses. *Biomaterials* 1999.

References

- [48] Kumar a. S, Durai a. R, Sornakumar T. Wear behaviour of alumina based ceramic cutting tools on machining steels. *Tribol Int* 2006;39:191–7. doi:10.1016/j.triboint.2005.01.021.
- [49] Ravikiran A. Water-lubricated sliding of Al₂O₃ against steel. *Wear* 1993;171:33–9.
- [50] Erickson LC, Blomberg a., Hogmark S, Bratthäll J. Tribological characterization of alumina and silicon carbide under lubricated sliding. *Tribol Int* 1993;26:83–92. doi:10.1016/0301-679X(93)90016-T.
- [51] Ravikiran A, Nagarajan VS, Biswas SK, Pramila Bai BN. Effect of speed and pressure on dry sliding interactions. *J Am Ceram Society* 1995;78:356–64.
- [52] Ravikiran A, Subbanna GR, Pramila Bai BN. Effect of interface layers formed during dry sliding of zirconia toughened alumina (ZTA) and monolithic alumina against steel. *Wear* 1996;192:56–65. doi:10.1016/0043-1648(95)06754-X.
- [53] Ravikiran A, Jahanmir S. Effect of contact pressure and load on wear of alumina. *Wear* 2001;251:980–4. doi:10.1016/S0043-1648(01)00739-6.
- [54] Kumar S, Bhattacharyya A, Mondal DK, Biswas K, Maity J. Dry sliding wear behaviour of medium carbon steel against an alumina disk. *Wear* 2011;270:413–21. doi:10.1016/j.wear.2010.12.007.
- [55] Beliardouh NE, Nouveau C, Walock MJ, Jacquet P. A study of the wear performance of duplex treated commercial low-alloy steel against alumina and WC balls. *Surf Coatings Technol* 2014;259:483–94. doi:10.1016/j.surfcoat.2014.10.042.
- [56] Senthil Kumar A, Raja Durai A, Sornakumar T. The effect of tool wear on tool life of alumina-based ceramic cutting tools while machining hardened martensitic stainless steel. *J Mater Process Technol* 2006;173:151–6. doi:10.1016/j.jmatprotec.2005.11.012.
- [57] Narutaki N, Yamane Y, Hayashi K, Hoshi T. Cutting Performance and Wear Characteristics of an Alumina-Zirconia Ceramic Tool in High-speed Face Milling. *CIRP Ann - Manuf Technol* 1991;40:49–52. doi:10.1016/S0007-8506(07)61931-3.
- [58] Ravikiran A, Nagarajan VS, Biswas SK, Bai BNP. Effect of Speed and Pressure on Dry Sliding Interactions of Alumina against Steel 1993;64:356–64.
- [59] Ravikiran A, Pramila Bai BN. High speed sliding of Al₂O₃ pins against an En-24 steel disc 1991;13:1991.
- [60] Ravikiran A, Pramila Bai BN. High Speed sliding of Al₂O₃ pins against an En-24 steel disc 1993;13:296–304.
- [61] Beliardouh NE, Nouveau C, Walock MJ, Jacquet P. A study of the wear performance of duplex treated commercial low-alloy steel against alumina and WC balls. *Surf Coatings Technol* 2014;259:483–94. doi:10.1016/j.surfcoat.2014.10.042.
- [62] He YJ, Winnubst a. J a., Schipper DJ, Bakker PMV, Burggraaf a. J, Verweij H. Friction and wear behaviour of ceramic-hardened steel couples under reciprocating sliding motion. *Wear* 1995;184:33–43. doi:10.1016/0043-1648(94)06544-6.
- [63] García E. Improving friction and wear conditions in grinding. Practical application and fundamental study. University of Basque Country, 2014.

- [64] Brinksmeier E, Heinzl C, Wittmann M. Friction, cooling and lubrication in grinding. *CIRP Ann - Manuf Technol* 1999;48:581–98. doi:10.1016/S0007-8506(07)63236-3.
- [65] Anderson D, Warkentin A, Bauer R. Experimental and numerical investigations of single abrasive-grain cutting. *Int J Mach Tools Manuf* 2011;51:898–910. doi:10.1016/j.ijmachtools.2011.08.006.
- [66] Hahn RS. On the Mechanics of the Grinding Process Under Plunge Cut Conditions. *J Eng Ind* 1966;88:72. doi:10.1115/1.3670895.
- [67] Kannappan S, Malkin S. Effects of grain size and operating parameters on the mechanics of grinding. *J Eng Ind* 1972;94:833. doi:10.1115/1.3428258.
- [68] Öpöz TT, Chen X. Experimental investigation of material removal mechanism in single grit grinding. *Int J Mach Tools Manuf* 2012;63:32–40. doi:10.1016/j.ijmachtools.2012.07.010.
- [69] Hanasaki S, Touge M. Study of the electrolytic grinding mechanism using a single-diamond cutting tool with a wear flat area. *Wear* 1990;139:285–301. doi:10.1016/0043-1648(90)90051-B.
- [70] Tanaka K, Koshy P. A pneumatic sensor for grinding wheel condition monitoring. *Precis Eng* 2018. doi:10.1016/j.precisioneng.2018.09.005.
- [71] Tian YB, Liu F, Wang Y, Wu H. Development of portable power monitoring system and grinding analytical tool. *J Manuf Process* 2017;27:188–97. doi:10.1016/j.jmapro.2017.05.002.
- [72] Patnaik Durgumahanti US, Singh V, Venkateswara Rao P. A New Model for Grinding Force Prediction and Analysis. *Int J Mach Tools Manuf* 2010;50:231–40. doi:10.1016/j.ijmachtools.2009.12.004.
- [73] Badger JA, Torrance AA. Comparison of two models to predict grinding forces from wheel surface topography. *Int J Mach Tools Manuf* 2000;40:1099–120. doi:10.1016/S0890-6955(99)00116-9.
- [74] Hamdi H, Dursapt M, Zahouani H. Characterization of abrasive grain's behavior and wear mechanisms. *Wear* 2003;254:1294–8. doi:10.1016/S0043-1648(03)00158-3.
- [75] Vettivel SC, Selvakumar N, Narayanasamy R, Leema N. Numerical modelling, prediction of Cu-W nano powder composite in dry sliding wear condition using response surface methodology. *Mater Des* 2013;50:977–96. doi:10.1016/j.matdes.2013.03.072.
- [76] Guo C, Chen Y. Thermal modeling and optimization of interrupted grinding. *CIRP Ann* 2018;67:321–4. doi:10.1016/j.cirp.2018.04.083.
- [77] Li C, Zhang F, Meng B, Liu L, Rao X. Material removal mechanism and grinding force modelling of ultrasonic vibration assisted grinding for SiC ceramics. *Ceram Int* 2017;43:2981–93. doi:10.1016/j.ceramint.2016.11.066.
- [78] Zhang Y, Li C, Ji H, Yang X, Yang M, Jia D, et al. Analysis of grinding mechanics and improved predictive force model based on material-removal and plastic-stacking mechanisms. *Int J Mach Tools Manuf* 2017;122:81–97. doi:10.1016/j.ijmachtools.2017.06.002.

- [79] Wiederkehr P, Siebrecht T, Potthoff N. Stochastic modeling of grain wear in geometric physically-based grinding simulations. *CIRP Ann* 2018;67:325–8. doi:10.1016/j.cirp.2018.04.089.
- [80] Ahrens M, Damm J, Dagen M, Denkena B, Ortmaier T. Estimation of Dynamic Grinding Wheel Wear in Plunge Grinding. *Procedia CIRP* 2017;58:422–7. doi:10.1016/j.procir.2017.03.247.
- [81] Malkin S, Cook NH. The wear of grinding wheels. Part 1: Attritious wear. *J Eng Ind* 1971;93(4):1120–8.
- [82] Besmann TM, Kulkarni NS, Vienna JD, Spear KE. Predicting phase equilibria of spinel-forming constituents in waste glass systems. *Ceram Trans* 2005;168:121–31.
- [83] Pepper S V. Shear strength of metal-sapphire contacts. *J Appl Phys* 1976;47:801–8. doi:10.1063/1.322711.
- [84] Malkin S. The wear of grinding wheels. Part2: Fracture wear. *J Eng Ind* 1971:1129–33.
- [85] Butler D., Blunt L., See B., Webster J., Stout K. The characterisation of grinding wheels using 3D surface measurement techniques. *J Mater Process Technol* 2002;127:234–7. doi:10.1016/S0924-0136(02)00148-6.
- [86] Tamaki J, Kitagawa T. Evaluation of surface topography of metal-bonded diamond wheel utilizing three-dimensional profilometry. *Int J Mach Tools Manuf* 1995;35:1339–51.
- [87] Hosokawa A, Mashimo K, Yamada K, Ueda T. Evaluation of Grinding Wheel Surface by Means of Grinding Sound Discrimination. *JSME Int J Ser C Mech Syst Mach Elem Manuf* 2004;47:52–8. doi:10.1299/jsmec.47.52.
- [88] Yasui H, Hiraki Y, Sakata M. Development of automatic image processing system for evaluation of wheel surface condition in ultra-smoothness grinding. *Proc 16th Annu Meet ...* 2001.
- [89] Adibi H, Rezaei SM, Sarhan AAD. Grinding Wheel Loading Evaluation Using Digital Image Processing. *J Manuf Sci Eng* 2013;136:011012. doi:10.1115/1.4025782.
- [90] Gopan V, Wins KLD. Quantitative Analysis of Grinding Wheel Loading Using Image Processing. *Procedia Technol* 2016;25:885–91. doi:10.1016/j.protcy.2016.08.198.
- [91] Vidal G, Ortega N, Bravo H, Dubar M, Gonzalez H. An Analysis of Electroplated cBN Grinding Wheel Wear and Conditioning during Creep Feed Grinding. *Metals (Basel)* 2018;8. doi:10.3390/met8050350.
- [92] Brinksmeier E, Aurich JC, Govekar E, Heinzl C, Hoffmeister HW, Klocke F, et al. Advances in modeling and simulation of grinding processes. *CIRP Ann - Manuf Technol* 2006;55:667–96. doi:10.1016/j.cirp.2006.10.003.
- [93] Hecker RL, Ramoneda IM, Liang SY. Analysis of wheel topography and grit force for grinding process modeling. *J Manuf Process* 2003;5:13–23. doi:10.1016/S1526-6125(03)70036-X.
- [94] Singh V, Venkateswara Rao P, Ghosh S. Development of specific grinding energy model. *Int J Mach Tools Manuf* 2012;60:1–13. doi:10.1016/j.ijmachtools.2011.11.003.

- [95] Liu Q, Roy A, Tamura S, Matsumura T, Silberschmidt V V. Micro-cutting of single-crystal metal: Finite-element analysis of deformation and material removal. *Int J Mech Sci* 2016;118:135–43. doi:10.1016/j.ijmecsci.2016.09.021.
- [96] Moulik PN, Yang HTY, Chandrasekar S. Simulation of thermal stresses due to grinding. *Int J Mech Sci* 2001;43:831–51. doi:10.1016/S0020-7403(00)00027-8.
- [97] Rentsch R, Inasaki I. Effects of fluids on the surface generation in material removal processes - Molecular dynamics simulation. *CIRP Ann - Manuf Technol* 2006;55:601–4. doi:10.1016/S0007-8506(07)60492-2.
- [98] Karkalos NE, Markopoulos AP, Kundrač J. Molecular Dynamics Model of Nano-metric Peripheral Grinding. *Procedia CIRP* 2017;58:281–6. doi:10.1016/j.procir.2017.03.189.
- [99] Guo X, Li Q, Liu T, Zhai C, Kang R, Jin Z. Molecular dynamics study on the thickness of damage layer in multiple grinding of monocrystalline silicon. *Mater Sci Semicond Process* 2016;51:15–9. doi:10.1016/j.mssp.2016.04.013.
- [100] Shiari B, Miller RE, Klug DD. Multiscale simulation of material removal processes at the nanoscale. *J Mech Phys Solids* 2007;55:2384–405. doi:10.1016/j.jmps.2007.03.018.
- [101] Ren J, Hao M, Lv M, Wang S, Zhu B. Molecular dynamics research on ultra-high-speed grinding mechanism of monocrystalline nickel. *Appl Surf Sci* 2018;455:629–34. doi:10.1016/j.apsusc.2018.06.042.
- [102] Guo C, Campomanes M, McIntosh D, Becze C, Green T. Optimization of continuous dress creep-feed form grinding process. *CIRP Ann - Manuf Technol* 2003;52:259–62. doi:10.1016/S0007-8506(07)60579-4.
- [103] Karpuschewski B, Wehmeier M, Inasaki I. Grinding monitoring system based on power and acoustic emission sensors. *CIRP Ann* 2000;49:235–40. doi:10.1016/S0924-0136(96)02444-2.
- [104] Midha PS, Zhu CB, Trmal GJ. Optimum selection of grinding parameters using process modelling and knowledge based system approach. *J Mater Process Technol* 1991;28:189–98. doi:10.1016/0924-0136(91)90218-4.
- [105] Challen JM, Oxley PLB. An explanation of the different regimes of friction and wear using asperity deformation models. *Wear* 1979;53:229–43. doi:10.1016/0043-1648(79)90080-2.
- [106] Rabiye M, Lee J, Wei Z. Roughness after flat grinding by electroplated wheel. 8th CIRP Conf. High Perform. Cut. (HPC 2018), vol. 77, 2018, p. 303–6. doi:10.1016/j.chemphys.2005.04.012.
- [107] Zhang Y, Fang C, Huang G, Xu X. Modeling and simulation of the distribution of undeformed chip thicknesses in surface grinding. *Int J Mach Tools Manuf* 2018;127:14–27. doi:10.1016/j.ijmactools.2018.01.002.
- [108] Rom M, Brakhage KH, Barth S, Wrobel C, Mattfeld P, Klocke F. Mathematical modeling of ceramic bond bridges in grinding wheels. *Math Comput Simul* 2018;147:220–36. doi:10.1016/j.matcom.2017.02.002.
- [109] Aurich JC, Biermann D, Blum H, Brecher C, Carstensen C, Denkena B, et al. Modelling and simulation of process: Machine interaction in grinding. *Prod Eng* 2009;3:111–20.

- doi:10.1007/s11740-008-0137-x.
- [110] Doman DA, Warkentin A, Bauer R. A survey of recent grinding wheel topography models. *Int J Mach Tools Manuf* 2006;46:343–52. doi:10.1007/978-94-007-2512-6_76.
- [111] Torrance AA. Modelling abrasive wear. *Wear* 2005;258:281–93. doi:10.1016/j.wear.2004.09.065.
- [112] Klocke F, Barth S, Wrobel C, Weiß M, Mattfeld P, Brakhage KH, et al. Modelling of the Grinding Wheel Structure Depending on the Volumetric Composition. *Procedia CIRP* 2016;46:276–80. doi:10.1016/j.procir.2016.04.066.
- [113] Chen X, Rowe WB. Analysis and simulation of grinding process. Part I: Generation of the grinding wheel surface. *Int J Mach Tools Manuf* 1996;36:871–82. doi:10.1093/eurheartj/ehu271.
- [114] Torrance AA, Badger JA. Relation between the traverse dressing of vitrified grinding wheels and their performance. *Int J Mach Tools Manuf* 2000;40:1787–811. doi:10.1016/S0890-6955(00)00015-8.
- [115] Osa JL, Sánchez JA, Ortega N, Iordanoff I, Charles JL. Discrete-element modelling of the grinding contact length combining the wheel-body structure and the surface-topography models. *Int J Mach Tools Manuf* 2016;110:43–54. doi:10.1016/j.ijmachtools.2016.07.004.
- [116] Jiang JL, Ge PQ, Bi WB, Zhang L, Wang DX, Zhang Y. 2D / 3D ground surface topography modeling considering dressing and wear effects in grinding process. *Int J Mach Tools Manuf* 2013;74:29–40.
- [117] Chiu N, Malkin S. Computer Simulation for Cylindrical Plunge Grinding 1993;42:383–7.
- [118] Novoselov Y, Bratan S, Bogutsky V. Analysis of Relation between Grinding Wheel Wear and Abrasive Grains Wear. *Procedia Eng* 2016;150:809–14. doi:10.1016/j.proeng.2016.07.116.
- [119] Yu T, Bastawros AF, Chandra A. Experimental and modeling characterization of wear and life expectancy of electroplated CBN grinding wheels. *Int J Mach Tools Manuf* 2017;121:70–80. doi:10.1016/j.ijmachtools.2017.04.013.
- [120] Adibi H, Rezaei SM, Sarhan AAD. Analytical modeling of grinding wheel loading phenomena. *Int J Adv Manuf Technol* 2013;68:473–85. doi:10.1007/s00170-013-4745-z.
- [121] Hwang TW, Evans CJ, Malkin S. High Speed Grinding of Silicon Nitride With Electroplated Diamond Wheels, Part 2: Wheel Topography and Grinding Mechanisms. *J Manuf Sci Eng* 2000;122:42. doi:10.1115/1.538909.
- [122] Ardashev D V. Mathematic model of the blunting area of an abrasive grain in grinding processes, with account of different wear mechanisms. *Procedia Eng* 2015;129:500–4. doi:10.1016/j.proeng.2015.12.049.
- [123] Maheo L, Dau F, André D, Charles JL, Iordanoff I. A promising way to model cracks in composite using Discrete Element Method. *Compos Part B Eng* 2015;71:193–202. doi:10.1016/j.compositesb.2014.11.032.
- [124] Fillot N, Iordanoff I, Berthier Y. Modelling third body flows with a discrete element

- method-a tool for understanding wear with adhesive particles. *Tribol Int* 2007;40:973–81. doi:10.1016/j.triboint.2006.02.056.
- [125] Iordanoff I, Berthier Y, Descartes S, Heshmat H. A Review of Recent Approaches for Modeling Solid Third Bodies. *J Tribol* 2002;124:725–35. doi:10.1115/1.1467632.
- [126] Goupil A, Iordanoff I, Charles JL, Rinchet A. Modelling of polishing tools for high spatial frequency defect correction on aspherical surfaces. *Key Eng Mater* 2013;554–557:1232–1241. doi:10.4028/www.scientific.net/KEM.554-557.1232.
- [127] Lou S, Jiang X, Scott PJ. Application of the morphological alpha shape method to the extraction of topographical features from engineering surfaces. *Meas J Int Meas Confed* 2013;46:1002–8. doi:10.1016/j.measurement.2012.09.015.
- [128] Klocke F, Maye J, Engelhorn R, Weirich T. Micro-Analysis of the Contact Zone of Tribologically Loaded Second- Phase Reinforced Sol-Gel-Abrasives. *CIRP Ann - Manuf Technol* 2002;51:245–50.
- [129] Leclerc W. Discrete element method to simulate the elastic behavior of 3D heterogeneous continuous media. *Int J Solids Struct* 2017;121:86–102. doi:10.1016/j.ijsolstr.2017.05.018.
- [130] Koshy P, Jain VK, Lal GK. Stochastic simulation approach to modelling diamond wheel topography. *Int J Mach Tools Manuf* 1997;37:751–61.
- [131] Rasim M, Mattfeld P, Klocke F. Analysis of the grain shape influence on the chip formation in grinding. *J Mater Process Technol* 2015;226:60–8.
- [132] Cooper WL, Lavine AS. Grinding process size effect and kinematics numerical analysis. *ASME* 2000;122:59–69.
- [133] André D, Iordanoff I, Charles JL, Néauport J. Discrete element method to simulate continuous material by using the cohesive beam model. *Comput Methods Appl Mech Eng* 2012;213–216:113–25. doi:10.1016/j.cma.2011.12.002.
- [134] Incropera F, Dewitt D, Bergman T, Lavine A. Fundamentals of heat and mass transfer. Sixth Edit. United States of America: John Wiley and Sons; 2007.
- [135] Rowe WB. Thermal analysis of high efficiency deep grinding. *Int J Mach Tools Manuf* 2001;41:1–19. doi:10.1016/S0890-6955(00)00074-2.
- [136] Tan Y, Yang D, Sheng Y. Discrete element method (DEM) modeling of fracture and damage in the machining process of polycrystalline SiC 2009;29:1029–37. doi:10.1016/j.jeurceramsoc.2008.07.060.
- [137] www.yakuru.fr/granoo (last seen 01/2019) 2019.